April 2014

Heat Transfer into Wall Panel Connections from Residential Scale Fires

John Philip Morrissey
Worcester Polytechnic Institute

Nicholas Robert Martin
Worcester Polytechnic Institute

Trevor Mitchell Rancourt
Worcester Polytechnic Institute

Zachary Thomas Gendreau
Worcester Polytechnic Institute

Heat Transfer into Wall Panel Connections from Residential Scale Fires

Project Number: FP13

A Major Qualifying Project

submitted to the faculty of

WORCESTER POLYTECHINIC INSTITUTE

in partial fulfillment of the requirements for the

Degree of Bachelor of Science

in Mechanical Engineering

by

_____

Zachary Gendreau

_____

Nicholas Martin

_____

John Morrissey

_____

Trevor Rancourt

Date Submitted: May 1, 2014

Approved:

_____

Prof. Nicholas A Dembsey, Advisor

Abstract

Construction of homes and buildings using panels manufactured off site is a growing method of pre-fabrication. Known as panelized construction, this method of building assembly has gained popularity in recent years. With this increase in use, the need to learn more about the fire performance of panels is crucial. The connections at which these panels come together are of particular interest. The long term goal of this work is to numerically simulate connection performance based on an assumed orientation and material properties. This project uses inert materials in physical models as well as a commercial conduction code to study heat transfer into the connections. Inert materials allow for a close match between the physical model and the conduction code. Several of the most commonly used connection orientations were exposed to residential scale fires. The heat transfer measured in the physical models was compared to that simulated using the conduction code. These comparisons will be presented in the context of evaluating the ability of the conduction code to simulate connection heat transfer.

Acknowledgments

Throughout our project, there have been several individuals that have guided us and lead us to where we are today. We would like to acknowledge their support, as the success of our project would not have been possible without them.

Our team would like to thank our advisor, Nicholas Dembsey, for providing this project opportunity to us, as well as providing his expertise and knowledge to the benefit of our group. His guidance throughout the duration of our project is much appreciated.

We would also like to thank Randy Harris, WPI's Fire Lab Manager, who helped us with all aspects of our experiments conducted in the lab. The project would not be possible without his help.

We also want to thank Rich O'Meara from Core Composites for generously providing prefabricated fiber reinforced polymer panels for us to test in the lab.

Table of Authorship

Section	Author(s)	Editor(s)
Abstract	Trevor Rancourt, Nicholas Martin	Zachary Gendreau
Introduction	John Morrissey, Nicholas Martin, Zachary Gendreau	Trevor Rancourt
Background	Trevor Rancourt, John Morrissey, Nicholas Martin	Zachary Gendreau
Physical Model	John Morrissey, Trevor Rancourt	Nicholas Martin
Thin-Skin Calorimeter Calibration	Nicholas Martin	John Morrissey
Computational Model	Zachary Gendreau, Trevor Rancourt	Nicholas Martin
Results	Nicholas Martin	Trevor Rancourt
Conclusions	Zachary Gendreau	John Morrissey

Table of Contents

List of Equations

List of Figures

List of Tables

Introduction

Construction of homes and buildings using panels manufactured off site is a growing method of pre-fabrication. Known as panelized construction, this method of building assembly has gained popularity in recent years. With this increase in use, the need to learn more about the fire performance of panels is crucial. The connections at which these panels come together are of particular interest. These connections come in many different geometries, of which a few are common and needed to be tested. The geometries selected were found to be the most useful in our testing and relevant to the field of study. For full scale testing of these connections, physical models were designed and built with an approximate coordination with National Fire Protection Association testing standards to fit our needs.

The next step in this project was to simulate the physical model in computational software in order to make testing of these connections in the future much more practical. Using cone calorimeter calibration to specify boundary conditions, the computational model could be compared to the conditions of the physical model. This allowed for continued testing and results comparison showing where the two models differ and what steps were needed to correct them.

Background

Panelized Construction

Structural insulated panels have been around since the 1930's when they were experimented with after the technology was used in aircraft [1]. Structural insulated panels, or SIPs as they are known, are built from an insulating layer of rigid polymer foam between two structural boards. The foam and boards can be made from many different materials; however the foam is primarily polystyrene or polyurethane while the board can be anything from sheet metal to carbon fiber [1]. The most common residential SIPs are made using Oriented Strand Board, a type of plywood. These panels require a component that connects two panels together known as a spline. Dimensional lumber can be used but this creates thermal bridging, so manufacturers use many methods such as overlapping.

All structurally insulated panels are built in much the same way with a foam core sandwiched by sheathing materials; however the connections have very different methods. These fall into a few basic categories, joints with separate splines or molded overlaps, and mechanical or adhesive bonds [2]. A combination of splines and bonds is how panels are put together with the most common being separate splines, typically 2x4 or 2x6 lumber, with construction adhesives and screws to connect them in

residential construction. New designs include mechanical locks with overlapping sheathing materials that keep the 'r-value' of the foam core consistent.

Panelized Construction Connections

There are many different ways that wall panels may be connected in the field. After analyzing the most commonly used joint geometries, three types of panelized construction joints were studied in this project. Our decision process was made by studying common building practices, analyzing patents, and looking at panelized construction company websites. The research done for these geometries may be seen in Appendix A.

Building Codes

Fiber reinforced polymer use in building construction is covered in the 2009 International Building Codes [3]. Chapter 6, Section 2602 of these codes defines fiber-reinforced polymers (FRPs) to consist of reinforcement fibers that have been impregnated with a fiber-binding polymer that has been molded and hardened. Chapter 6, Section 2612 of these codes explains the requirements and uses of FRPs in construction. FRPs must all be clearly labeled at the construction site. The label must include information about the manufacturer and how it will be used. This label must be provided by an approved agency. The uses of FRPS are broken down into interior finishes, decorative materials and trim, light-transmitting materials and for exterior wall covering [3].

FRPs can be used for interior finishes if comply with chapter 8 of the 2012 IBC which covers interior finishes [4]. Section 803 sets the limits for interior wall and ceiling finishing materials. If the finish is thicker than .9mm it needs to pass fire tests. The materials are grouped into class A, B, or C depending on the flame spread and smoke-developed index. They can also be tested using the room corner test using NFPA 286 (Section 801). The class defines where the material can be used in certain structures. The class requirements vary depending on the type of building and if automatic sprinkler systems are installed (Section 801) [4].

When FRPs are used as a decorative material or trim they need to comply with section 806. This type of trim must meet different standards then other materials. When the area of the trim is 20 percent of less of the wall area, it needs to have a flame spread index of 25. When the area of the trim is 10 percent or less the flame spread index needs to be 75 or less. It also needs to use the fire blocking and be separated from the exterior wall by being attached to metal base or other noncombustible material [4].

When used as a light transmitting material FRPs need to comply with sections 2606 through 2611 [4]. These sections have additional specifications that need to be met. They need to have a self-ignition temperature of 343 degrees centigrade or higher; a smoke –developed index no greater than 450 and a smoke density rater not greater than 75 (Chapter 26, Section 6). They also need to be able to withstand the usual loads. Even with these standards there are some structures that they may not be used in with automatic sprinklers. Section 2607 and 2608 limit the amount of limit the amount that can be used on exterior walls and the maximum height that it can be installed. If the structure includes automatic sprinklers, the amount that can be used is increased. There are similar limitations when the material is used for roofing or skylights. These amounts are also modified when automatic sprinkler systems have been installed. The last section deals with the limitations when these materials are used for interior signs. To pass an inspection they need to be fully encased in metal, not have an area greater than 20 percent of the wall and not be larger than 24 square feet (Chapter 26, Section 11) [4].

FRPs can also be used on the exterior surface of buildings. They need to fire standards along with snow loads and earthquake loads. For most construction types the exterior walls must obey sections 2603.5.1 through 2603.5.7. The resistance rating must be determined using ASTM E 119 or UL 263. There are exceptions when FRPs are installed on building that are 40feet or less above grade. The flame-spread index must be 200 or less. The FRP cannot exceed 10 percent of the wall area if the fire separation distance is 5 feet or less. If the fire separation distance is greater than 5 feet there is not limitation on the percent of wall area [4].

These limitations have allowed FRPs to be used more easily in construction. It also insures that they will be used only where code allows and there are controls over how they are manufactured.

Fire Testing

In order to properly test the physical models, testing standards commonly used in industry were researched. The governing standards that were discovered included ASTM E84 [5], NFPA 286 [6], and FM Global Fire Tests [7]. These standards provided information on surface burning characteristics, evaluating a room corner test and standard fire scenarios. The details of these standards can be found in Appendix B.

Physical Model

Panel Geometry

The three connection geometries used in our testing are shown in their respective drawings below. These panels were built using inert materials instead of typical construction materials for multiple reasons. Continuous testing without degradation of the materials, constant thermal transfer, and easier thermal mapping were the primary reasons that allowed for more accurate results. More information on the selection of these materials can be found in the materials catalog in Appendix C.

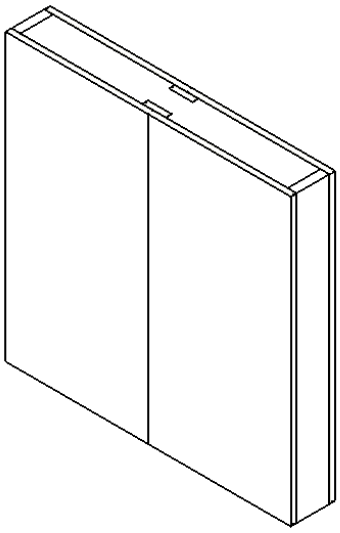

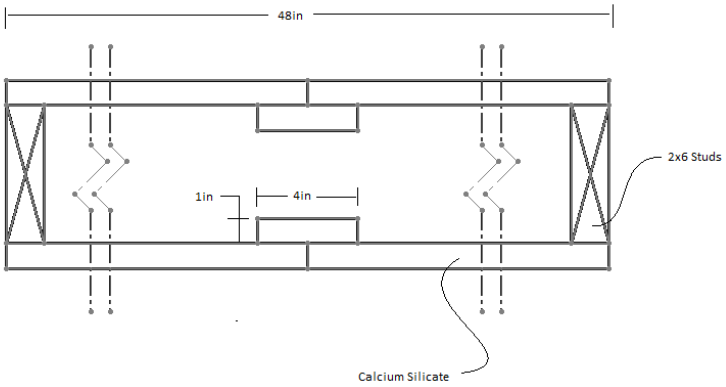

Figure 1: Butt Joint - Spline

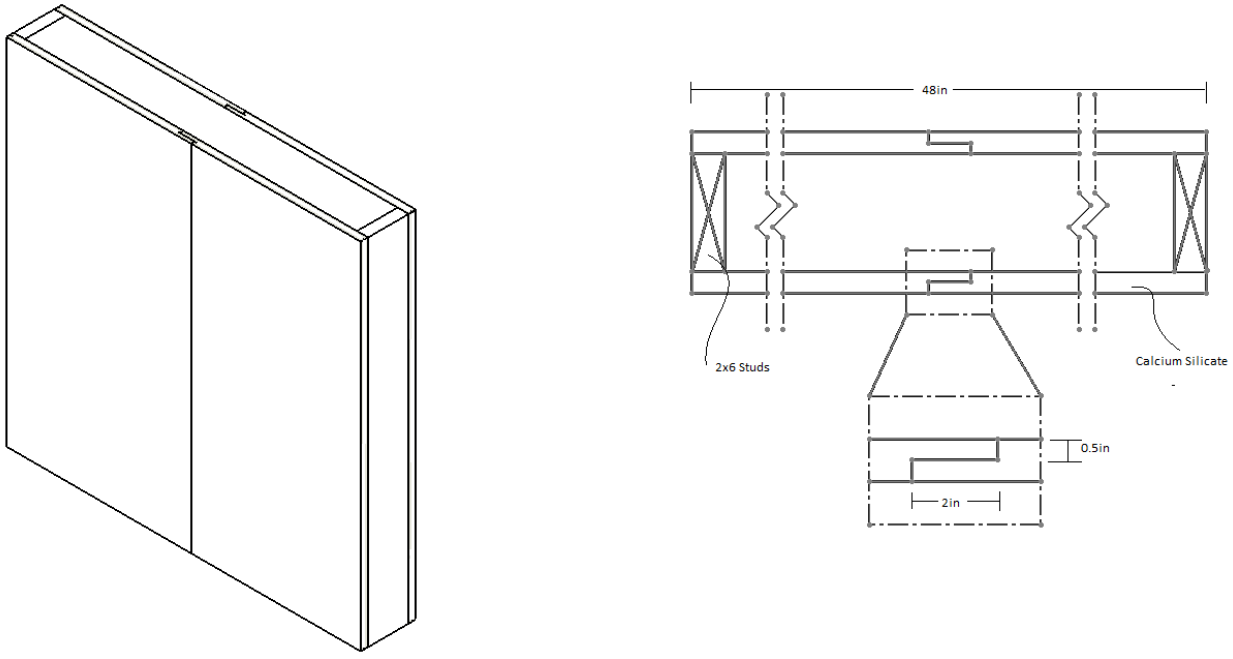

Figure 2: Butt Joint - Overlap

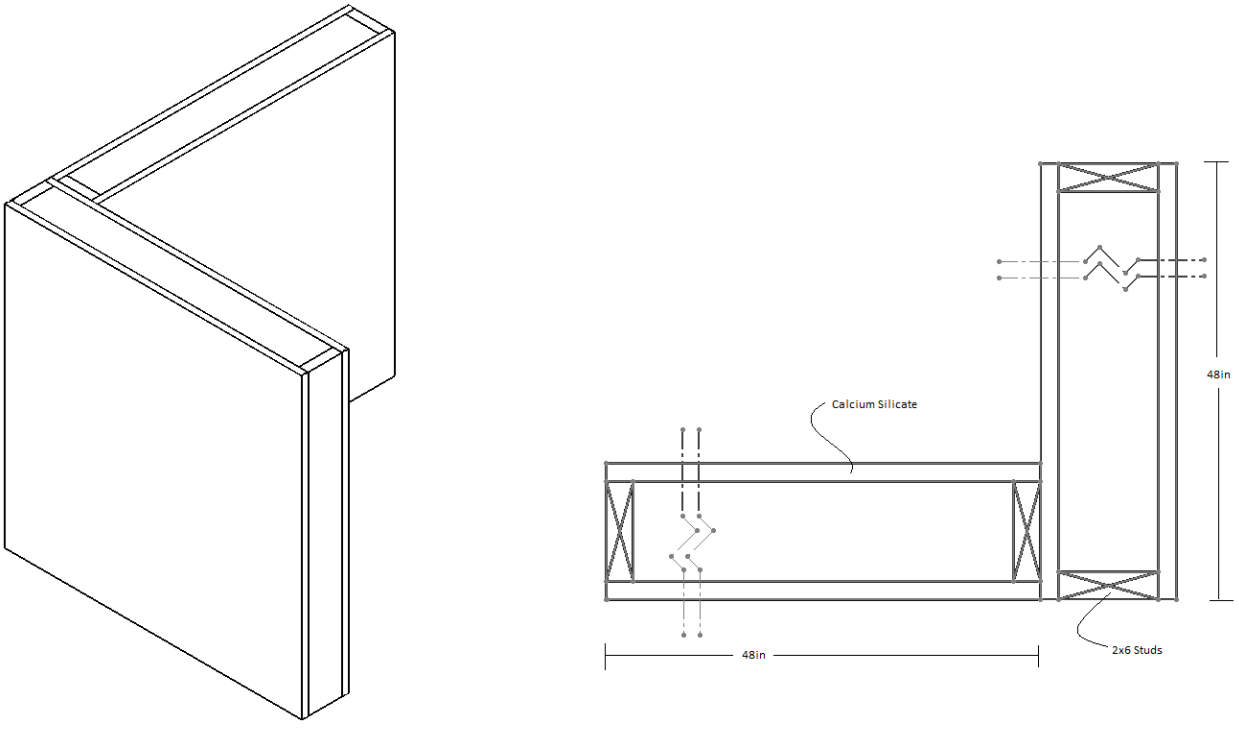

Figure 3: Corner Joint

These panels were constructed separately and designed to fit into rigs which would allow for full scale testing on an 8’ high section. These panels were installed into full scale rigs in order to simulate an entire wall. These rigs are made from typical construction materials and are not instrumented. The materials were replaced as necessary between tests to keep results as consistent as possible. Descriptions and diagrams of these panels and rigs are in Appendix D.

It is important to note that due to the difficulty to perfectly seal the panel connections, a set gap size (1/8”) was placed in all of the experimental models. We set the gap size to a known dimension so we could match the experimental model with the physical model. By instrumenting this gap, we can determine the effect the air flow has on the gap in the physical model versus the computational model which only considers stagnant air within the same gap.

Instrumentation

Figures displaying the instrumentation layouts of the various testing geometries are shown below. The instrumentation is located primarily on the front connection of the panel unless otherwise noted. Descriptions of these figures and of the instruments themselves can be found in Appendix E.

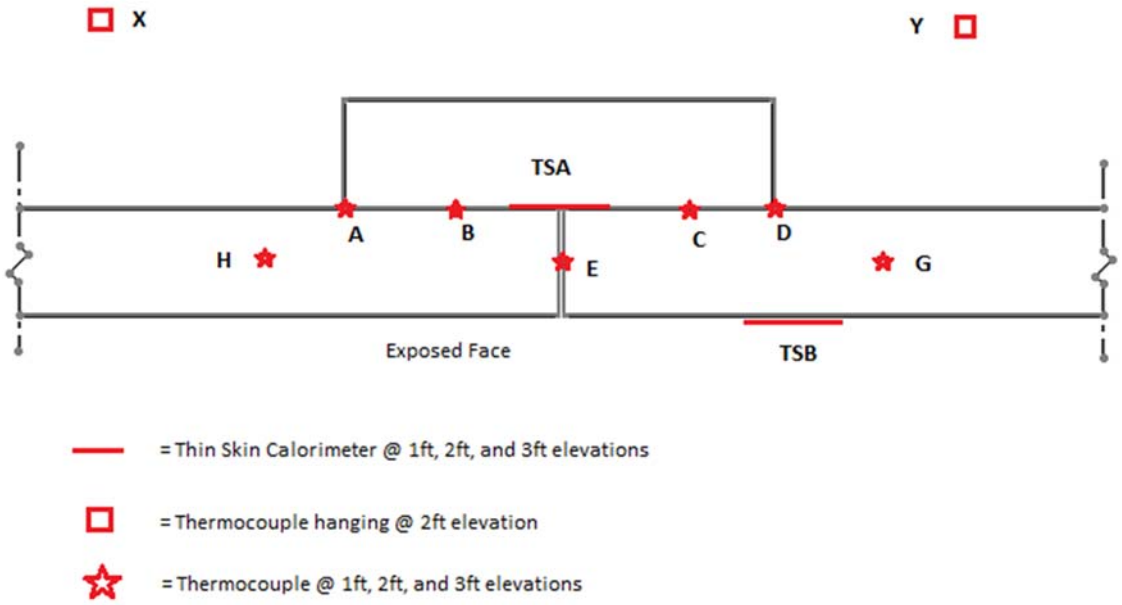

Figure 4: Spline Joint Instrumentation (not to scale)

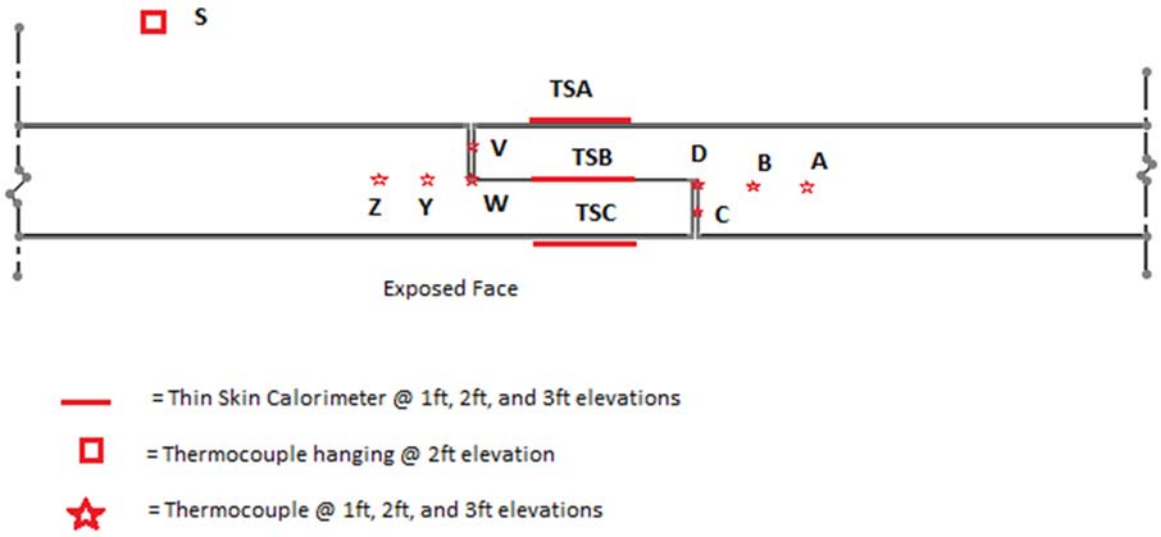

Figure 5: Overlap Joint Instrumentation (not to scale)

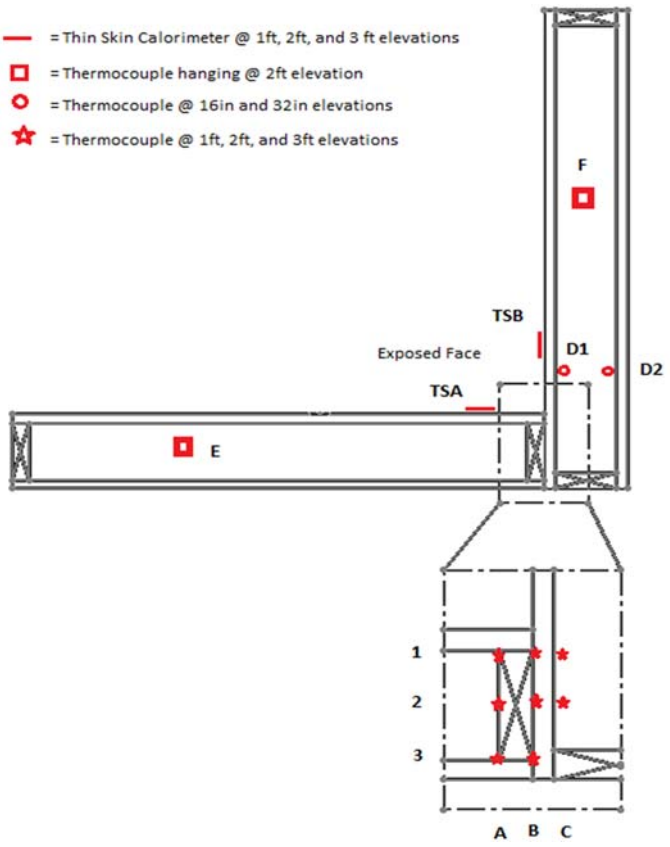

Figure 6: Corner Joint Instrumentation (not to scale)

Thin-Skin Calorimeter Calibration

Thin skin calorimeters were calibrated using a cone calorimeter to find the contact conductance between the stainless steel plate and the calcium silicate board. The thin skin calorimeters were constructed following the ASTM E-459 standard [8]. The calibration exercise used the energy balance equation below.

$$\rho c\delta \frac{dT_s}{dt} = \alpha_s q"_i - \varepsilon_s \sigma\left(T_s{}^4 - T_\infty{}^4\right) - h_{conv}(T_s - T_\infty) - h_{total}(T_s - T_{substrate})$$

Equation 1: Thin-Skin Calorimeter Calibration Energy Balance Equation

Where:

Component	Description	Variables
$\rho c\delta \frac{dT_s}{dt}$	Energy Storage in the plate	ρ – density of the plate c – specific heat of the plate δ – thickness of the plate T_s – temperature of the plate
$\alpha_s q"_i$	Incident heat flux	α_s – absorptivity of the plate $q"_i$ – incident heat flux
$\varepsilon_s \sigma\left(T_s{}^4 - T_\infty{}^4\right)$	Radiation loss	ε_s – emissivity of the plate σ – Stefan-Boltzmann constant T_∞ – ambient temperature
$h_{conv}(T_s - T_\infty)$	Convective loss	h_{conv} – convective heat transfer coefficient
$h_{total}(T_s - T_{substrate})$	Contact Conductance	h_{total} – contact conductance heat transfer coefficient $T_{substrate}$ – surface temperature of the calcium silicate

Table 1: Energy Balance Equation Terms

By using a cone calorimeter, we set a known incident heat flux (25kW, 50kW, and 75kW) to the thin skin calorimeter assembly for a duration of 10 minutes. In addition, we coated the stainless steel plate with a high temperature black matte spray paint to give an absorptivity and emissivity of the plate close to 1. We assumed a value of 0.9. It is also assumed that the convective heat transfer coefficient for air ranges from 5 W/(m^{2}K) to 25 W/(m^{2}K). For simplicity, we assumed an average value of 15 W/(m^{2}K) in the calibration. The remaining unknown variables in the energy balance equation is the contact conductance heat transfer coefficient (h_{total}) and the surface temperature of the calcium silicate ($T_{substrate}$). We used the finite difference method [9] in order to find these values. This exercise defined the gap across the stainless steel plate and the calcium silicate board.

It is important to note that the contact conductance heat transfer coefficient is a linear approximation of the heat flowing from the stainless steel plate to the calcium silicate board. The linear approximation is used because the temperatures in the physical experiments are not high enough for radiation to become a significant factor. The linear approximation can be seen below.

$$h_{total} = 4\varepsilon_s \sigma {T_s}^3 + h_{contact}$$

Equation 2: Heat Transfer Coefficient

At extremely high temperatures, for example in the 75kW incident heat flux calibration test, this radiation becomes significant. In these cases, the radiation term above must be used in the calibration [10].

A schematic of the thin-skin calorimeter assembly can be seen below. It includes a 2in by 2in stainless steel thin-skin calorimeter plate 1.2mm thick, two 1in thick slabs of calcium silicate board with a thermocouple placed in between. A notch was drilled out in between the two calcium silicate slabs to feed the wires through for the thermocouple and thin skin calorimeter. Thermal grease was used for the thermocouple at depth to create near perfect thermal contact between the two calcium silicate slabs. The assembly was held together with two bolts secured with washers and nuts. In addition, a ceramic blanket was used to insulate the surroundings of the assembly to reduce the heat transfer to as one-dimensional as possible. The gap shown below is exaggerated for demonstration purposes.

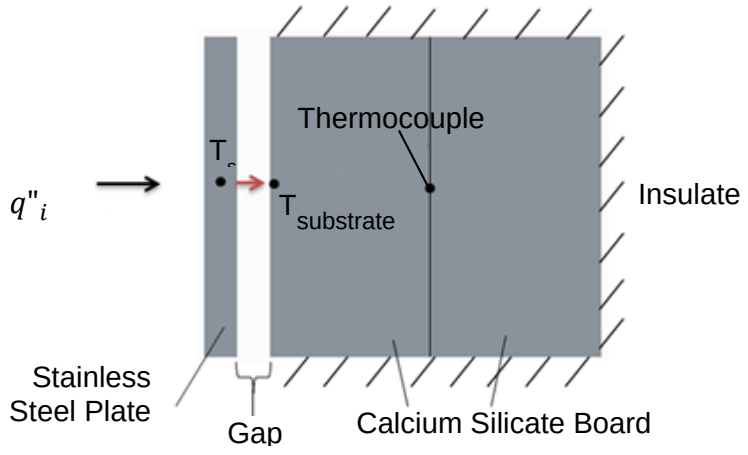

Figure 7: Cone Calorimeter Setup

Calibration Results

The contact conductance heat transfer coefficient was determined to be 650 W/(m^{2}K). The results of the 50 kW incident heat flux calibration test can be seen in the graph below.

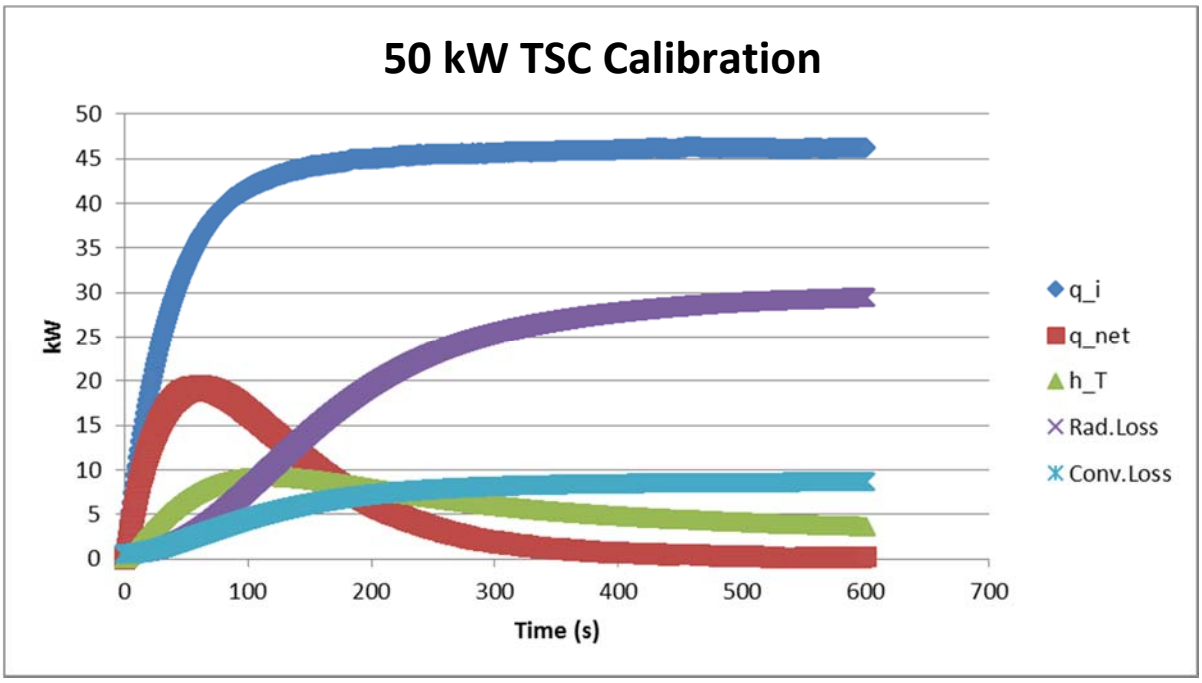

Figure 8: Thin Skin Calibration Results

The graph above shows each of the components of the energy balance equation. The blue line indicates the incident heat flux from the cone calorimeter, the red line indicates the net heat flux of the plate, the green line indicates the contact conductance between the stainless steel plate and the calcium silicate, the purple line indicates radiation losses, and the light blue line indicates the convective losses.

This calibration exercise was used as a baseline to validate the computational model. The contact conductance heat transfer coefficient found in the calibration exercise was used as the front face boundary condition in the computer simulations. For additional information on the calibration exercise, see Appendix F.

Computational Model

We selected COMSOL® Multiphysics 4.4 [11] as the conduction code for the computational model. COMSOL® uses the finite element method to solve engineering and physics models. We used the conduction code to compute different node temperatures throughout the panel connection geometry to use as a comparison with the same nodes in the experimental model.

Thin Skin Calorimeter Calibration

The project group used the thin skin calorimeter calibration exercise as a baseline to validate the computational model. In order to do this, the calibration exercise was simulated using the conduction code. The computational model uses the following general heat transfer equation:

$$\frac{\delta T}{\delta t} = \frac{k}{\rho c}\frac{\delta^2 T}{\delta x^2}$$

Equation 3: General Heat Transfer Equation

In order to get accurate results, boundary conditions needed to be defined in the computational model to match the experimental model. For the exposed face, the stainless steel plate material properties was neglected in the model as only the temperature of the plate (T_s) was considered using the following boundary condition:

$$h_{total}(T_s - T_{substrate}) = -k\frac{\delta T}{\delta x}$$

Equation 4: Boundary Condition Equation

Since the temperature of the plate changes with respect to time, a third order polynomial of time was fitted to the plate temperature profile. This function was used to set T_s as a function of time. For example, the third order polynomial function for the 50kW calibration test is:

$$T_s = (1 * 10^{-5})t^3 - 0.013t^2 + 4.7186\text{t} + 332$$

A similar approach was used for the 25kW and 75kW calibration tests. The heat transfer coefficient, h_{total} = 650 W/(m^{2}K), was that found in the calibration exercise described in the previous section.

Since the experimental model surroundings were insulated, an insulating boundary condition was placed in the computational model for the surroundings:

$$-k\frac{\delta T}{\delta x} = 0$$

Equation 5: Insulating Boundary Condition Equation

Another boundary condition in the computational model was perfect thermal contact between the two calcium silicate slabs:

$$-k\frac{\delta T}{\delta x} = -k\frac{\delta T}{\delta x}$$

Equation 6: Thermal Contact Boundary Equation

This is an accurate simulation since thermal grease was used in the experimental model between the calcium silicate pieces to simulate near perfect thermal contact. The figure below is the model used in the conduction code.

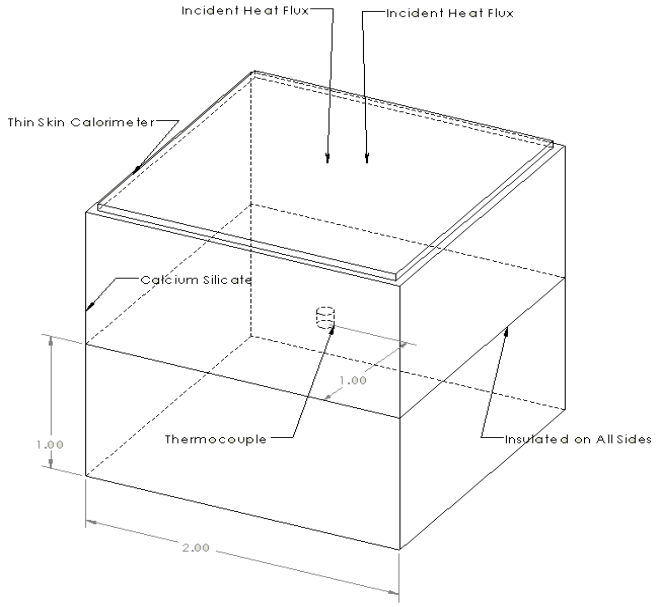

Figure 9: Computational model of think skin calibration

As seen in the figure above, a node was placed in the center of the model in between the two slabs of calcium silicate. This is the same place the thermocouple was placed in the experimental model. Comparisons between the 50 kW experimental model and computational model can be seen below.

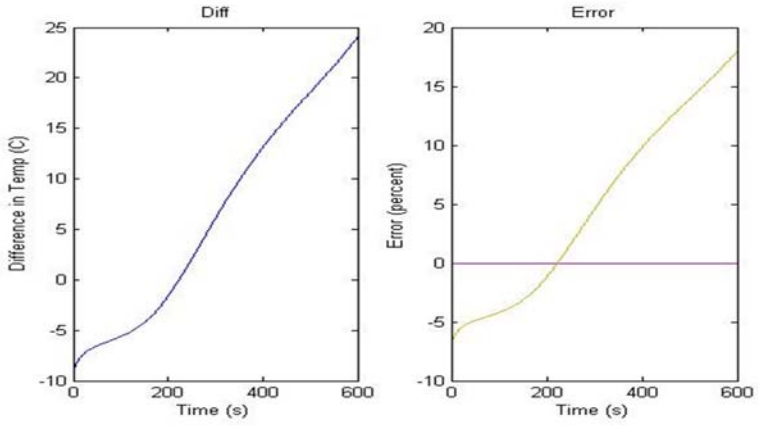

Figure 10: Graphs at point 1, difference in temperature and percent error

From the figure above we can see that the maximum difference is 25 °C which is a reasonable value. The graphs below were calculated using the following equations.

$$Error = \frac{Temp_{COMSOL} - Temp_{Physical}}{Temp_{Physical}} * 100$$

Equation 7: Error Equation

$$Difference = Temp_{COMSOL} - Temp_{Physical}$$

Equation 8: Difference between computational and physical

Our computational model has now been validated and can be used in our full scale fire testing.

Full Scale Experimental Model

In order to simplify the computational model, only the exposed face panel connection was modeled. To execute this simplification, boundary conditions needed to be defined to match the experimental model. These boundary conditions include the following:

- A front face heat flux from the fire. This was calculated using thin skin calorimeters on the front face of the experimental models. The mathematical description of this boundary condition is below. The heat transfer coefficient used for this boundary condition is 650 W/(m^{2}K), the value found in the thin skin calorimeter calibration exercise. The temperature profile of the plate, T_s (data from the experimental model), was fitted with a third order polynomial function of time.

$$h_{total}(T_s - T_{substrate}) = -k\frac{\delta T}{\delta x}$$

Equation 9: Third Order Polynomial Function of Time

- The air gaps that are present in the joint are represented as stagnate air, as only conduction is considered. One of the main goals of this project was to find out how much of an impact the air flow has on the gap.
- The back of the exposed panel was modeled with convective cooling due to the natural convection produced within an enclosed space. The heat transfer coefficient for this boundary condition is 1.4 W/(m^{2}K). The calculation for this value can be found in Appendix G.

$$-k\frac{\delta T}{\delta x} = h_{enclosure}\left(T_{back\ face} - T_{eclosed\ air}\right)$$

Equation 10: Enclosed Space Equation

The initial condition is that all points in the model start at the same temperature at t = 0.

$$T = T_{\infty}$$

The table below shows the material properties for calcium silicate and air. The properties for air are averaged between 20 C and 400 C. These values were used as the material properties in the computational model.

Material	Density (kg/m^3)	Thermal Conductivity (W/mK)	Heat Capacity (J/kgK)
Calcium Silicate Board	590	0.125	800
Air	0.0844	0.0363	1023.7

Table 2: Material Properties used in computations

Each panel connection was simulated using the computational model setup with the above boundary conditions. The front face boundary condition was different for each since the temperature profiles for the front face thin skin calorimeters were different in each test. Each of these temperature profiles were fitted with a third order polynomial of time as described in the previous section. The third order polynomial temperature profile used in the spline joint was the following:

$$T_s\,[K] = (6 * 10^{-6})t^3 - 0.0072t^2 + 2.8096t + 328$$

The third order polynomial temperature profile used in the overlap joint was the following:

$$T_s\,[K] = (9 * 10^{-6})t^3 - 0.0099t^2 + 3.6396t + 293$$

The third order polynomial temperature profile used in the corner joint was the following:

$$T_s\,[K] = (1 * 10^{-5})t^3 - 0.0115t^2 + 4.3222t + 288.6$$

The last term in each of the polynomial function denotes the initial condition temperature for each of the joints. Ideally, each of the tests would start at room temperature (~290K), but due to time constraints this was not possible for each test. It is also important to note that only one elevation was analyzed for each panel connection due to time constraints.

The geometry of the joints used in the computational model can be seen in the figures below. Note that perfect thermal contact is assumed at any point where on piece of calcium silicate meets calcium silicate. The mesh size starts at 10^{-3} inches at the joint and grows at a rate of 1.1 (node

separation is no greater than 110 percent of the previous node separation) to a maximum of 0.1 inches away from the joint.

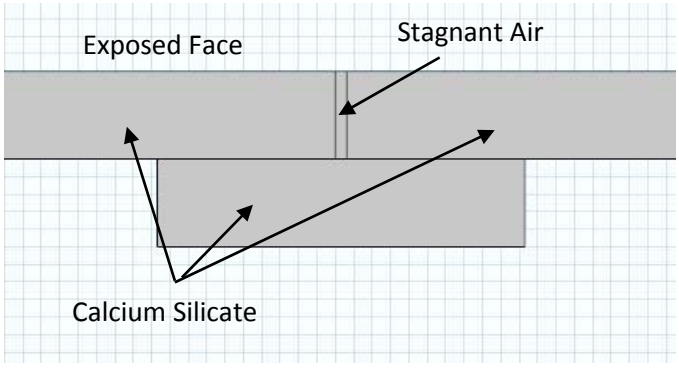

Figure 12: Spline Joint Computational Model

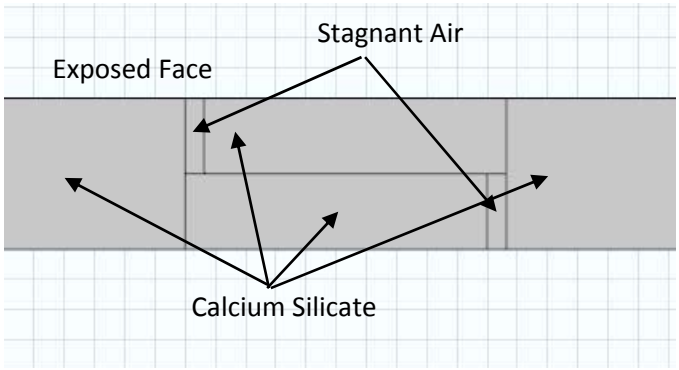

Figure 11: Overlap Joint Computational Model

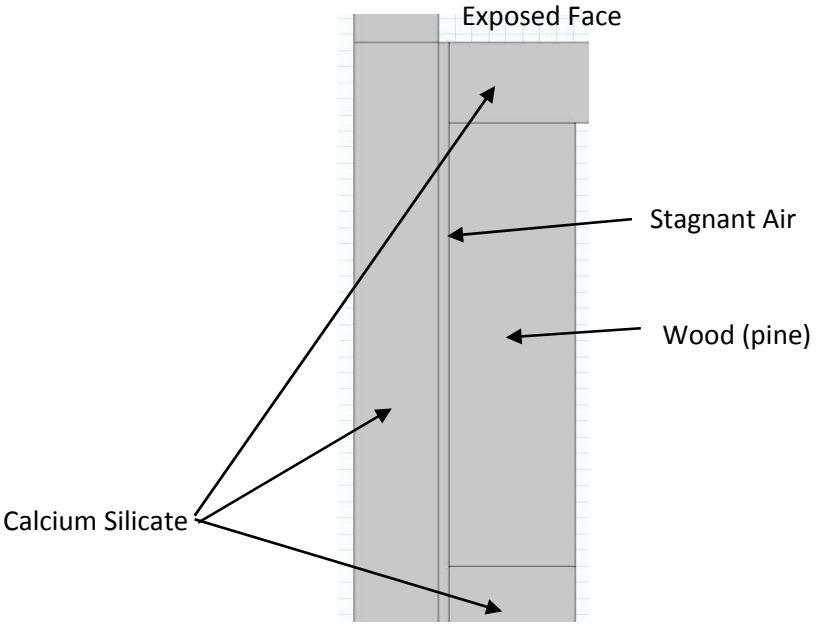

Figure 13: Corner Joint Computational Model

The results of the computational model was then compared to the results of the experimental model. We compared the results to see how well the computational model simulated the experimental model and to see the effect of the air flow had on the gap.

Results

Data was taken from the experimental testing on full scale models and compared to the computational models simulated in COMSOL®. Each geometry yielded varying results but showed overall trends used to make conclusions about the ability of the program to simulate real fire tests. The front face of each joint was modeled quite successfully in the computer due to the extensive work using the cone calorimeter to find optimal front face boundary conditions. The primary focus of the results deals with the heat transfer at depth.

Butt Joint 1 – Spline

The primary difference between the physical model and the computational model proved to be the temperature readings within the exposed air gap as seen in the graph below. The graph below refers to the instrumentation in Figure 4 for the spline joint. The depths shown correspond to the following temperature nodes: 0" is thin skin B, 0.5" is thermocouple E, 1" is thin skin A, and 2" is thermocouple F.

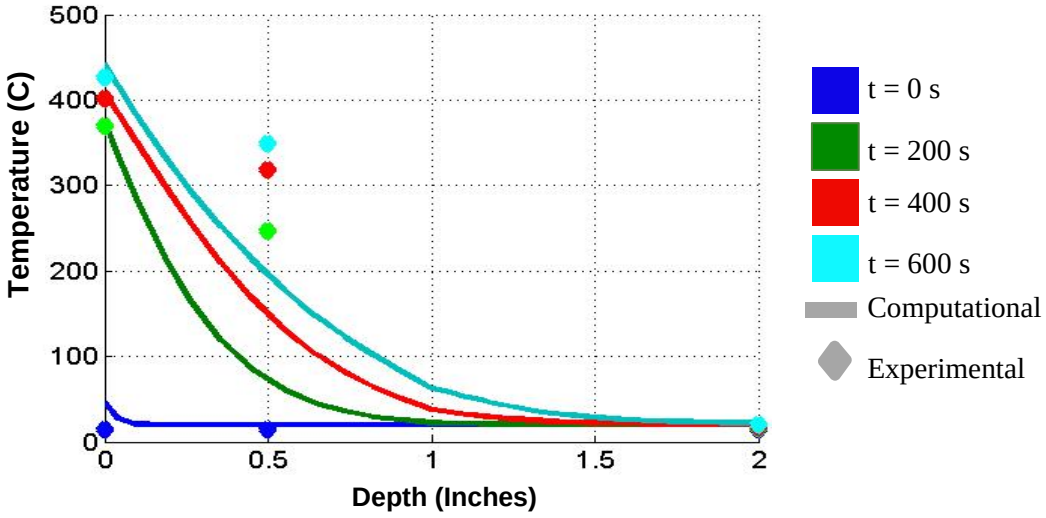

Figure 14: Spline Joint Temperature vs. Depth

The gap inside the joint between the two sheets in the front skin was 0.125 inch wide and 1 inch deep. This gap allowed for significant airflow in the physical model during fire testing. This airflow was not present in the computational model since the gap boundary condition was treated as stagnant air,

as only conduction was considered. This difference is obvious in the temperature node at 0.5 inch depth, which has convective heating in the physical model and insulating properties in the computational model. This reason explains the much lower temperatures in the computational model. Additional data from the instrumentation of the physical model in the spline joint is shown in Appendix H.

Butt Joint 2 – Overlap

The results for this joint are similar to those from the spline joint. However, the differences in temperatures between the physical model and computational model are much smaller than in the spline joint. The change is possibly due to the differences in air gap depth between the spline joint and overlap joint. In the spline joint, the gap reaches a maximum depth of 0.5 inches, whereas the overlap joint only reaches a maximum depth of 0.25 inches. With a greater depth, there is more insulating air between the fire and the instrumentation, resulting in in lower temperatures for the computational model. Another reason for this difference could be that our back face boundary condition is not as accurate as in the spline joint model. The computational data suggests a higher heat transfer coefficient is needed for the convective cooling on the back of the exposed face to match the experimental data. A higher heat transfer coefficient would lower the temperatures on the back face in the computational model. The data comparing the temperature versus depth parameterized by time is shown below. This graph refers to the instrumentation shown in Figure 5 of the overlap joint. The depths shown correspond to the following temperature nodes: 0" is thin skin C, 0.25" is thermocouple C, 0.5" is thermocouple D, and 1" is thin skin A.

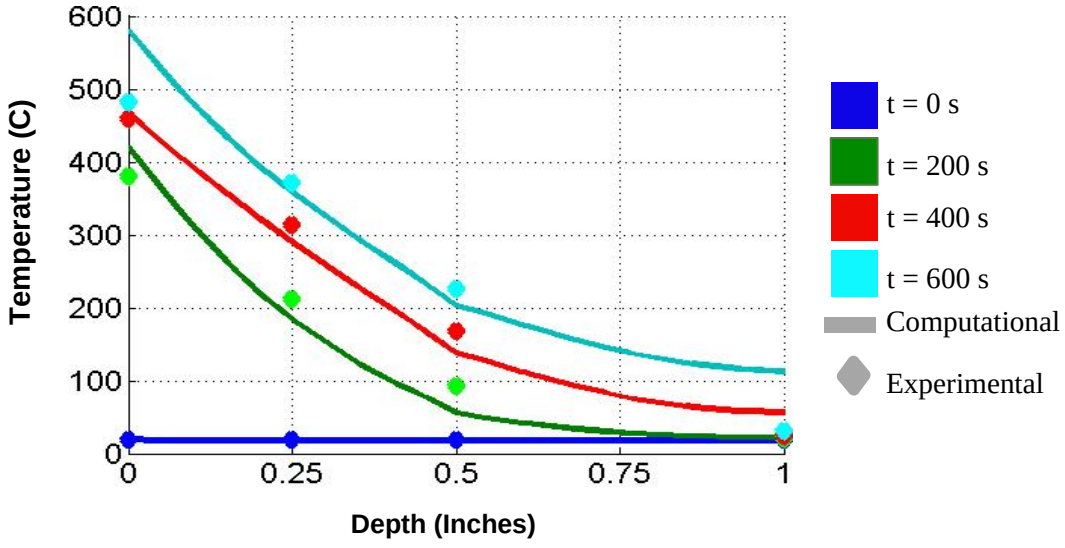

Figure 15: Overlap Joint Temperature vs. Depth

The data trends are similar to the spline joint, but the physical data and computational data are much closer for the reasons stated above. The results still demonstrate that the air flow in the gap is convectively heating the instrumentation in the physical model. The data from the physical model instrumentation in the overlap joint is shown in Appendix H.

Corner Joint

The test data from the corner joint shows similar trends to both the spline joint and overlap joint. The data showing temperature vs. depth parameterized by time is shown in the graph below. This graph refers to the instrumentation shown in Figure 6 of the corner joint. The depths shown correspond to the following temperature nodes: 0" is thin skin A, 1" is thermocouple B1, 3.75" is thermocouple B2, and 6.25" is thermocouple B3.

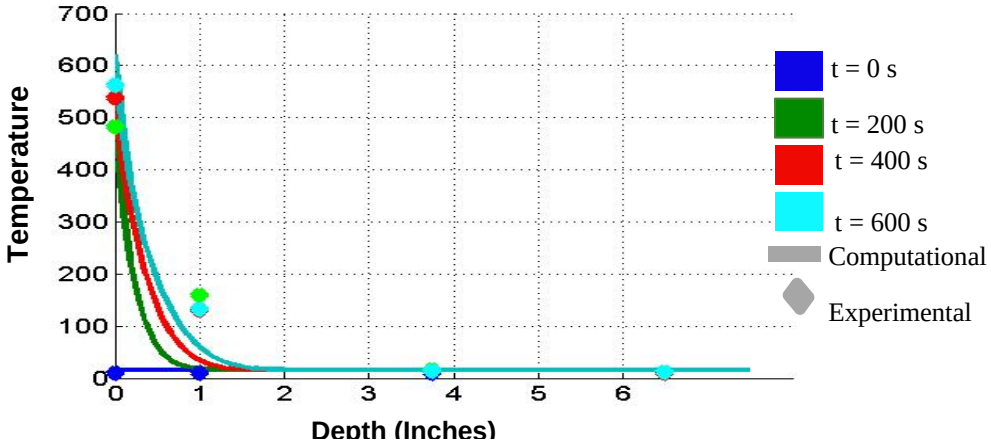

Figure 16: Corner joint Temperature vs. Depth

The obvious difference in the results from the corner joint to the butt joint results are due to the increased depth in the corner joint. The gap between panel sections in this joint is also 0.125 inch wide, but is 7.5 inches deep. The air flow does not penetrate deep though the gap, but still provides convective heating at the 1 inch node.

Summary

The difference between the first node of each joint and its computational counterpart is shown in a summarization graph below. This graph shows that the joints with larger gaps have much more of an impact on the temperature profile and a larger difference between the physical model and the computational results.

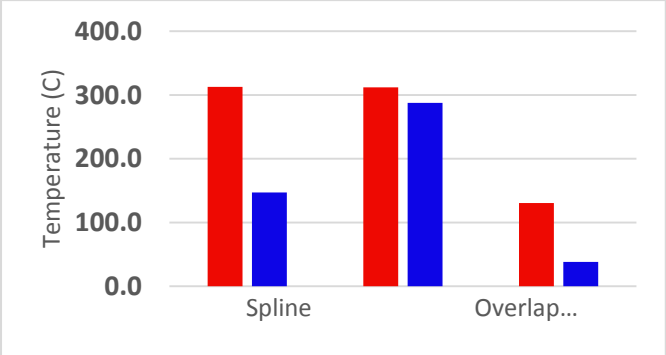

Figure 17: Data Summary after 400 seconds

Conclusions

As the physical model was developed, new boundary conditions, equations, and testing procedures needed to be worked out to fit those needs. Some of these included testing trials, conduction codes, convective cooling, and gap air flow.

The compilation of data from the physical tests shows consistent trends, which allows the data to be used. More accurate data could have been averaged out of many tests, but due to time constraints and lab availability, only enough tests were done to rationalize the data.

The computational model was developed using boundary conditions imposed by early testing and refined by data found by calibrating thin skin calorimeters underneath a cone calorimeter. This work developed a contact conductance between the stainless steel plate and calcium silicate board for use as the front face boundary condition in the computational model. Natural convection in an enclosure was investigated to determine the boundary condition of the inside face of the exposed panel.

The significant difference between the computational model and the experimental model proves that air flow in the small gap between panels has a major influence on the temperature of the joint. To further improve the computational model, the gap needs to be better characterized to include this air flow. Overall, the computational model was able to simulate the experimental model with relative accuracy. With improved boundary conditions, i.e. the flow of air in the gap, a more accurate computational model can be developed.

References

[1] Maxwell, Steve. "Pressure-Treated SIP Foundations Are Warm, Dry and Easy to Build -." *Steve Maxwell Magazine* n.d.: n. pag. Web. 2013 Sept. 10. <http://stevemaxwell.ca/pressure-treated-sip-foundations-are-warm-dry-and-easy-to-build/>.

[2] Vaidya, Amol S. *Lightweight Composites for Modular Panelized Construction*. University of Alabama at Birmingham, n.d. Web. 2013 Sept. 15.

[3] *International Building Code 2009*. Country Club Hills, IL: International Code Council, 2009. Print.

[4] *2012 International Building Code*. Country Club Hills, IL: ICC, 2011. Print.

[5] "ASTM E-84: Standard Test Method for Surface Burning Characteristics of Building Materials." American Society of Testing and Materials, 2001. Web. Sept. 2013. <https://law.resource.org/pub/us/cfr/ibr/003/astm.e84.2001.pdf>.

[6] "NFPA 286: Standard Methods of Fire Tests for Evaluating Contribution of Wall and Ceiling Interior Finish to Room Fire Growth." 2011. National Fire Protection Association, 2010. Web. Sept. 2013.

[7] "American National Standard for Evaluating." FM Global, Dec. 2007. Web. Sept. 2013. <http://www.fmglobal.com/assets/pdf/fmapprovals/4880ansi.pdf>.

[8] "ASTM E-459: Standard Test Method for Measuring Heat Transfer Rate Using a Thin-Skin Calorimeter." 2011. ASTM International, 2011. Web. Oct. 2013.

[9] Bergman, Theodore L., Adrienne S. Lavine, Frank P. Incropera, and David P. Dewitt. *Fundamentals of Heat and Mass Transfer*. 7th ed. Hoboken, NJ: John Wiley & Sons, 2011. Print.

[10] Alston, Jarrod J. "Room/Corner Fire Calibration Data: Marine Composite Screening Specimens." Thesis. Worcester Polytechnic Institute, 2004. WPI. Web. Feb. 2014. <https://www.wpi.edu/Pubs/ETD/ Available/etd-0527104-180727/unrestricted/jja_ms_thesis_20040527.pdf>.

[11] *Introduction to Comsol Multiphysics®*. 4.4th ed. COMSOL, 2013. Print.

Appendix A: Panelized Construction Background

Structural insulated panels have been around since the 1930's when they were experimented with after the technology was used in aircraft. Structural insulated panels, or SIPs as they are known, are built from an insulating layer of rigid polymer foam between two structural boards. The foam and boards can be made from many different materials; however the foam is primarily polystyrene or polyurethane while the board can be anything from sheet metal to carbon fiber. The most common residential SIPs are made using Oriented Strand Board, a type of plywood. These panels require a component that connects two panels together known as a spline. Dimensional lumber can be used but this creates thermal bridging, so manufacturers use many methods such as overlapping.

All structurally insulated panels are built in much the same way with a foam core sandwiched by sheathing materials; however the connections have very different methods. These fall into a few basic categories, joints with separate splines or molded overlaps, and mechanical or adhesive bonds. A combination of splines and bonds is how panels are put together with the most common being separate splines, typically 2x4 or 2x6 lumber, with construction adhesives and screws to connect them in residential construction. New designs include mechanical locks with overlapping sheathing materials that keep the r-value of the foam core consistent.

The benefits of using these pre built panels include construction cost, life cycle cost, structural performance and thermal performance. The construction cost of SIPs is equivalent to that of standard stick building due to the major decrease in labor cost. All SIPs are pre built based on the building's design which makes assembly on site simple. This reduces labor costs which is a high percentage of overall construction costs. The improved thermal performance also helps life cycle cost by decreasing the amount of energy needed in the building. SIPs have a much higher effective R-value than normal construction with much less thermal bridging, which occurs when dimensional lumber or something with little insulating value that touches both the inside surface and outside surface. With all three primary layers acting together the structural abilities of SIPs are much higher than conventional framing. The layers act as an I-beam where the foam is the webbing and the sandwich boards as the flanges. The boards resist tension and compression while the foam core prevents buckling and racking. In comparison tests against conventional framing, SIPs were found to have a strength of 2000 lbs per linear foot of wall.

There has been extensive work with panelized construction with different materials, however using lighter materials such as fiber reinforced polymers (FRP) has not been fully realized. Using lighter

materials could make costs go down and ease of construction go up. New materials are being developed to work toward a more “green” approach. Natural fiber reinforced polymeric composites are being used as structural sandwich panels which gives a low carbon footprint as well as cost effective production.

Two types of panelized construction joints were studied in this project. Joints typically using an adhesive connection and joints using only fastener connections. Some of these geometries can use one or both of these methods.

Using an adhesive glue is a very common form of joint connection. This form of bonding allows load to be transferred efficiently between two adherents. The adhesives also increase the structural efficiency of the laminated structure. Some issues of adhesives come from localized flaws affecting joint strength, long time for surface preparation as well as edge effects due to higher stress concentrations. Adhesives may include glues, foams, foam spray, caulk or other synthetic material. Some panels may employ only adhesives. In this form, only adhesive is used to connect two panels. A commonly used adhesive is encapsulated adhesive 36.

There are several other ways in which panels may be connected. The figure below illustrates a few of the possible geometries of joints that are acceptable.

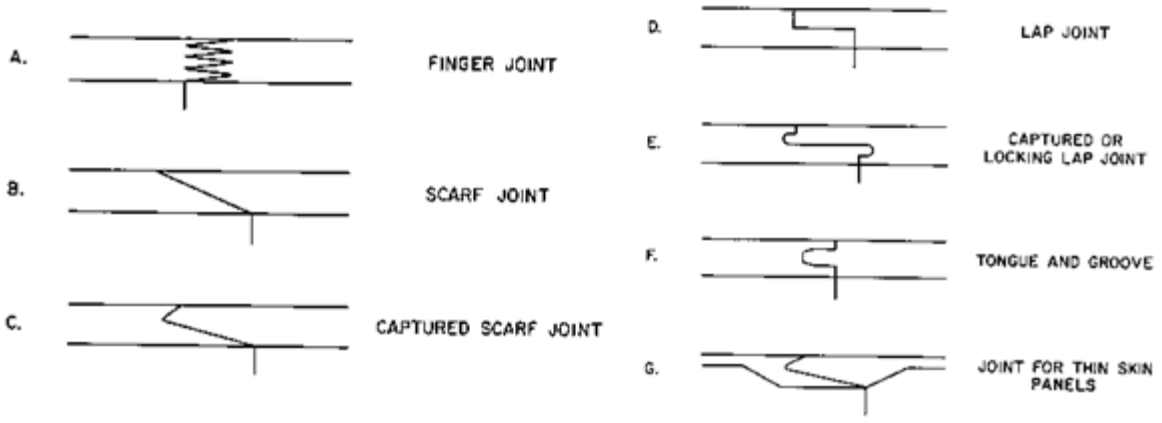

Figure 18: Common Panelized Construction Wall Panel Connection Geometries

Another form of adhesive bonding uses splines. Splines are pieces of material that connect two panels and are the same height as the wall panel core. The splines are bonded to achieve desired strength and fit in between grooves in the panels. Many times, these splines are also stabilized with

panel screws to ensure strong stability. The splines are coated with the adhesive and put into one side of the panels, then the other panel is then fitted into the spline to form a tight fit. The screws of fasteners are then inserted to finish the connection. The figure below shows a common way that these pieces may come be connected. Often times with splines, the connections are made on two parallel panels, not on the corners. Other connections from the one shown below can be seen in Appendix A.

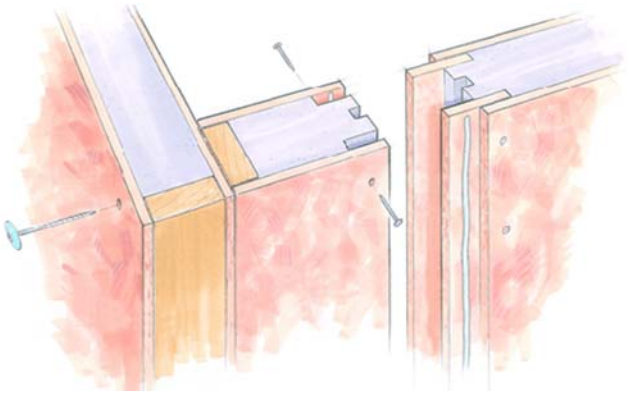

Appendix B: Fire Testing

ASTM E84 – Standard Test Method for Surface Burning Characteristics of Building Materials

This test, known as the "tunnel test," measures flame growth on the underside of a horizontal test subject. The tunnel is 25 ft. by 1.8 ft. by 1.0 ft., and the test material acts as the tunnel's roof. Two gas burners placed at one end of the tunnel provide approximately 89 kW of heat while air and combustible gases are ventilated through the tunnel for a duration of 10 minutes. The source flame takes up the first 5 ft. of the tunnel, and the progress of the flame across the test material is visually measured. The smoke emissions are measured using an optical sensor. Using this information, the Flame Spread Index (FSI) can be determined. This scale is based on set parameters where asbestos-cement board has a FSI of 0 while red oak has a FSI of 100. A rating of 100 indicates that the tip of the flame reaches the end of the tunnel at the 10 minute mark of the test. Based on a material's FSI, it is classified in one of three categories.

	Flame Spread Index	**Smoke Developed Index**
Class A	0-25	0-450
Class B	26-75	0-450
Class C	76-200	0-450

Figure 19: Material Flame Class

The FSI scale is linear, so a rating of 25 indicates the tip of the flame reached 25% of the tunnel by the end of the 10 minute test. If a material has a FSI of 200, then the flame tip reached the end of the tunnel in half of the time of the test. The Smoke Developed Index (SDI) is measured by the optical density of the smoke. Red oak has a SDI of 100. The higher the rating for the SDI, the denser the smoke produced by the material.

The incident heat flux produced in a tunnel test experiment by William Parker in 1977 reached a maximum of 40 kW/m^2, which can be seen in Appendix B.

NFPA 286 – Standard Methods of Fire Tests for Evaluating Contribution of Wall and Ceiling Interior Finish to Room Fire Growth

NFPA 286, known as the room corner test, "measures certain fire performance characteristics of finish wall and ceiling covering materials in an enclosure under specific fire exposure conditions." The test "determines the extent to which the finish covering materials may contribute to fire growth in a

room and the potential for fire spread beyond the room under particular conditions simulated" NFPA 286, 2011).

The test criteria include an 8 ft. by 12 ft. floor plan with an 8 ft. high ceiling constructed with wood framing. A 30 in. wide doorframe must be at the center of one of the 9 ft. walls. The exterior must be covered with 5/8 in. gypsum wall board. The flame source must be a propane fuel burner, which must be placed in either corner opposite of the doorway. The procedure for the test is to first set the flame source at a 40 kW output for 5 minutes, then a 160 kW output for an additional 10 minutes.

The incident heat flux produced by a test similar to NFPA 286 (specifically UBC 42-2), conducted by Williamson and Mowrer in 1991, and averaged approximately 60 kW/m^2. The test UBC 42-2 is also a room corner test with similar room size and similar fuel source output. More specifically, the room size is 7.87 ft. by 11.8 ft. by 7.87 ft. The fuel source output is 40 kW for the first 5 minutes, then 150 kW for an additional 10 minutes. The heat flux maps for this experiment can be seen in Appendix B.

The room corner test must be split into four quadrants, with a thermocouple on the ceiling of each quadrant. Three additional thermocouples must be located at the ceiling directly above the flame source, the center of the room, and at the doorway. The thermocouples must be Bare Type K Chromel-Alumel. An optical sensor must be used to test the smoke emissions and a Schmidt-Boelter calorimeter must be placed on the floor in the center of the room. The figure belowindicates the locations of the thermocouples and heat flux gauge.

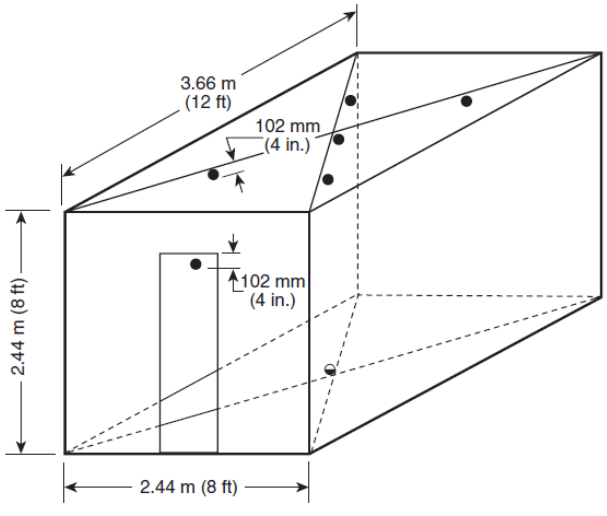

● = Thermocouples —each 102 mm (4 in.) below ceiling, with one additional thermocouple over the burner, and 102 mm (4 in.) below the ceiling.

◒ = Calorimeter on floor — 26 mm (1.1 in.) above floor.

In addition, two paper targets must be placed on the floor at the positions indicated in the figure below.

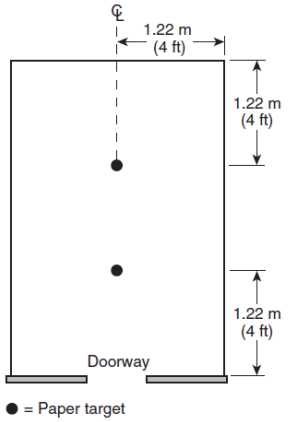

These paper targets are used as flashover indicators per NFPA 286. According to NFPA 286, flashover has occurred when any two of the following conditions have been met:

1. The Heat Release Rate of the fire exceeds 1 MW
2. The heat flux at the floor exceeds 20 kW/m^2
3. The average upper layer temperature exceeds 600 °C
4. Flames exit the doorway
5. Paper target on the floor auto-ignites

Additional instrumentation includes those in the exhaust duct. These include a bidirectional probe to measure gas velocity, thermocouples to measure the temperature in the exhaust duct, a gas sampling tube to measure the oxygen, carbon dioxide, and carbon monoxide concentrations of the fire, and an optical sensor to measure smoke density.

FM Global Fire Tests

FM Global conducts two different fire tests room corner tests. One is a 25 ft. high ceiling and the other is a 50 ft. ceiling. The assembly is made up of three panels: two to create a corner and one to act as the roof. The ignition source is a 750 lb. wood crate, 42 in. by 42 in., and 5 ft. high located in the corner 1 ft. from the walls.

These tests are run to obtain FM Global approval for large warehouse assemblies. For FM Global acceptance to the maximum height of 30 ft., assemblies cannot support a self-propagating fire which reaches the limits of the test at 25 ft., as evidence by flaming or material damage. The duration of the

test is 15 minutes or until the limits have been reached. For FM Global acceptance to the maximum height of 50 ft., assemblies must first pass the 30 ft. high corner test, and cannot support a self-propagating fire which reaches the limits of the test at 50 ft. as evidenced by flaming or material damage. The duration of the test is also 15 minutes or until the limits have be reached.

An FM Global 50 ft. corner tests produces a maximum heat flux of approximately 125 kW/m^2 (Alpert, 2002), as indicated in the figure in Appendix B.

The incident heat flux produced in a tunnel test experiment by William Parker in 1977 reached a maximum of 40 kW/m^2 as seen in the figure below.

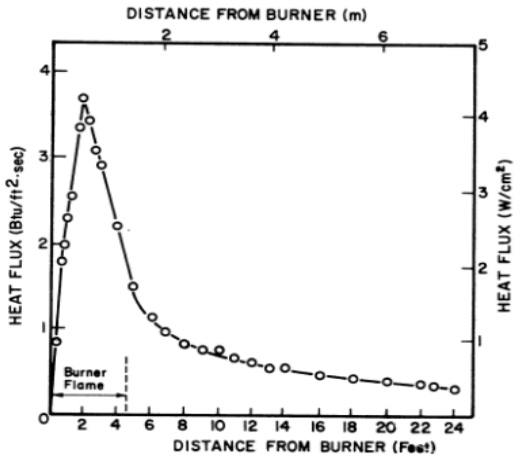

The incident heat flux produced by a test similar to NFPA 286 (specifically UBC 42-2), conducted by Williamson and Mowrer in 1991, averaged approximately 60 kW/m^2. The test UBC 42-2 is also a room corner test with similar room size and similar fuel source output. More specifically, the room size is 7.87 ft. by 11.8 ft. by 7.87 ft. The fuel source output is 40 kW for the first 5 minutes, then 150 kW for an additional 10 minutes. The heat flux maps for this experiment can be seen below.

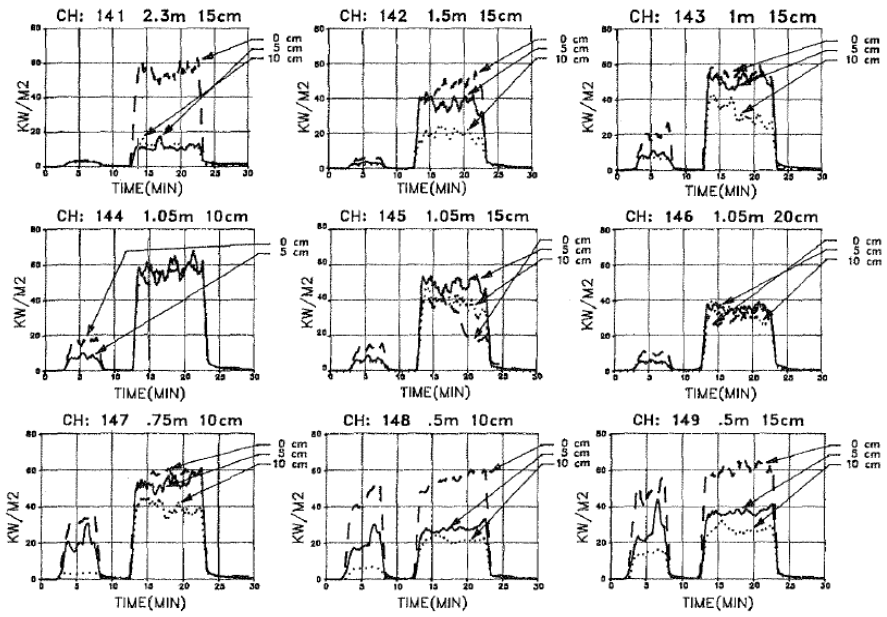

The measurements in each graph are read from certain distances above the source flame and certain distances away from the wall.

An FM Global 50 ft. corner tests produces a maximum heat flux of approximately 125 kW/m^2 (Alpert, 2002), as indicated in the figure below.

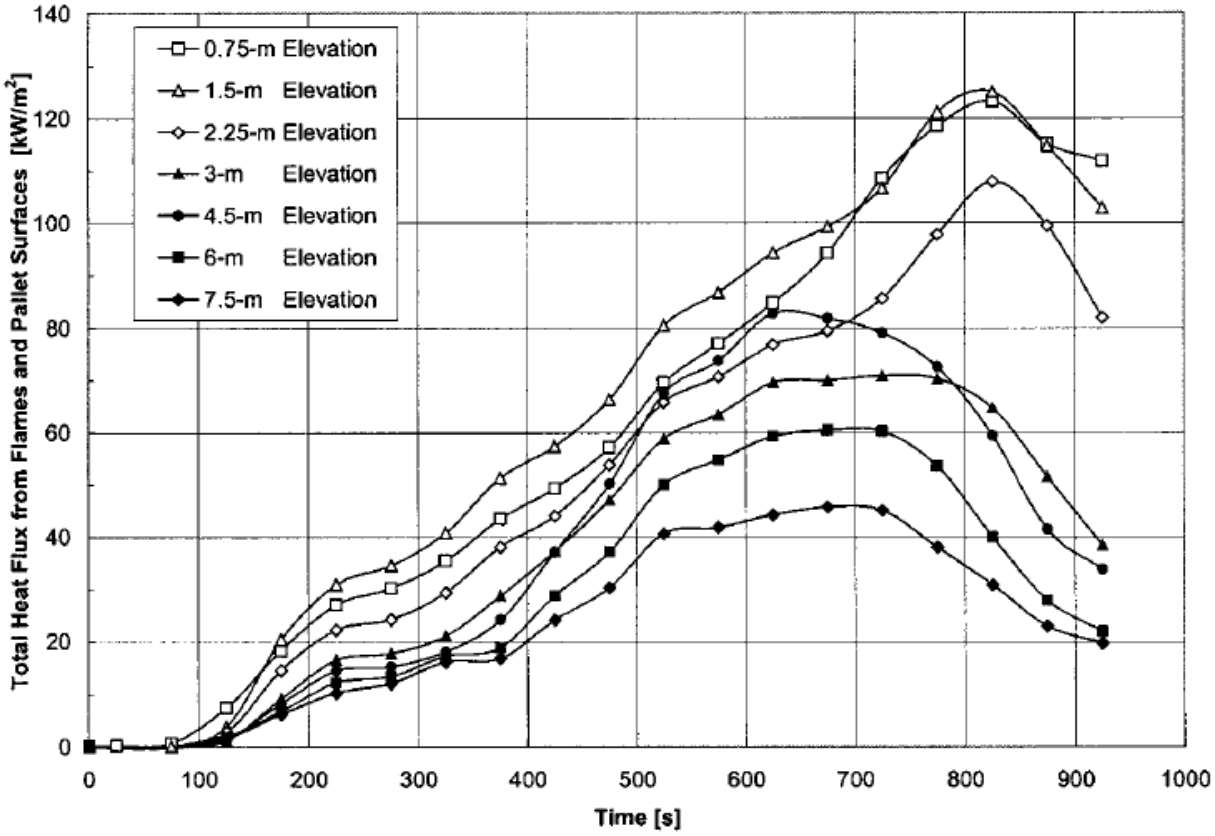
0.75-m Elevation
1.5-m Elevation
2.25-m Elevation
3-m Elevation
4.5-m Elevation
6-m Elevation
7.5-m Elevation
Total Heat Flux from Flames and Pallet Surfaces [kW/m²]
Time [s]
0
20
40
60
80
100
120
140
0
100
200
300
400
500
600
700
800
900
1000

Appendix C: Materials Catalog

Sheathing Materials

Oriented Strand Board (OSB) – Wood particles combined with glue and pressed to form plywood of sorts. Most common material used in residential construction because of its availability and low cost. Has high weight but equally high strength which allows for sturdy structures. Typically finished with gypsum board for fire performance and finish characteristics.

Sheet Metal (Steel) – Produced in rolls which allows for unlimited sizing options. Used almost exclusively for industrial applications for its durability and strength. Very heavy and expensive with limited structural allowances which results in needed structural supports.

Plywood – Very similar to OSB in almost all areas, with slightly higher costs and less availability. Can come stronger and with more desirable finishes. Fire performance is also similar and retardants can be added into the layers to increase performance.

Fiber Cement Siding – Poured cement mixed with fibers to form a matrix and pressed into sheets. The fibers add strength and fracture toughness which also helps improve fire testing results. Extremely common in industrial construction and commercial buildings. Only used when foam cores are reinforced with structural steel or concrete.

Magnesium Board – Used in the form of magnesium oxide which creates a type of natural cement. High utility with many available finishes and sizes. Low overall availability creates higher than average production cost until mass production becomes available. The fire performance matches that of type x drywall which in non-flammable in terms of building codes. Difficulties include cost, ease of installation, weight and availability.

Fiberglass Mat Gypsum – A combination of fiberglass reinforcing fibers in a mat that supports gypsum to make a structural panel. Has many of the same fire qualities as type x drywall with the glass fibers providing continued support during burn testing. Weight can be reduced overall by eliminating drywall as a finish material. Cost is high and increases with size of production panel size.

Carbon Fiber Reinforced Polymers – Many different combinations of fibers and polymers exist with polymers having many possibilities of fire retardants that can be added to improve performance. Production costs as well as availability are moderate but could improve with increased demand. Weight is extremely low which is the highest point of consideration for use in panelized construction.

Core Materials

Expanded Polystyrene – Thermosetting polystyrene is fire resistant which would be required in panelized construction due to the structural needs of the foam. Adding fire retardants help in this application. Cost is low with unlimited availability and options for construction.

Extruded Polystyrene – Extremely similar to expanded polystyrene but with a higher density which results in a higher thermal value. Also provides a higher resistance as a water barrier. Cost is slightly higher as well as weight and production capacity.

Polyurethane Foam – Better fire resistance than polystyrene but with greater environmental impact. Slightly higher density which provides a better R-value.

Sheet Materials Data:

Material	Density (kg/m^3)	Specific Heat (J/kg. °C)	Glass Temp (°C)	Max Service Temp (°C)	Thermal Conductivity (W/m. °C)
OSB	750	1710	102	140	0.14
Steel (AISI 205)	7900	530	1450	787	17
Plywood (5 Ply)	800	1710	102	140	0.15
Fiber Cement	2300	867	2500	1060	0.9
Magnesium Board	3580	1030	2860	2130	60
Glass Mat Gypsum	1300	1710	102	140	0.14
Epoxy SMC	1700	1340	167	184	6.3

Core Materials Data:

Material	Density (kg/m^3)	Specific Heat (J/kg. °C)	Glass Temp (°C)	Max Service Temp (°C)	Thermal Conductivity (W/m. °C)
Expanded Polystyrene	27	1220	92	87	0.036
Extruded Polystyrene	53	1220	92	87	0.04
Thermoplastic Polyurethane	64	1630		177	0.0305
Thermoset Polyurethane		1750	100	135	0.316

Example Test Results for Composite Resins:

Tabe 1. FILLED HALOGENATED Resin Systems

Resin	A	B	C	D
ASTM E-84				
FSI	20	20	20	20
SDI	850	700	700	900
ASTM E162				
FSI	15	5	10	5
ASTM E662				
Flaming				
D1.5	26	1.9	7.6	9.7
D4.0	420	170	230	580
Dmax	590	550	530	660
Non-Flaming				
D1.5	0.29	0.36	0.29	1
D4.0	8.5	11	10	49
Dmax	350	300	210	320

Appendix D: Panel Description

Butt Joint 1:

The joint is in the middle of the panel with a spline behind it. The spline is made of the same material and thickness as the outer skin of the panel. Screws attach the spline to the outer skin every 16 inches or where applicable and on both sides of the joint. The prototype design skin is made from 2 layers of ½ inch sheetrock while the test design is made from 1 inch calcium silicate.

The joint panel is made 4 feet by 4 feet to decrease material costs and make instrumentation easier. The panel fits into a rig that extends it to a full 4 foot by 8 foot panel with similar properties to best be able to test the joint geometry. The back of the panel is removable to allow for instrumentation and repairs.

Butt Joint 2:

The joint is an overlapping construction of the skin that is centered on the middle of the panel. This overlapping construction is designed for strength and thermal properties as well as ease of installation. The overlapping joint is half the thickness and two inches long with a reverse pattern to lock with. A single screw attaches both skins through the joint at every 16 inches or where applicable.

The panel is made to the same overall dimensions as butt joint 1 so as to make them both compatible to the same rig. This will allow testing of the panels to be quick with only minor repairs need to the rig. The back of the panel is removable to allow for instrumentation and repairs.

Corner Joint 1:

The corner joint is made similar to the butt joints that attach at the ends. This allows for simple construction on site. The panels assemble in a step by step process to increase strength and allow the corner to be inserted into a rig to allow full 8 foot testing. The skins, as with the other joints, are made from 1 inch calcium silicate while the prototype is made from 2 layers of ½ inch sheetrock. There are no screws needed in the joint other than those holding the side panels together making the corner.

Butt Joint Rig:

The rig is designed to allow both butt joints to fit into it while making the test a full 8 feet. The spot for the joint panels allows for them to fit in as well as ceramic blanket to prevent skewed data from changes in the fire flow. There is a support structure made from studs that allow for a free standing structure that will last for all tests required. The skins above and below the test panel are made from

two layers of ½ inch sheetrock which allows the outer layer to be removed after each test. This is to keep the integrity of the sheetrock for future tests.

Corner Joint Rig:

The rig is designed to allow the corner joint test panel to fit in to a spot that keeps the test panel at an ideal height of two to six feet. The rig is made of the same construction techniques as the joint geometry. The skin of the rig is made of two layers of ½ inch sheetrock for the same reasons as the butt joint rig. This is to be able to remove the outer layer after each test which keeps the rigs properties through each test.

Appendix E: Instrumentation

Instrumentation – Thermocouples

To provide data on the temperatures within the wall geometry, thermocouples will be placed at different areas and elevations within the wall geometry. The main purpose of the project is to determine the heat flow through the geometry. Since thin-skin calorimeter heat flux gauges are limited to one-dimensional heat flow, the thermocouples were placed in pairs in order to calculate an estimate of heat flow from one thermocouple to the other using Fourier's Law:

$$\dot{q}" = -k\frac{dT}{dx}$$

Thermocouples will also be placed in pairs horizontally and vertically surrounding the screws that fasten the joint geometry assembly. The purpose of these thermocouples is to use Fourier's Law to determine what affect the fasteners have on the heat flow through the joint geometry.

For the first prototype test, the thermocouples were placed in pairs at different elevations on each side of the seam. As prototype testing continues, the number and locations of the thermocouples will evolve into the best possible instrumentation for true testing. The thermocouples were constructed with Type K 30-gauge high temperature glass insulated thermocouple wire. The team picked 30-gauge thermocouple wire for its small size yet strong durability in comparison to the much more fragile 36-gauge thermocouple wire.

Instrumentation – Thin-skin Calorimeters

Thin-skin calorimeters were chosen as a simple means to calculate the incident heat flux moving through the joint connection geometry and were constructed in accordance to ASTM-E459. The group conducted archival research in order to determine the appropriate thermocouple wire diameter to plate thickness ratio to obtain necessary response characteristics as directed by ASTM-E459. A design that was analyzed by Keltner and Bickle in 1976 involved 36-gauge thermocouple wire attached to a 1mm thick plate. This leaves a ratio of approximately 1 to 10. Another design analyzed by Alston in 2004 involved 24-gauge thermocouple wire attached to a 1.6mm thick plate. This design produces a ratio of approximately 1 to 3. A Gardon heat flux gauge was used as a practical limit of thermocouple wire diameter to plate thickness ratio since the gauge is extremely thin. The ratio produced by this gauge is approximately 1 to 1. With this range of thermocouple wire diameter to plate thickness ratios, the group was able to determine appropriate sizing for use in testing.

In true testing, the group will use 25.4mm x 25.4mm (1” x 1”) stainless steel plates approximately 1mm thick. The small plate size will be ideal when inserting the thin-skin calorimeters within the joint geometry. The plates will be wired on the unexposed surface of the stainless steel plate with Type K 24-gauge high temperature glass insulated thermocouple wire. This produces a ratio of approximately 1 to 2, well within the range determined above.

The plates used in the first prototype test were constructed of 50.8mm x 50.8mm (2” x 2”) stainless steel plates approximately 1.2mm thick, and were sprayed with a high-temperature black matte spray paint to bring the plate emissivity close to 1. These dimensions were chosen for easy accessibility in the WPI Fire Science Laboratory. The plates were wired using Type K high temperature glass insulated 24-gauge high temperature glass insulated thermocouple wire. These thin-skin calorimeters fit within the above range at an approximate ratio of 1 to 2. The thermocouple wire used in the thin-skin calorimeter application is a thicker gauge than the thermocouple wire used for the thermocouples because of the difficulty of welding 30-gauge thermocouple wire to the plates.

During testing, the thin-skin calorimeters will produce a temperature data point. In order to determine a net heat flux, the following equation must be used:

$$q"_{net} = \rho c \delta \frac{dT}{dt}$$

This is the storage term, or heat build-up of the plate, in the conservation of energy equation:

$$Storage = In - Out$$

In order to calculate the incident heat flux, the heat losses must be accounted for as shown in the following equation:

$$\rho c \delta \frac{dT_s}{dt} = \alpha_s q"_i - \varepsilon_s \sigma \left(T_s{}^4 - T_\infty{}^4\right) - h_{conv}(T_s - T_\infty) - (h_{total})(T_s - T_{substrate})$$

The left-hand side of the equation is the storage term of the equation, which is the rate of increase in energy stored per unit area of the plate, calculated by multiplying the thermal capacitance of the plate material by the rate of change of temperature of the plate surface with respect to time, $\frac{dT_s}{dt}$. The thermal capacitance is a product of the material density, ρ, specific heat, c, and thickness, δ. The first term of the right-hand side of the equation is the fraction of incident energy absorbed by the plate from the fire. The second term is the energy emitted by the material to the environment via radiation. Since the plate was sprayed with a high temperature black matte spray paint, the absorptivity, α_s, and

emissivity, ε_s, is near one. The third term is the convective heat loss from the surface. The variable h_{conv} is the convective heat transfer coefficient and the variable T_g is the gas temperature of the fire plume. The last term on the right-hand side is the heat losses into the wall assembly via radiation, $4\varepsilon_b \sigma {T_s}^4 (T_s - T_1)$, and conduction, $h_{cr}(T_s - T_1)$. The variable ε_b is the emissivity of unexposed plate, h_{cr} is the contact resistance heat transfer coefficient, and T_1 is the surface temperature of the substrate behind the plate. An additional loss term can be used for the lateral heat conduction across the plate. However, this term can be ignored because of the relative size of the plate in comparison to the fire (Alston, 2004, 160-162).

The group determined that the thin-skin calorimeters will be placed as indicated by the black rectangles on the figures below. The below figures are top view cut-outs of each geometry. The plates will be at three different elevations.

Instrumentation Figures

Butt-Joint 1 (Spline – not to scale)

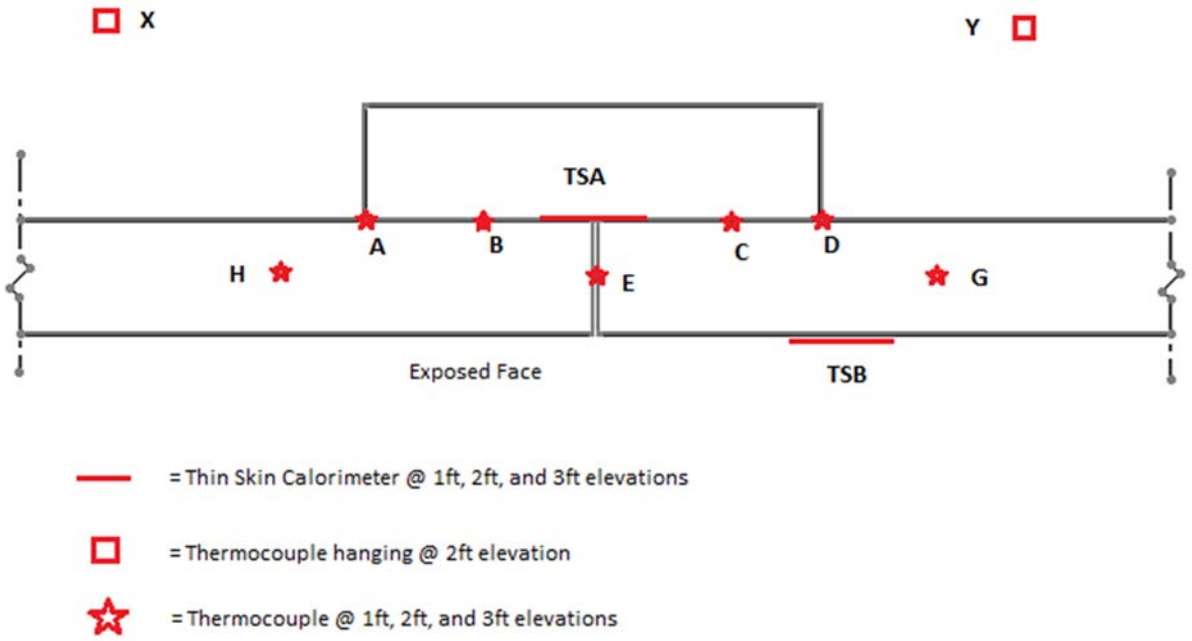

Butt-Joint 2 (Overlap – not to scale)

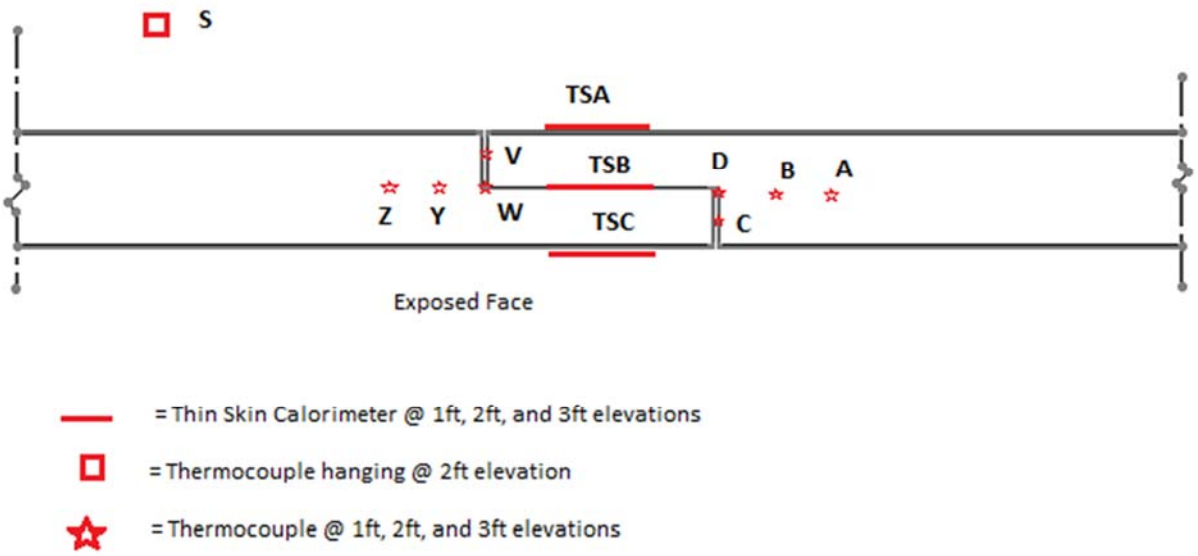

Corner Joint (not to scale)

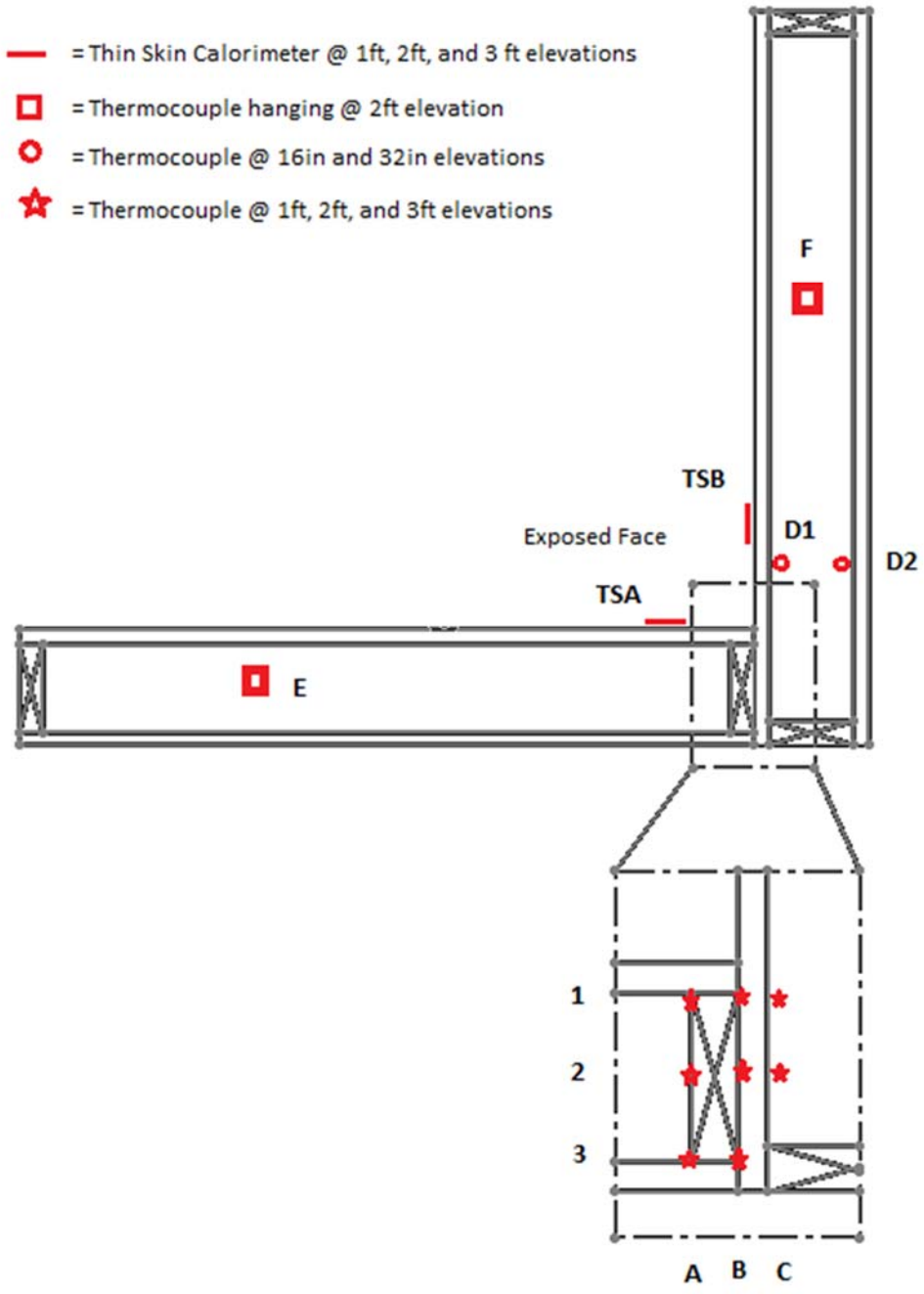

These locations were chosen based on the main goal of the project of determining heat flow and the limitations of thin-skin calorimeters. At each elevation, the plates must be staggered to prevent any interruption of the heat flow through the joint geometry.

Appendix F: Thin-Skin Calorimeter Calibration

As a one-dimensional problem, the finite difference equation and boundary conditions can be applied directly.

$$\frac{\partial T}{\partial t} = \alpha \frac{\delta^2 T}{\delta x^2}; \quad where\ \alpha = \frac{k}{\rho c}$$

$$B.C.(x = 0): \ -k\frac{\delta T}{\delta x} = h_{total}(T_{plate} - T_{substrate})$$

$$B.C.(x = 50.8mm): \quad -k\frac{\delta T}{\delta x} = 0$$

$$I.C.: \quad T(x,t) = T(x,0) = T_0$$

The finite difference method splits the substrate into a prescribed number of nodes and uses explicit (or implicit) numerical equations to find the temperature of each node at each time step using the known boundary conditions. The figure below illustrates how the substrate can be split into nodes of thickness Δx.

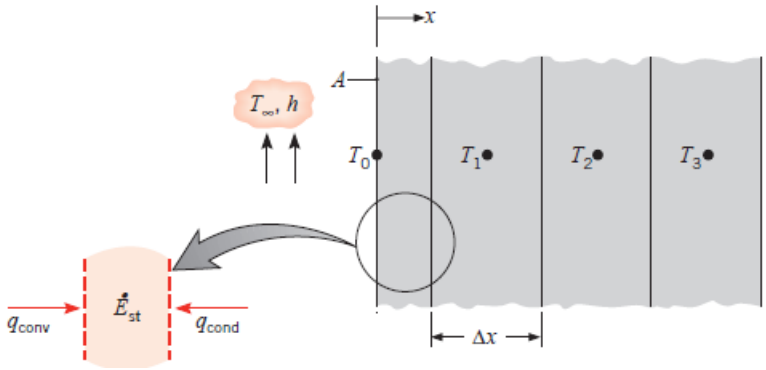

Each node temperature must be solved using an energy balance equation and its corresponding boundary conditions. The surface boundary condition can be quantified as a convective boundary condition where the temperature of the "fluid" is the temperature of the plate. The heat transfer coefficient is $h_{contact}$ which remains unknown and will be calculated later. The interior nodes can be quantified using pure conduction from one node to the other.

It is important to note that although you can prescribe a value for the node thickness, Δx, you cannot do so for the time step, Δt. You must use a stability criterion in order to stabilize numerically induced oscillations in the results that occur when you use the explicit method of the finite difference method. The stability criterion for an interior node (conduction) is defined below.

$$\Delta t = \frac{F_0(\Delta x)^2}{\alpha}$$

F_0 is the Fourier's Number, and the stability criterion follows that $F_0 \leq \frac{1}{2}$ (Bergman, 332). Since the surface node involves convection, we must also meet a second stability criterion. The stability criterion for a surface node (convection) follows that $F_0(2 + Bi) \leq \frac{1}{2}$, where Bi = Biot Number and is defined as:

$$Bi = \frac{h_{total} * \delta}{k}$$

We can now begin the finite difference method calculations seen below. (Note: the superscript 'p' in the equations below denotes the time step. E.g. when t=0, p=0; when t=Δt, p=1; when t=2*Δt, p=2; and so on).

Surface node:

$$Storage = In - Out$$

$$\rho c \Delta x \frac{dT}{dt} = h_{total}\left(T_{plate} - T_0\right) + \frac{k}{\Delta x}(T_1 - T_0)$$

$$\rho c \Delta x \frac{({T_0}^{p+1} - {T_0}^{p})}{\Delta t} = h_{total}\left({T_{plate}}^{p} - {T_0}^{p}\right) + \frac{k}{\Delta x}({T_1}^{p} - {T_0}^{p})$$

$${T_0}^{p+1} = {T_0}^{p} + \frac{h_{total}\Delta t}{\rho c \Delta x}\left({T_{plate}}^{p} - {T_0}^{p}\right) + \frac{k\Delta t}{\rho c (\Delta x)^2}({T_1}^{p} - {T_0}^{p})$$

$${T_0}^{p+1} = {T_0}^{p} + \frac{h_{total}\Delta t}{\rho c \Delta x}\left({T_{plate}}^{p} - {T_0}^{p}\right) + F_0({T_1}^{p} - {T_0}^{p})$$

To find the interior node equation, we used the same principal by conducting an energy balance. The result in explicit form is the following equation.

$${T_1}^{p+1} = F_0({T_2}^{p} + {T_0}^{p}) + (1 - 2F_0){T_1}^{p}$$

The end surface node is insulated. To quantify the temperature at this node, a numerical "trick" to continue to use the interior node equation is to put an imaginary node outside of the substrate. We then equate this node to the node preceding the end node. For example, if the end node is T_9, the imaginary node T_{10} is equal to the preceding node T_8. This "trick" simulates an insulated boundary condition.

In order to verify the numerical results, a known analytical solution for semi-infinite solids can be used that matches the surface convection boundary condition in our model. We used this equation to find the temperature in the solid at any point 'x' at any time 't'. The equation is below.

$$T(x,t) = T_i + (T_\infty - T_i)\left(erfc\left(\frac{x}{2\sqrt{\alpha t}}\right) - \left[\exp\left(\frac{hx}{k} + \frac{h^2 \alpha t}{k^2}\right)\right]\left[erfc\left(\frac{x}{2\sqrt{\alpha t}} + \frac{h\sqrt{\alpha t}}{k}\right)\right]\right)$$

$$where \quad erfc(\omega) = 1 - \mathrm{erf}(\omega)$$

Using the analytical solution, we verified that our numerical solution is correct. We then manipulated the contact conductance heat transfer coefficient h_{total} until the numerical analysis results matched the experimental results for the thermocouple at depth. We now have our two unknown values for the contact conductance heat transfer coefficient and the surface temperature of the substrate. This contact conductance heat transfer coefficient was used as the front face boundary condition for the COMSOL computer model.

Results

25 kW Incident Heat Flux Calibration Test

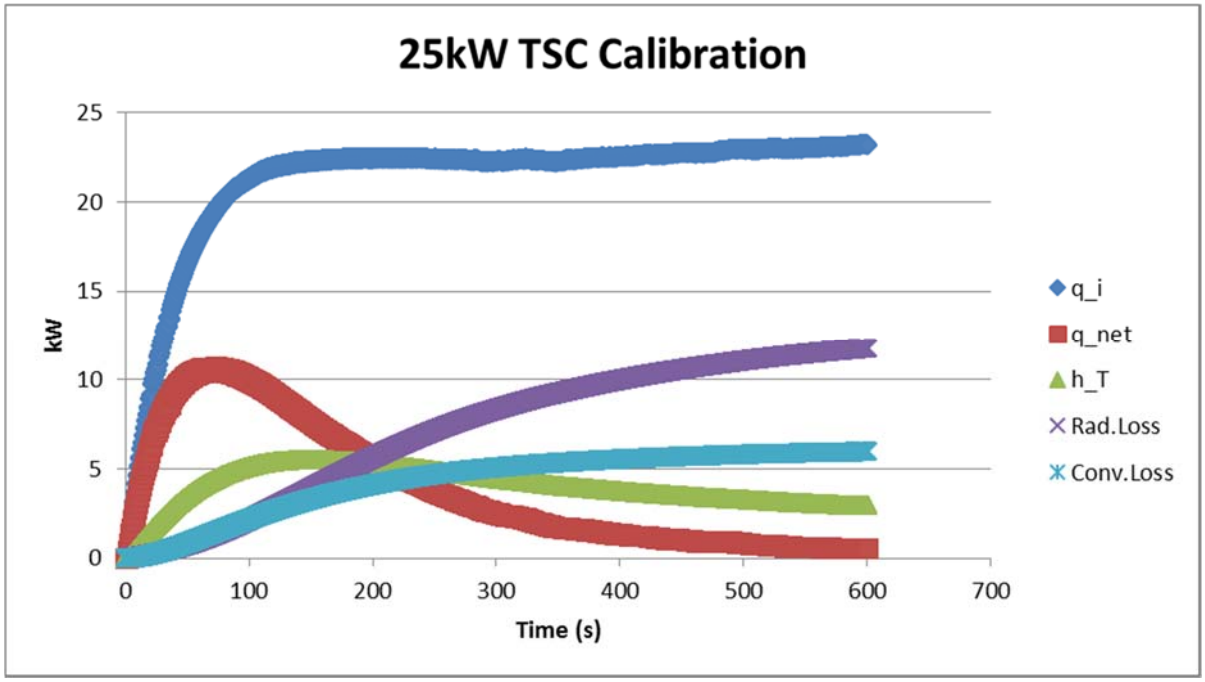

50 kW Incident Heat Flux Calibration Test

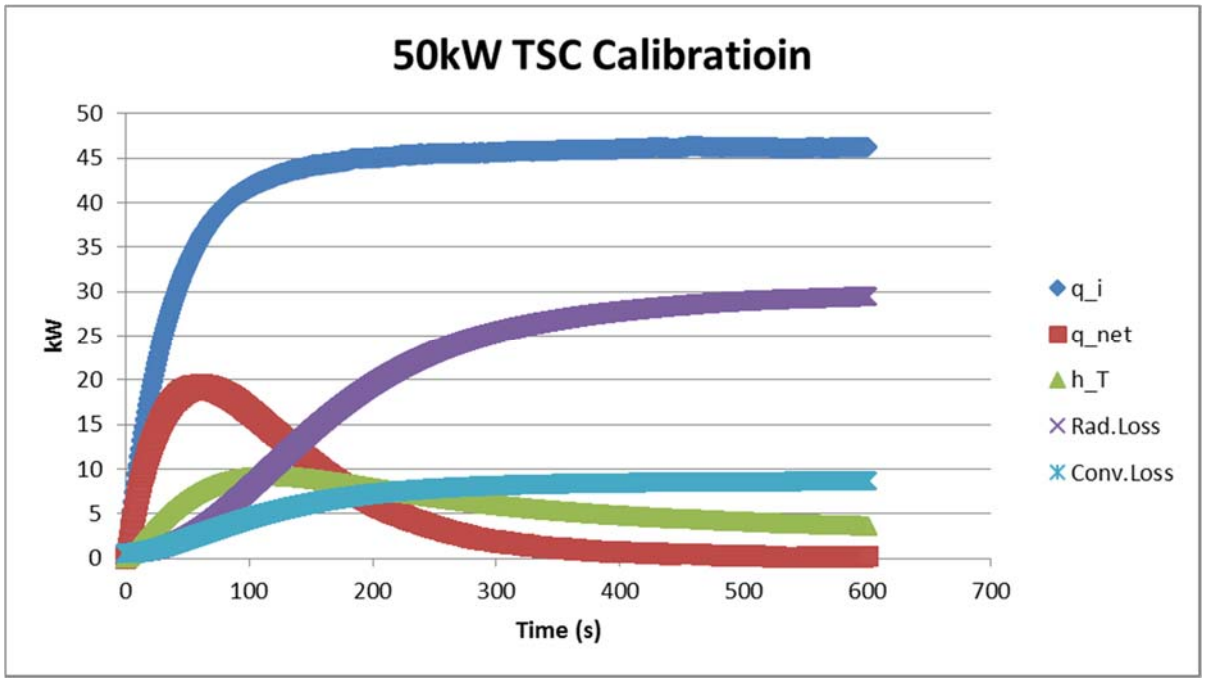

75kW Incident Heat Flux Calibration Test

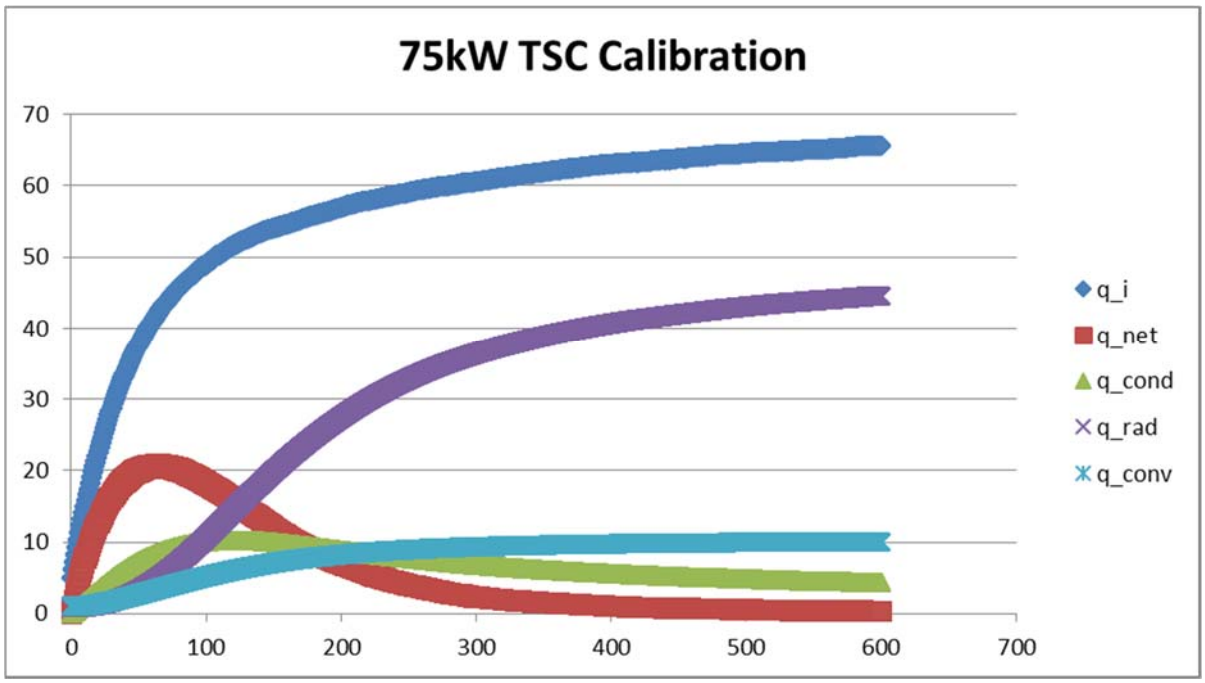

As seen in the 25kW and 50kW calibration graphs above, the response time of the plate is approximately 100 seconds. For the 75kW test, the response time is nearly doubled. The reason for this

discrepancy is because the linear approximation we used for the contact conductance heat transfer begins to break down. At the high temperatures produced in this test, radiation becomes significant.

Appendix G: Heat Transfer within Enclosed Space

The rigs that have been created have calcium silicate panels with an empty air gap in between. In general panelized construction, thermoset foam cores are sandwiched between the front and back panels. This foam will not melt away but rather char when exposed to fire for a long period of time. The calcium silicate is simulating the normal panels, and similarly, the air in between the panels in the rigs is simulating the foam core of normal panels. Air was chosen for the gap because it will not melt away and it will conduct heat that can be characterized. This is useful in that it will be able to be used for computer simulations of the rigs. This section analyzes the results of Butt Joint 2 prototype test and will be expanded to the rest of the rigs once further testing is complete.

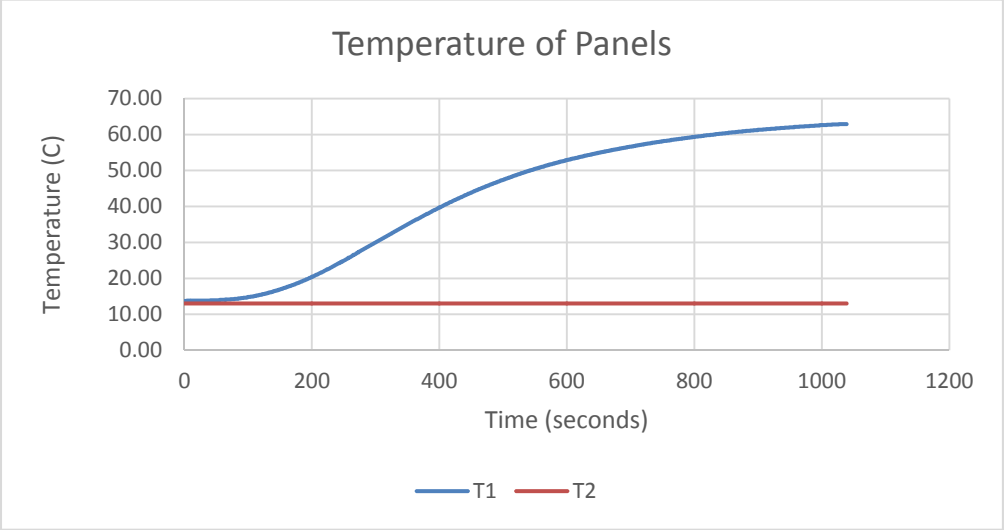

The graph above shows the temperature of the interior face of the two panels. T1 is the interior face of the front panel, the panel that was exposed to fire. This value was obtained by a thin skin calorimeter fastened to the middle of the back of the front panel. The values range from 13 C to 62 C. The value for T2 stays constant at 13 C. This was chosen as approximately the temperature of the room. In further tests, it would be helpful to have a thin skin calorimeter place on the interior face of the back panel as well.

The next temperature to consider is that of the air within the panels. This air is where natural convection would occur in this structure. In a previous test, thermocouples within the panels measured a temperature range of 15 C – 25 C of that interior air. The average of these (20 C) will be used for one of the calculations. To test under more demanding circumstances, the interior air temperature was again determined by averaging T1 and T2 at the peak temperature difference. This means that the

interior air temperature became 37.95 C, which was rounded to 40 C in order to obtain the physical properties of air that were needed.

The reason that these temperatures are needed is to compute the Rayleigh number of the interior cavity in the rig. This number is a dimensionless number that represents the amount of convection within this rig. Generally, if the Rayleigh number is below 1000, then the air within is stagnant because a conduction regime exists. To determine if a conduction regime is present in the rigs, the Rayleigh number was calculated for both interior air temperatures discussed above. The formula for the Rayleigh number is noted below.

$$R_{a_L} = \frac{g\beta(T_1 - T_2)L^3}{\alpha\nu}$$

$$R_{a_L} @\ t = 1039\ sec \longrightarrow \frac{9.81\frac{m}{s^2} * 0.00343\frac{1}{T} * (62.9^oC - 13^oC) *. 1397m^3}{2.12 * 10^{-5} * 1.51 * 10^{-5}} = 14{,}290{,}0669$$

The figure below shows the Rayleigh numbers for both interior air temperatures. Clearly, neither temperature generates a Rayleigh number less than 1000. This means that in both cases there is convection occurring within the panels. The range of values for the air at 20 C is approximately 200,000 – 15,000,000. The range for 40 C is approximately 150,000 to 10,000,000. The colder internal air results in a greater Rayleigh number, however, they are both within similar ranges.

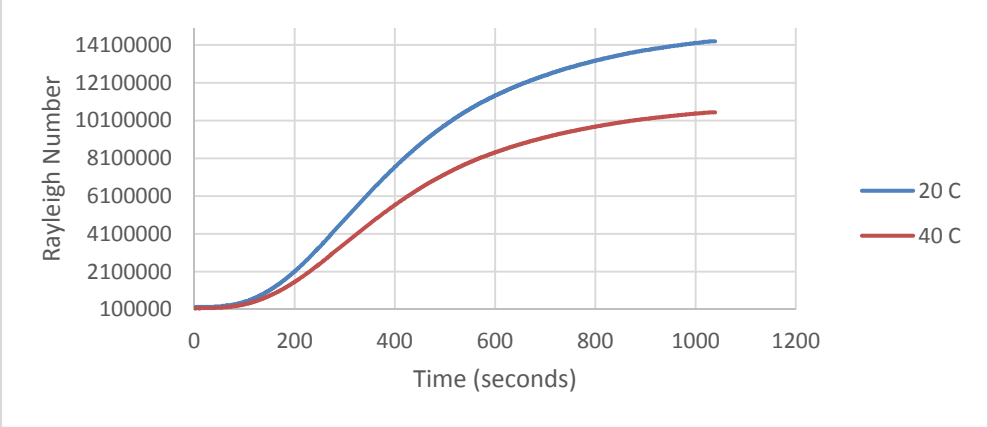

As stated before, the Rayleigh number ranges are: 20 C Range ($2 \times 10^5 – 15 \times 10^6$) and 40 C Range ($1.5 \times 10^5 – 10 \times 10^6$). In the figure below, those ranges both fall within the boundary layer regime section. This means there is laminar flow which is less substantial than turbulent and can be calculated easier.

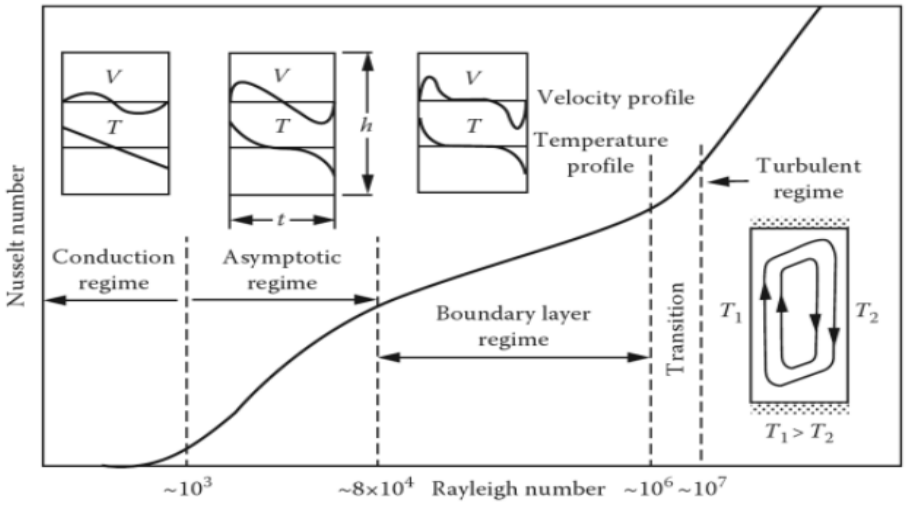

From this point, it is necessary to calculate the Nusselt number. This dimensionless value has several different equations that may be used. However, each correlation has conditions which the enclosed space must meet. H represents the height of the cavity and L is its thickness.

$$2 \leq \frac{H}{L} \leq 10 \qquad 2 \leq \frac{48}{5.5} \leq 10 \qquad 2 \leq 8.7 \leq 10 \checkmark$$

$$Prandl\ Number \leq 10^5 \qquad .7 \leq 10^5 \checkmark$$

$$10^3 \leq R_{a_L} \leq 10^{10} \checkmark$$

This scenario confirms all of the above conditions are acceptable, so the following equation will be used for the Nusselt number. Pr stands for the Prandtl number which is a coefficient based on air temperature. Also, H represents the height of the panel and L is the thickness as before. As the equation shows, the Nusselt number not only takes into account thickness of the cavity, but also height. Tong and Gerner (1986), analyzed natural convection in a partitioned air-filled rectangular enclosure and reported that placing a partition midway between the vertical walls results in greatest reduction in heat transfer. This topic will be analyzed in greater depth in the upcoming term.

$$N_{u_L} = 0.22\left(\frac{Pr}{0.2 + Pr}\right)^{0.28}\left(\frac{H}{L}\right)^{-\frac{1}{4}}$$

Below is a graph which represents the Nusselt value at both temperatures of the internal air. Clearly, they are very similar with a range of approximately 3-12. This value represents the amount of convective heat transfer over the amount of conductive heat transfer at the boundary layer.

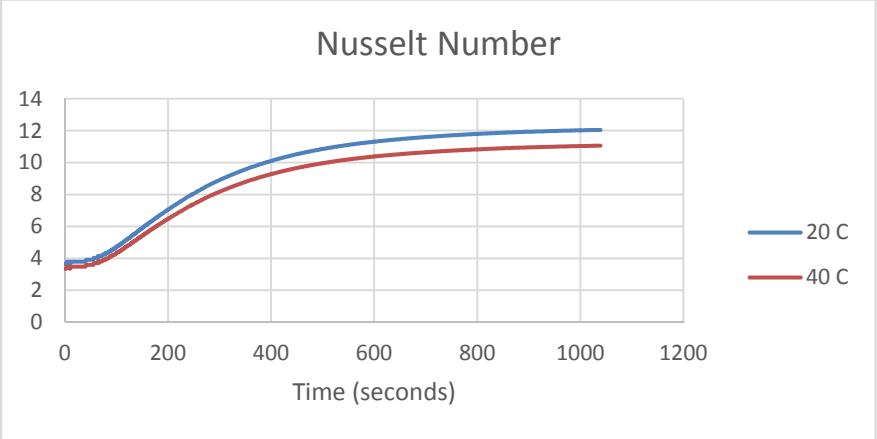

From the Nusselt value, the next step in determining the overall heat transfer within the cavity is determining the convective heat transfer coefficient. The equations below highlight this process. Again, L is the thickness of the cavity and k is the thermal conductivity of air.

$$Nu_L = \frac{h_{conv}L}{k} \Longrightarrow h_{conv} = \frac{Nu_L k}{L}$$

The graph below shows the convective heat transfer coefficient for both air temperatures. Similar to the graph above of the Nusselt number, these values are quite similar. This indicates that the effect of having a different internal air temperature is very minimal on this coefficient.

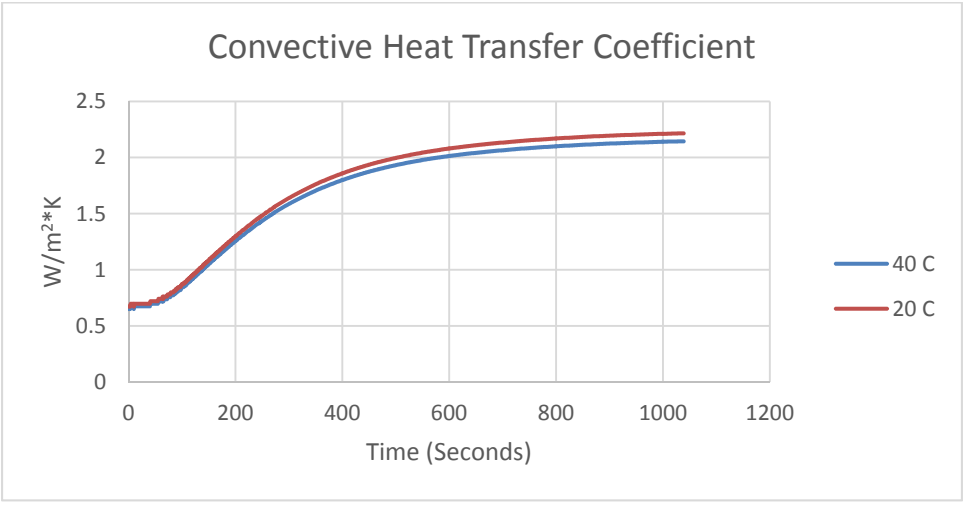

At this point, it was important to analyze both the convective and conductive heat flux through the space. The equations for both types of heat transfer are listed below.

$$\dot{q}"_{conv} = h_{conv}\Delta T \quad [\frac{W}{m^2}]$$

$$\dot{q}"_{cond} = \frac{k_{air}\Delta T}{\Delta x} \quad [\frac{W}{m^2}]$$

The graph below shows four lines, two for both conduction and convection at 20 C and 40 C. The temperatures minimally make a difference, as the lines for both convection and conduction are nearly on top of one another. However, it is clear that there is more convection than conduction in the cavity.

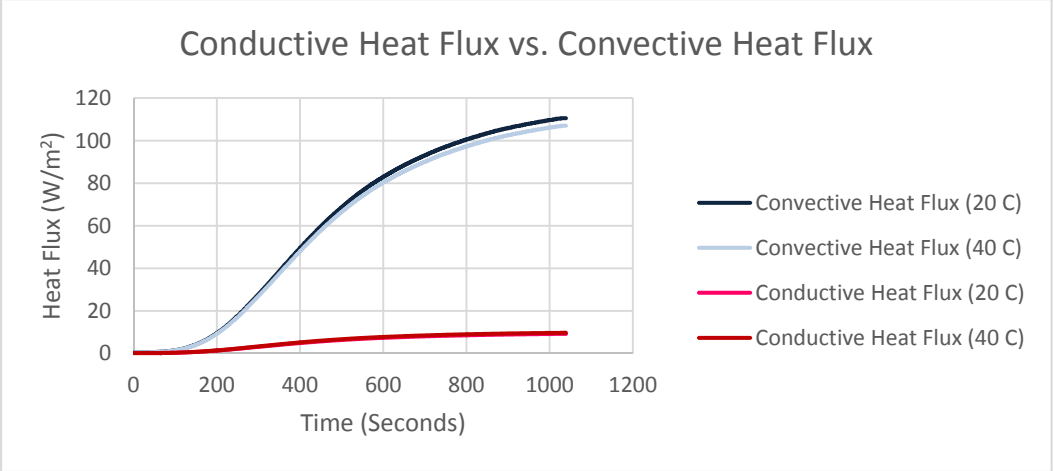

To get a more accurate graph of the relationship of conductive flux to convective flux, the graph below shows the ratio of convective over conductive.

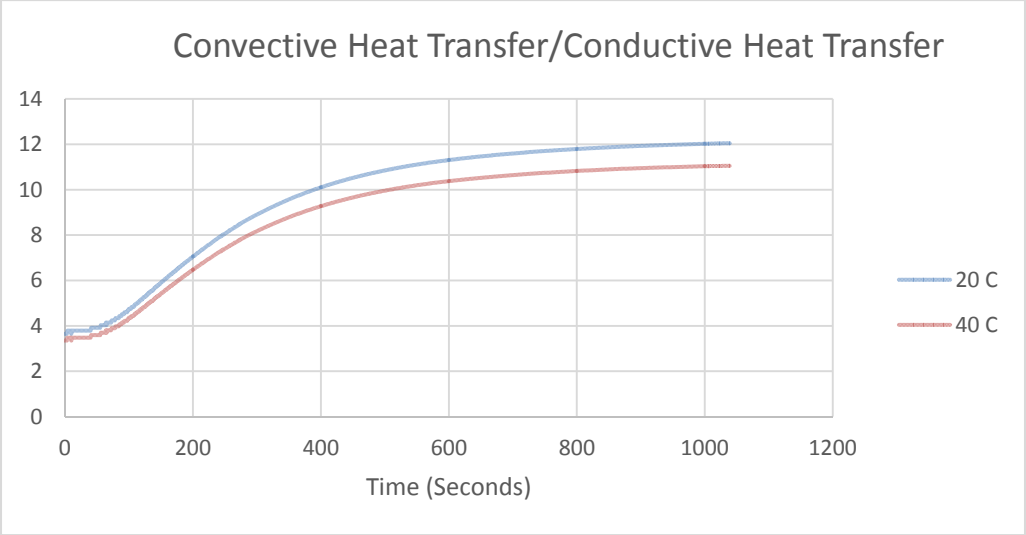

This means that throughout most of the test, there is nearly ten times the amount of convective heat flux than conductive heat flux. In the computer modeling, there will need to be adjustments made to show that the air is not stagnant within the cavity. Throughout testing, the heat flux will be monitored and recorded to create a more accurate simulation of the heat flow.

Appendix H: Physical Model Data

Spline Joint Data

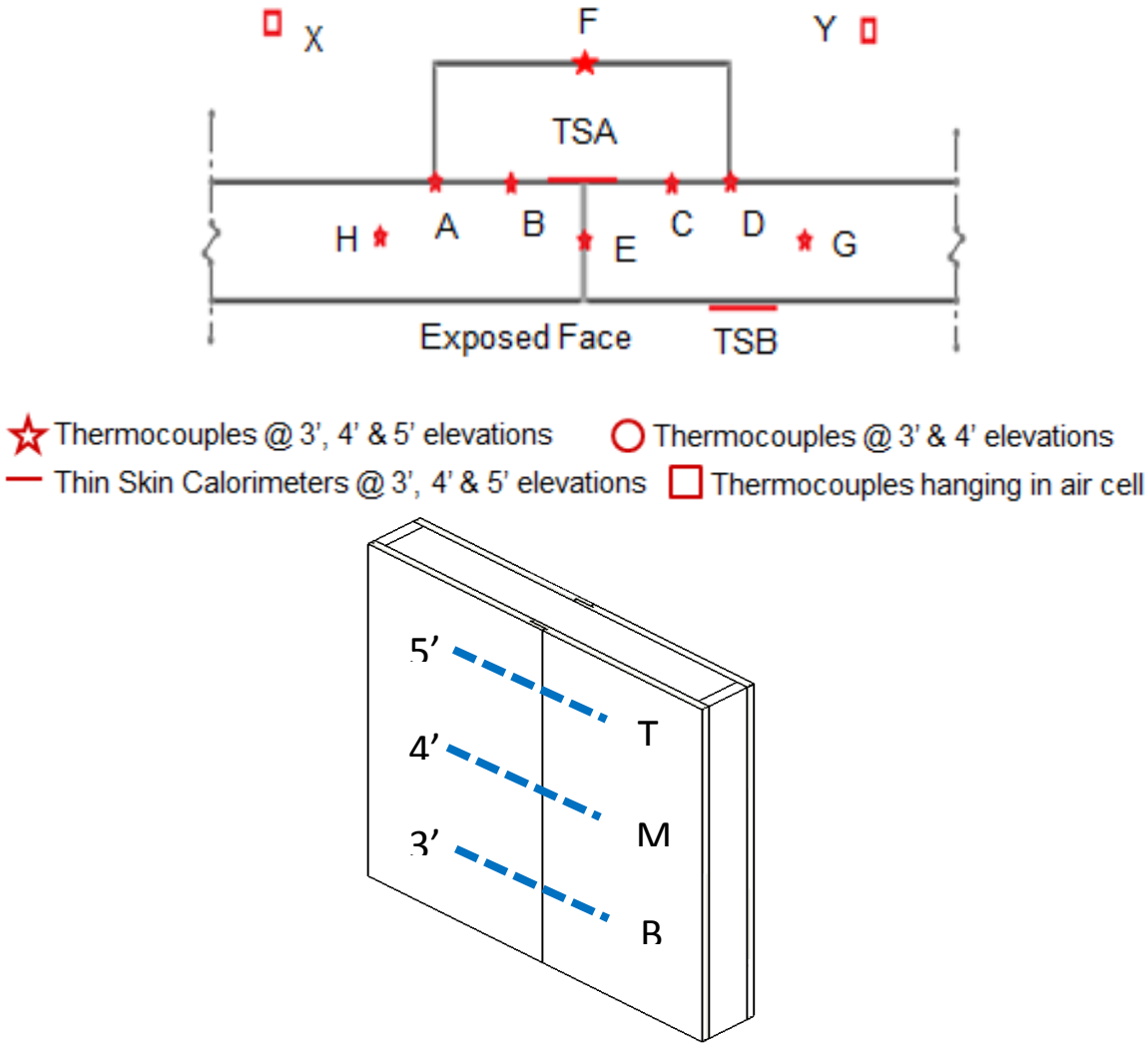

The above diagrams show the location of each instrument. If we are describing a thermocouple, the graph title will have two letters. The first letter of the title will designate the location of the instrument within the panel and can be seen in the top diagram. The second letter represents the elevation at which the instrument is located relative to the floor and may be seen in the bottom diagram. For think skin calorimeters, the first three letters before the dash designate the location of the instrument within the panel and can be seen in the top diagram. The letter after the dash represents the elevation at which the instrument is located relative to the floor and may be seen in the bottom diagram. Thermocouple X and Y are at a single elevation of 4 to 5 feet and represented by just their letter. The following graphs are temperature vs. time of the two experiments conducted, indicated by the legend.

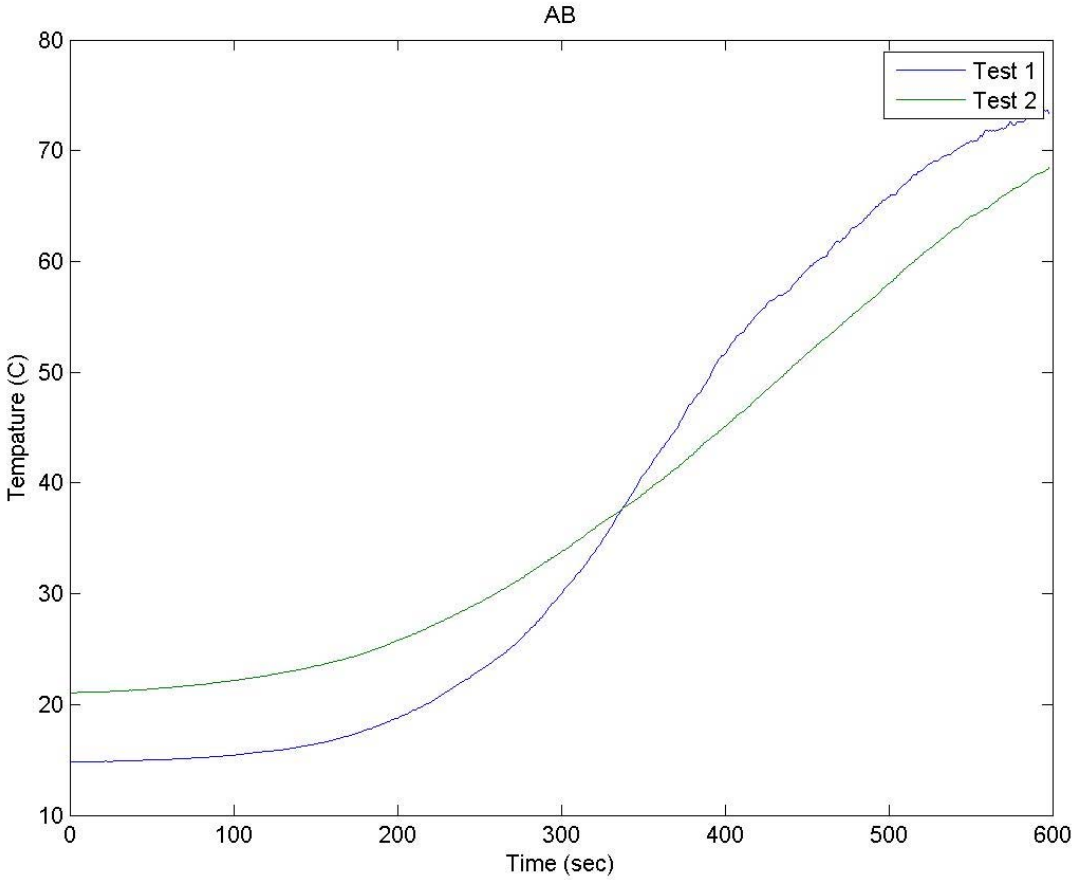
AB
Test 1
Test 2
Tempature (C)
Time (sec)
80
70
60
50
40
30
20
10
0
100
200
300
400
500
600

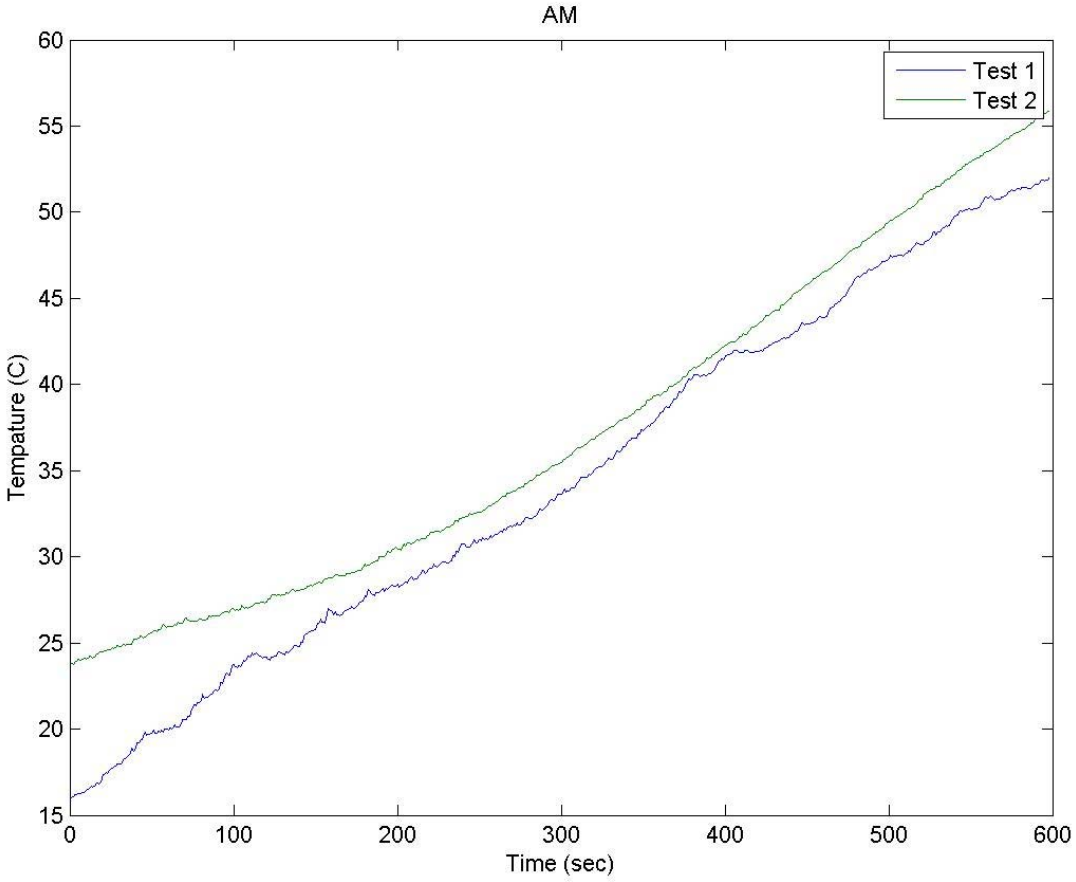
AM
Test 1
Test 2
Tempature (C)
Time (sec)
60
55
50
45
40
35
30
25
20
15
0
100
200
300
400
500
600

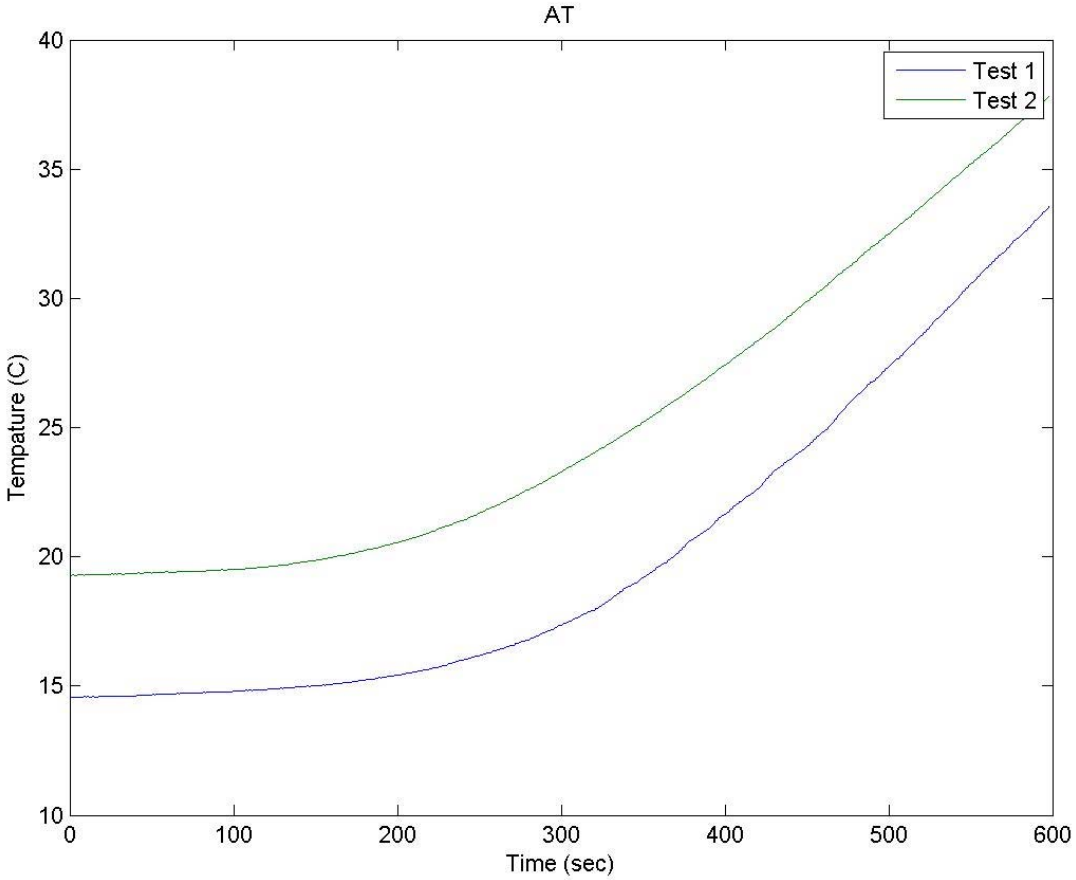
AT
Test 1
Test 2
Tempature (C)
Time (sec)
40
35
30
25
20
15
10
0
100
200
300
400
500
600

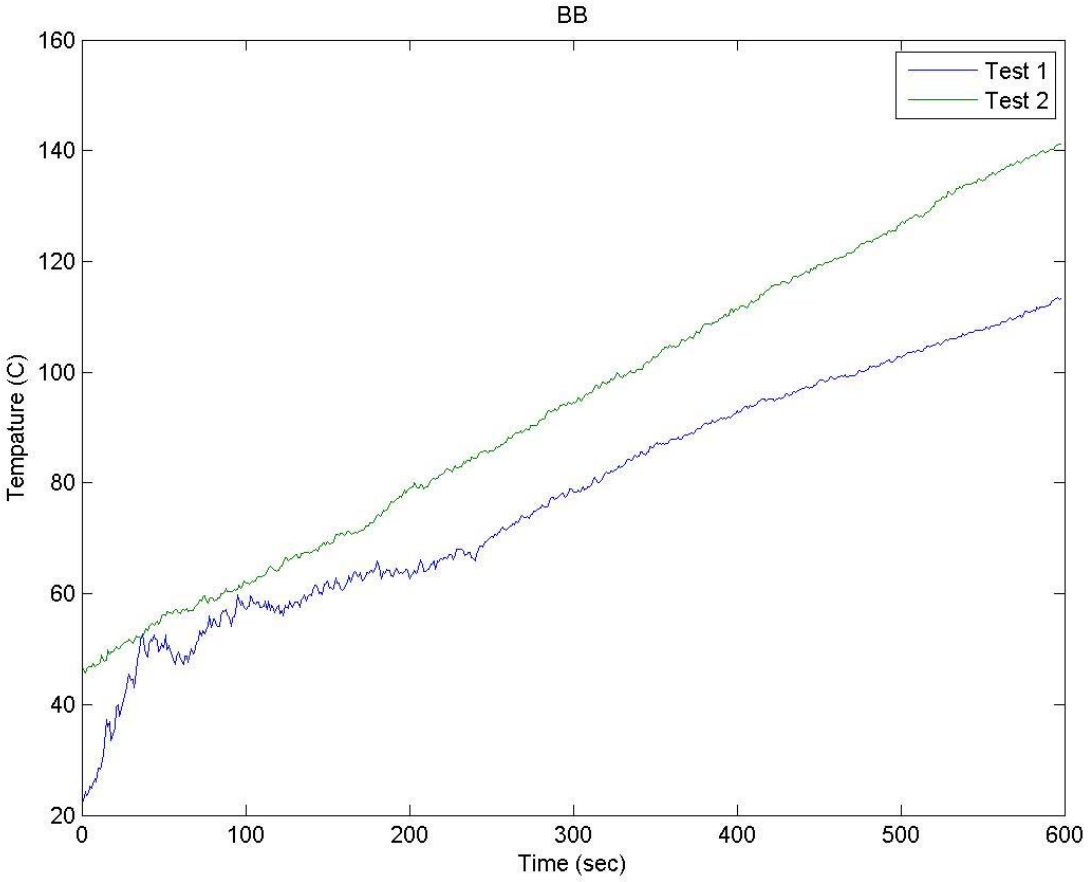
BB
Test 1
Test 2
Tempature (C)
Time (sec)
160
140
120
100
80
60
40
20
0
100
200
300
400
500
600

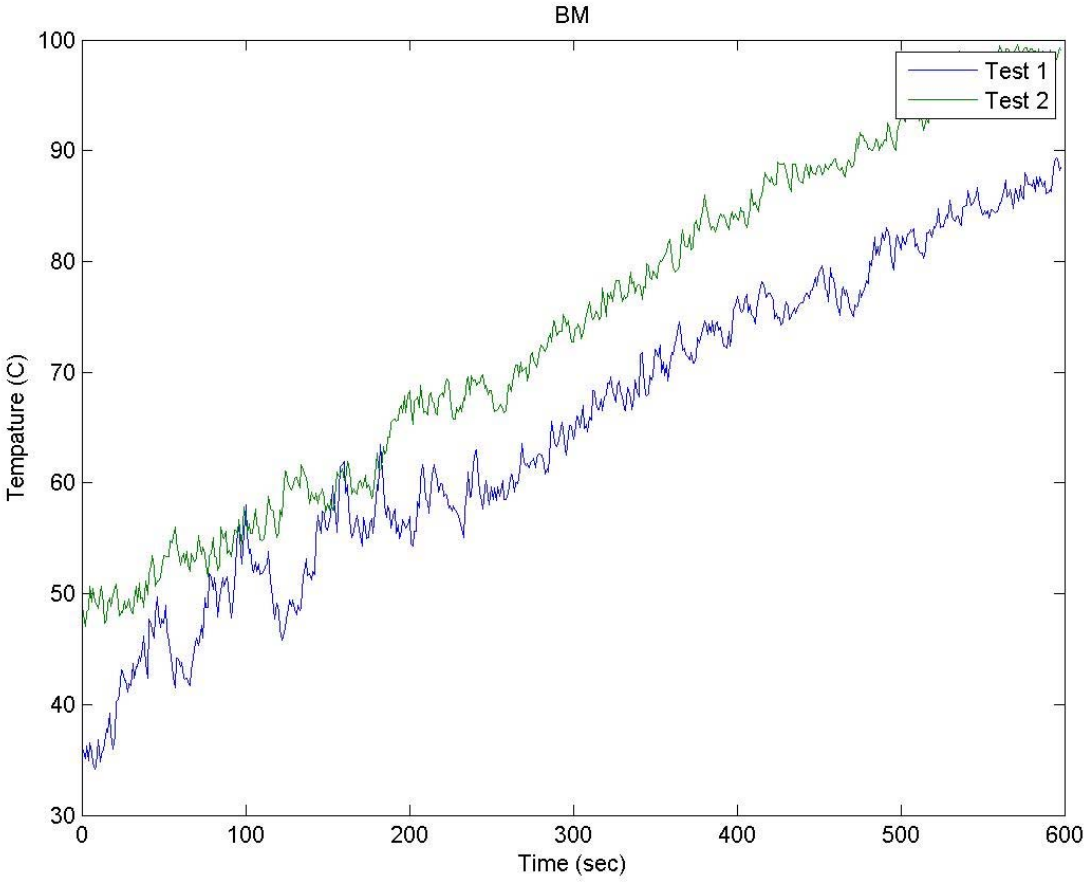
BM
Test 1
Test 2
Tempature (C)
Time (sec)
100
90
80
70
60
50
40
30
0
100
200
300
400
500
600

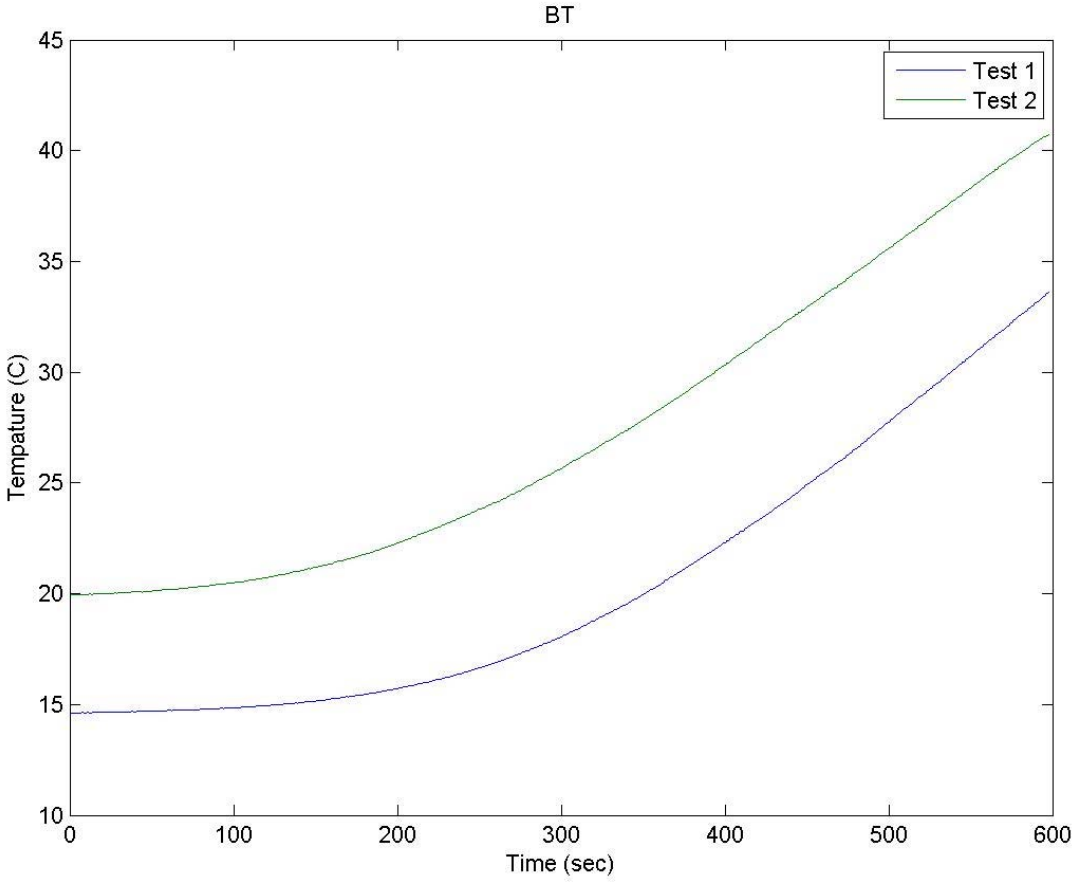
BT
Test 1
Test 2
Tempature (C)
Time (sec)
45
40
35
30
25
20
15
10
0
100
200
300
400
500
600

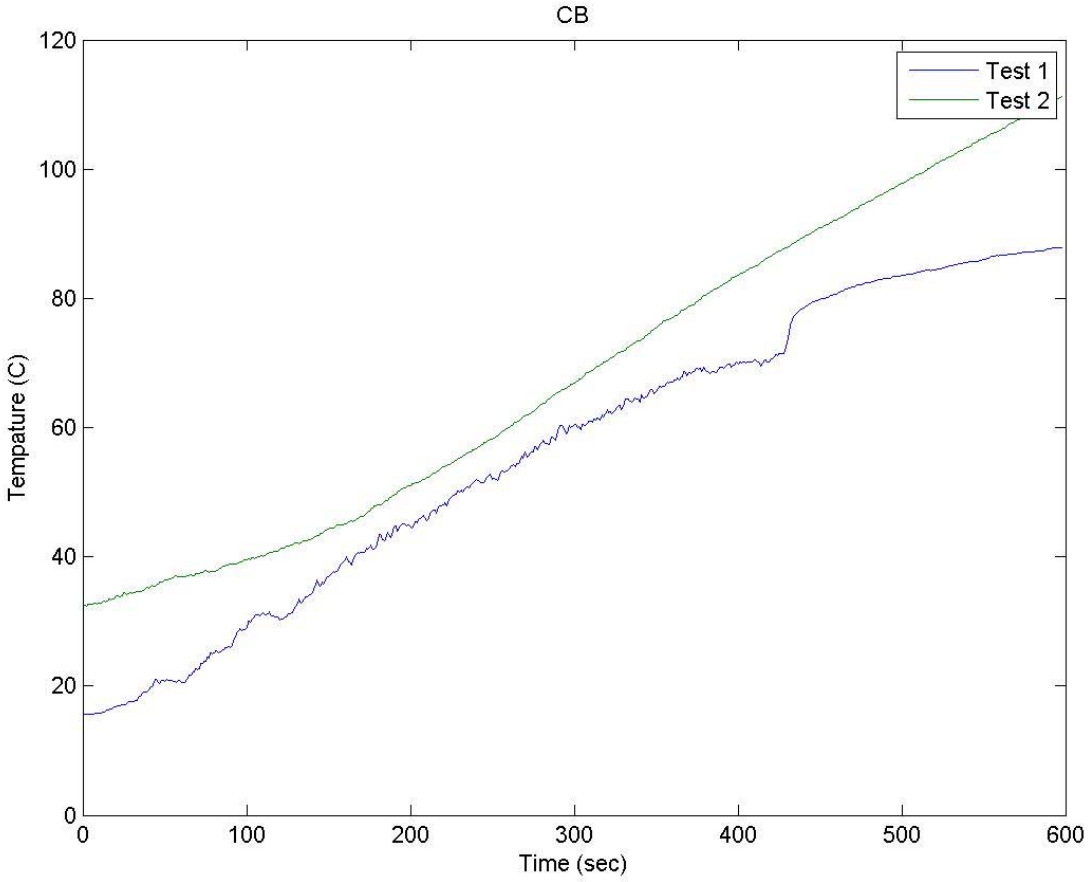
CB
Test 1
Test 2
Tempature (C)
Time (sec)
0
20
40
60
80
100
120
0
100
200
300
400
500
600

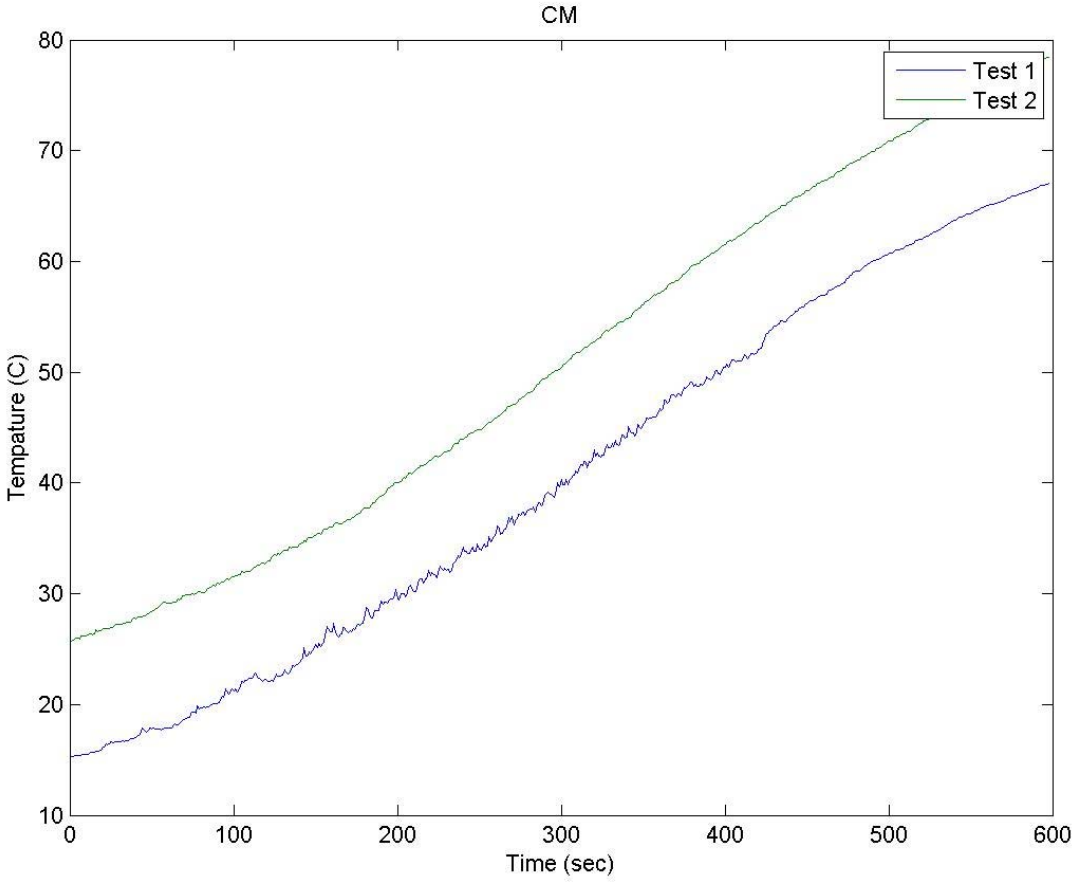
CM
Test 1
Test 2
Tempature (C)
Time (sec)
80
70
60
50
40
30
20
10
0
100
200
300
400
500
600

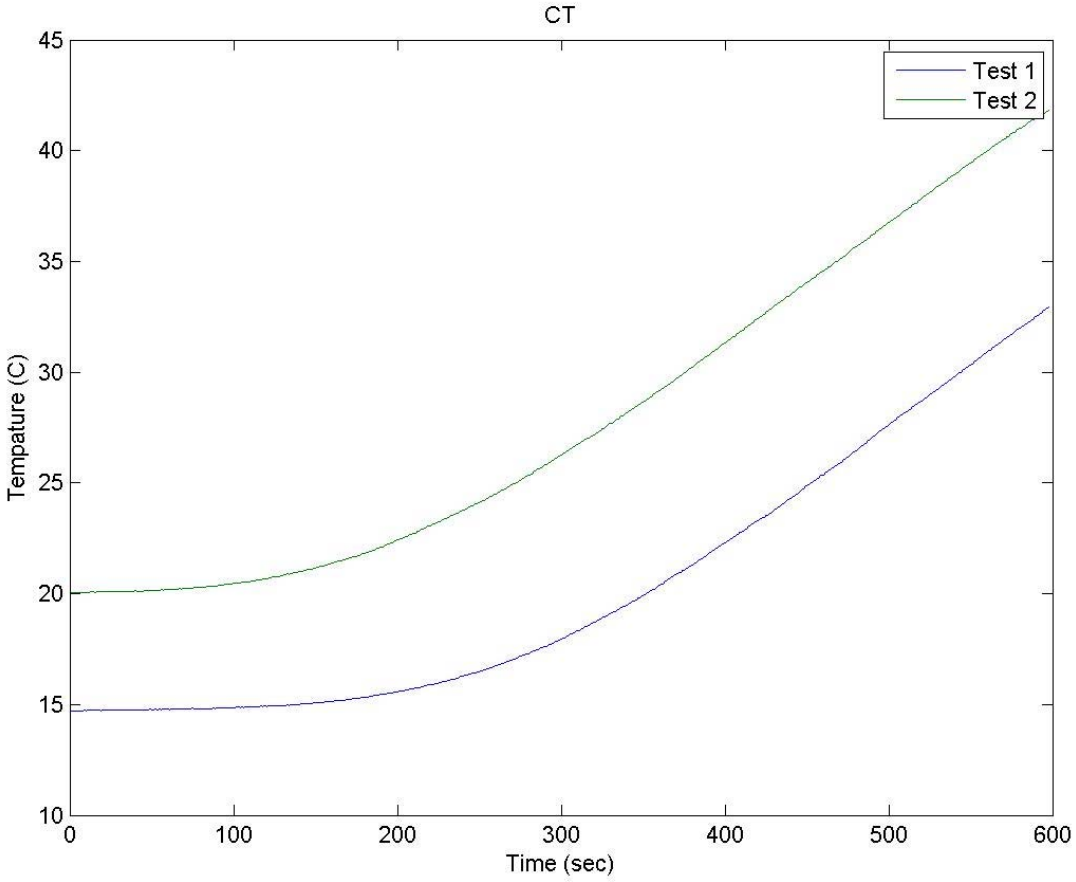
CT
Test 1
Test 2
Tempature (C)
Time (sec)
45
40
35
30
25
20
15
10
0
100
200
300
400
500
600

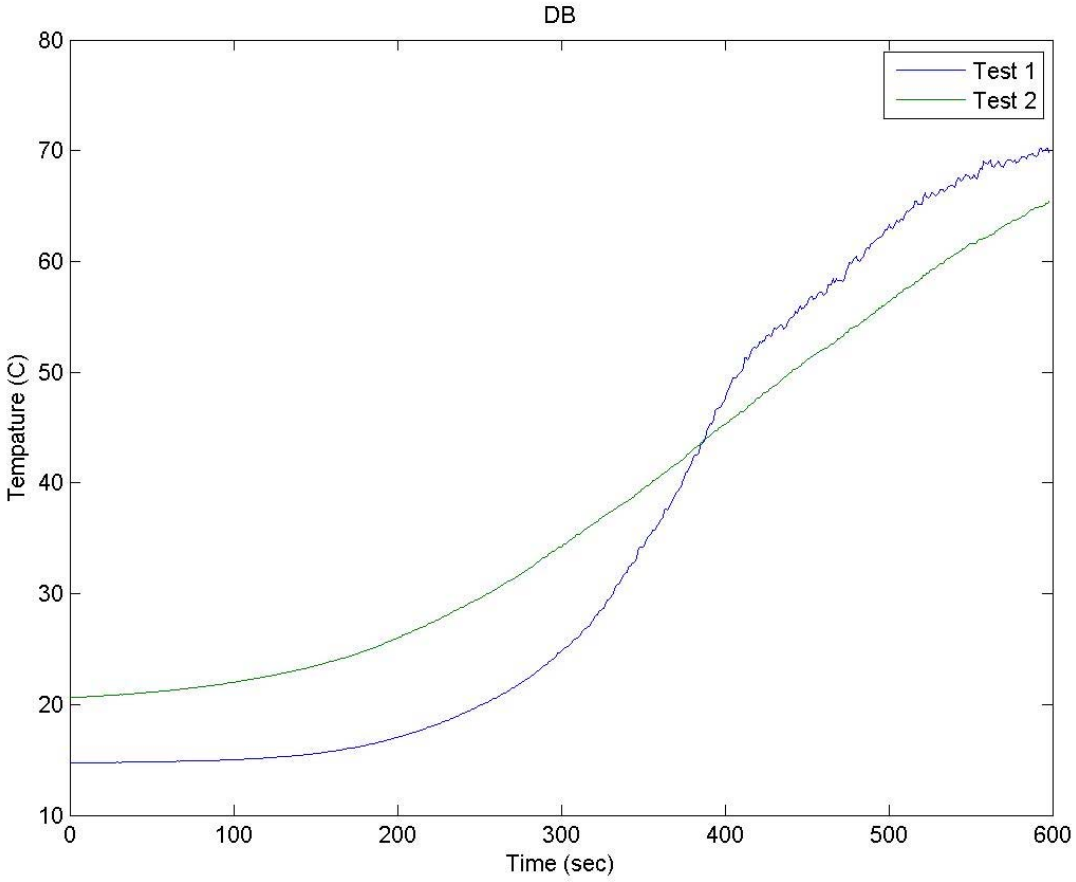
DB
Test 1
Test 2
Tempature (C)
Time (sec)
80
70
60
50
40
30
20
10
0
100
200
300
400
500
600

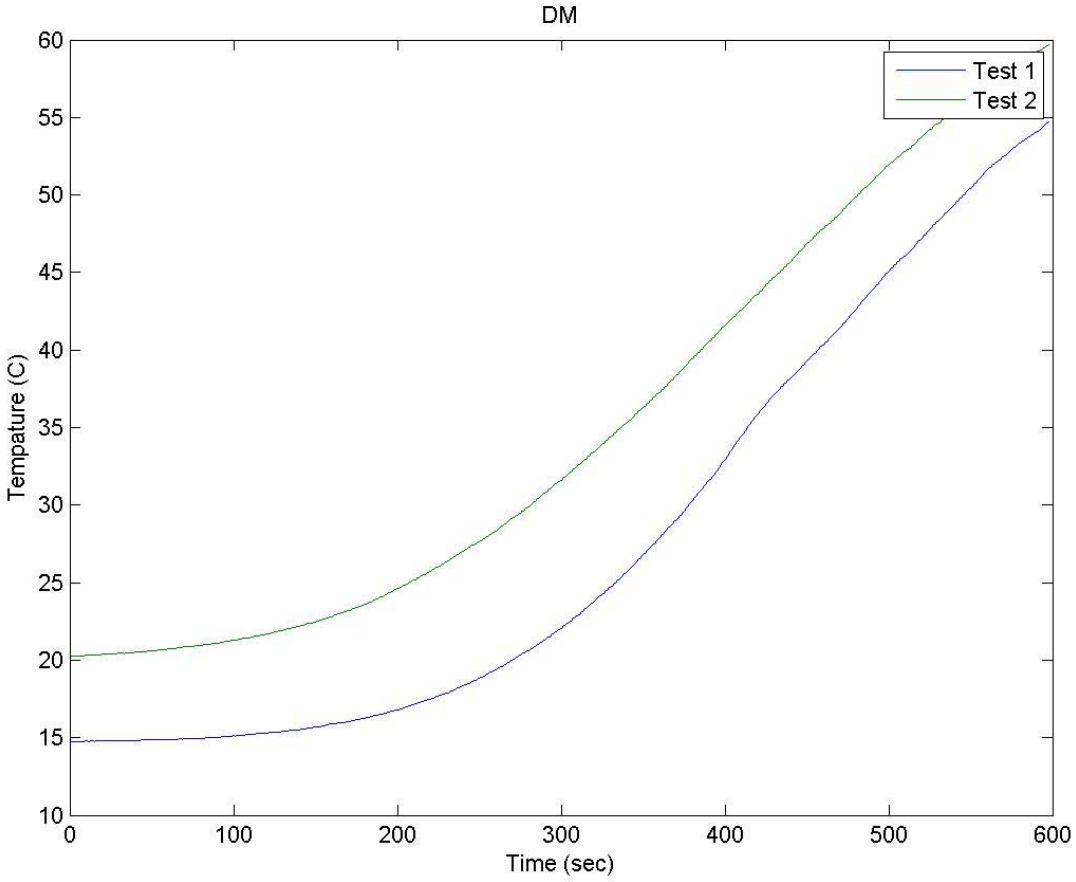
DM
Test 1
Test 2
Tempature (C)
Time (sec)
60
55
50
45
40
35
30
25
20
15
10
0
100
200
300
400
500
600

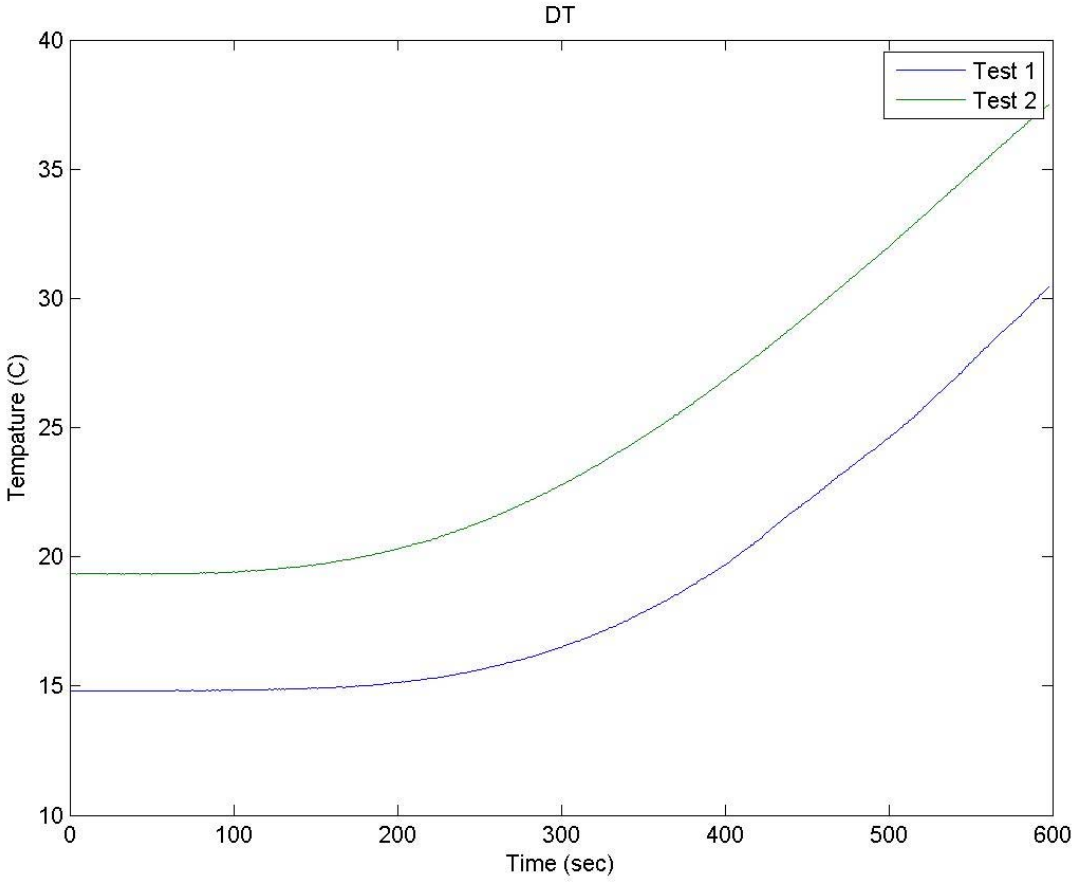
DT
Test 1
Test 2
Tempature (C)
Time (sec)
40
35
30
25
20
15
10
0
100
200
300
400
500
600

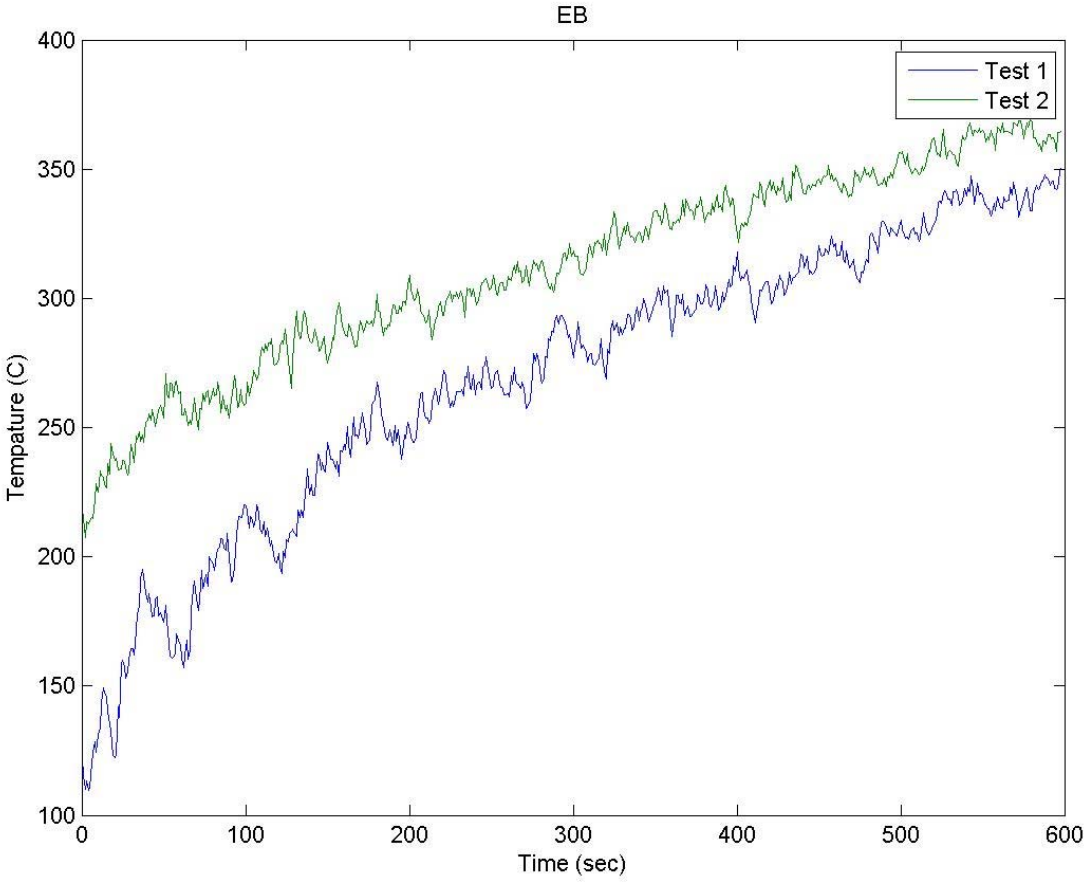
EB
Test 1
Test 2
Tempature (C)
Time (sec)
400
350
300
250
200
150
100
0
100
200
300
400
500
600

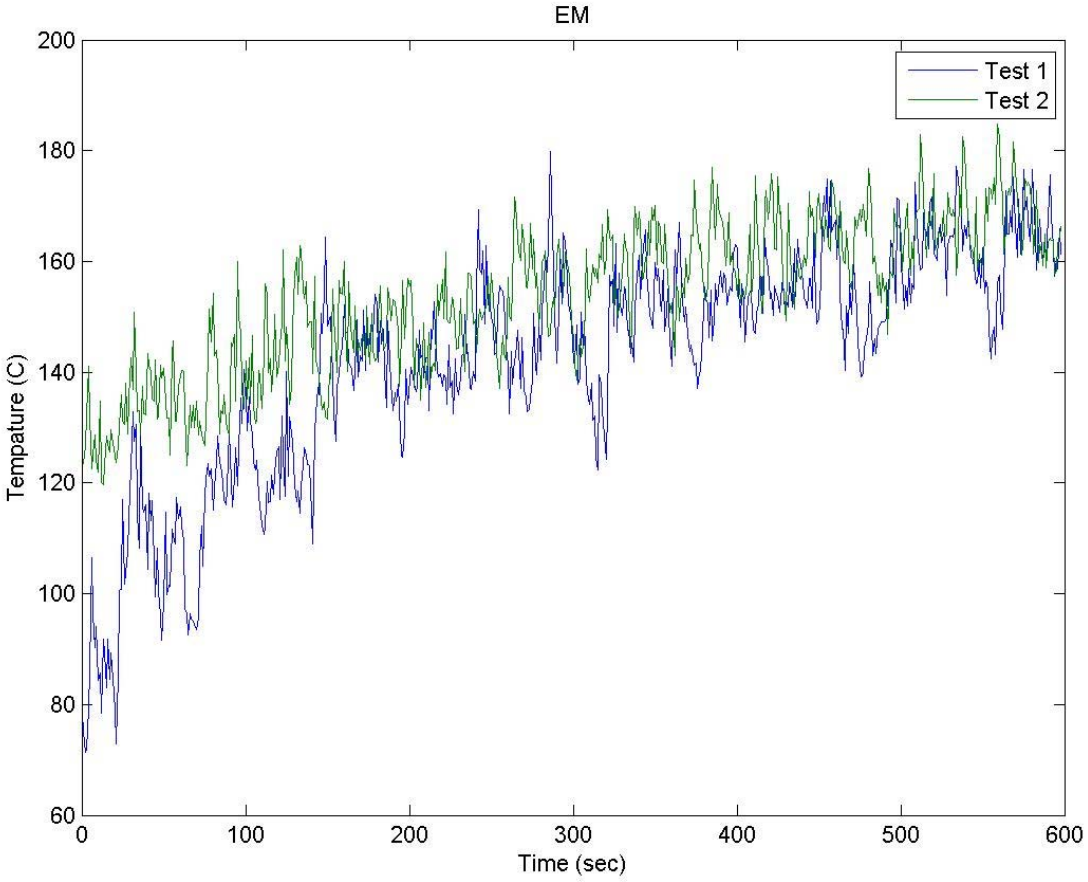
EM
Test 1
Test 2
Tempature (C)
Time (sec)
200
180
160
140
120
100
80
60
0
100
200
300
400
500
600

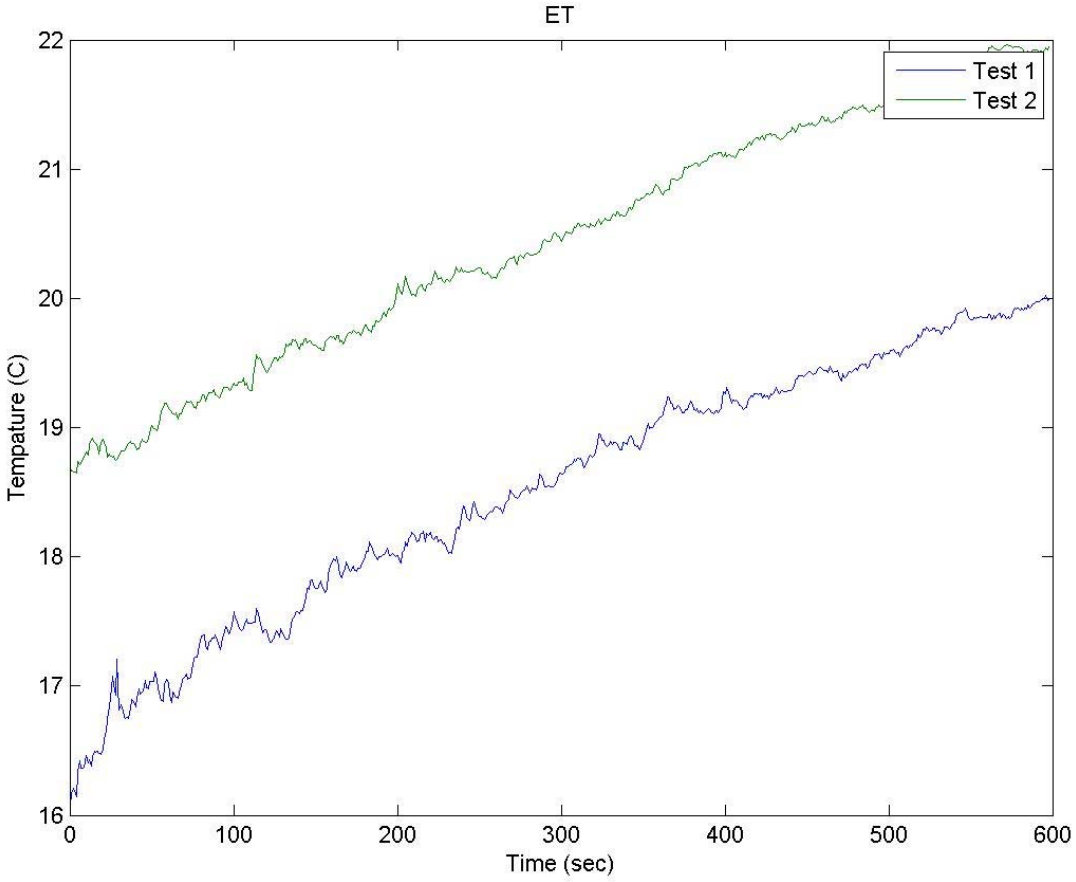
ET
Test 1
Test 2
Tempature (C)
Time (sec)
22
21
20
19
18
17
16
0
100
200
300
400
500
600

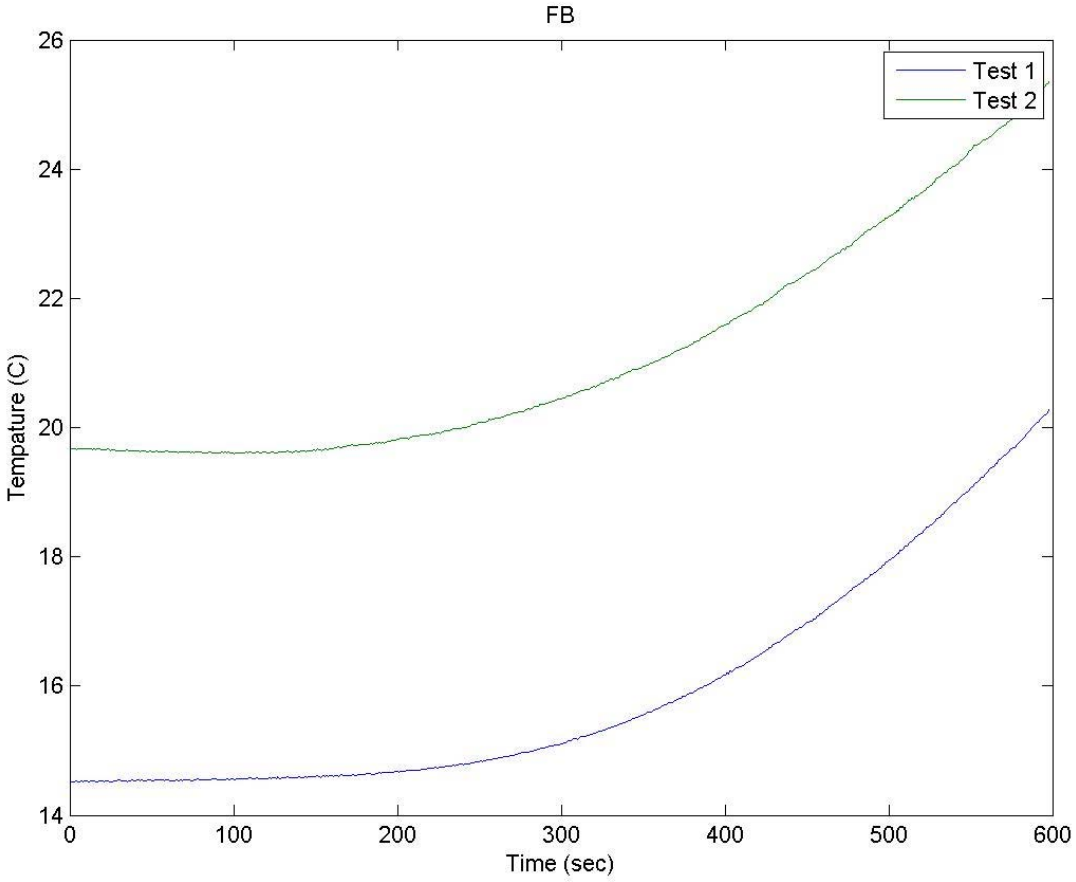
FB
Test 1
Test 2
Tempature (C)
Time (sec)
26
24
22
20
18
16
14
0
100
200
300
400
500
600

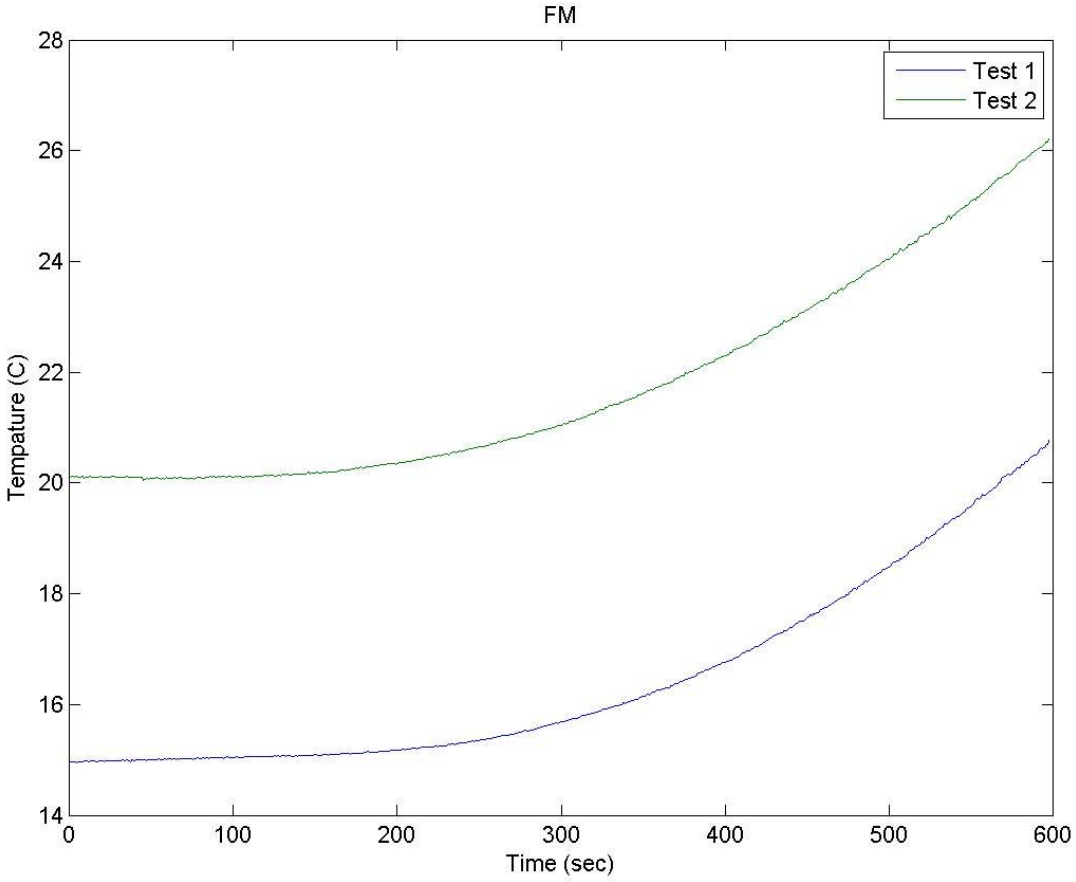
FM
Test 1
Test 2
Tempature (C)
Time (sec)
28
26
24
22
20
18
16
14
0
100
200
300
400
500
600

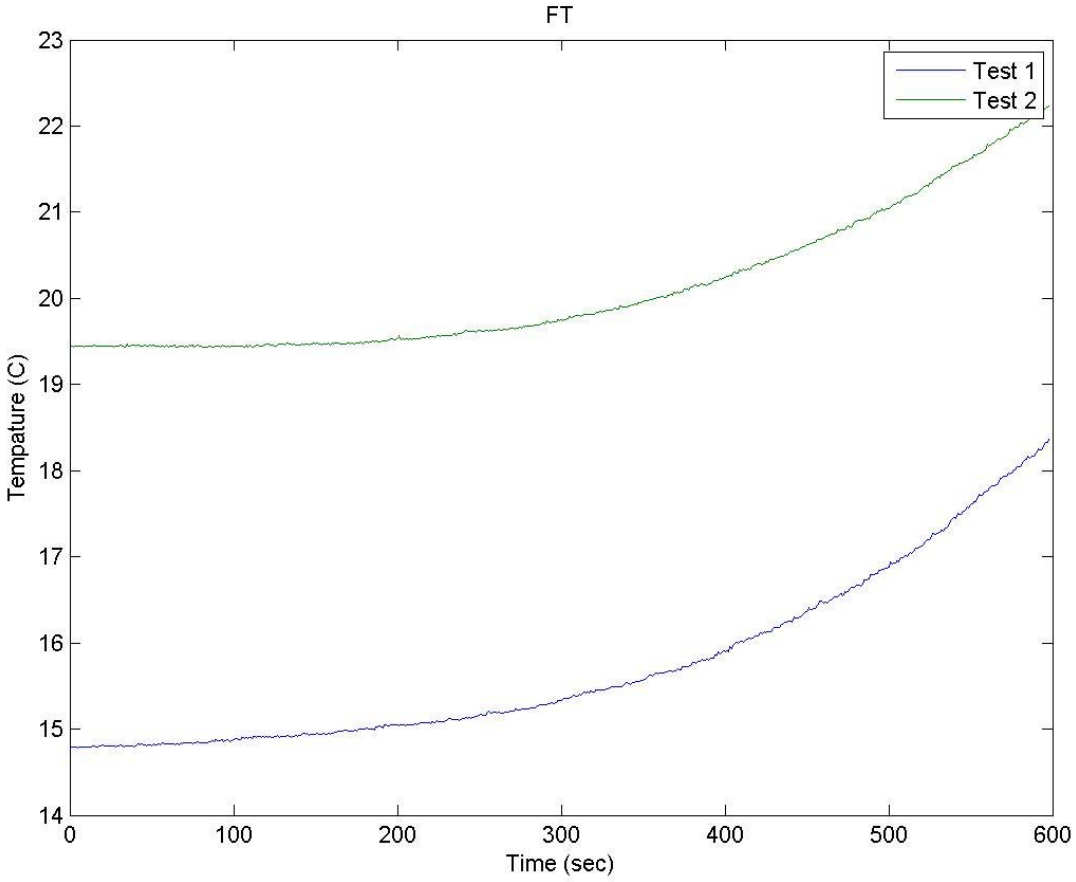
FT
Test 1
Test 2
Tempature (C)
Time (sec)
23
22
21
20
19
18
17
16
15
14
0
100
200
300
400
500
600

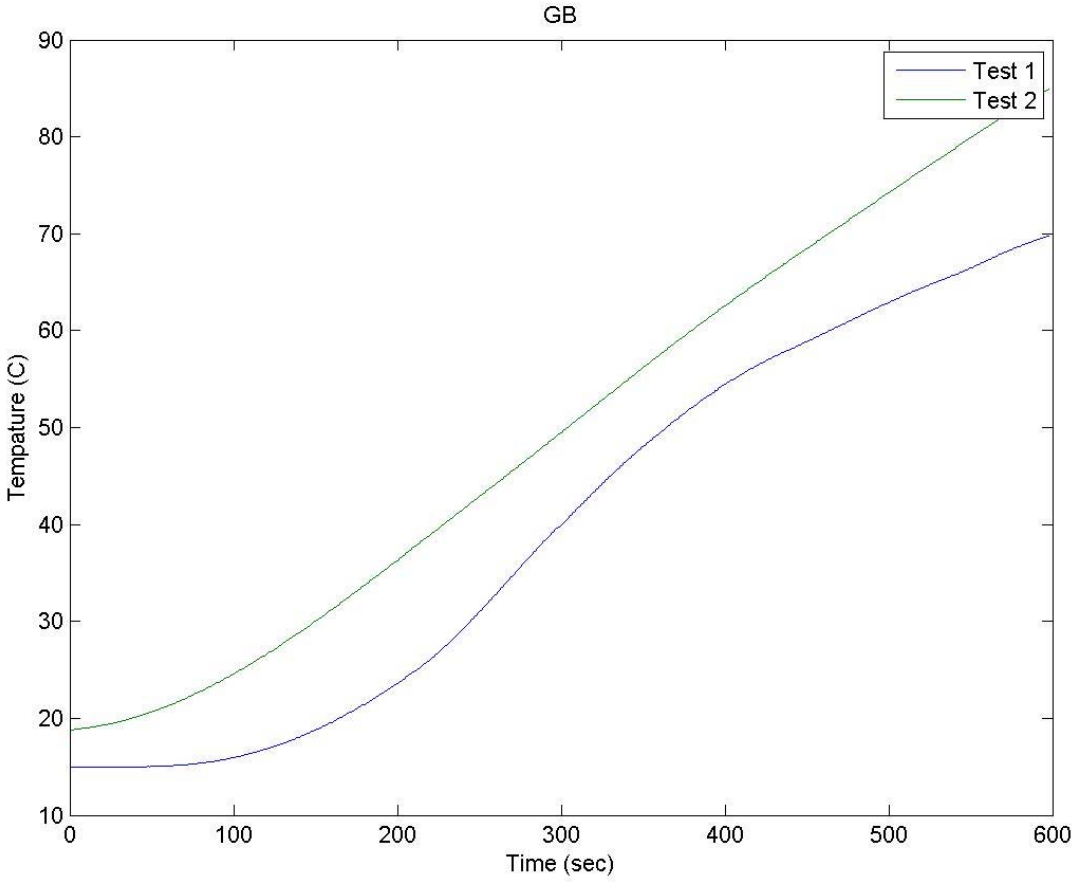
GB
Test 1
Test 2
Tempature (C)
Time (sec)
90
80
70
60
50
40
30
20
10
0
100
200
300
400
500
600

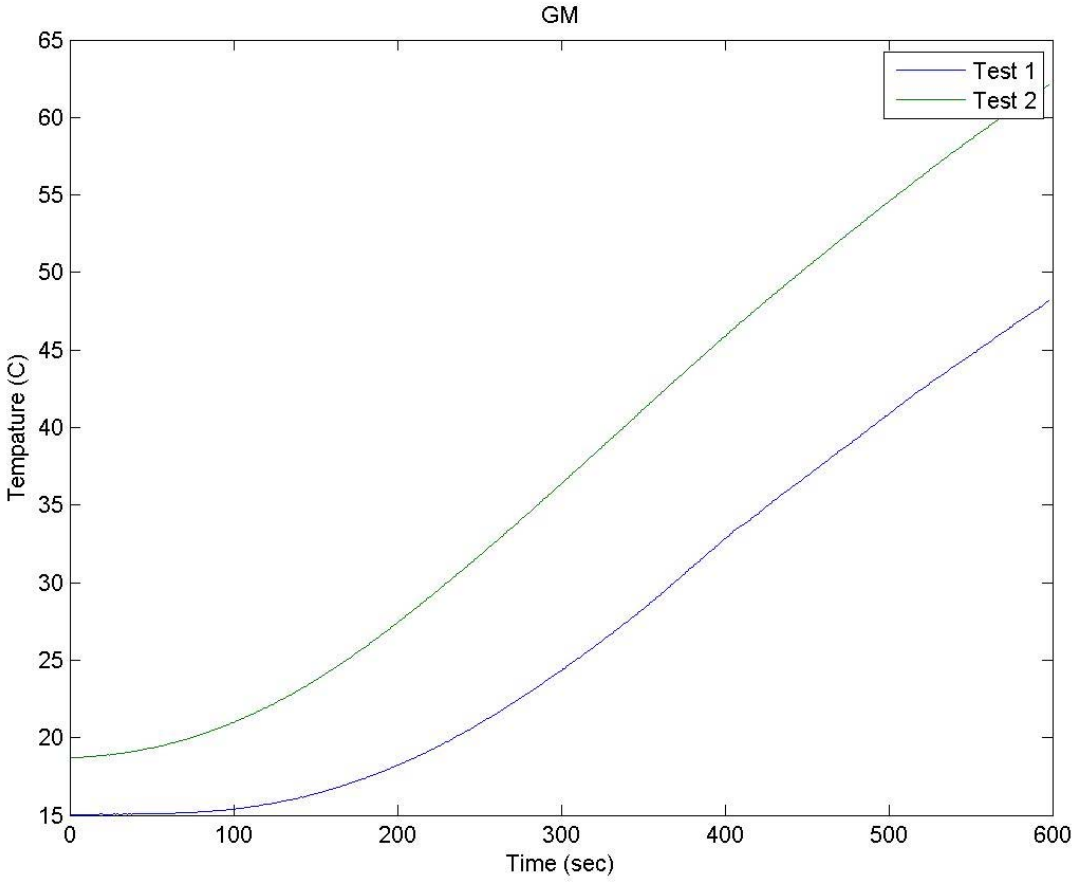
GM
Test 1
Test 2
Tempature (C)
Time (sec)
65
60
55
50
45
40
35
30
25
20
15
0
100
200
300
400
500
600

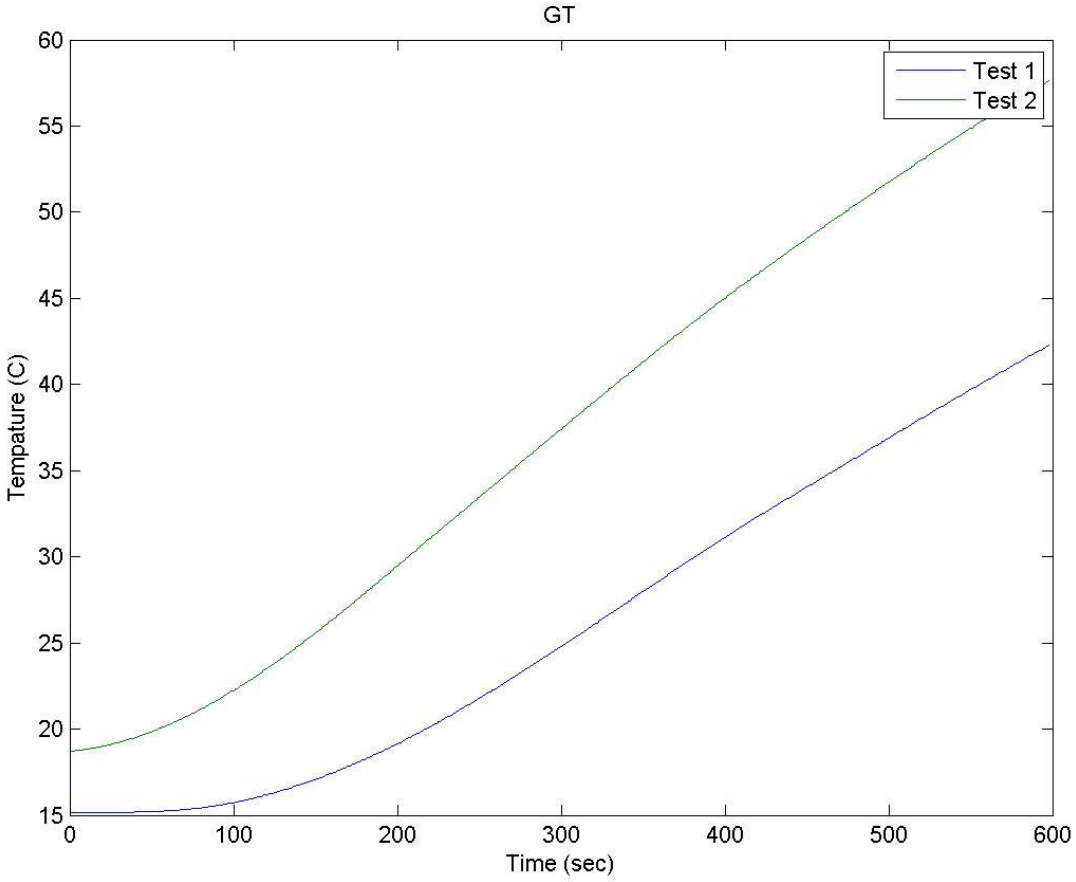
GT
Test 1
Test 2
Tempature (C)
Time (sec)
60
55
50
45
40
35
30
25
20
15
0
100
200
300
400
500
600

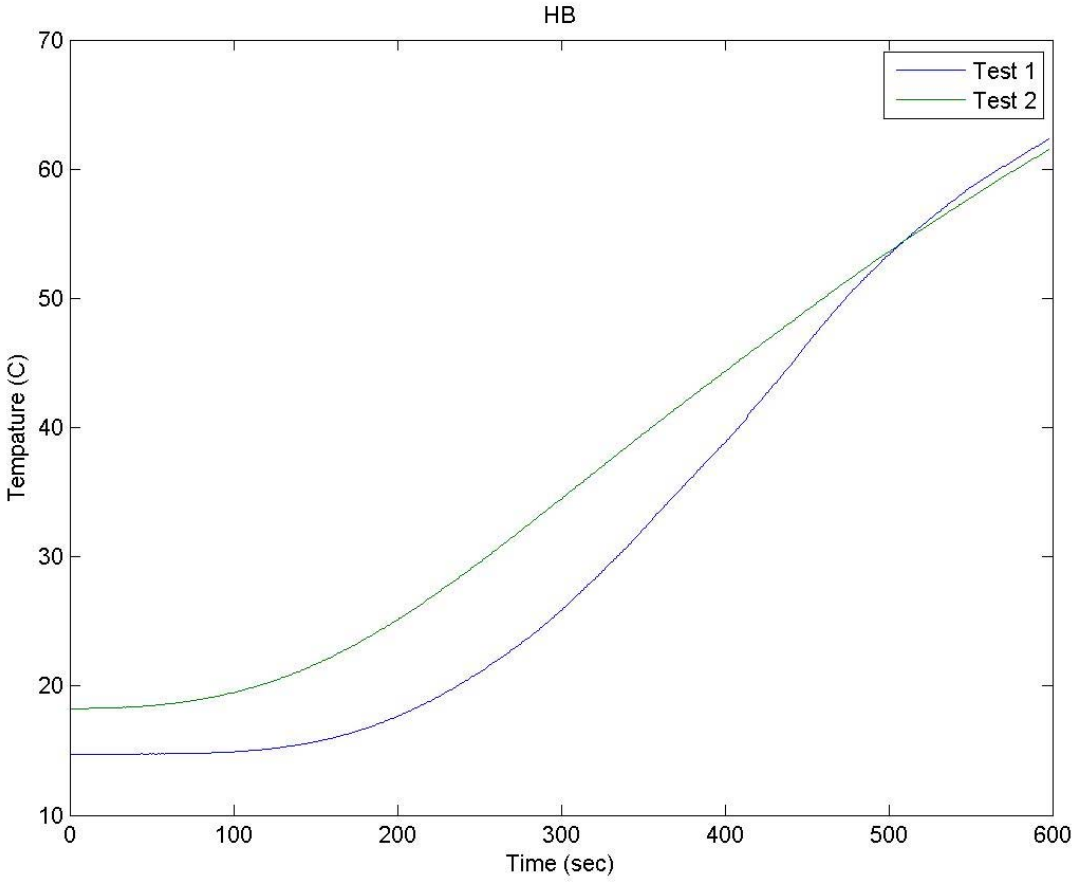
HB
Test 1
Test 2
Tempature (C)
Time (sec)
70
60
50
40
30
20
10
0
100
200
300
400
500
600

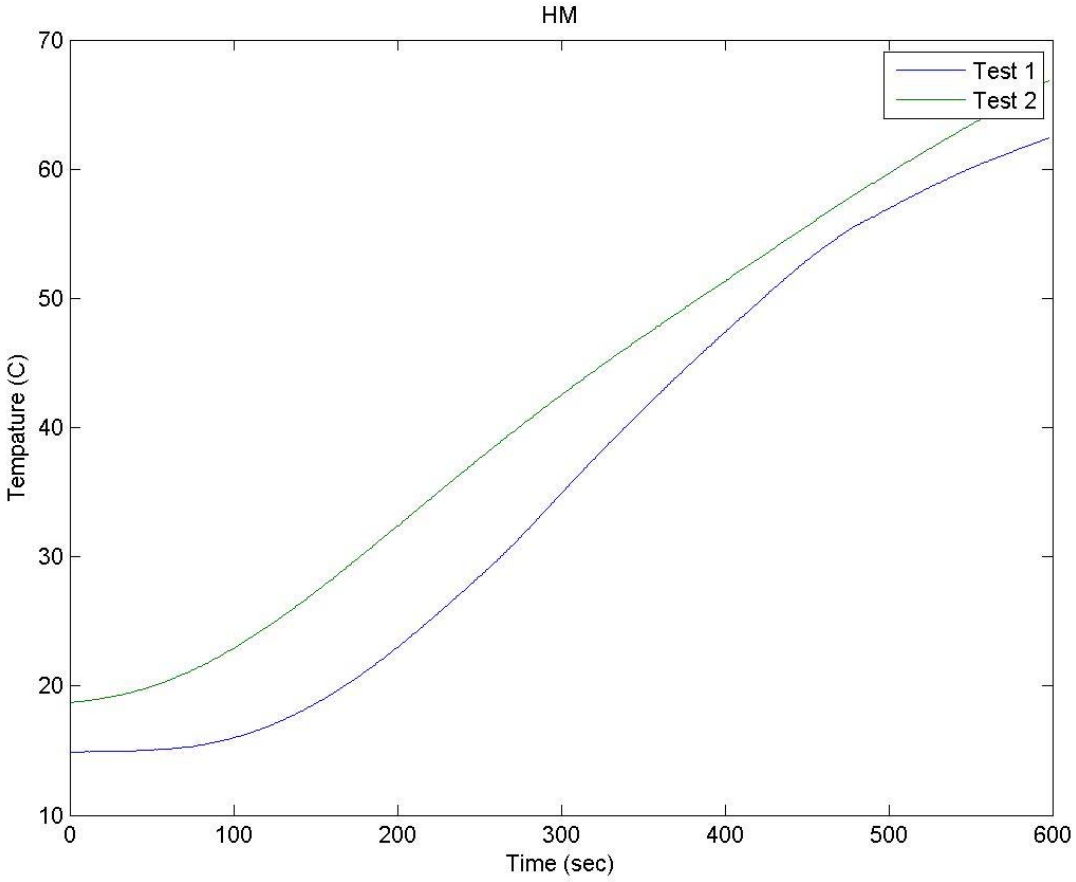
HM
Test 1
Test 2
Tempature (C)
Time (sec)
70
60
50
40
30
20
10
0
100
200
300
400
500
600

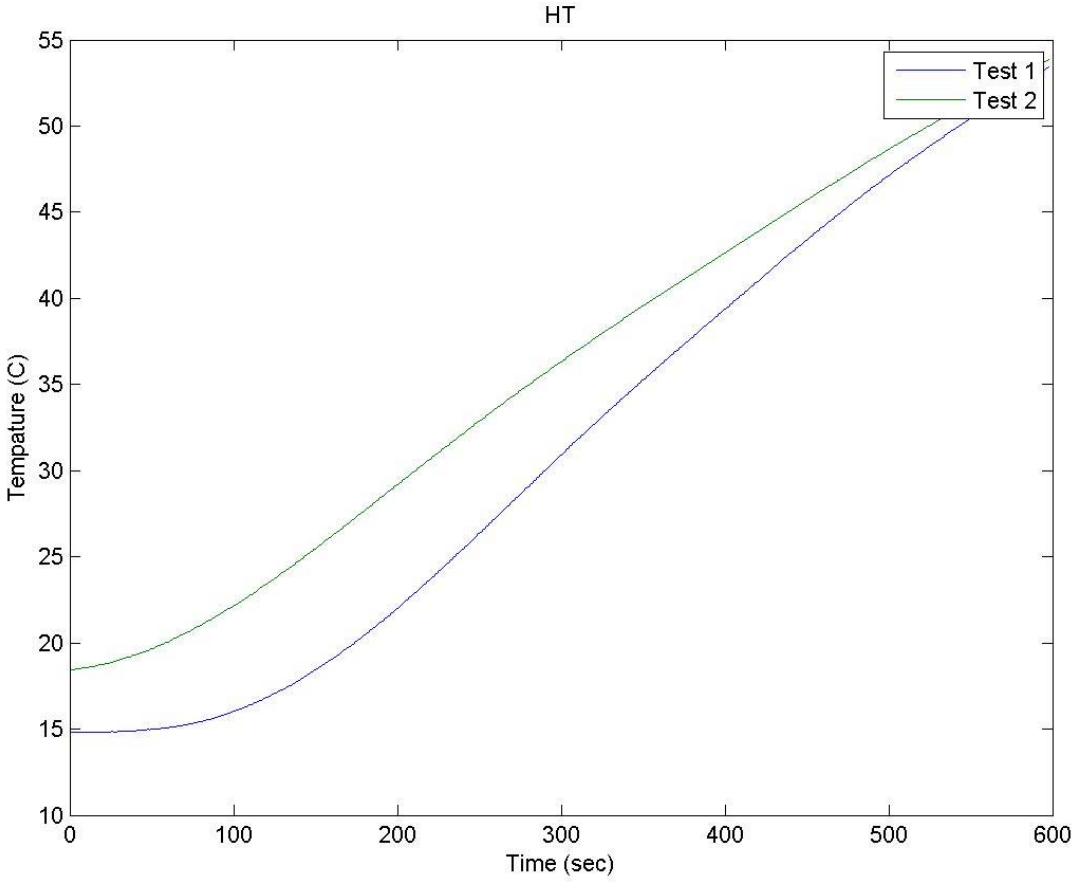
HT
Test 1
Test 2
Tempature (C)
Time (sec)
55
50
45
40
35
30
25
20
15
10
0
100
200
300
400
500
600

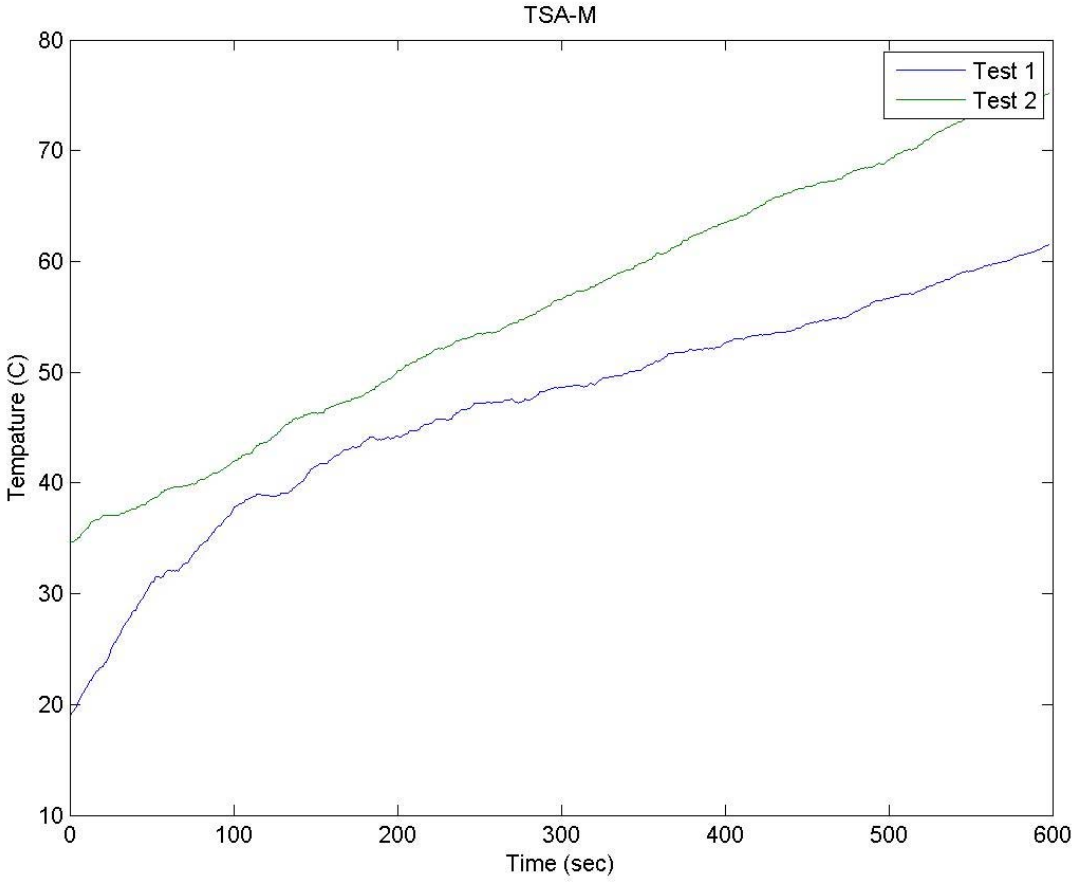
TSA-M
Test 1
Test 2
Tempature (C)
Time (sec)
80
70
60
50
40
30
20
10
0
100
200
300
400
500
600

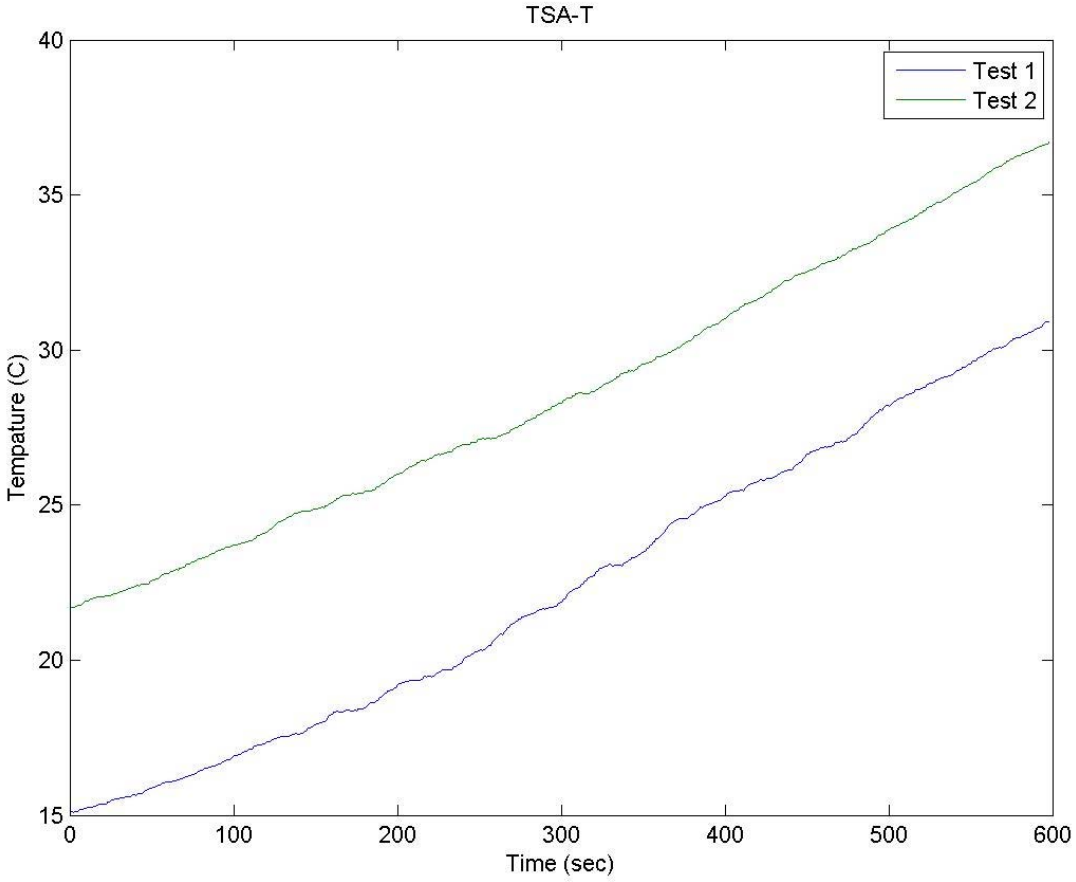
TSA-T
Test 1
Test 2
Tempature (C)
Time (sec)
40
35
30
25
20
15
0
100
200
300
400
500
600

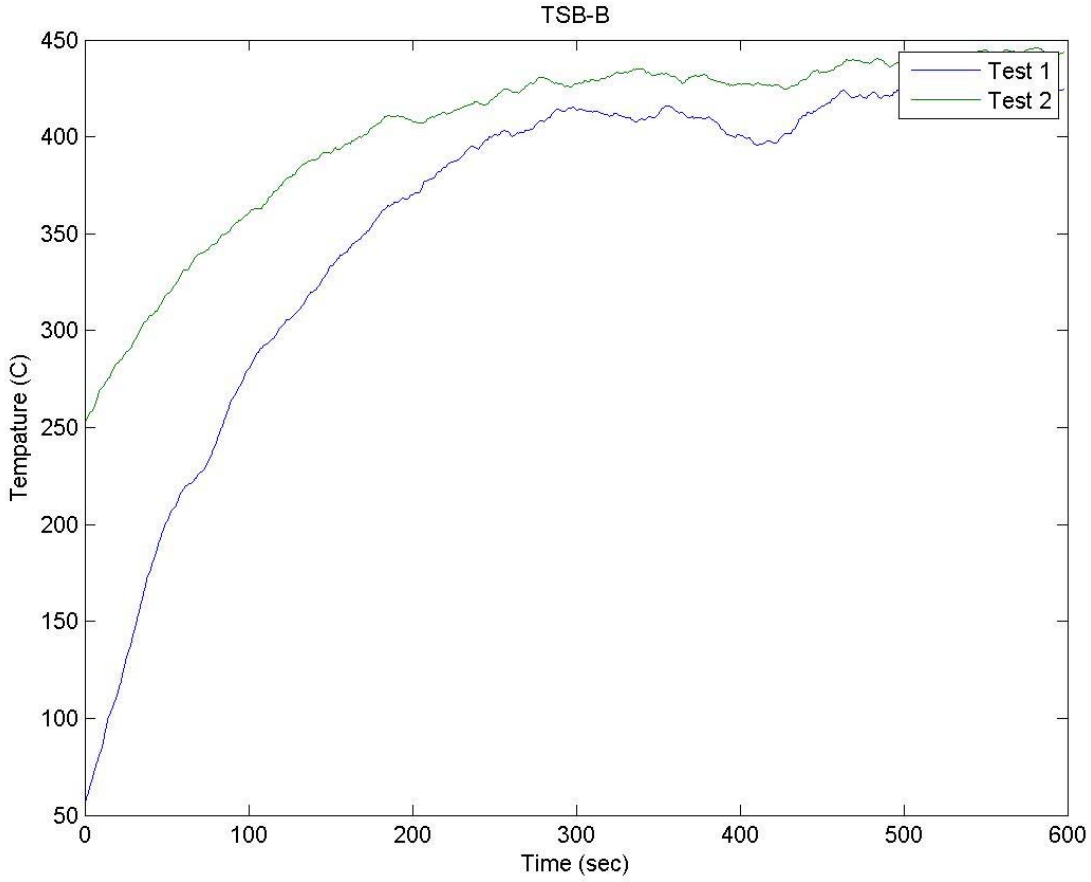
TSB-B
Test 1
Test 2
Tempature (C)
Time (sec)
450
400
350
300
250
200
150
100
50
0
100
200
300
400
500
600

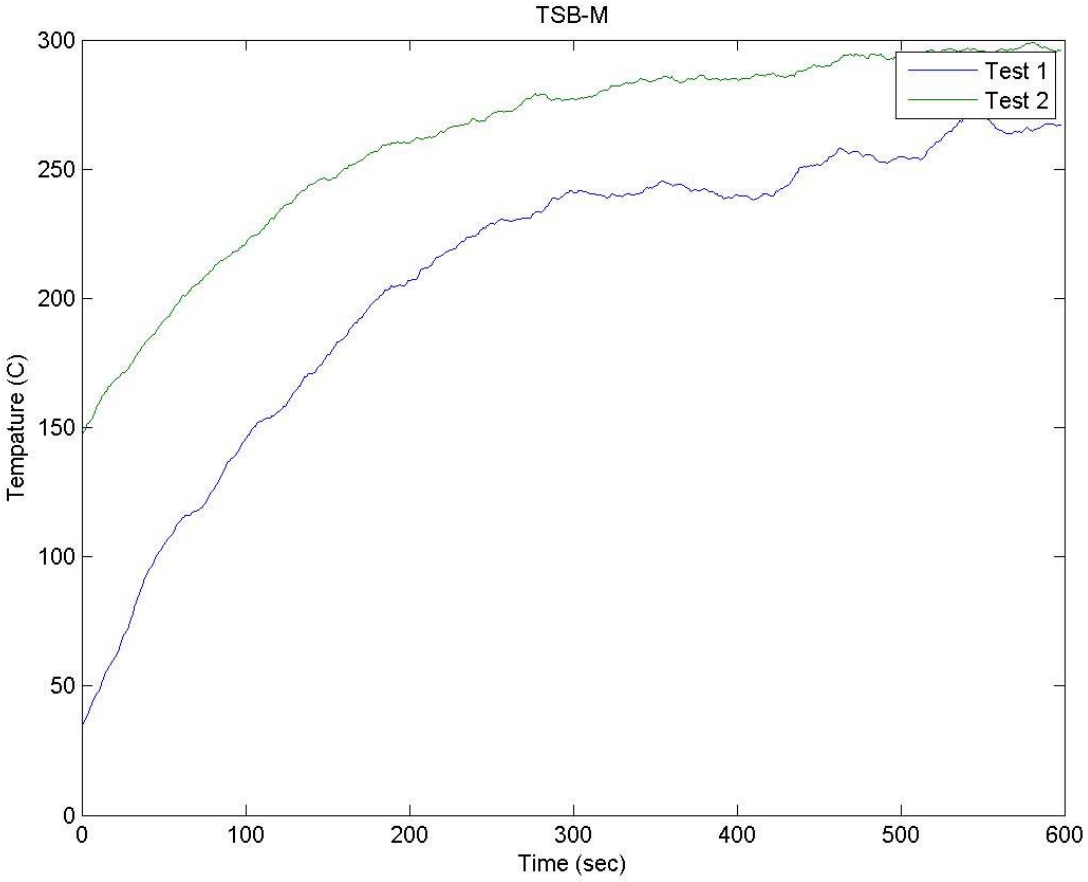
TSB-M
Test 1
Test 2
Tempature (C)
Time (sec)
0
50
100
150
200
250
300
0
100
200
300
400
500
600

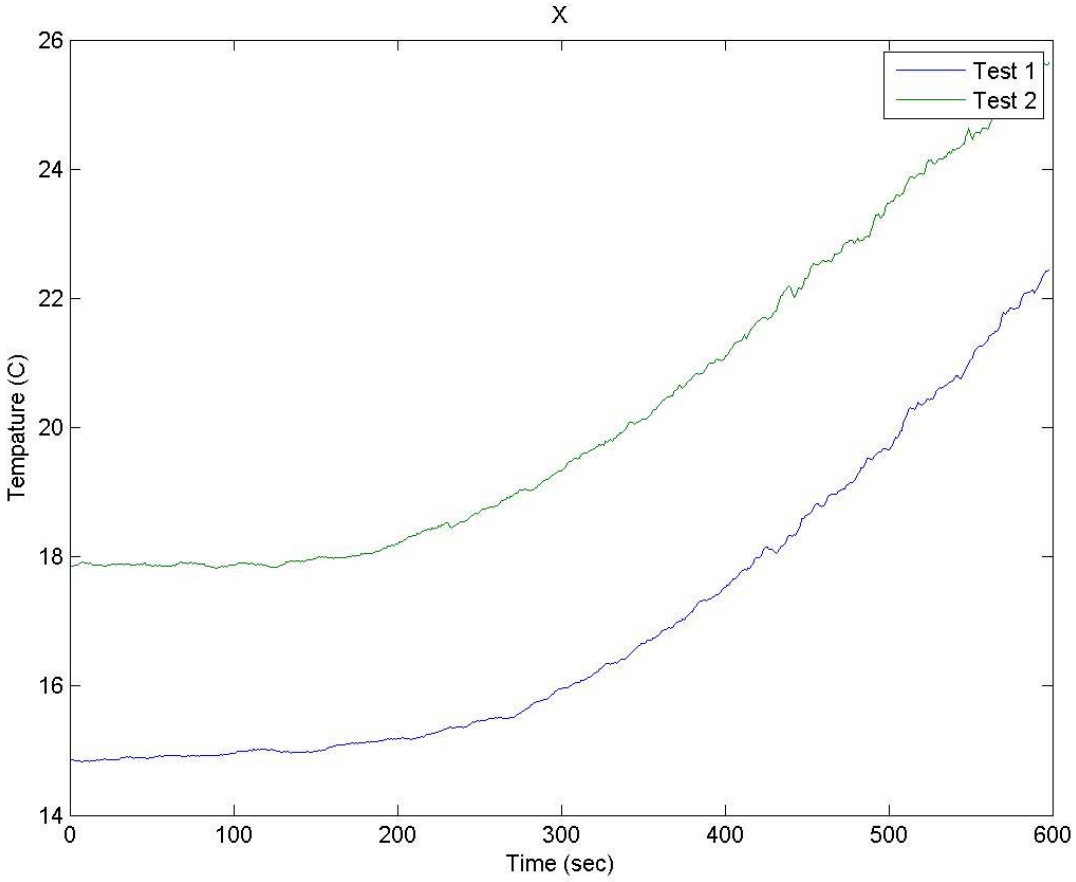
X
Test 1
Test 2
Tempature (C)
Time (sec)
26
24
22
20
18
16
14
0
100
200
300
400
500
600

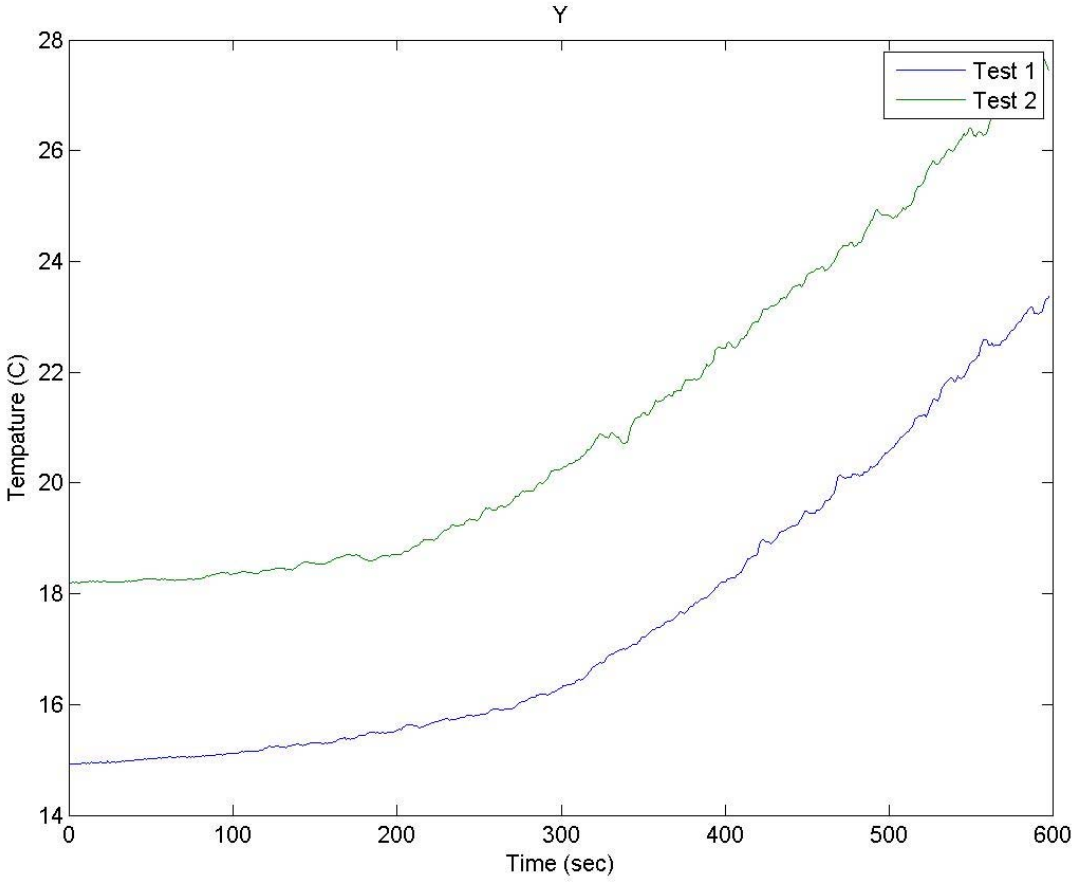
Y
Test 1
Test 2
Tempature (C)
Time (sec)
28
26
24
22
20
18
16
14
0
100
200
300
400
500
600

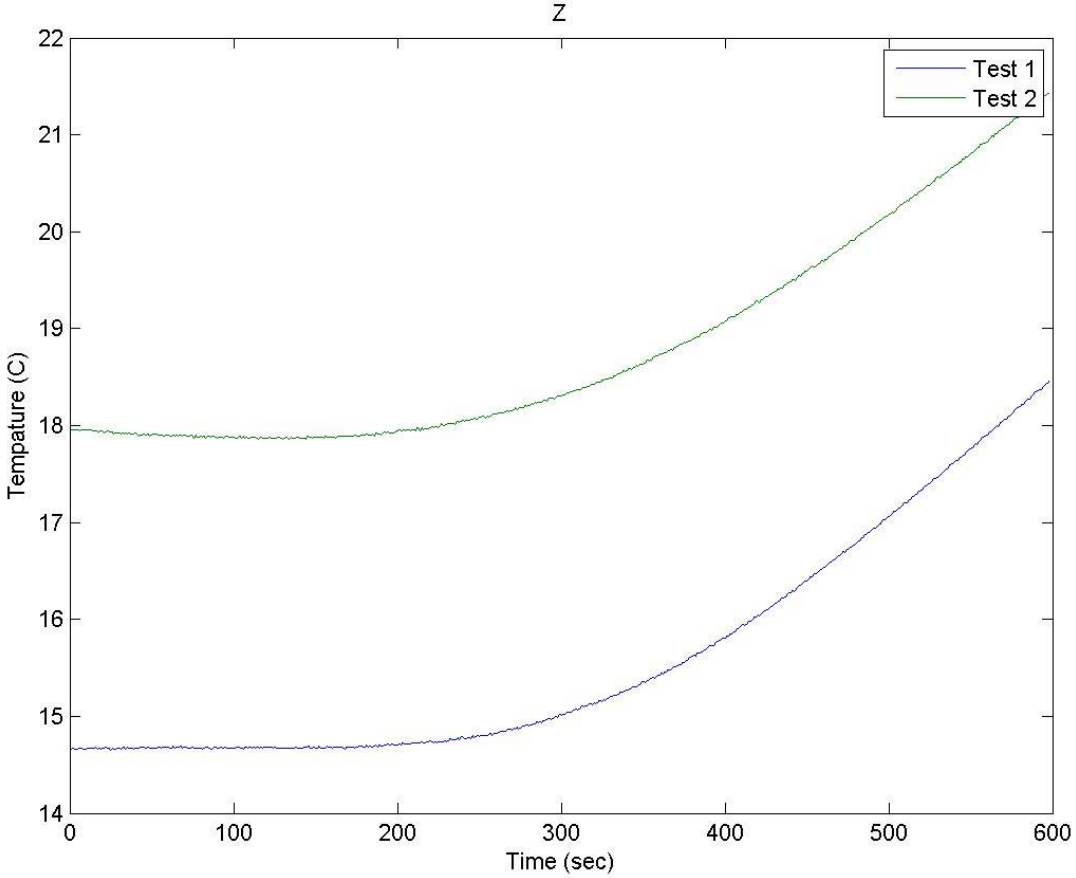
Z
Test 1
Test 2
Tempature (C)
Time (sec)
22
21
20
19
18
17
16
15
14
0
100
200
300
400
500
600

Overlap Joint Data

The following graphs are for the two test ran on the overlap joint.

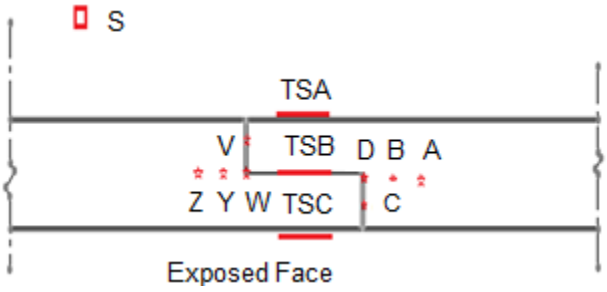

Thermocouples @ 3', 4' & 5' elevations
Thermocouples @ 3' & 4' elevations
Thin Skin Calorimeters @ 3', 4' & 5' elevations
Thermocouples hanging in air cell

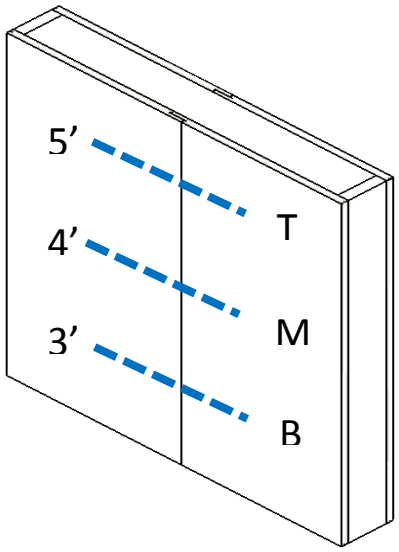

The above diagrams show the location of each instrument. If we are describing a thermocouple, the graph title will have two letters. The first letter of the title will designate the location of the instrument within the panel and can be seen in the top diagram. The second letter represents the elevation at which the instrument is located relative to the floor and may be seen in the bottom diagram. For think skin calorimeters, the first three letters before the dash designate the location of the instrument within the panel and can be seen in the top diagram. The letter after the dash represents the elevation at which the instrument is located relative to the floor and may be seen in the bottom diagram. Thermocouple S is at a single elevation of 4 to 5 feet and represented by just its letter. The following graphs are temperature vs. time of the two experiments conducted, indicated by the legend.

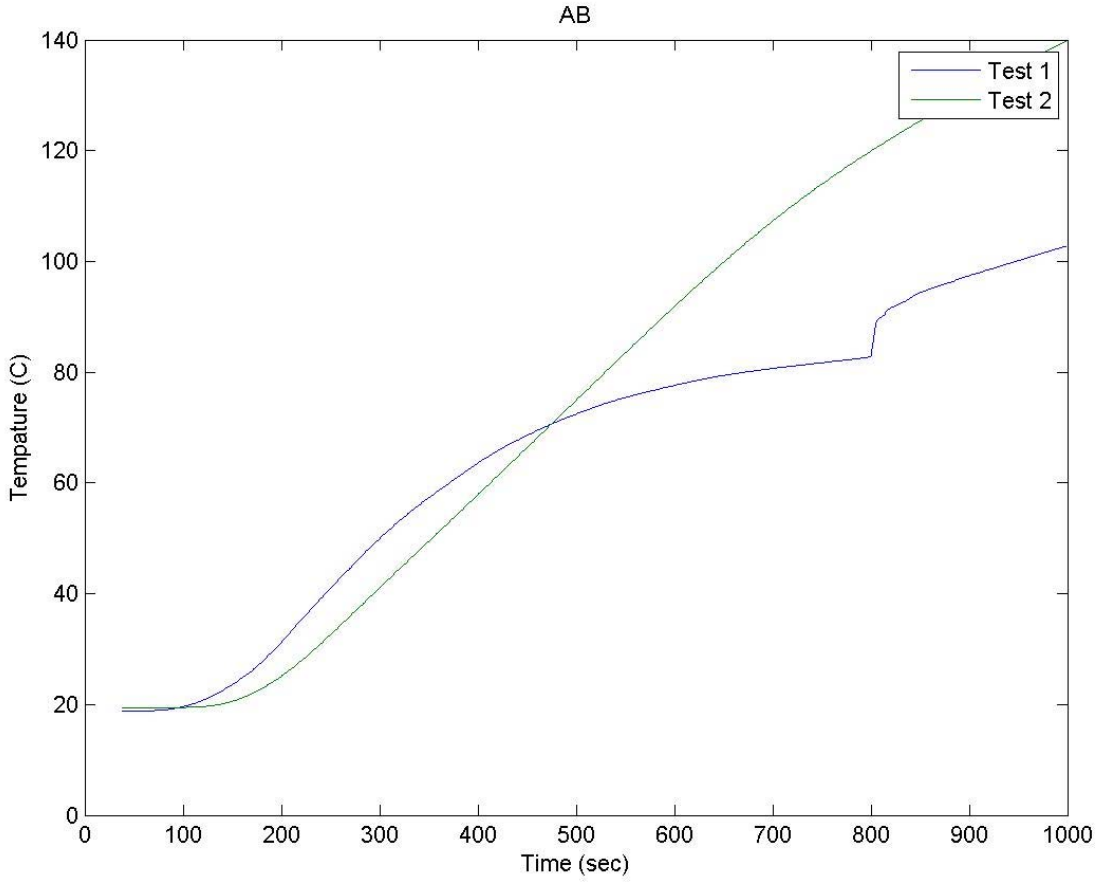
AB
Test 1
Test 2
Tempature (C)
Time (sec)
0
20
40
60
80
100
120
140
0
100
200
300
400
500
600
700
800
900
1000

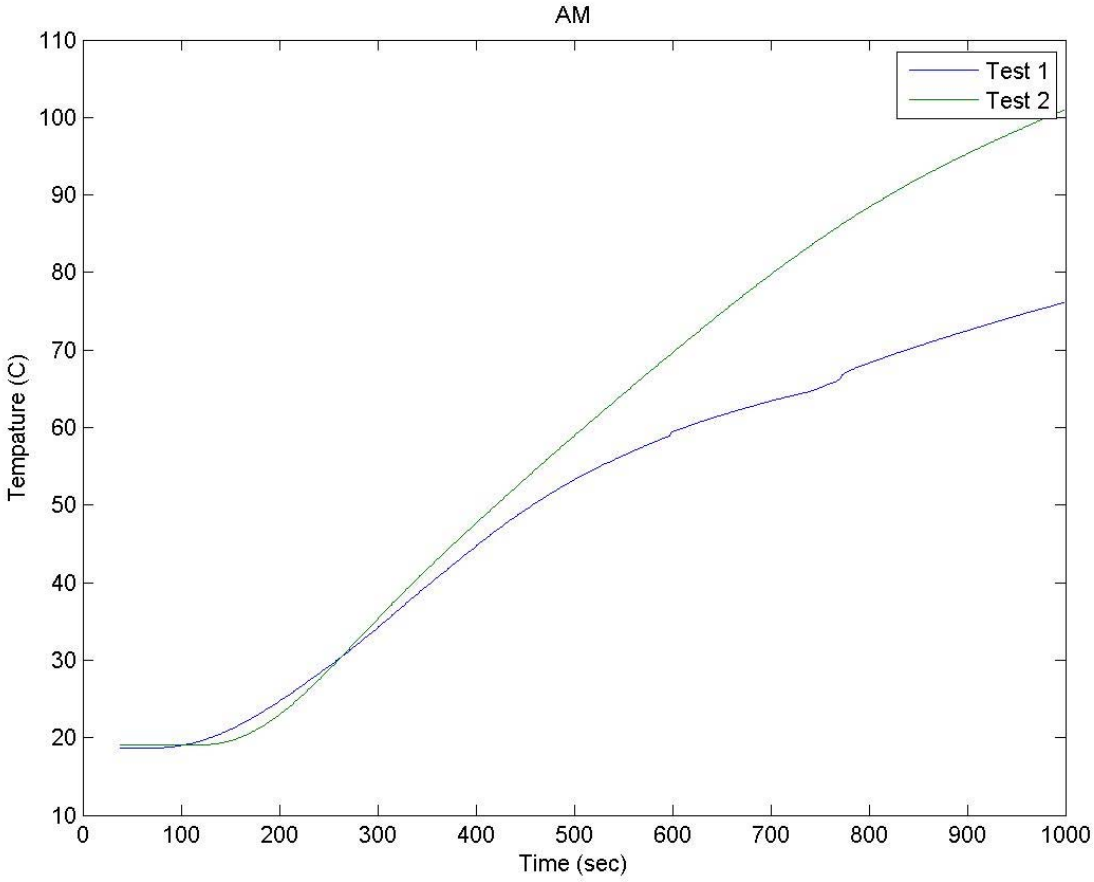
AM
Test 1
Test 2
Tempature (C)
Time (sec)
110
100
90
80
70
60
50
40
30
20
10
0
100
200
300
400
500
600
700
800
900
1000

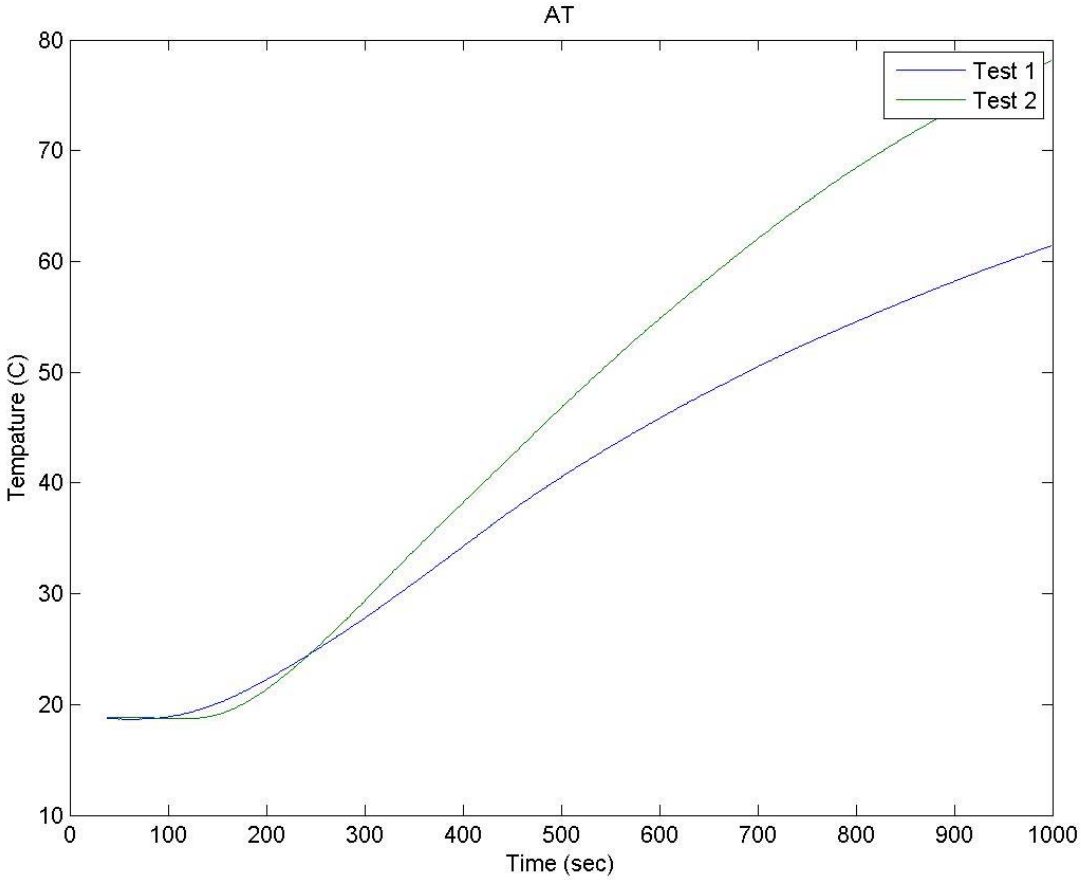
AT
Test 1
Test 2
Tempature (C)
Time (sec)
80
70
60
50
40
30
20
10
0
100
200
300
400
500
600
700
800
900
1000

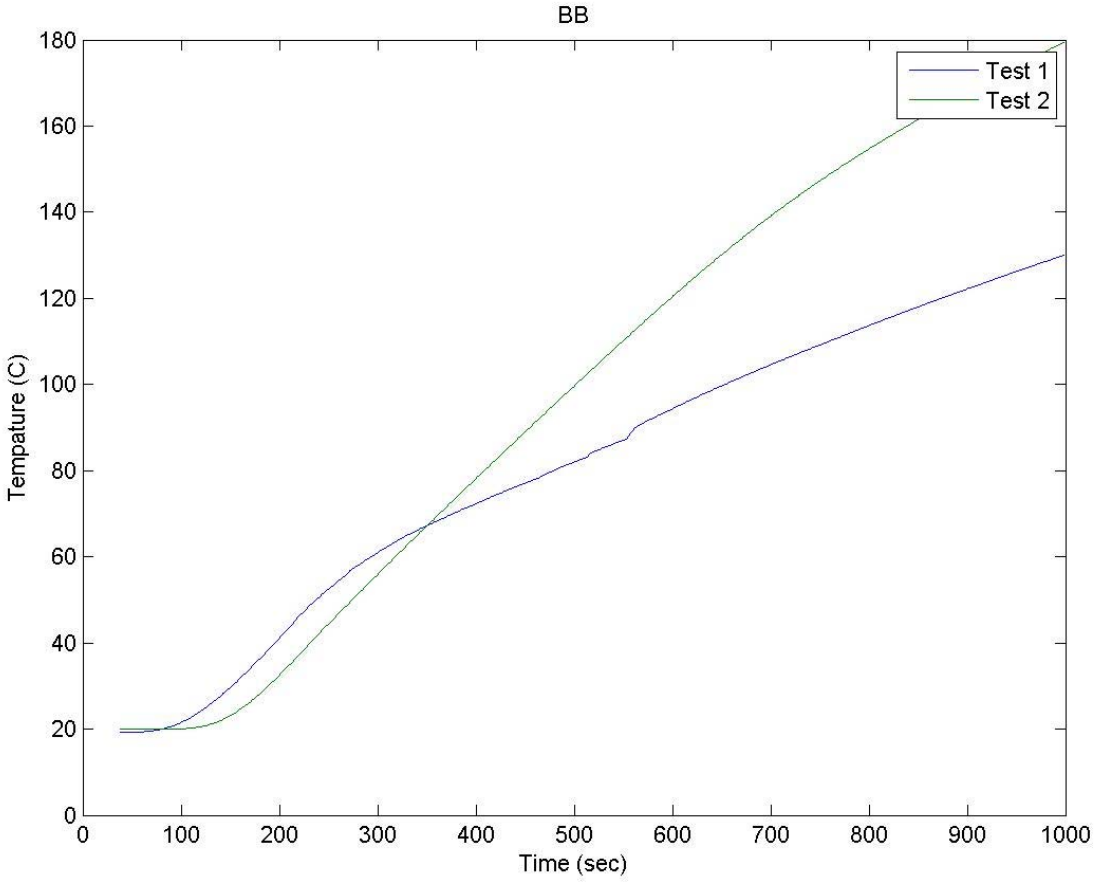
BB
Test 1
Test 2
Tempature (C)
Time (sec)
0
20
40
60
80
100
120
140
160
180
0
100
200
300
400
500
600
700
800
900
1000

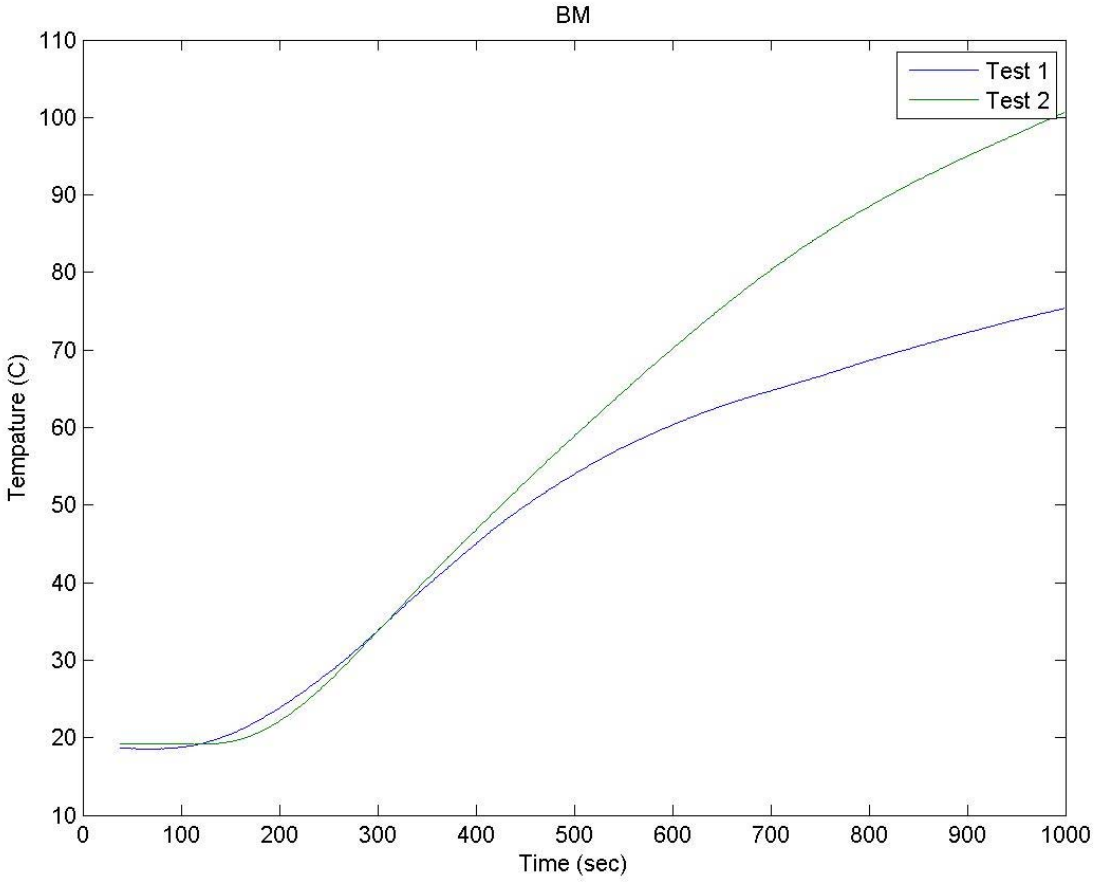
BM
Test 1
Test 2
Tempature (C)
Time (sec)
110
100
90
80
70
60
50
40
30
20
10
0
100
200
300
400
500
600
700
800
900
1000

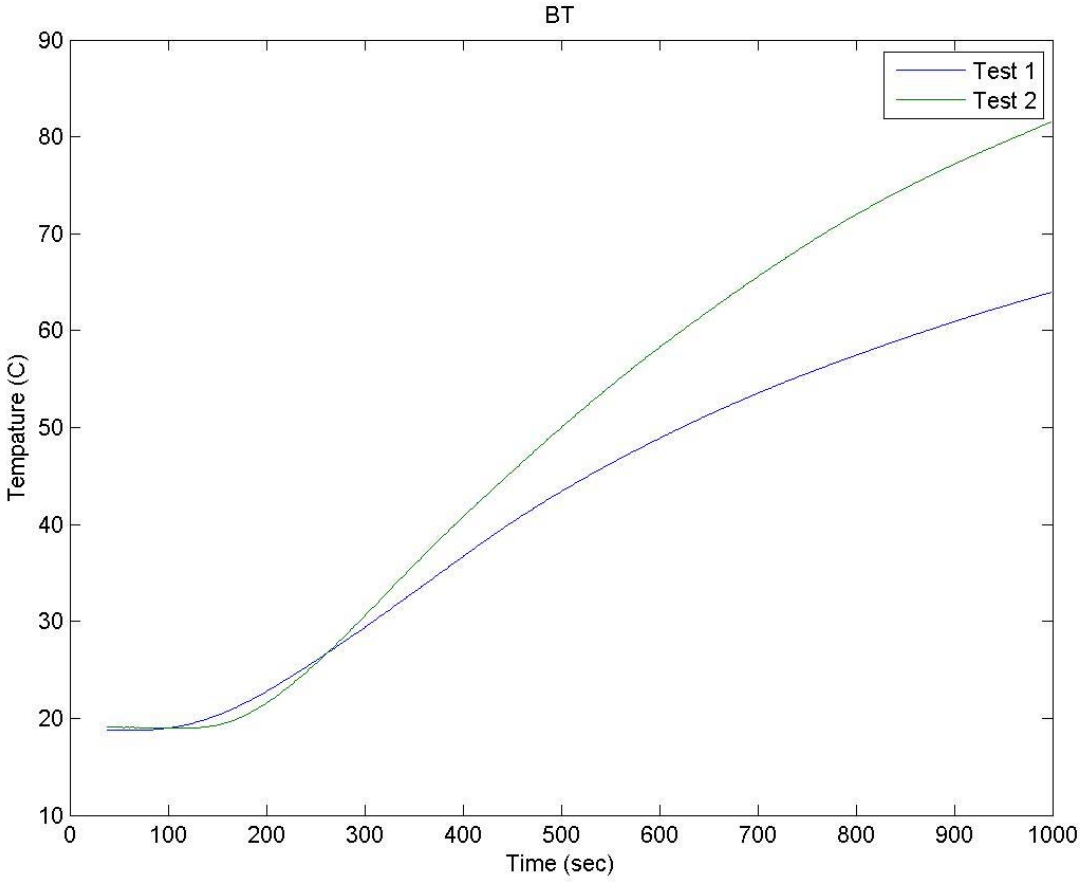
BT
Test 1
Test 2
Tempature (C)
Time (sec)
90
80
70
60
50
40
30
20
10
0
100
200
300
400
500
600
700
800
900
1000

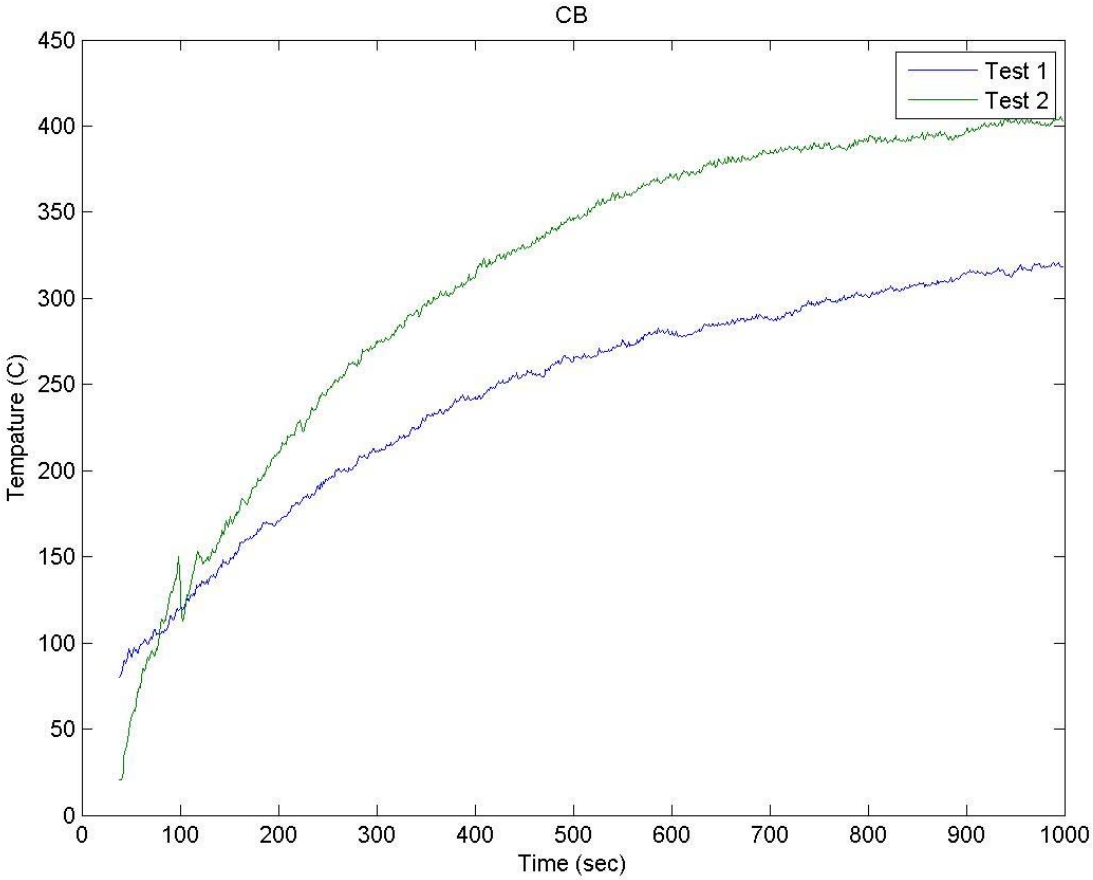
CB
Test 1
Test 2
Tempature (C)
Time (sec)
0
50
100
150
200
250
300
350
400
450
0
100
200
300
400
500
600
700
800
900
1000

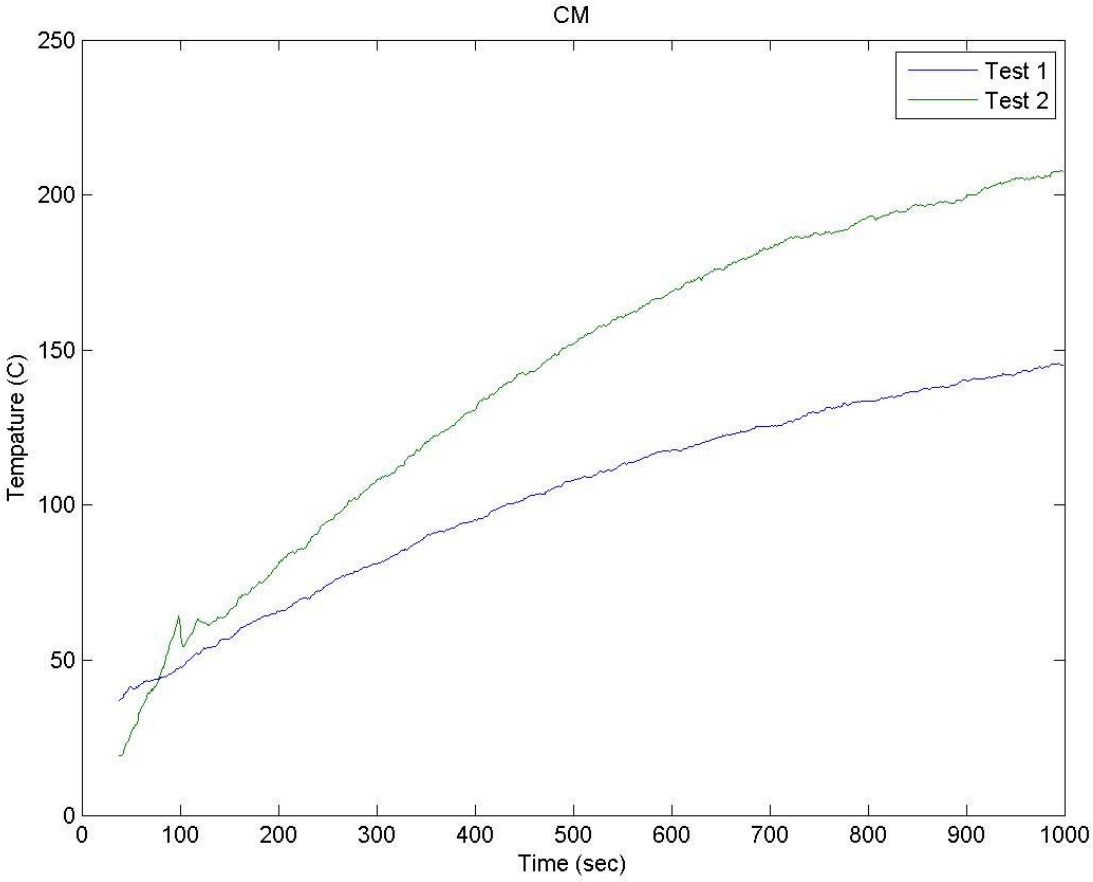
CM
Test 1
Test 2
Tempature (C)
Time (sec)
0
50
100
150
200
250
0
100
200
300
400
500
600
700
800
900
1000

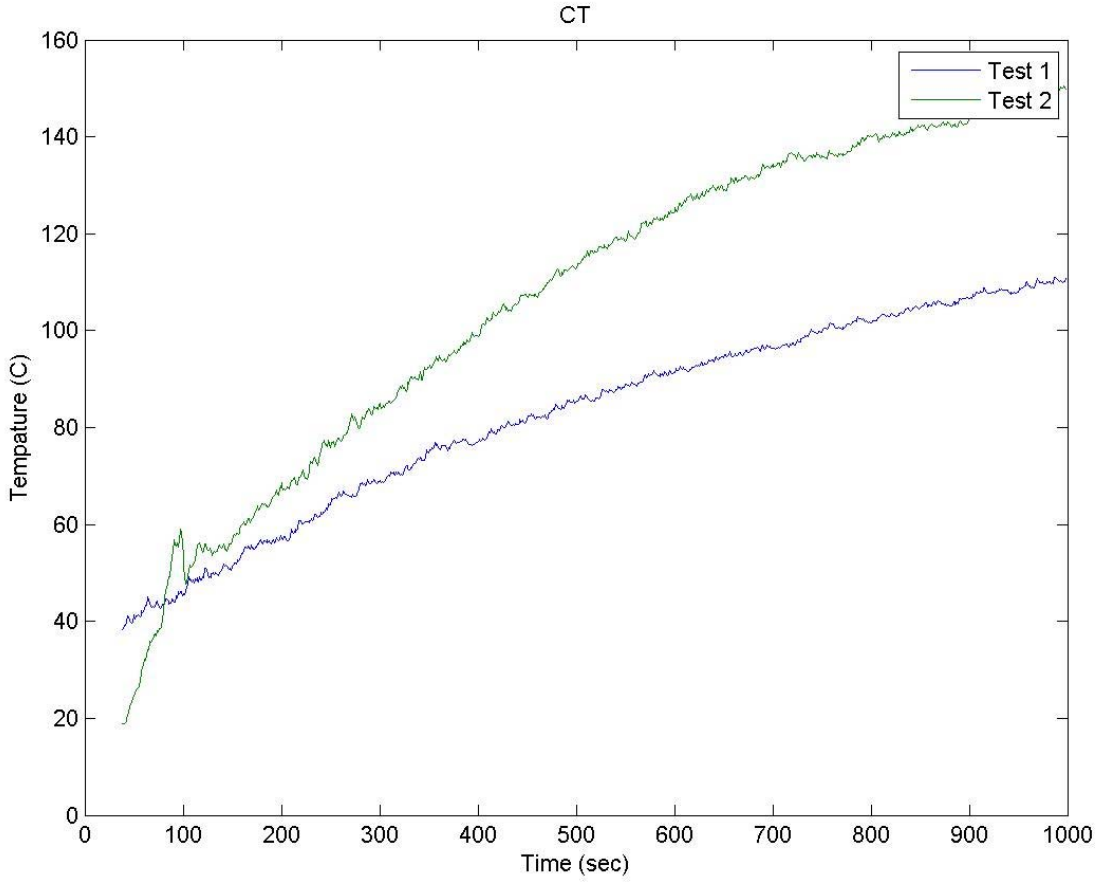
CT
Test 1
Test 2
Tempature (C)
Time (sec)
0
20
40
60
80
100
120
140
160
0
100
200
300
400
500
600
700
800
900
1000

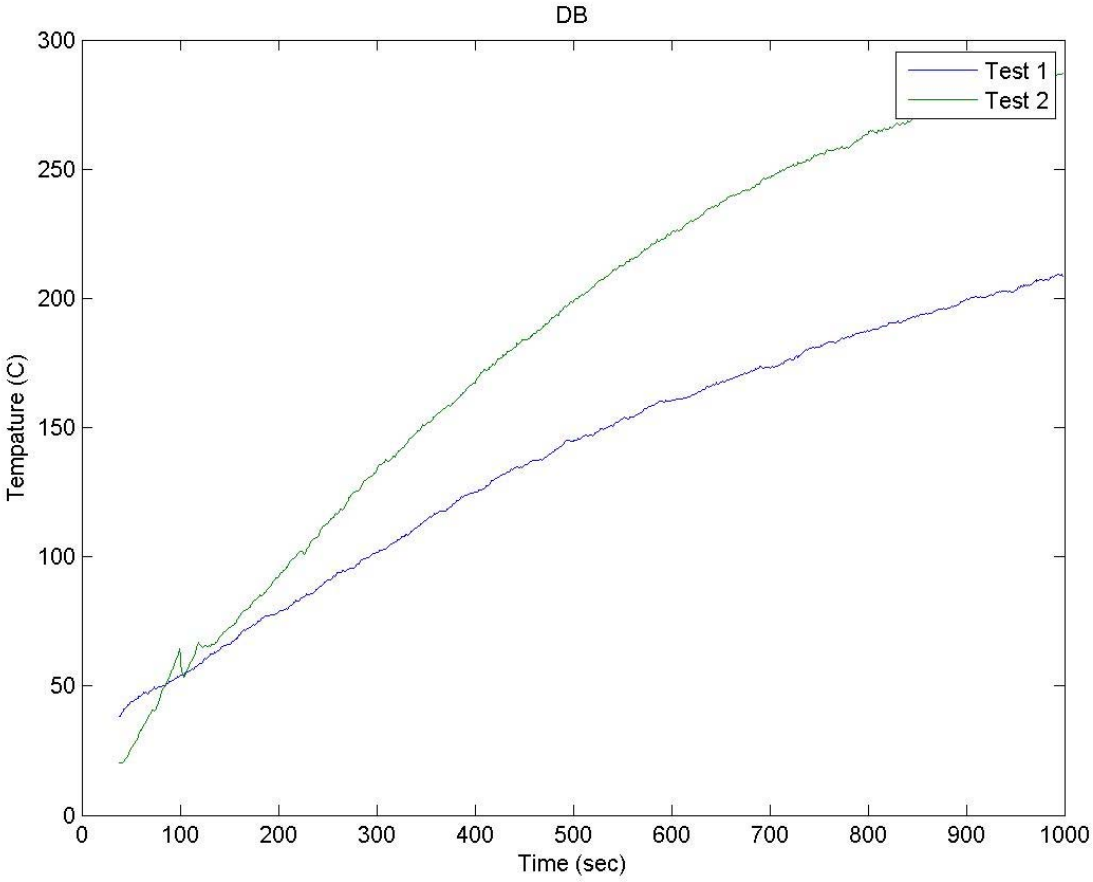
DB
Test 1
Test 2
Tempature (C)
Time (sec)
0
50
100
150
200
250
300
0
100
200
300
400
500
600
700
800
900
1000

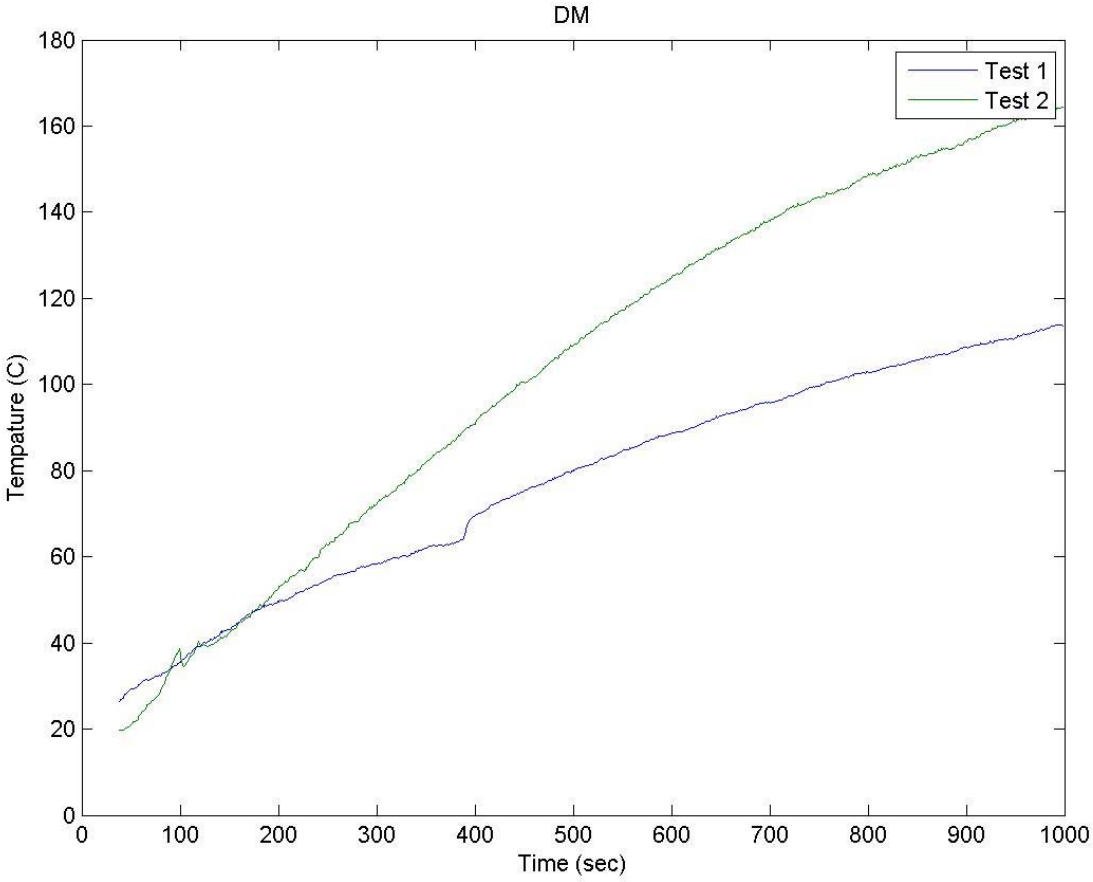
DM
Test 1
Test 2
Tempature (C)
Time (sec)
0
20
40
60
80
100
120
140
160
180
0
100
200
300
400
500
600
700
800
900
1000

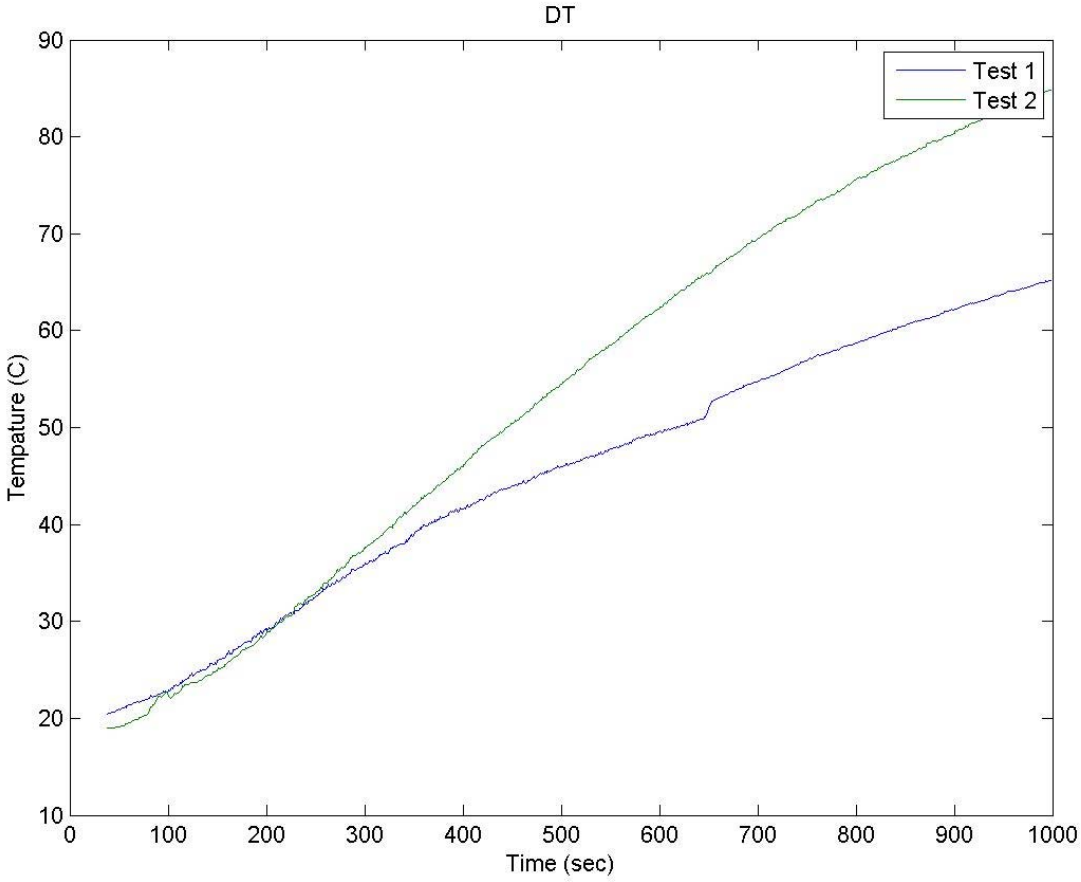
DT
Test 1
Test 2
Tempature (C)
Time (sec)
90
80
70
60
50
40
30
20
10
0
100
200
300
400
500
600
700
800
900
1000

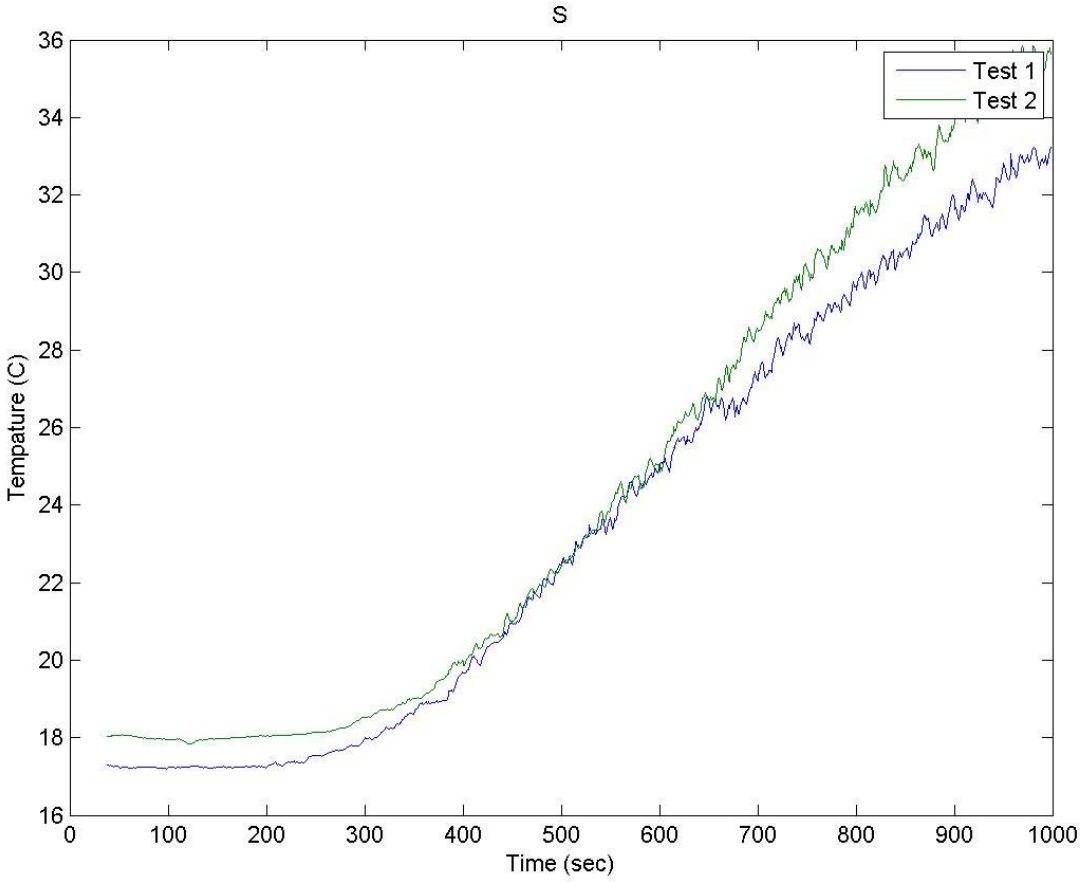
S
Test 1
Test 2
Tempature (C)
Time (sec)
36
34
32
30
28
26
24
22
20
18
16
0
100
200
300
400
500
600
700
800
900
1000

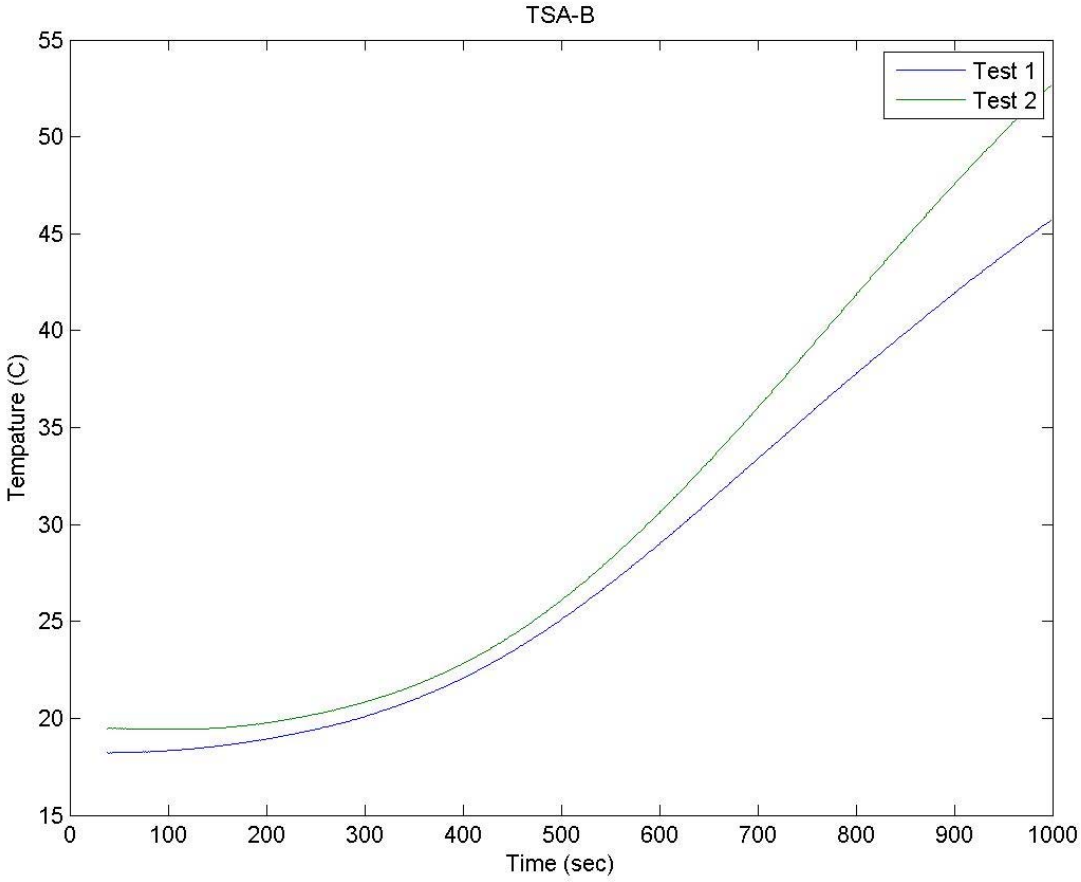
TSA-B
Test 1
Test 2
Tempature (C)
Time (sec)
55
50
45
40
35
30
25
20
15
0
100
200
300
400
500
600
700
800
900
1000

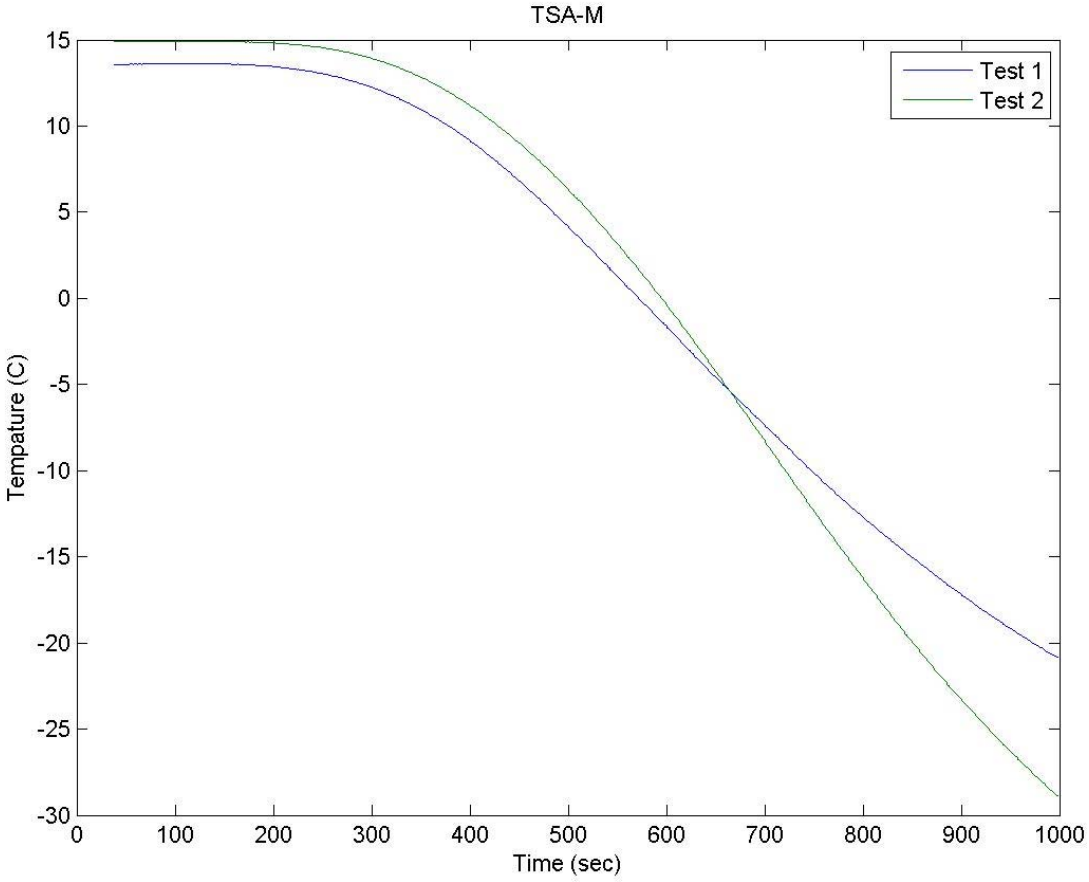
TSA-M
Test 1
Test 2
Tempature (C)
Time (sec)
15
10
5
0
-5
-10
-15
-20
-25
-30
0
100
200
300
400
500
600
700
800
900
1000

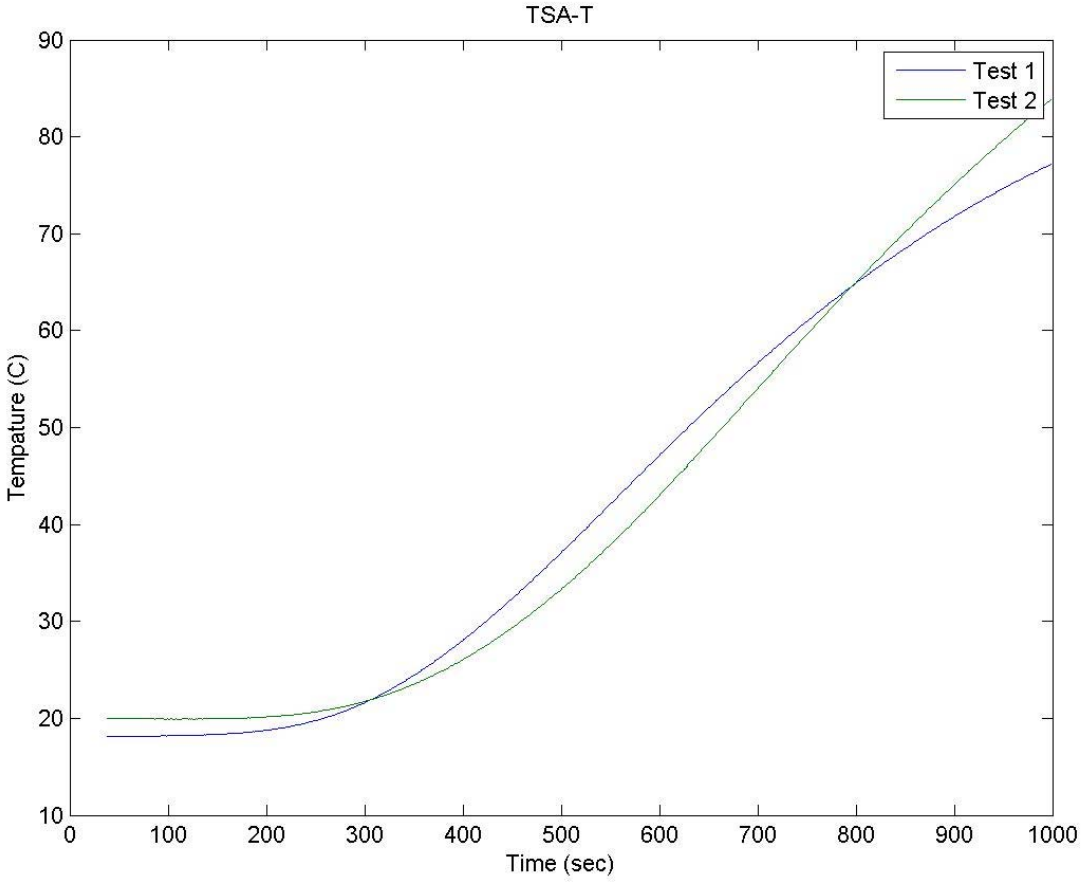
TSA-T
Test 1
Test 2
Tempature (C)
Time (sec)
90
80
70
60
50
40
30
20
10
0
100
200
300
400
500
600
700
800
900
1000

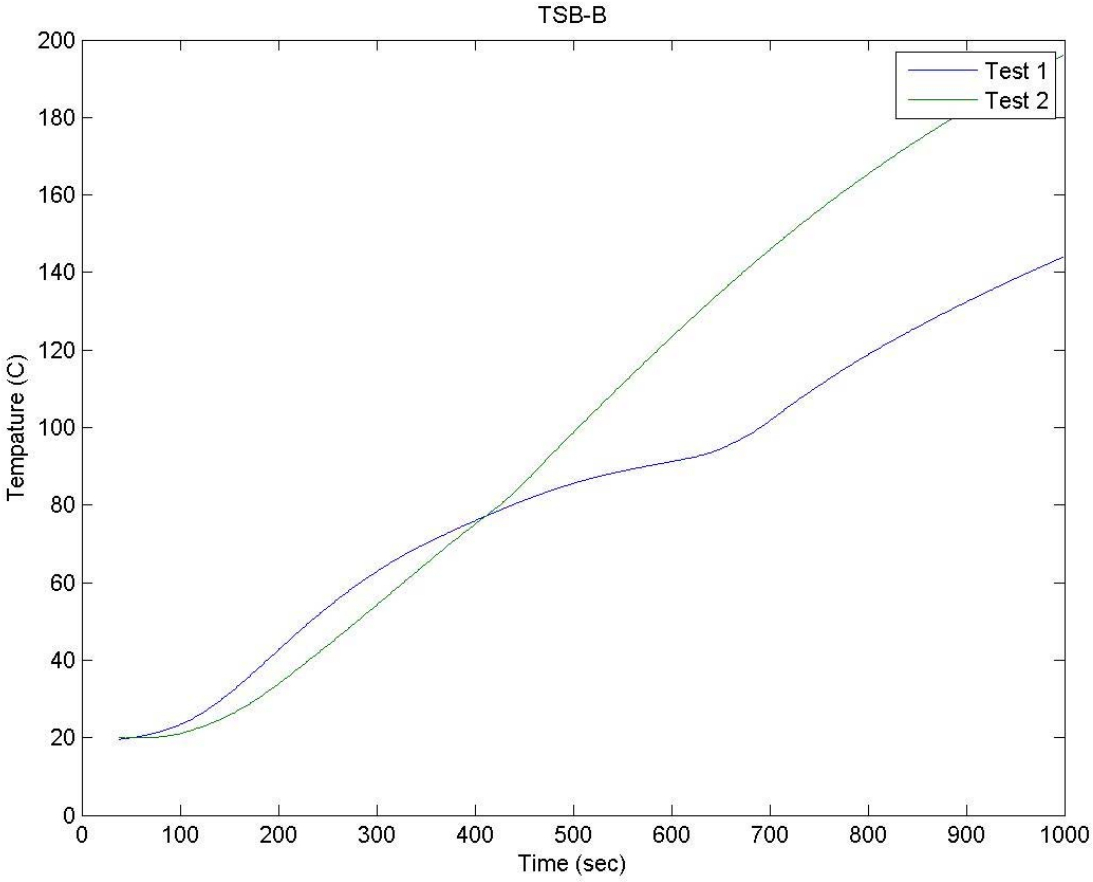
TSB-B
Test 1
Test 2
Tempature (C)
Time (sec)
0
20
40
60
80
100
120
140
160
180
200
0
100
200
300
400
500
600
700
800
900
1000

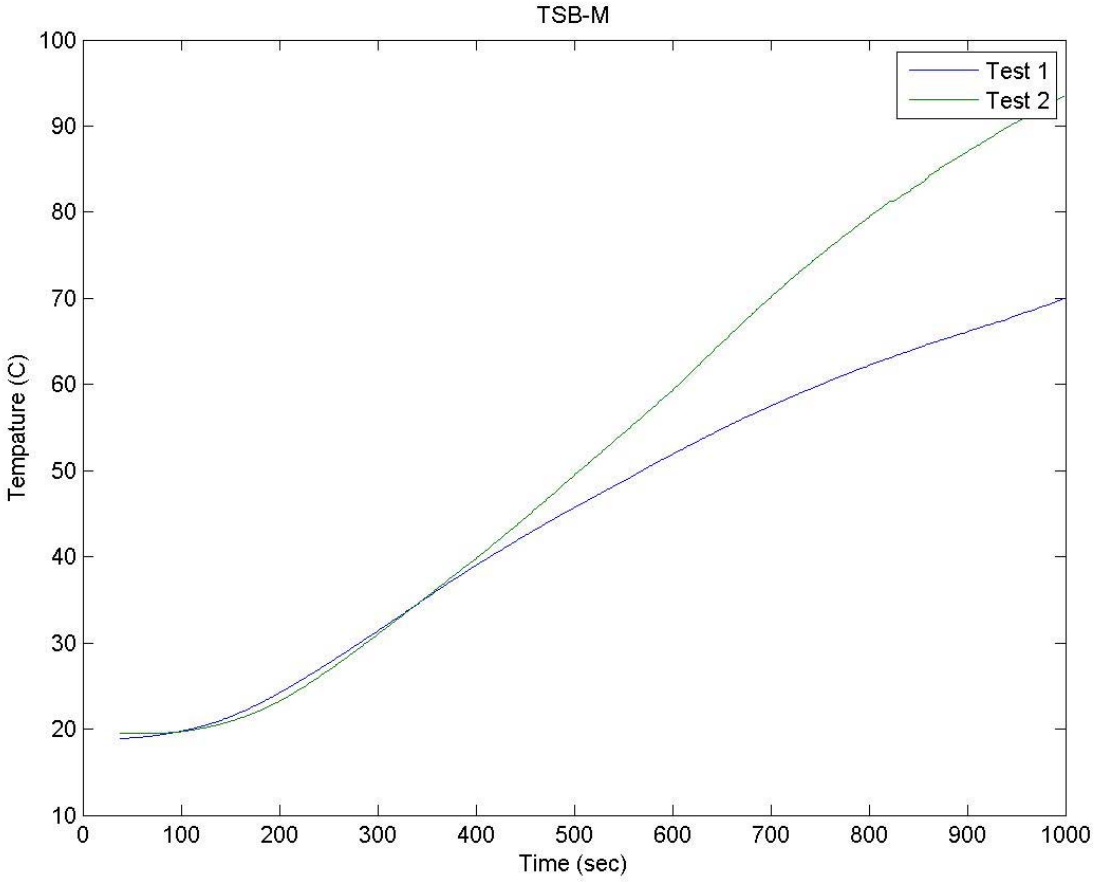
TSB-M
Test 1
Test 2
Tempature (C)
Time (sec)
100
90
80
70
60
50
40
30
20
10
0
100
200
300
400
500
600
700
800
900
1000

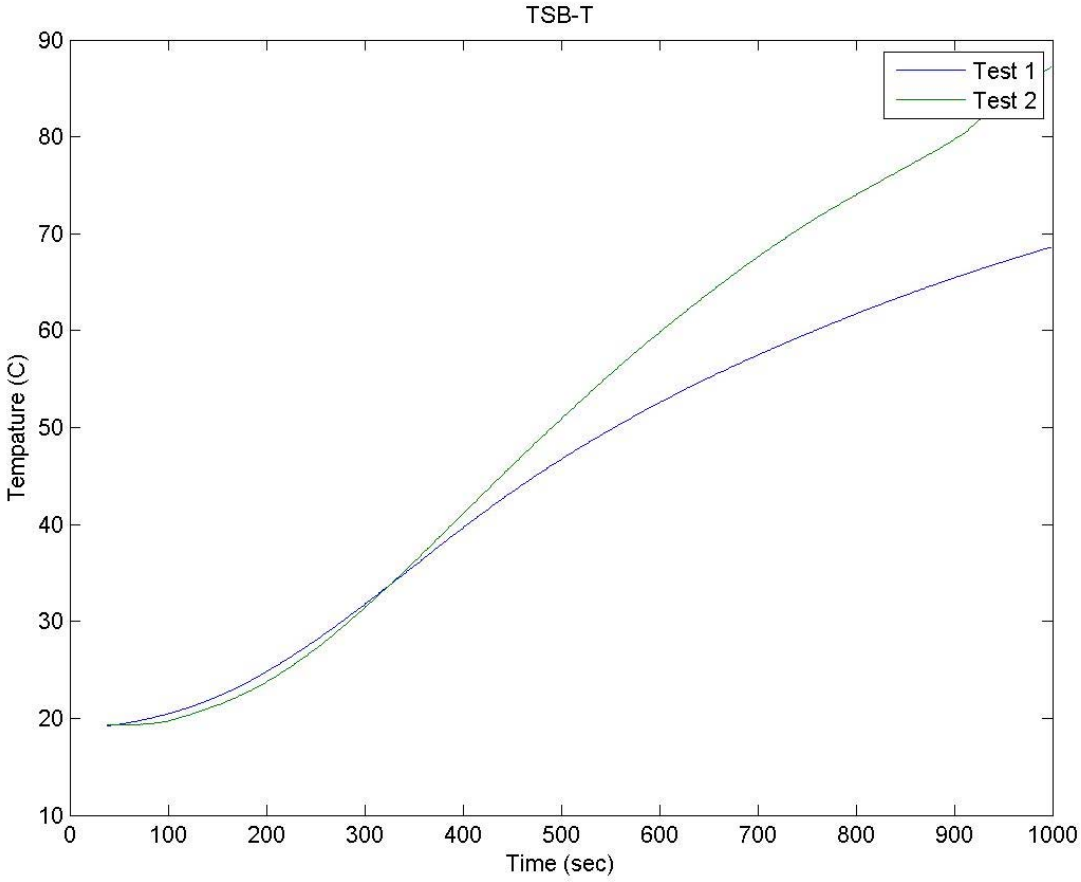
TSB-T
Test 1
Test 2
Tempature (C)
Time (sec)
90
80
70
60
50
40
30
20
10
0
100
200
300
400
500
600
700
800
900
1000

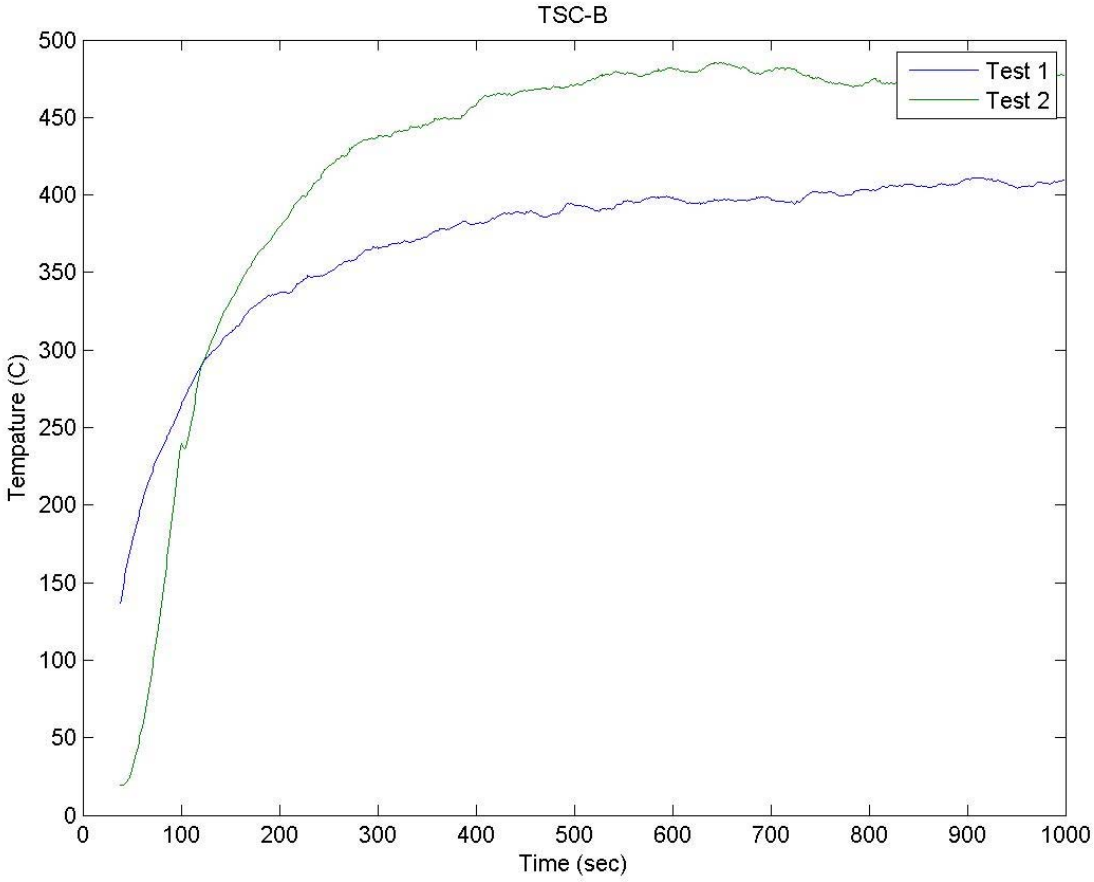
TSC-B
Test 1
Test 2
Tempature (C)
Time (sec)
0
50
100
150
200
250
300
350
400
450
500
0
100
200
300
400
500
600
700
800
900
1000

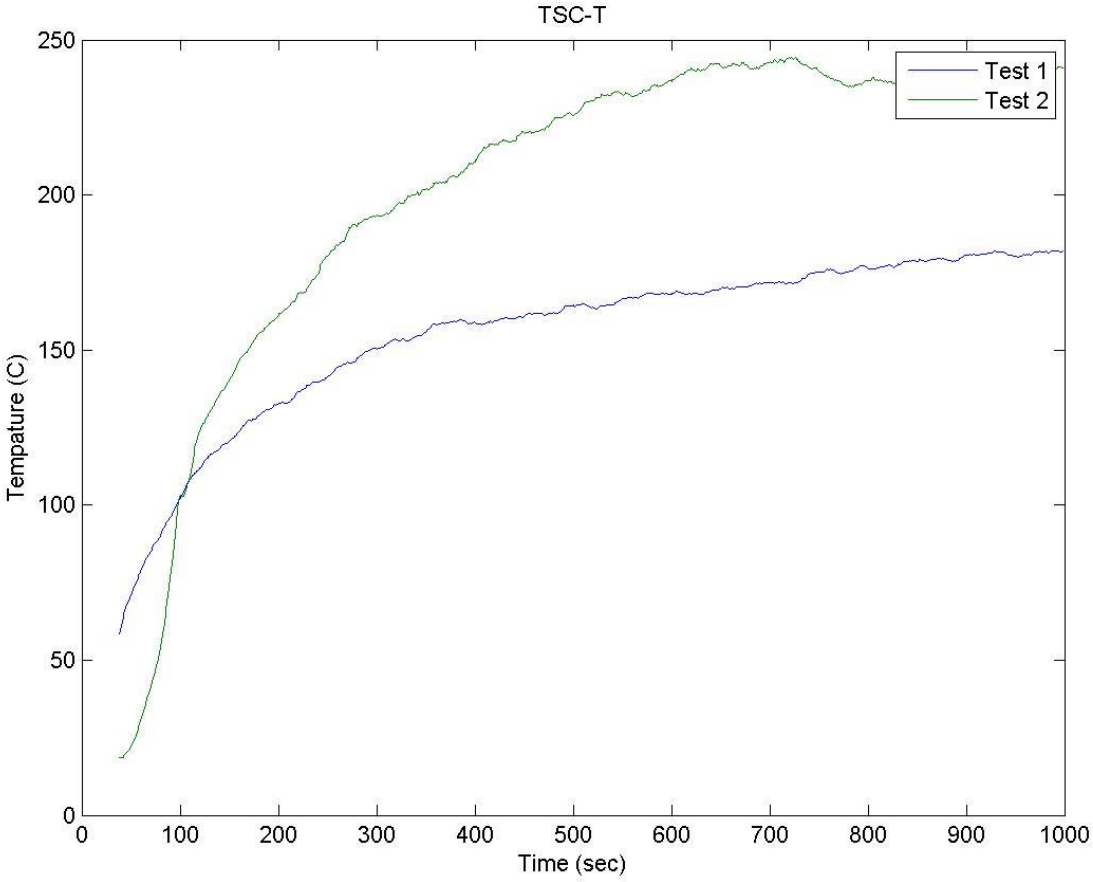
TSC-T
Test 1
Test 2
Tempature (C)
Time (sec)
0
50
100
150
200
250
0
100
200
300
400
500
600
700
800
900
1000

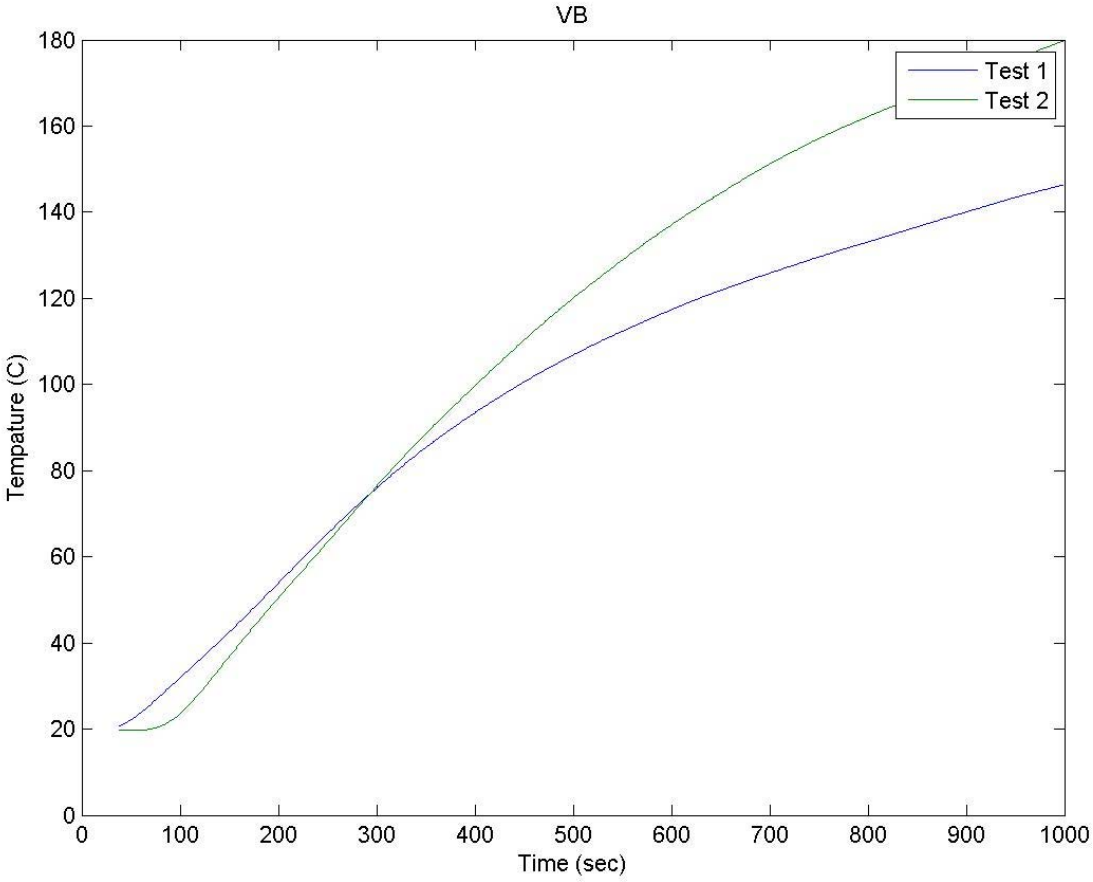
VB
Test 1
Test 2
Tempature (C)
Time (sec)
0
20
40
60
80
100
120
140
160
180
0
100
200
300
400
500
600
700
800
900
1000

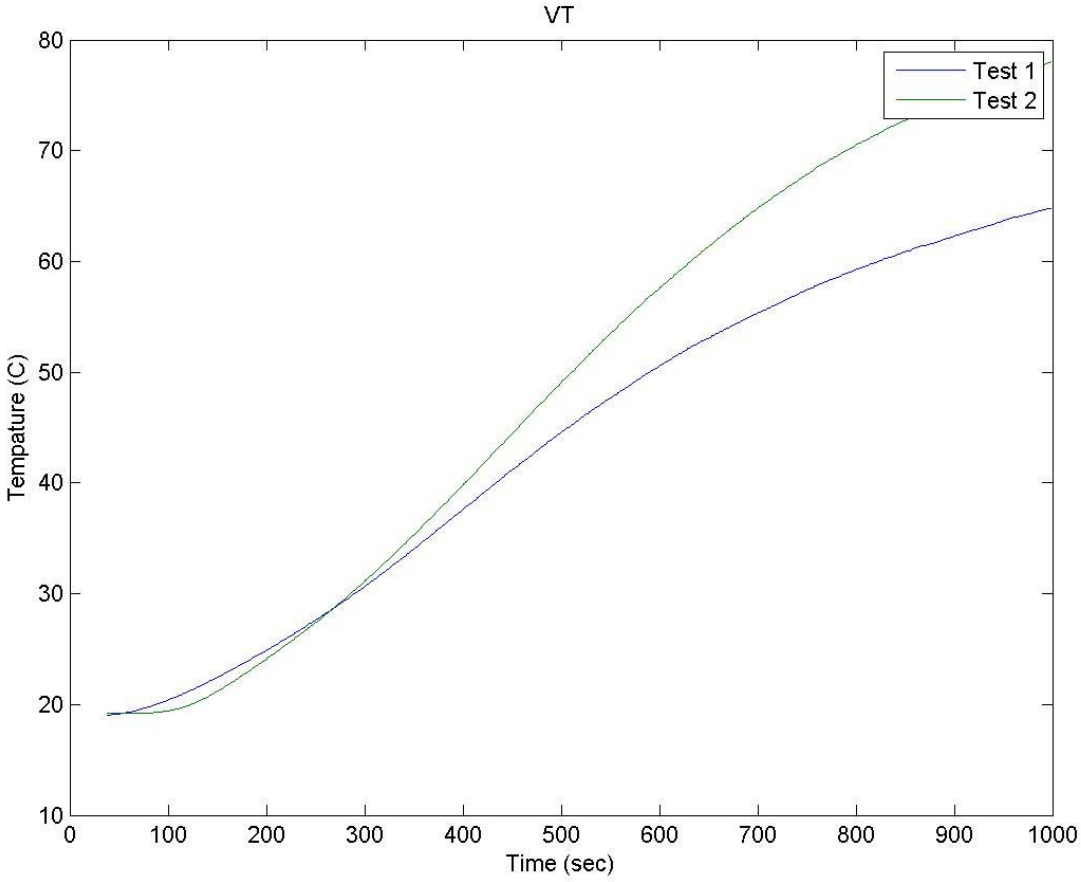
VT
Test 1
Test 2
Tempature (C)
Time (sec)
80
70
60
50
40
30
20
10
0
100
200
300
400
500
600
700
800
900
1000

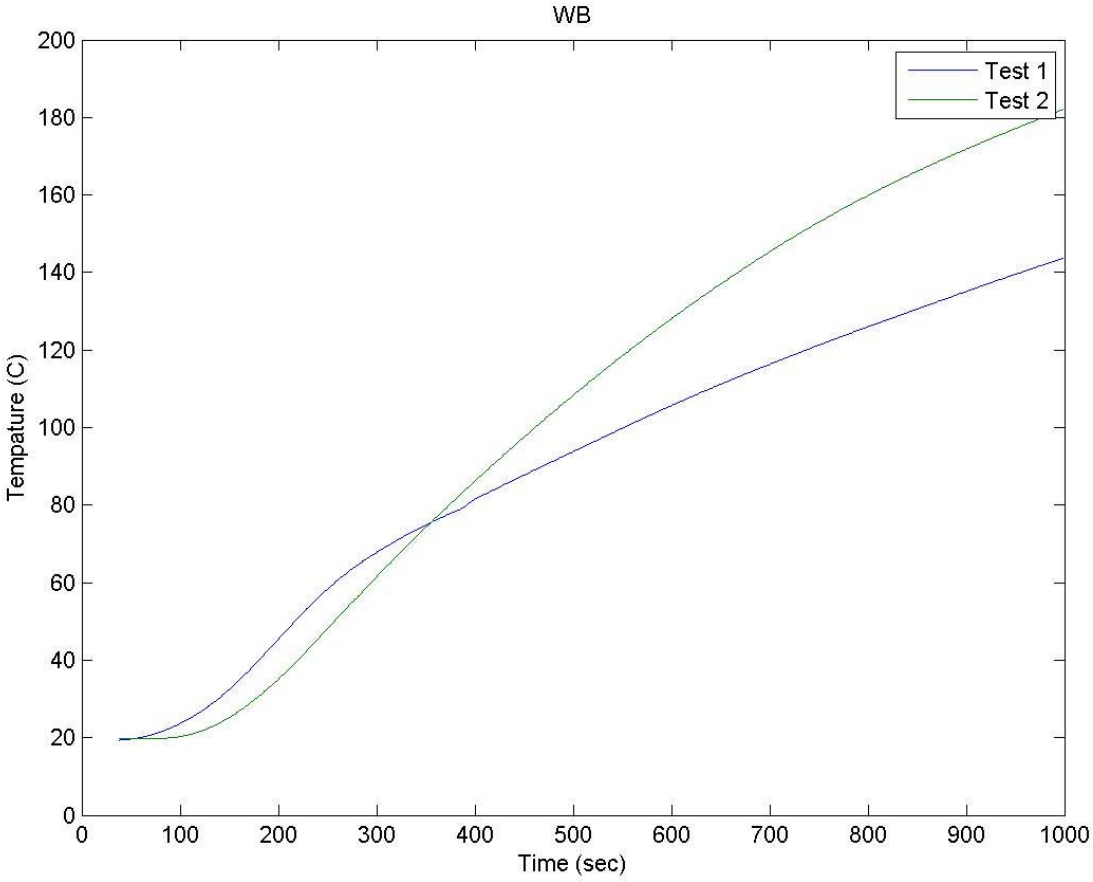
WB
Test 1
Test 2
Tempature (C)
Time (sec)
0
20
40
60
80
100
120
140
160
180
200
0
100
200
300
400
500
600
700
800
900
1000

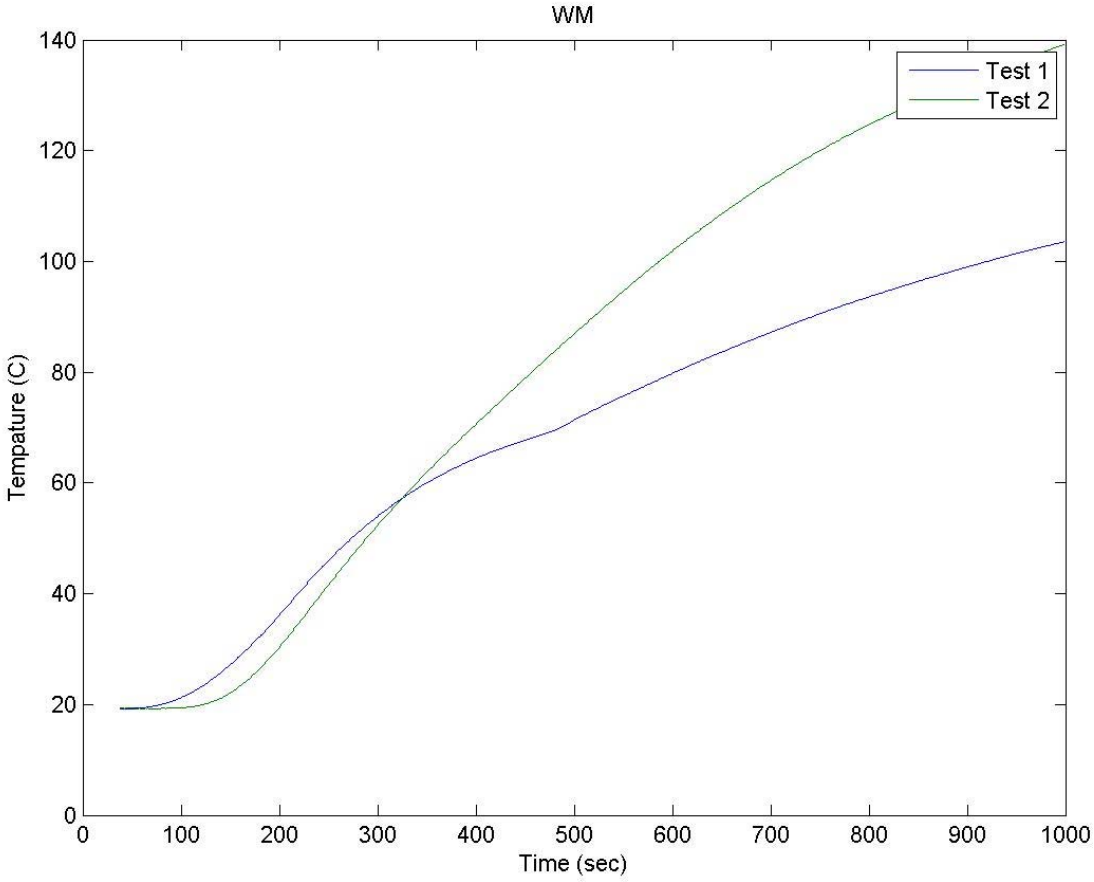
WM
Test 1
Test 2
Tempature (C)
Time (sec)
0
20
40
60
80
100
120
140
0
100
200
300
400
500
600
700
800
900
1000

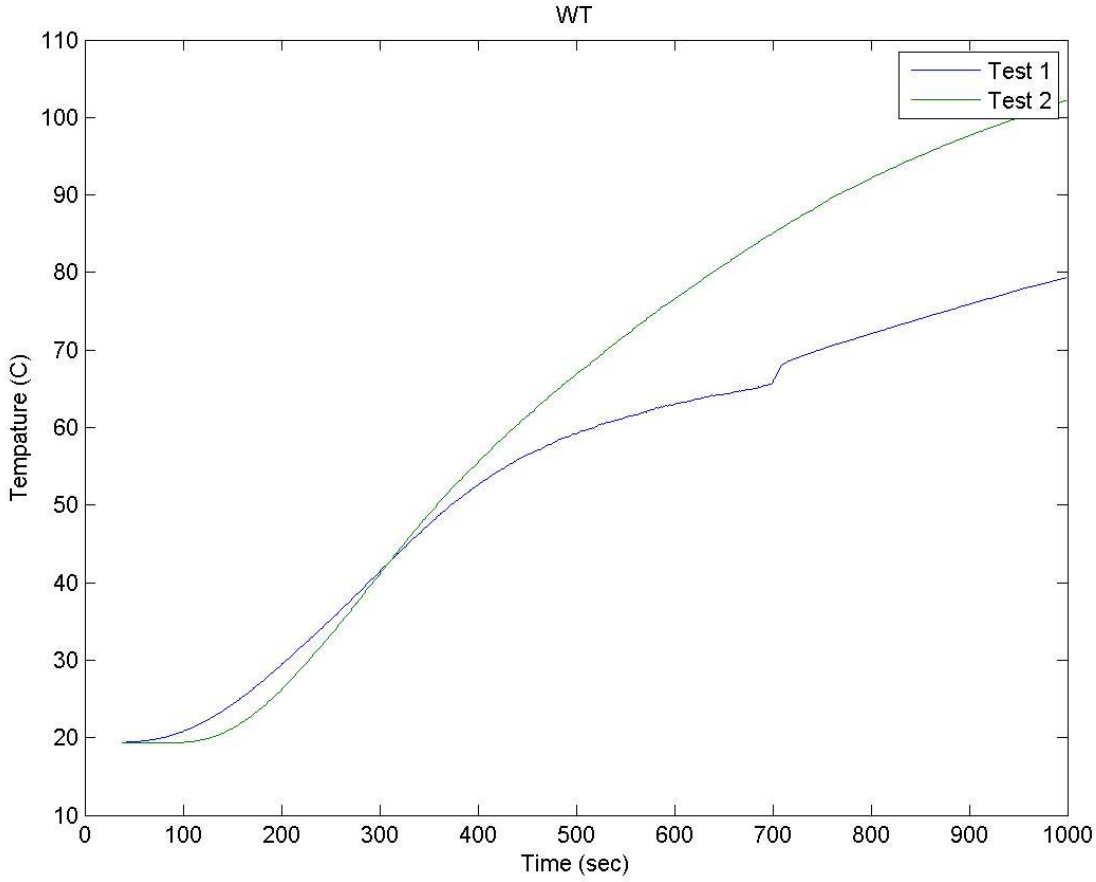
WT
Test 1
Test 2
Tempature (C)
Time (sec)
110
100
90
80
70
60
50
40
30
20
10
0
100
200
300
400
500
600
700
800
900
1000

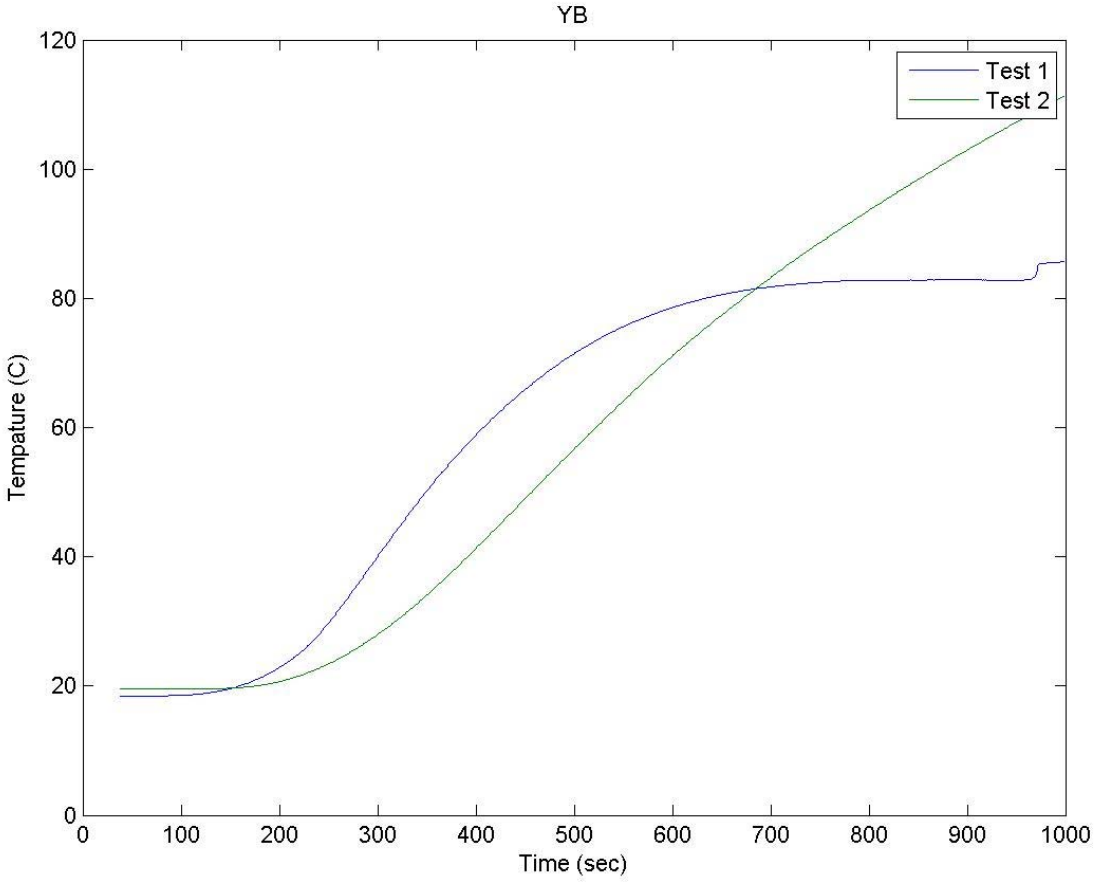
YB
Test 1
Test 2
Tempature (C)
Time (sec)
0
20
40
60
80
100
120
0
100
200
300
400
500
600
700
800
900
1000

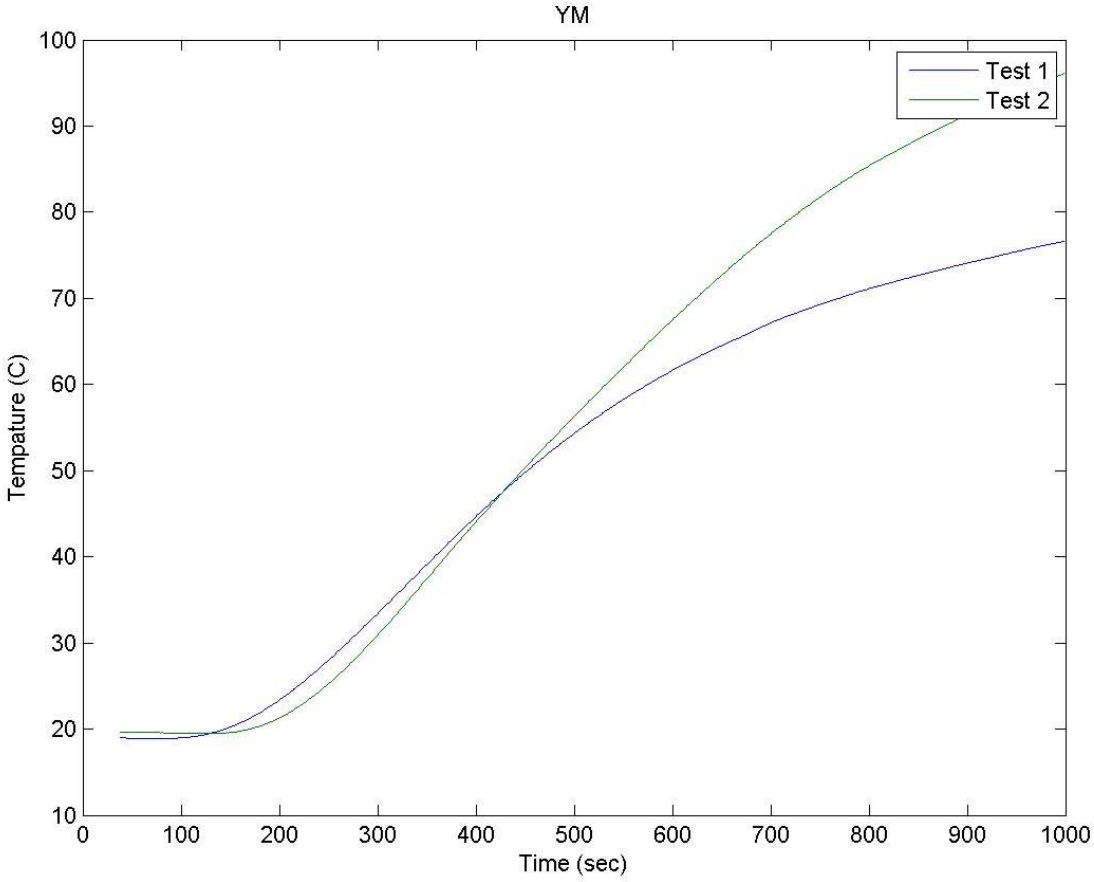
YM
Test 1
Test 2
Tempature (C)
Time (sec)
100
90
80
70
60
50
40
30
20
10
0
100
200
300
400
500
600
700
800
900
1000

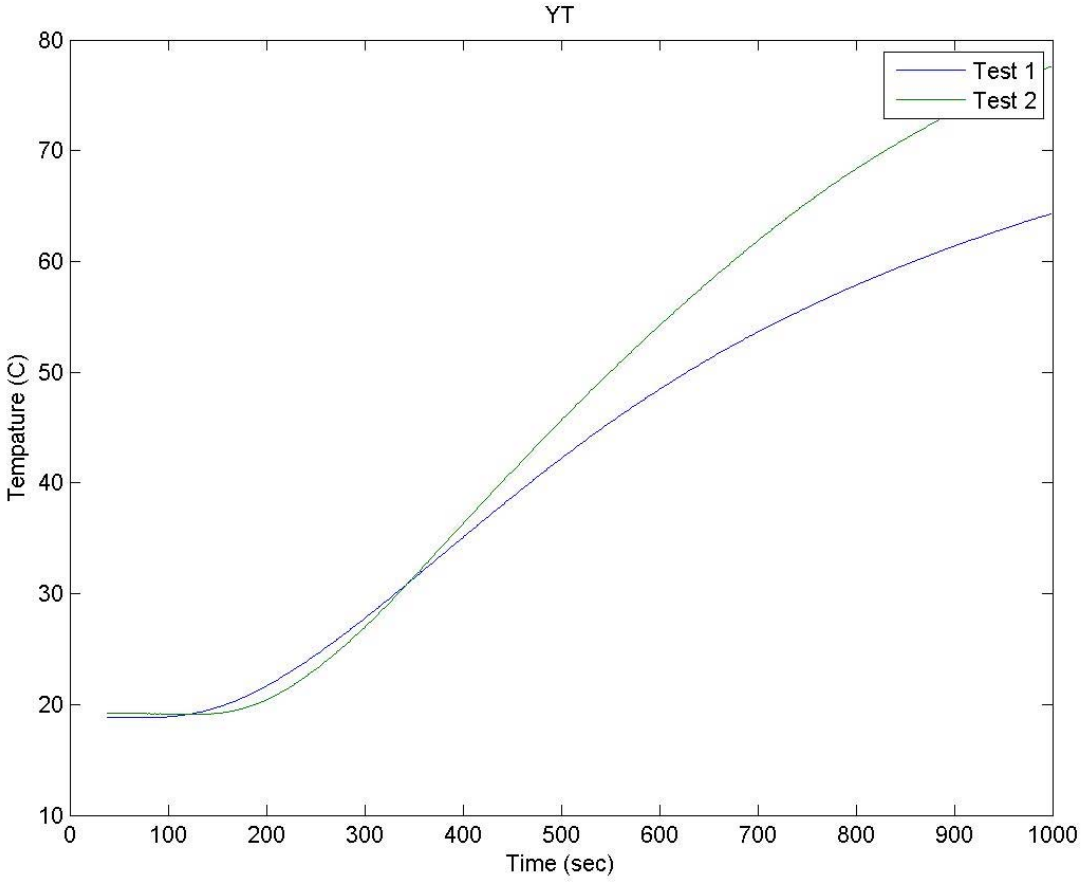
YT
Test 1
Test 2
Tempature (C)
Time (sec)
80
70
60
50
40
30
20
10
0
100
200
300
400
500
600
700
800
900
1000

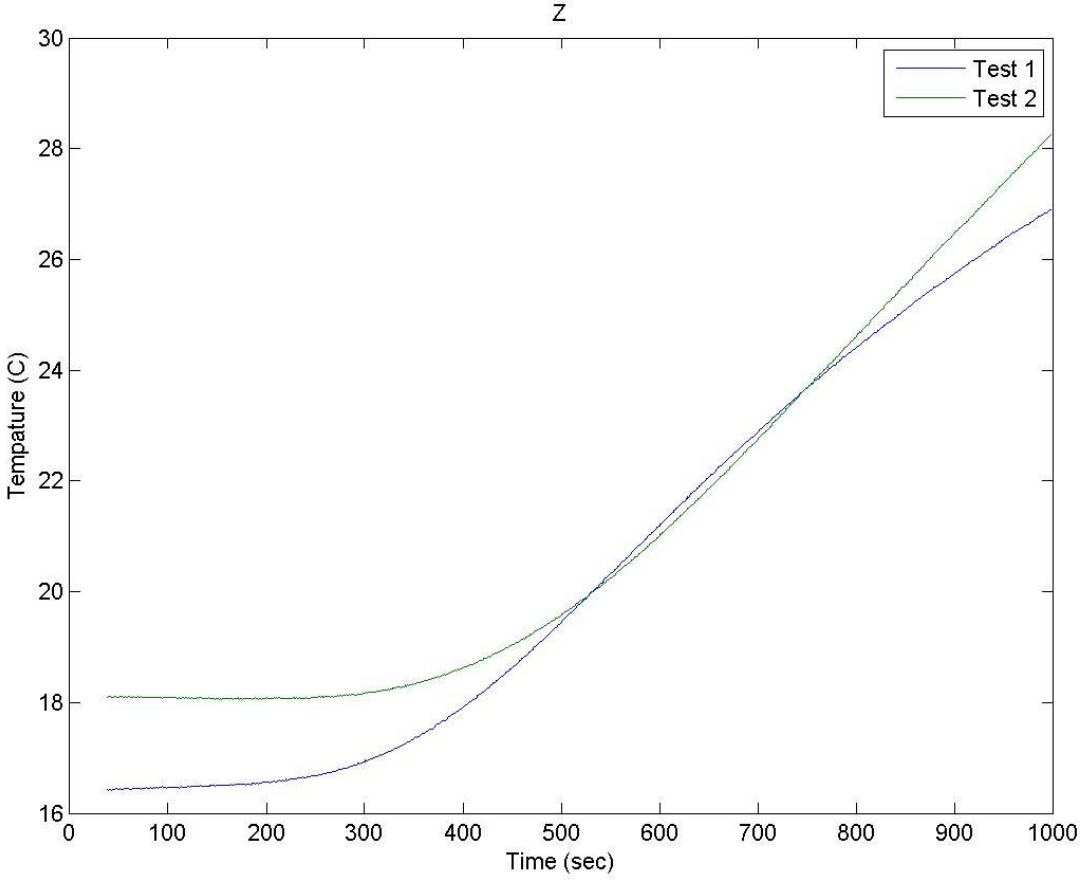
Z
Test 1
Test 2
Tempature (C)
Time (sec)
30
28
26
24
22
20
18
16
0
100
200
300
400
500
600
700
800
900
1000

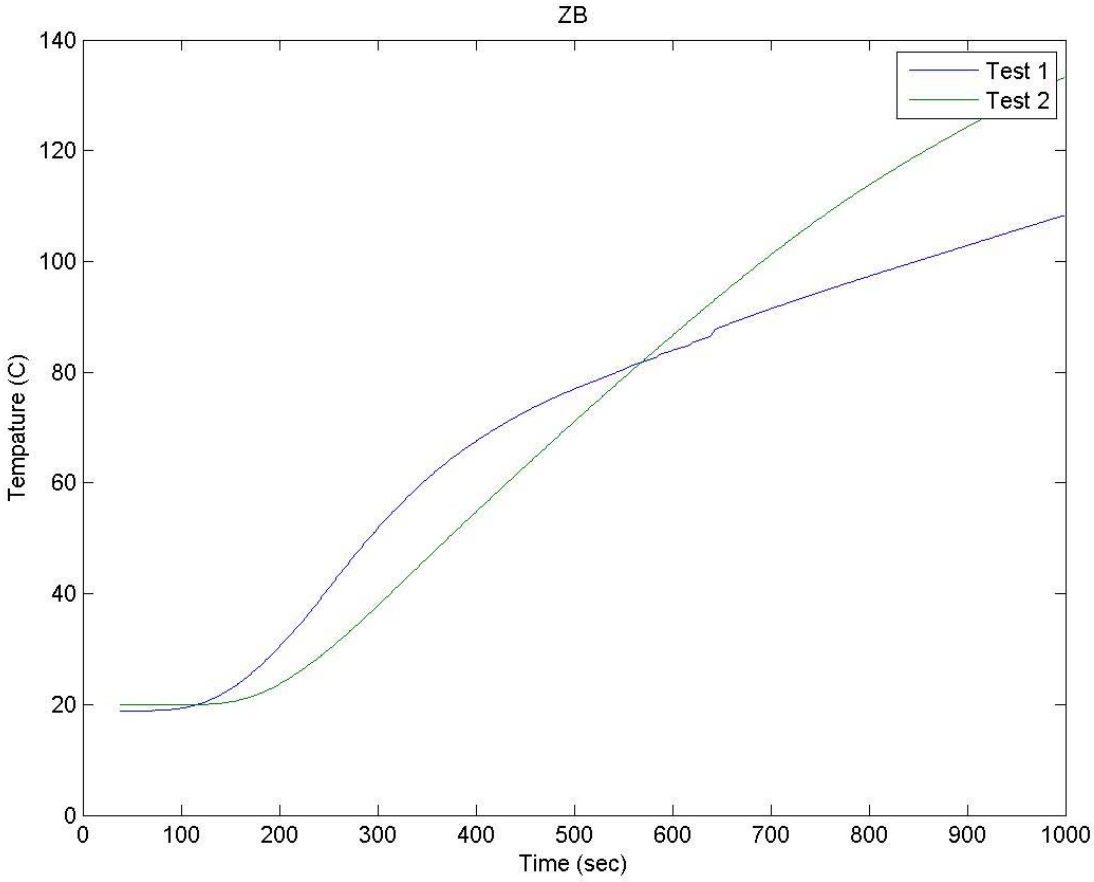
ZB
Test 1
Test 2
Tempature (C)
Time (sec)
0
20
40
60
80
100
120
140
0
100
200
300
400
500
600
700
800
900
1000

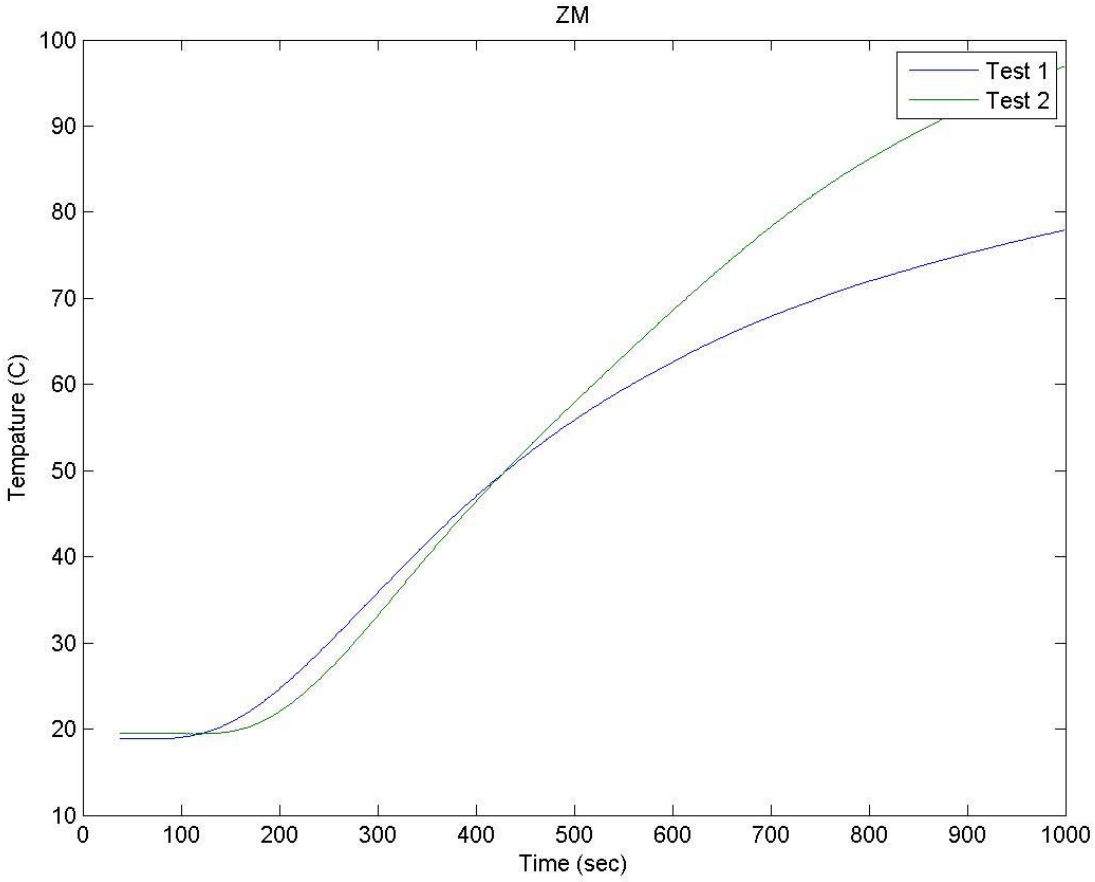
ZM
Test 1
Test 2
Tempature (C)
Time (sec)
100
90
80
70
60
50
40
30
20
10
0
100
200
300
400
500
600
700
800
900
1000

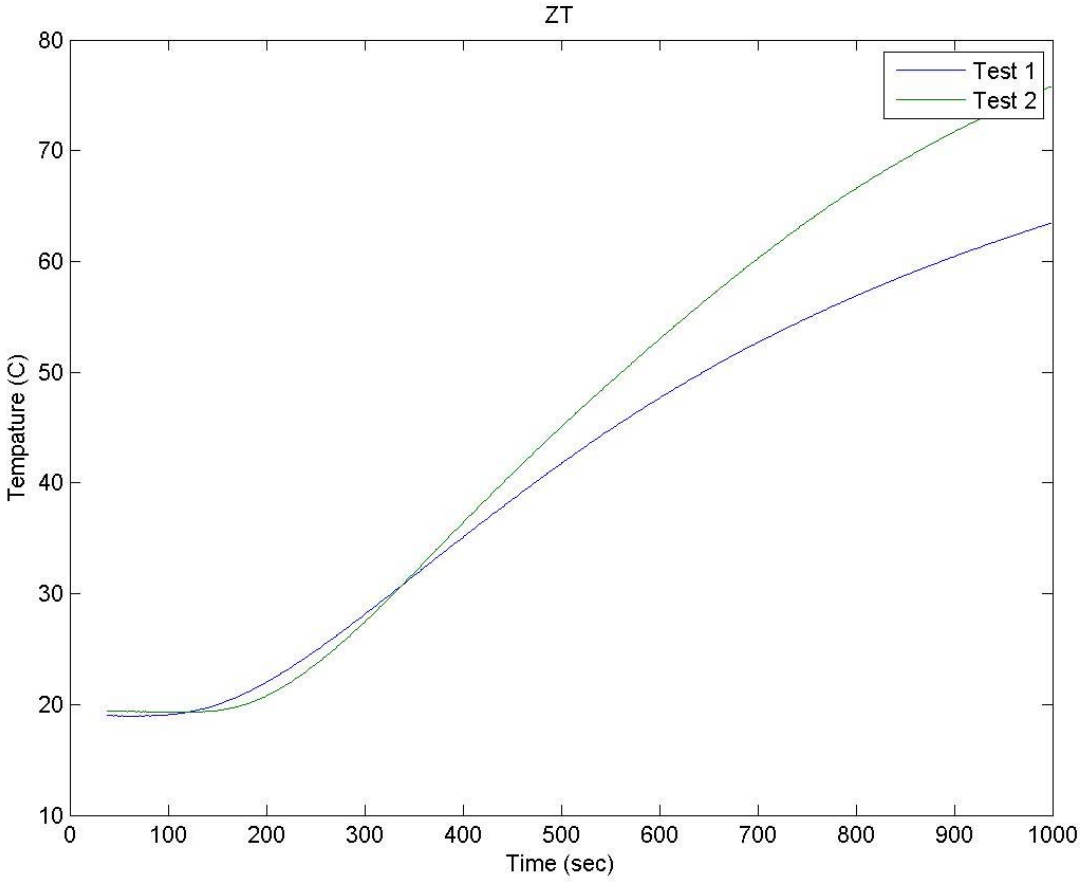

The following graphs are for the two test that were ran on the coner joint.

Corner Joint Data

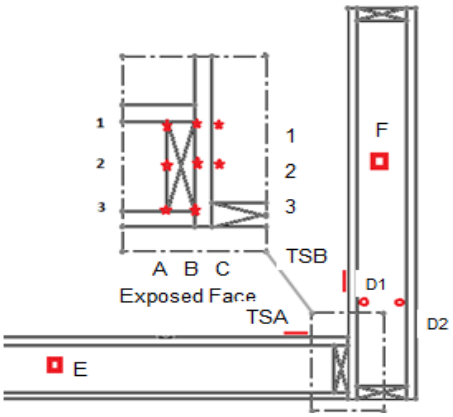

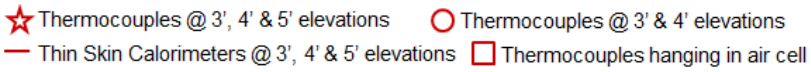

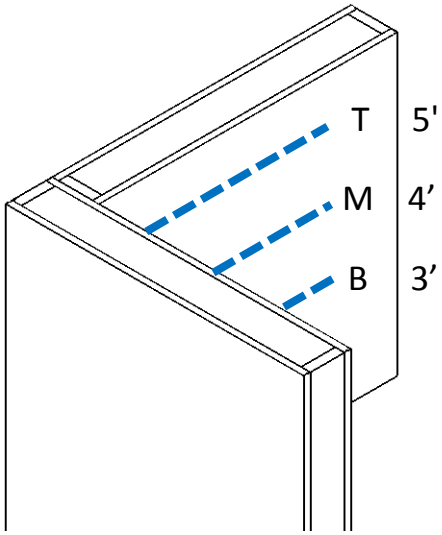

The above diagrams show the location of each instrument. If we are describing a thermocouple, the graph title will have two letters. The first letter of the title will designate the location of the instrument within the panel and can be seen in the top diagram. The second letter represents the elevation at which the instrument is located relative to the floor and may be seen in the bottom diagram. For think skin calorimeters, the first three letters before the dash designate the location of the instrument within the panel and can be seen in the top diagram. The letter after the dash represents the elevation at which the instrument is located relative to the floor and may be seen in the bottom diagram. Thermocouple E and F are at a single elevation of 4 to 5 feet and represented by just their letter. The following graphs are temperature vs. time of the two experiments conducted, indicated by the legend.

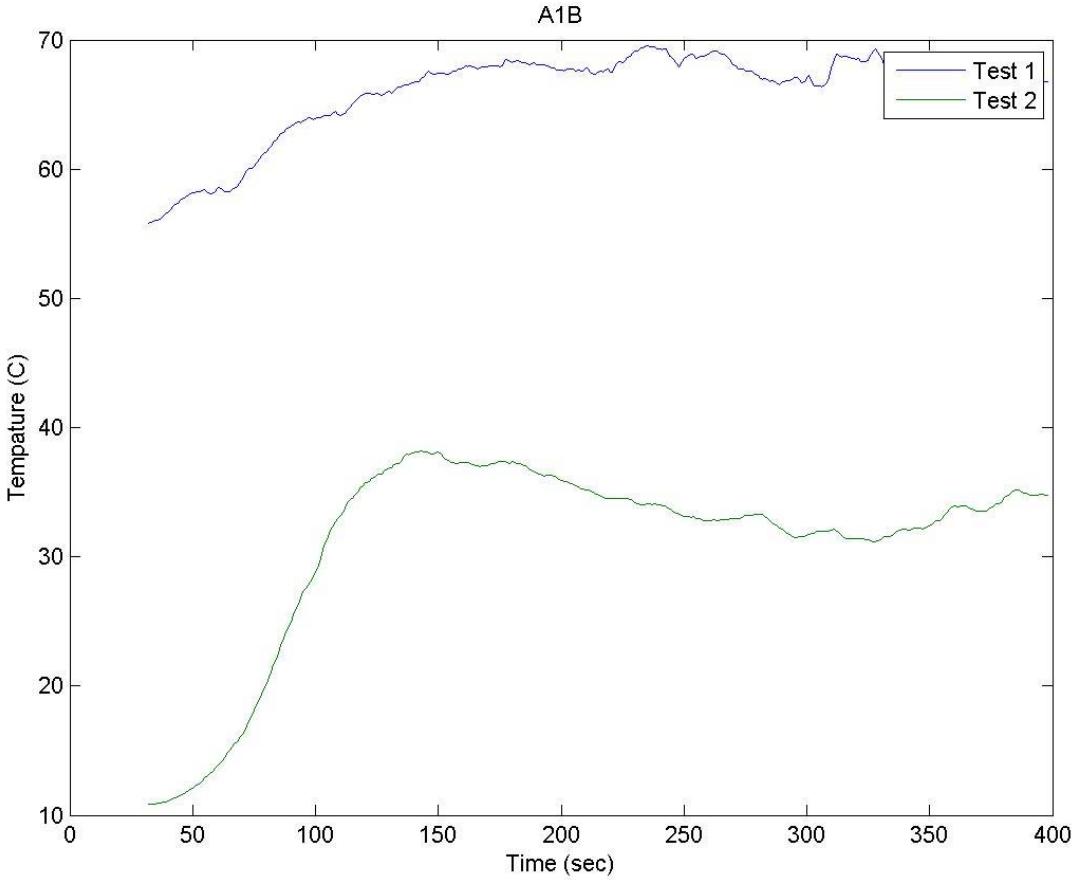
A1B
Test 1
Test 2
Tempature (C)
Time (sec)
70
60
50
40
30
20
10
0
50
100
150
200
250
300
350
400

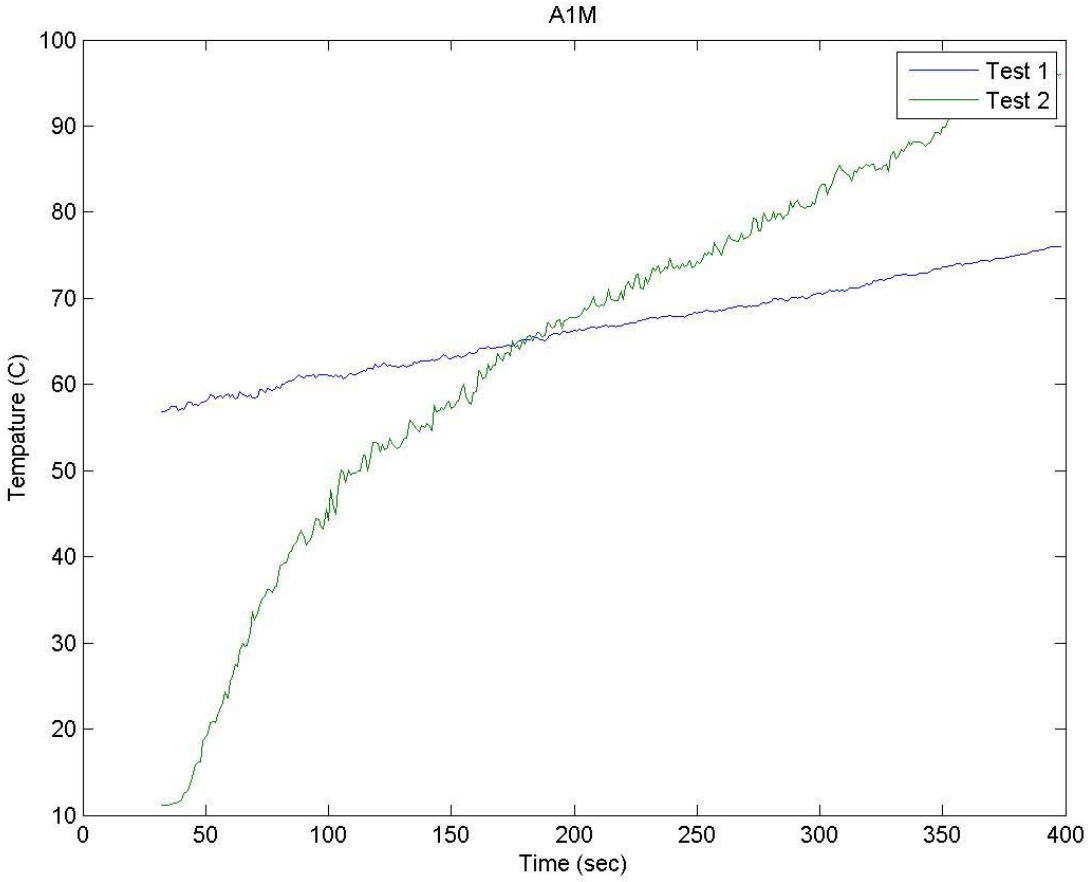
A1M
Test 1
Test 2
Tempature (C)
Time (sec)
100
90
80
70
60
50
40
30
20
10
0
50
100
150
200
250
300
350
400

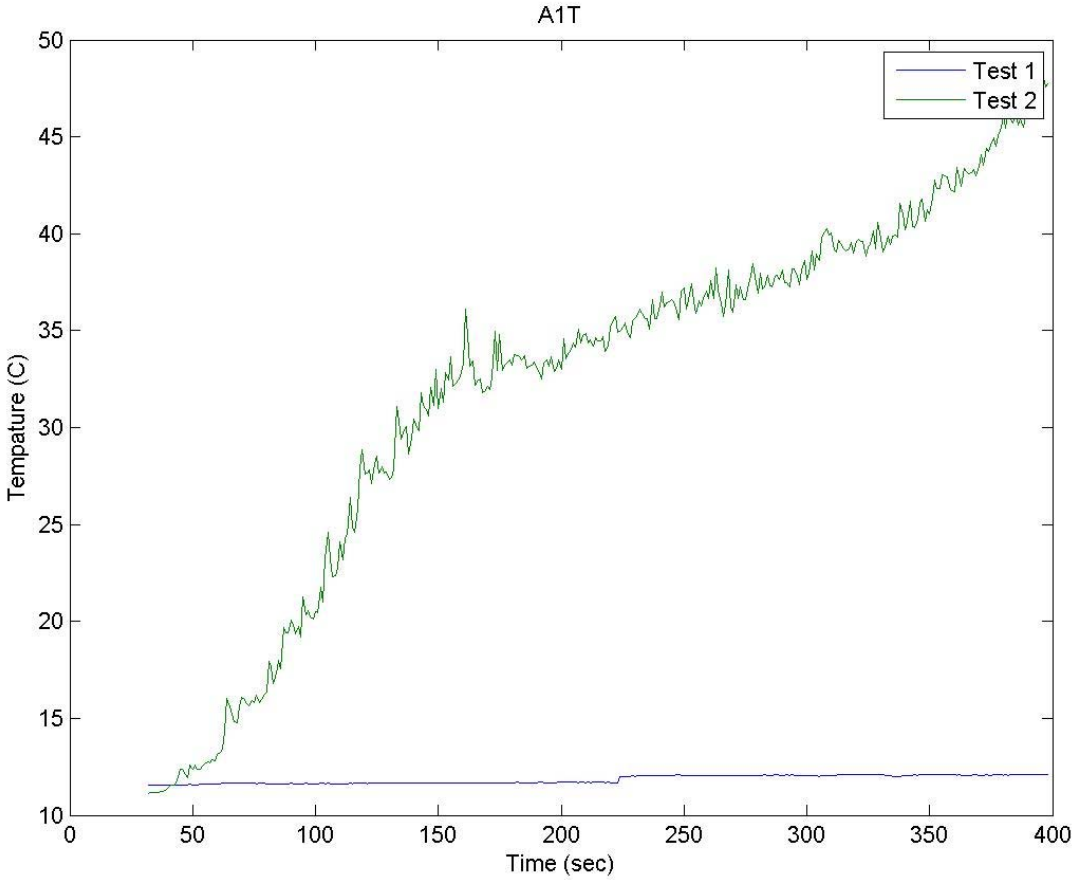
A1T
Test 1
Test 2
Tempature (C)
Time (sec)
50
45
40
35
30
25
20
15
10
0
50
100
150
200
250
300
350
400

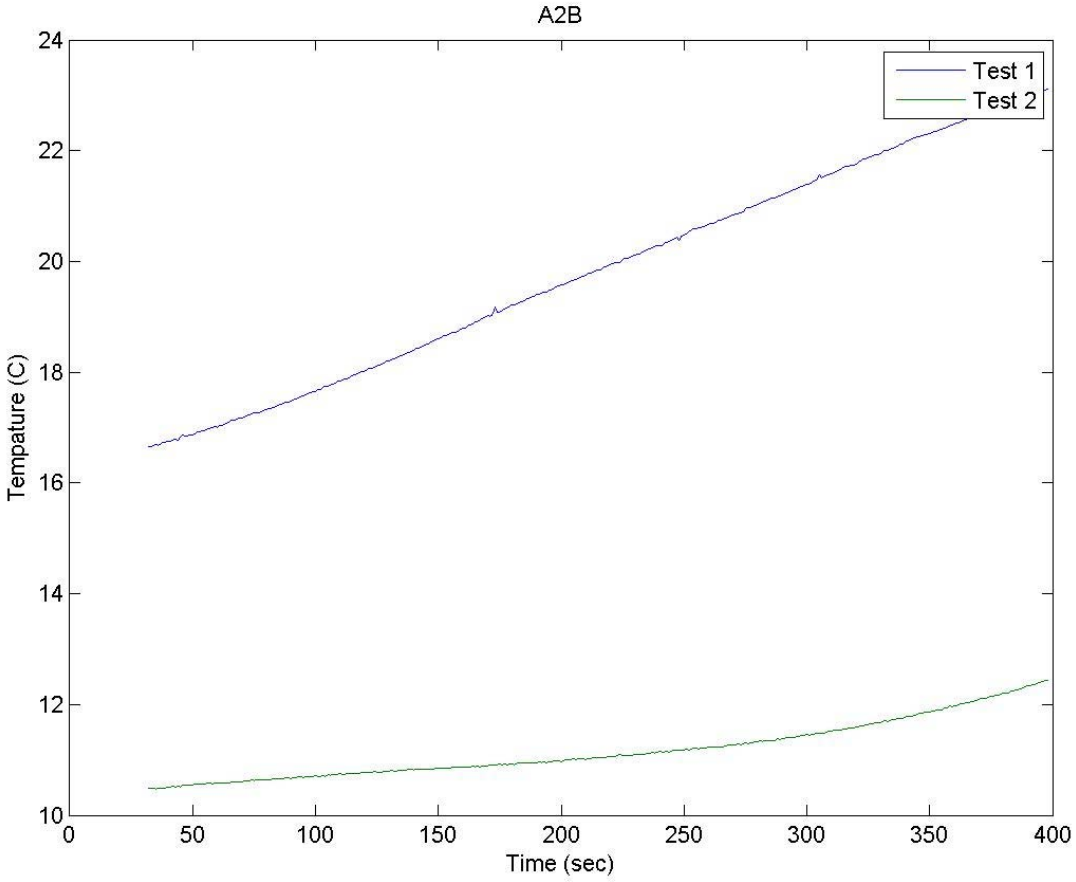
A2B
Test 1
Test 2
Tempature (C)
Time (sec)
24
22
20
18
16
14
12
10
0
50
100
150
200
250
300
350
400

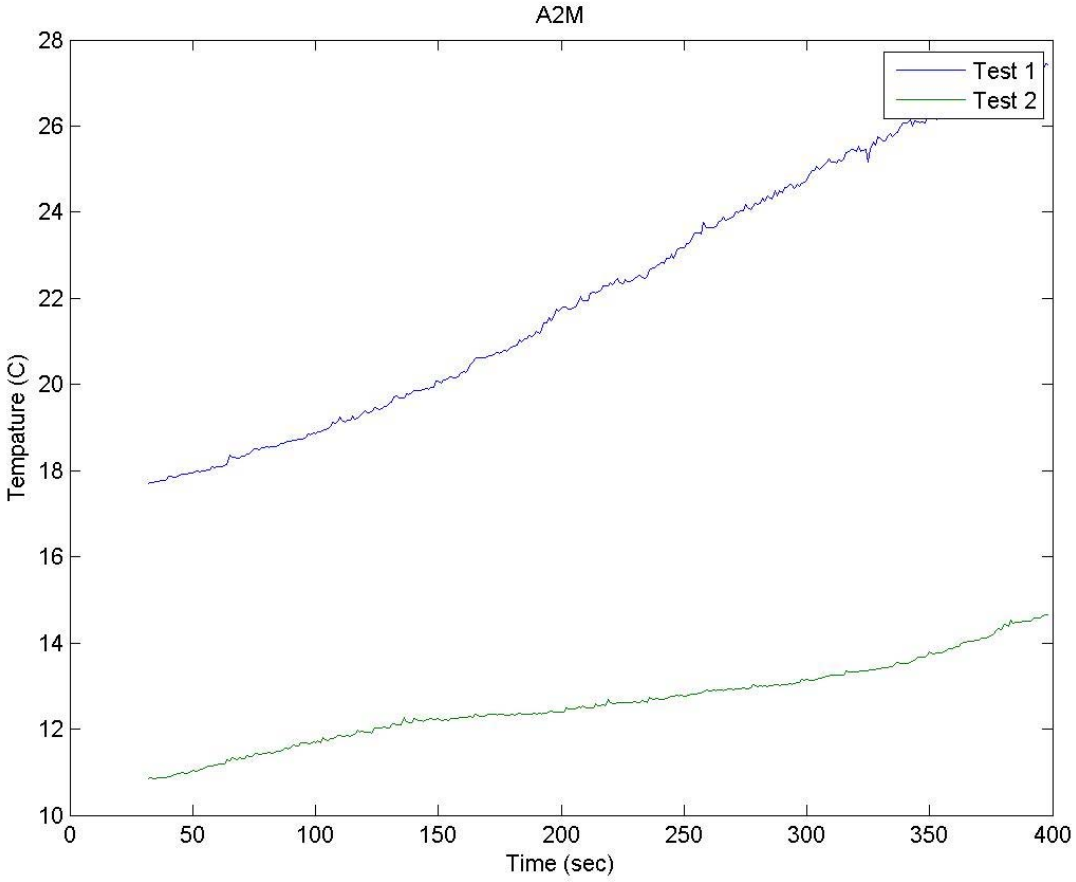
A2M
Test 1
Test 2
Tempature (C)
Time (sec)
28
26
24
22
20
18
16
14
12
10
0
50
100
150
200
250
300
350
400

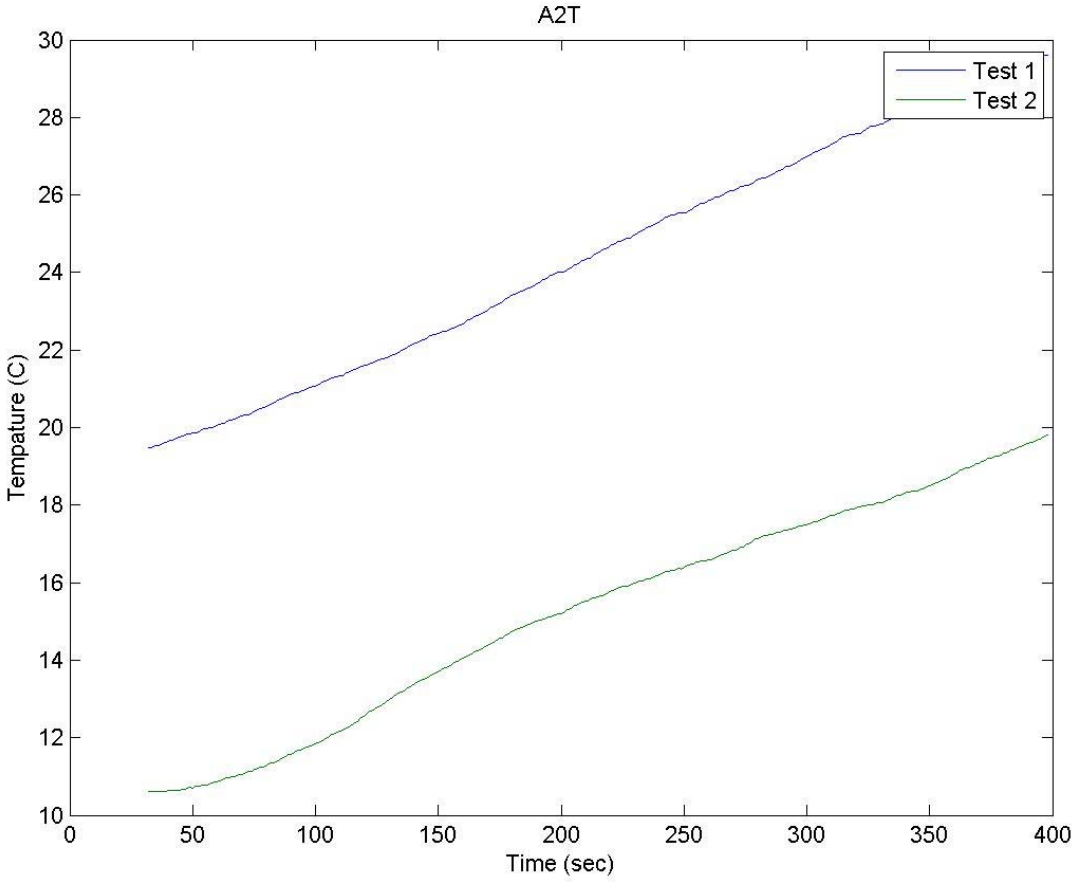
A2T
Test 1
Test 2
Tempature (C)
Time (sec)
30
28
26
24
22
20
18
16
14
12
10
0
50
100
150
200
250
300
350
400

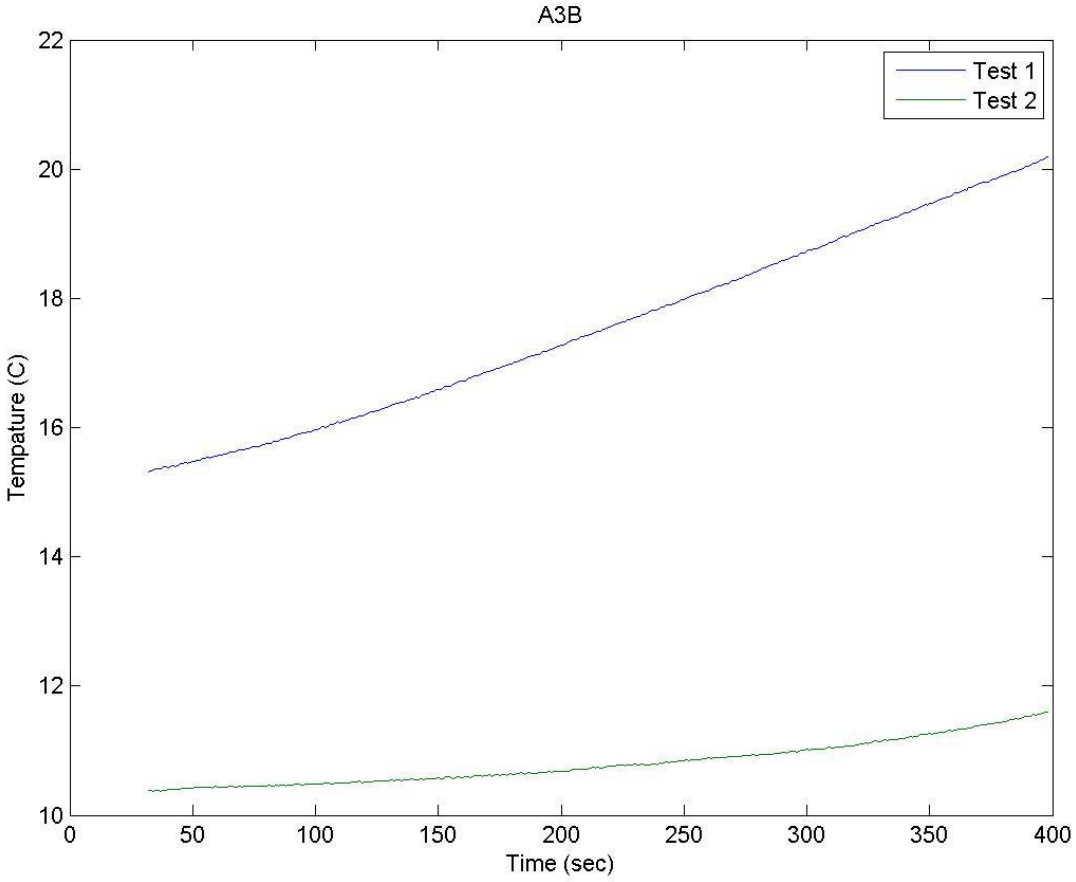
A3B
Test 1
Test 2
Tempature (C)
Time (sec)
22
20
18
16
14
12
10
0
50
100
150
200
250
300
350
400

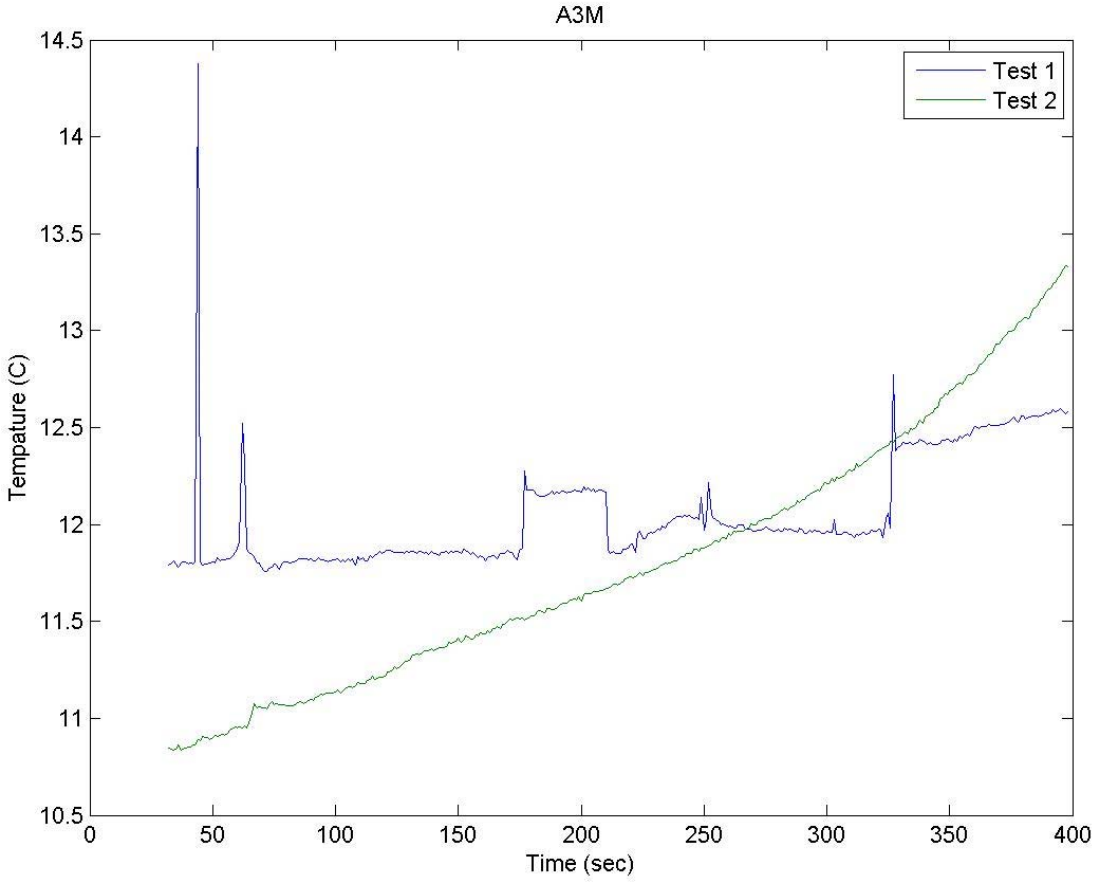
A3M
Test 1
Test 2
Tempature (C)
Time (sec)
14.5
14
13.5
13
12.5
12
11.5
11
10.5
0
50
100
150
200
250
300
350
400

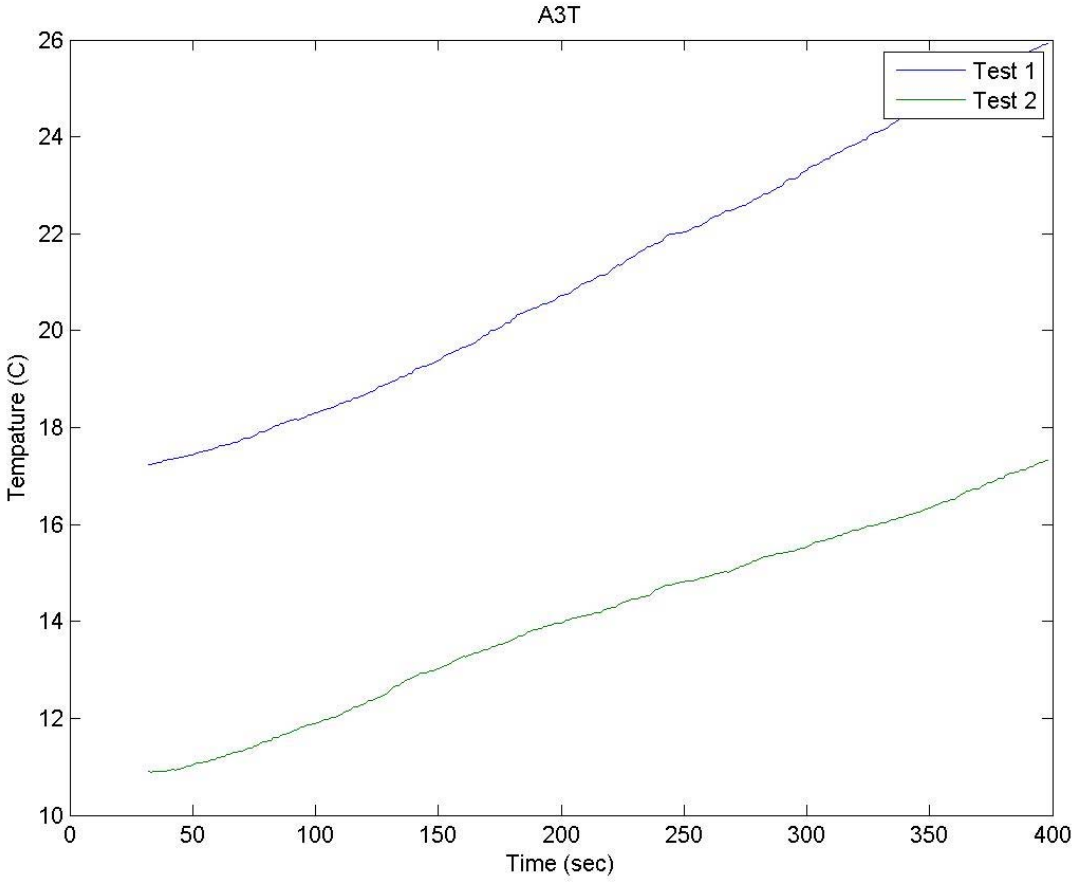
A3T
Test 1
Test 2
Tempature (C)
Time (sec)
26
24
22
20
18
16
14
12
10
0
50
100
150
200
250
300
350
400

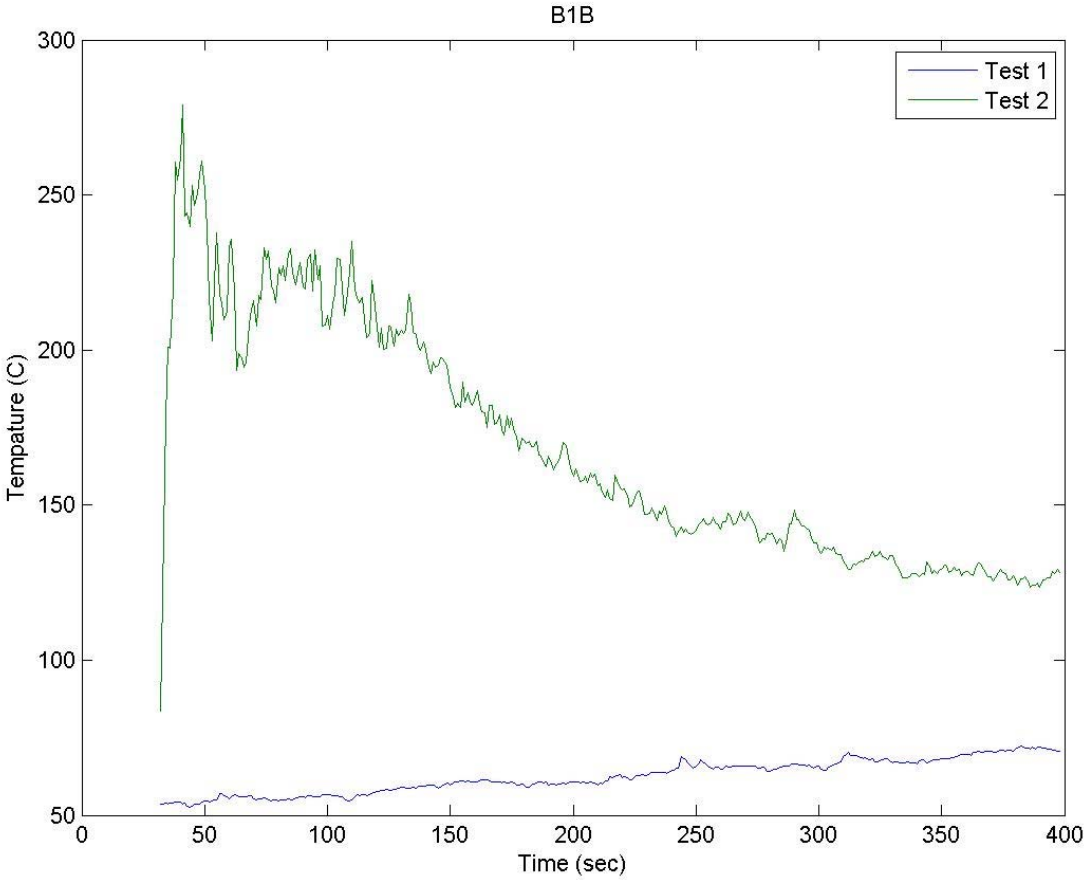
B1B
Test 1
Test 2
Tempature (C)
Time (sec)
300
250
200
150
100
50
0
50
100
150
200
250
300
350
400

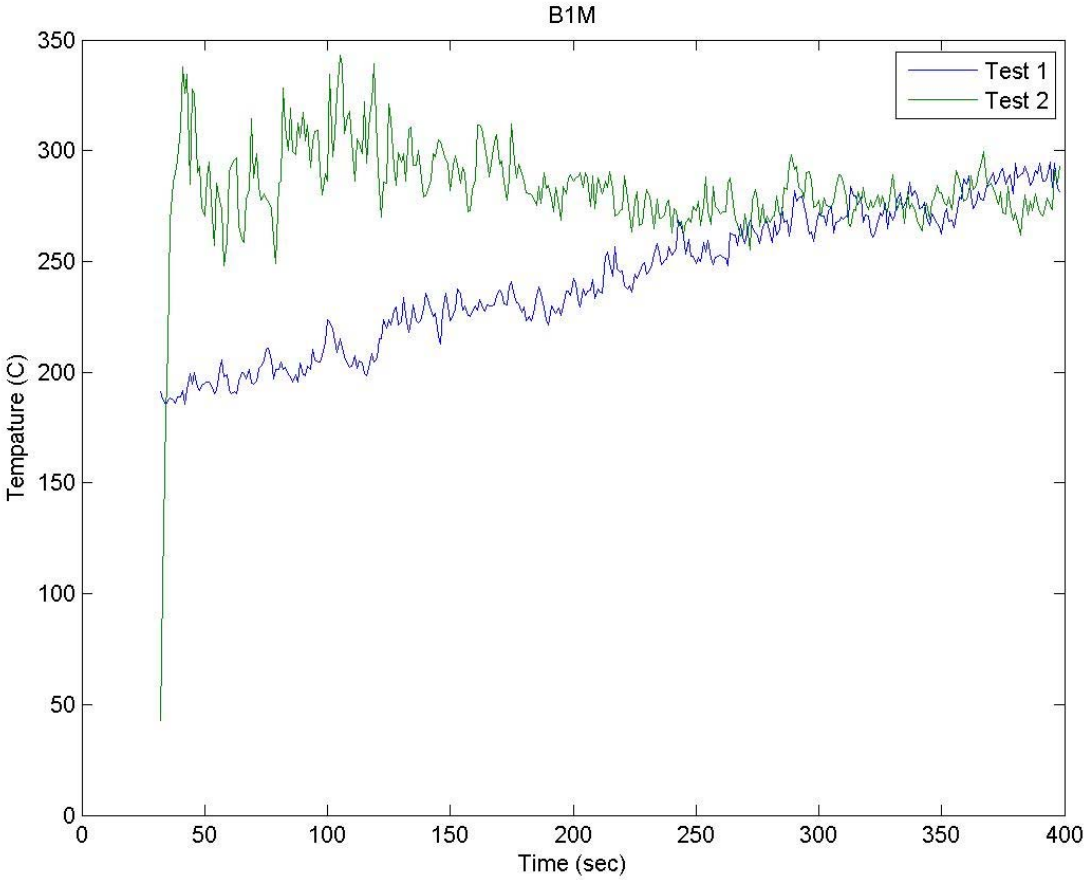
B1M
Test 1
Test 2
Tempature (C)
Time (sec)
0
50
100
150
200
250
300
350
400

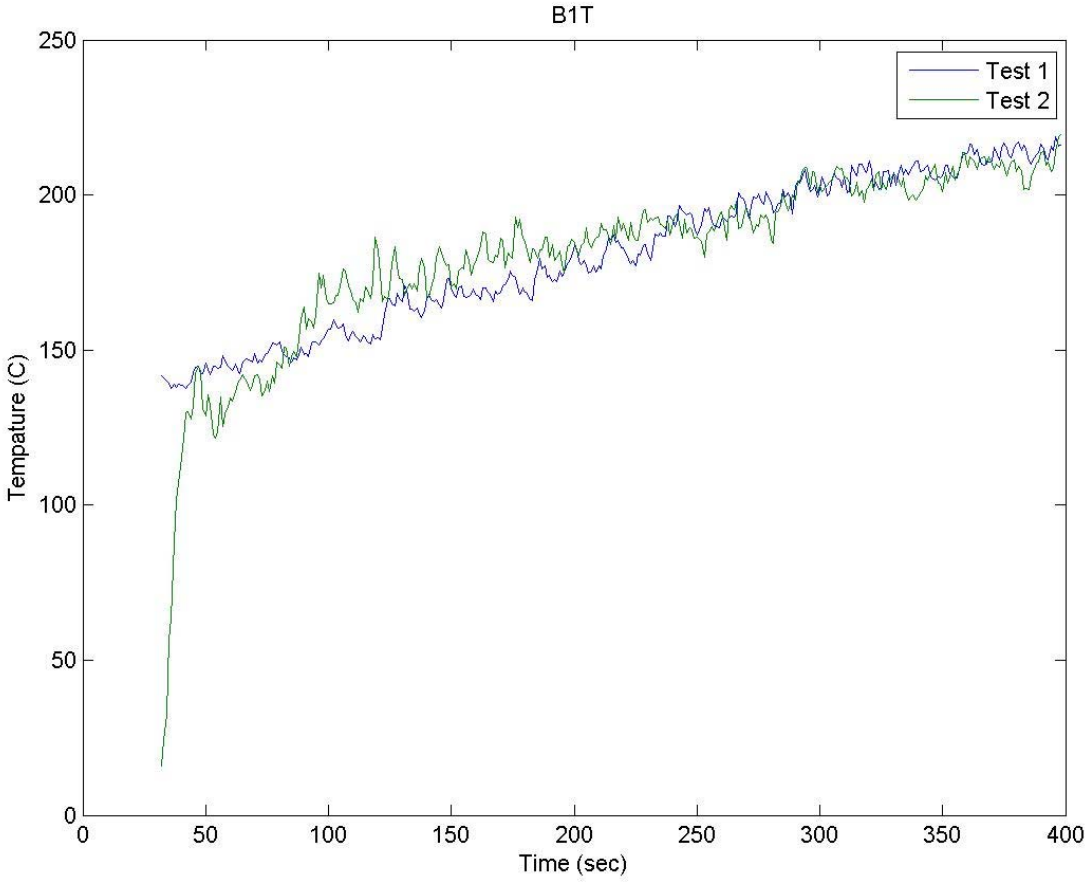
B1T
Test 1
Test 2
Tempature (C)
Time (sec)
0
50
100
150
200
250
300
350
400

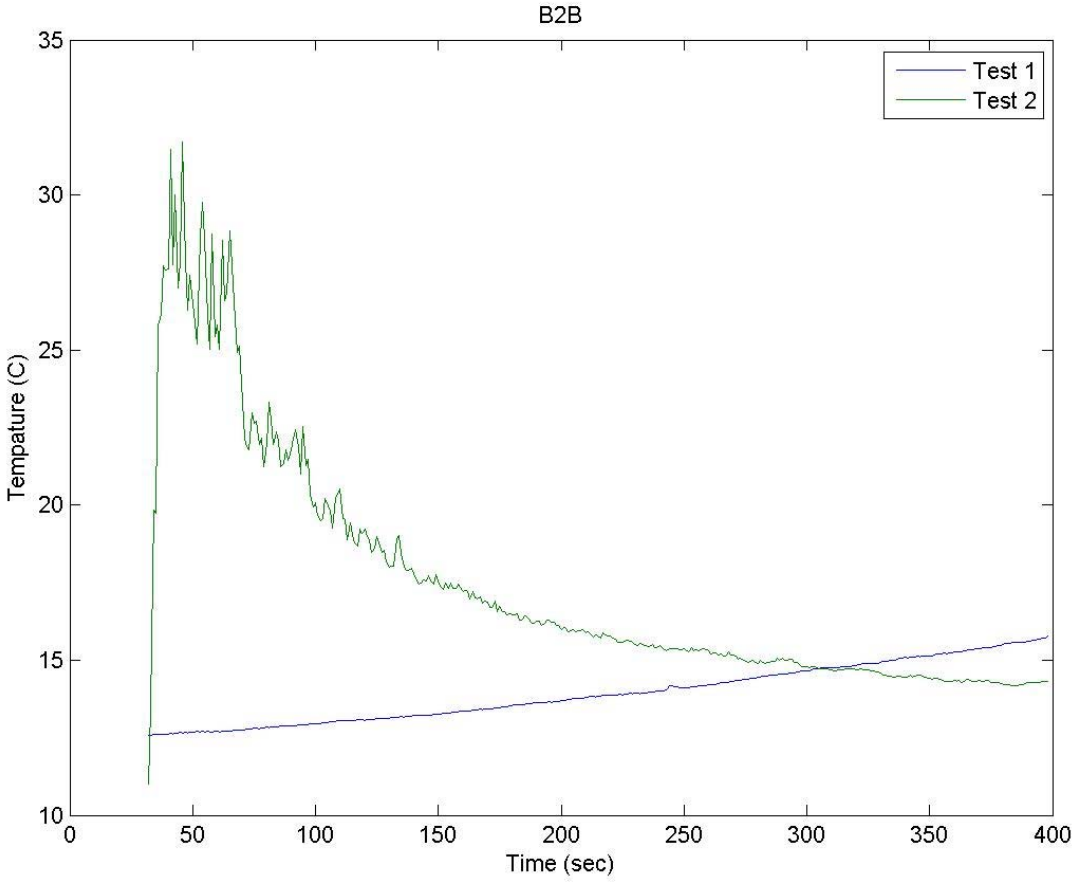
B2B
Test 1
Test 2
Tempature (C)
Time (sec)
35
30
25
20
15
10
0
50
100
150
200
250
300
350
400

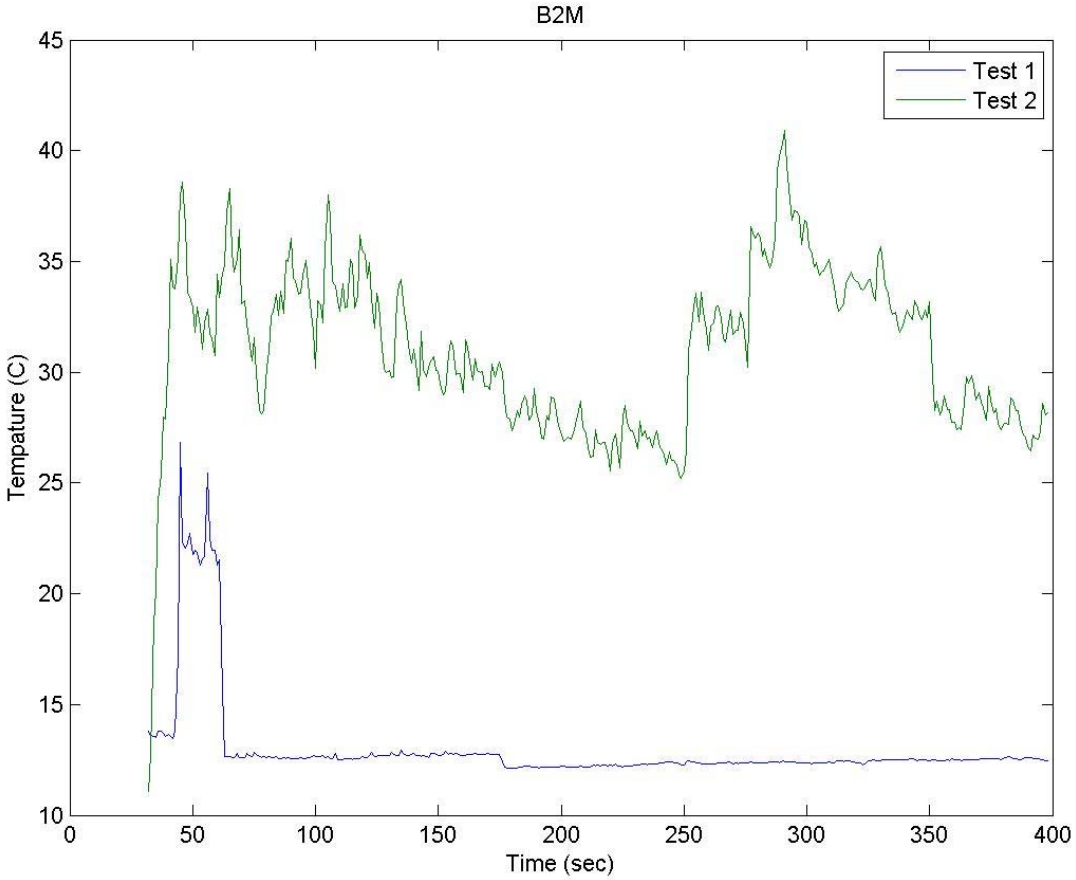
B2M
Test 1
Test 2
Tempature (C)
Time (sec)
45
40
35
30
25
20
15
10
0
50
100
150
200
250
300
350
400

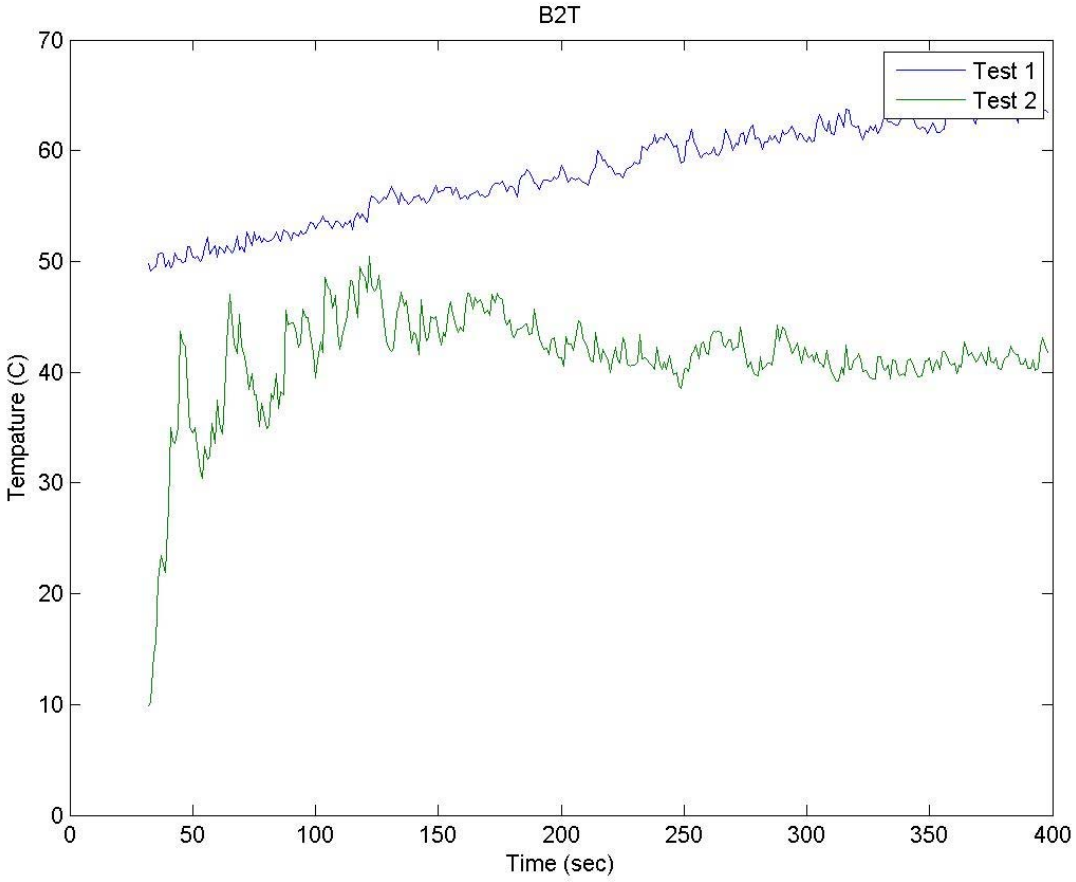
B2T
Test 1
Test 2
Tempature (C)
Time (sec)
0
10
20
30
40
50
60
70
0
50
100
150
200
250
300
350
400

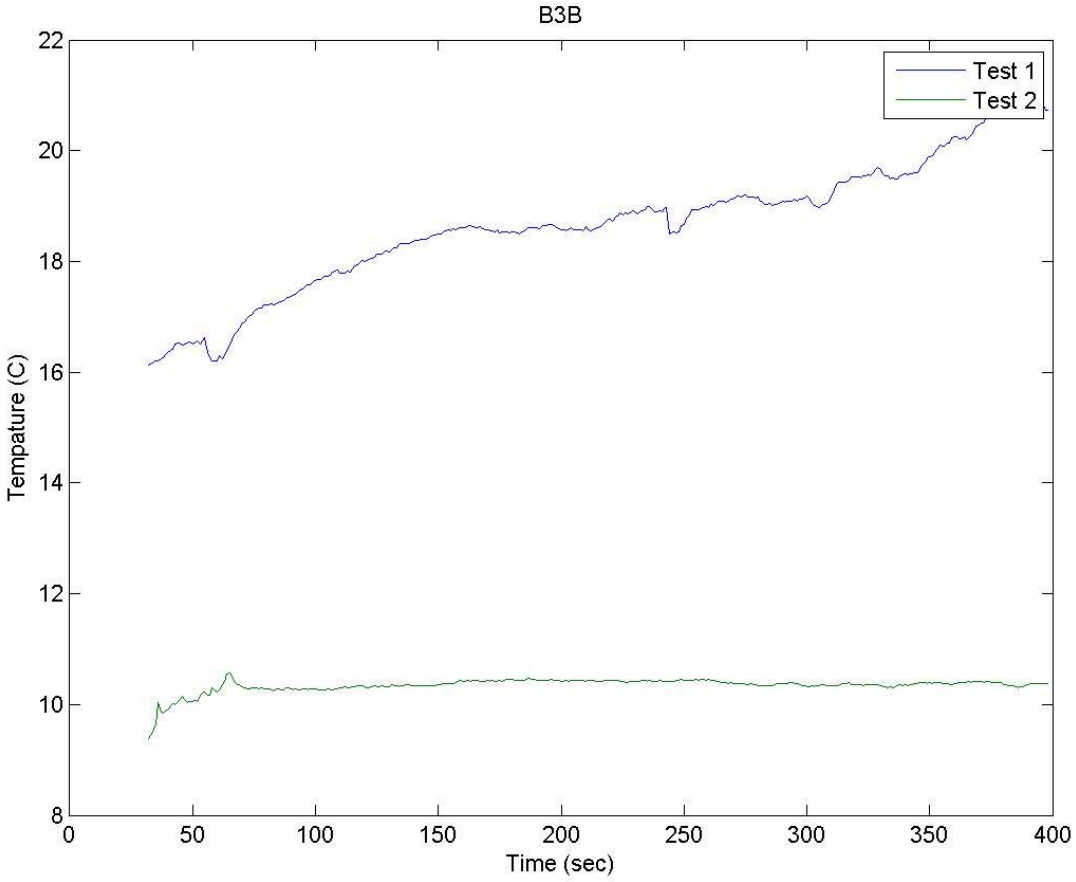
B3B
Test 1
Test 2
Tempature (C)
Time (sec)
22
20
18
16
14
12
10
8
0
50
100
150
200
250
300
350
400

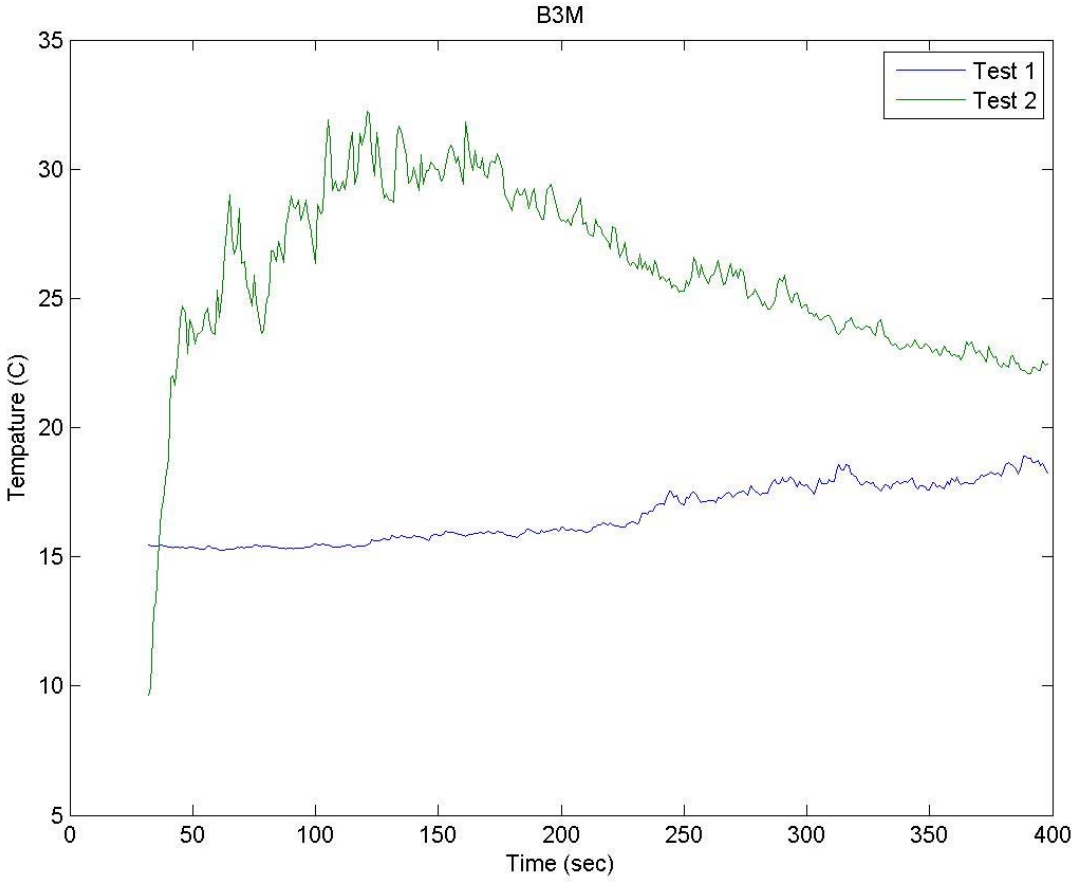
B3M
Test 1
Test 2
Tempature (C)
Time (sec)
35
30
25
20
15
10
5
0
50
100
150
200
250
300
350
400

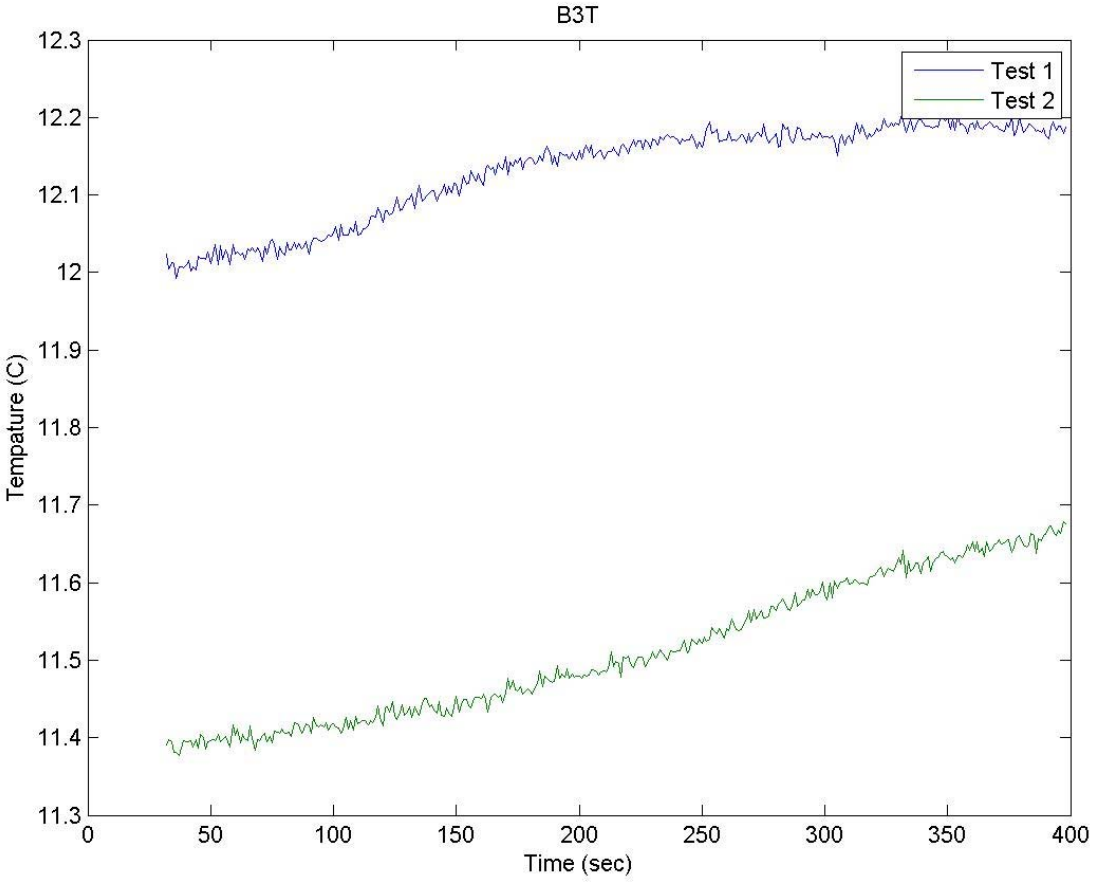
B3T
Test 1
Test 2
Tempature (C)
Time (sec)
12.3
12.2
12.1
12
11.9
11.8
11.7
11.6
11.5
11.4
11.3
0
50
100
150
200
250
300
350
400

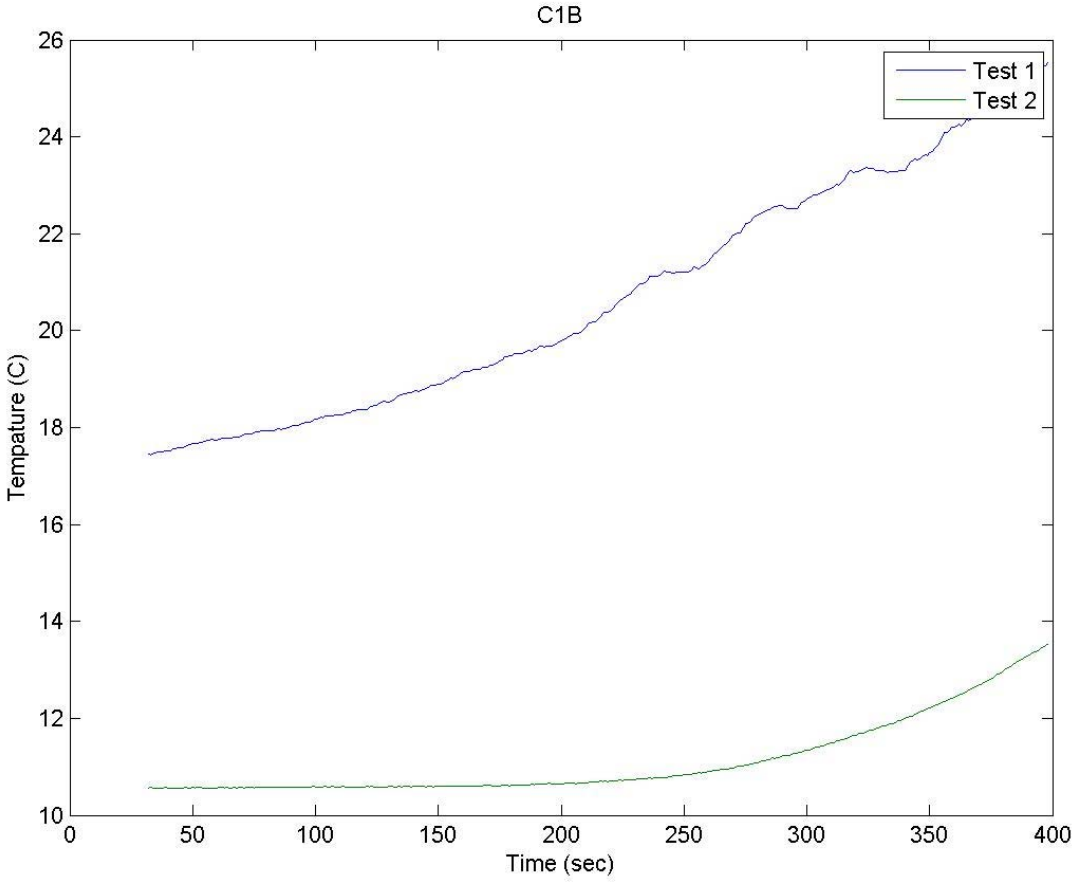
C1B
Test 1
Test 2
Tempature (C)
Time (sec)
26
24
22
20
18
16
14
12
10
0
50
100
150
200
250
300
350
400

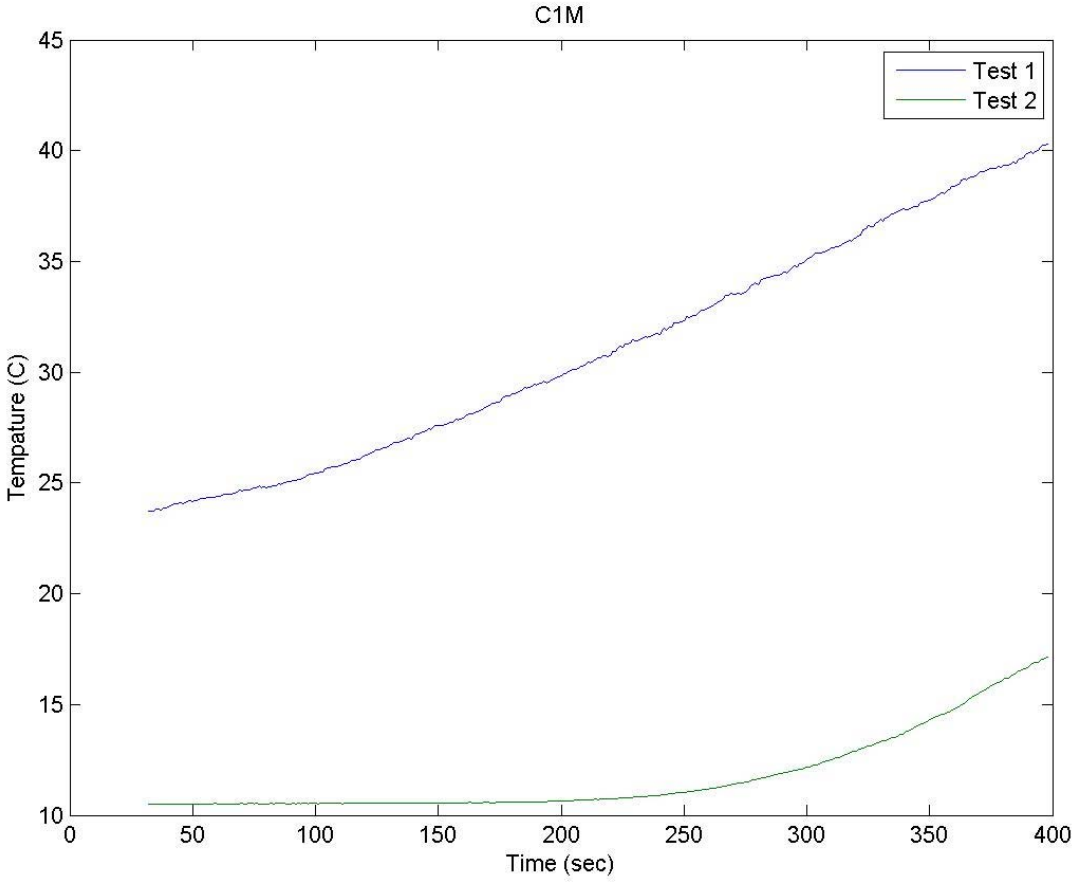
C1M
Test 1
Test 2
Tempature (C)
Time (sec)
45
40
35
30
25
20
15
10
0
50
100
150
200
250
300
350
400

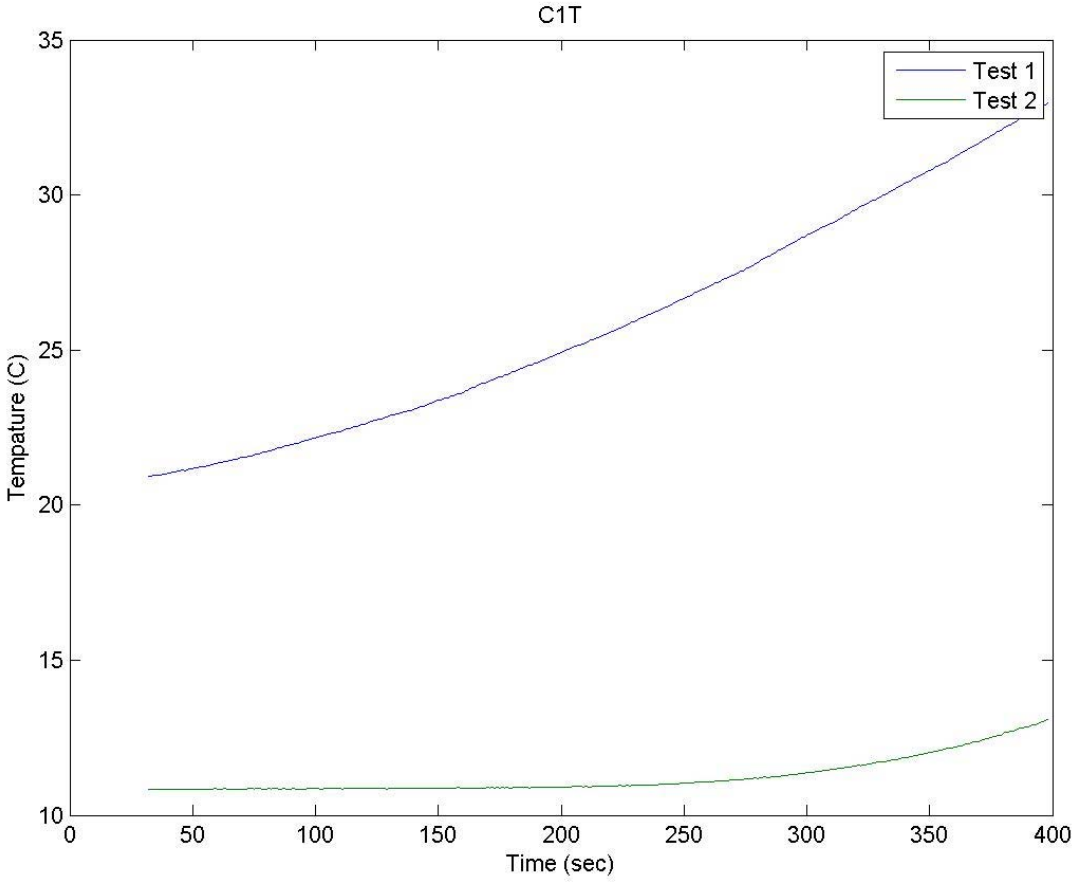
C1T
Test 1
Test 2
Tempature (C)
Time (sec)
35
30
25
20
15
10
0
50
100
150
200
250
300
350
400

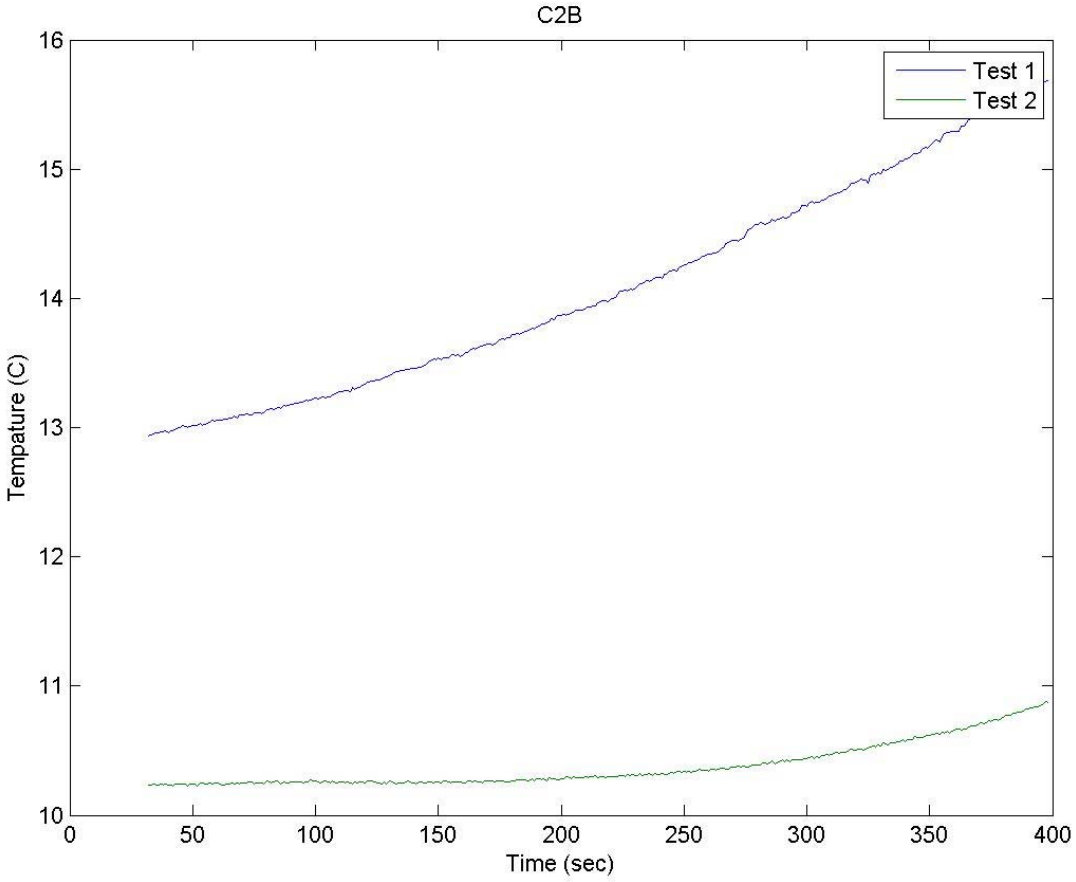
C2B
Test 1
Test 2
Tempature (C)
Time (sec)
16
15
14
13
12
11
10
0
50
100
150
200
250
300
350
400

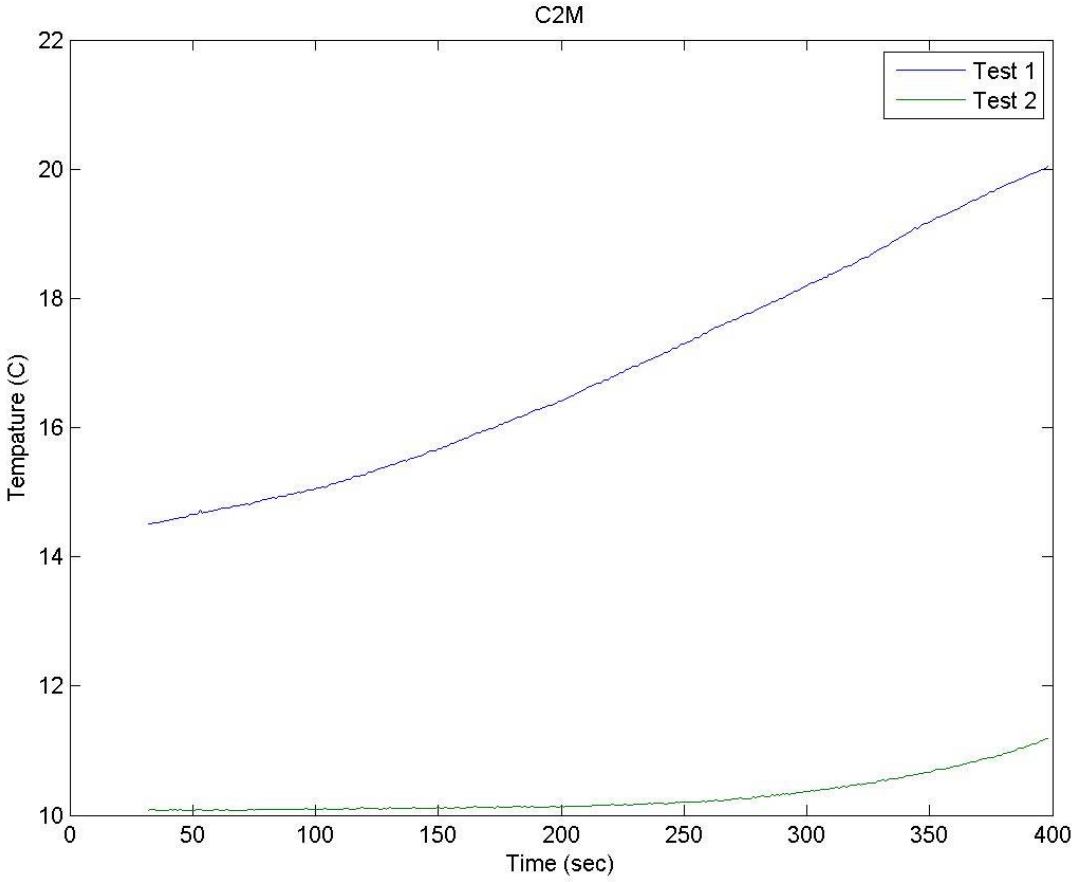
C2M
Test 1
Test 2
Tempature (C)
Time (sec)
22
20
18
16
14
12
10
0
50
100
150
200
250
300
350
400

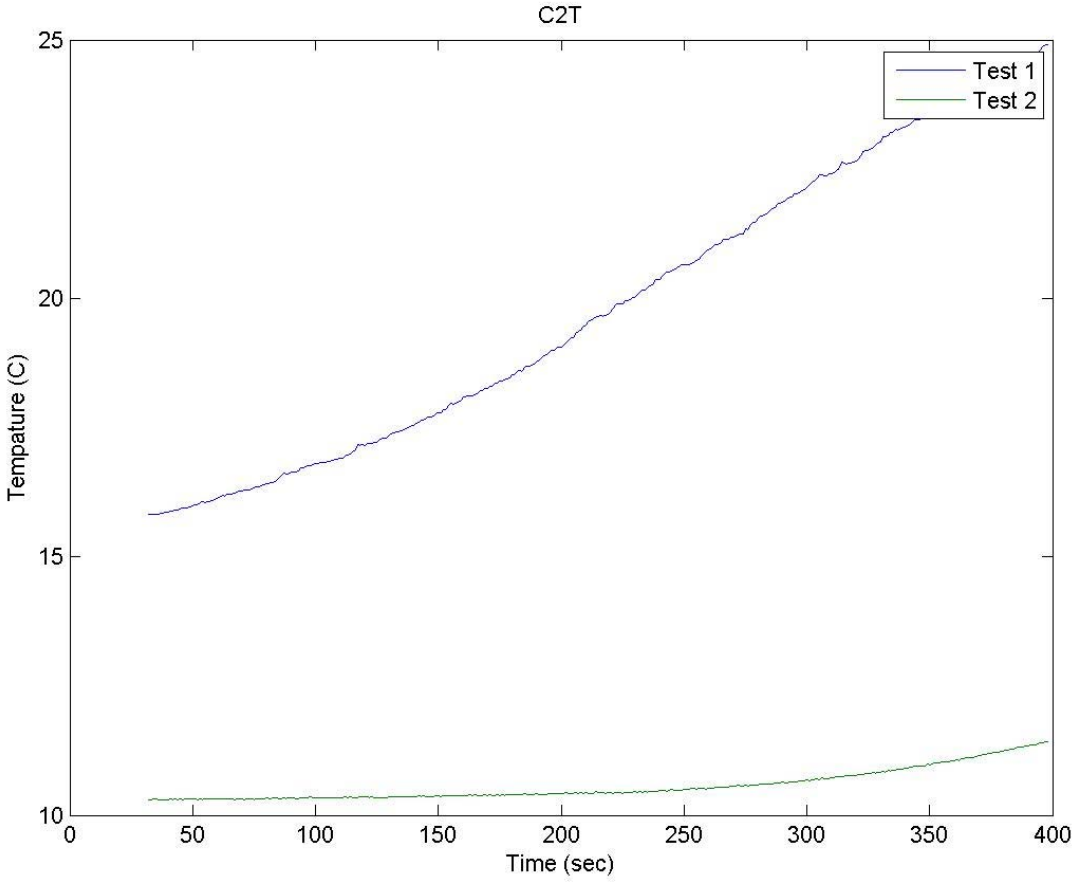
C2T
Test 1
Test 2
Tempature (C)
Time (sec)
25
20
15
10
0
50
100
150
200
250
300
350
400

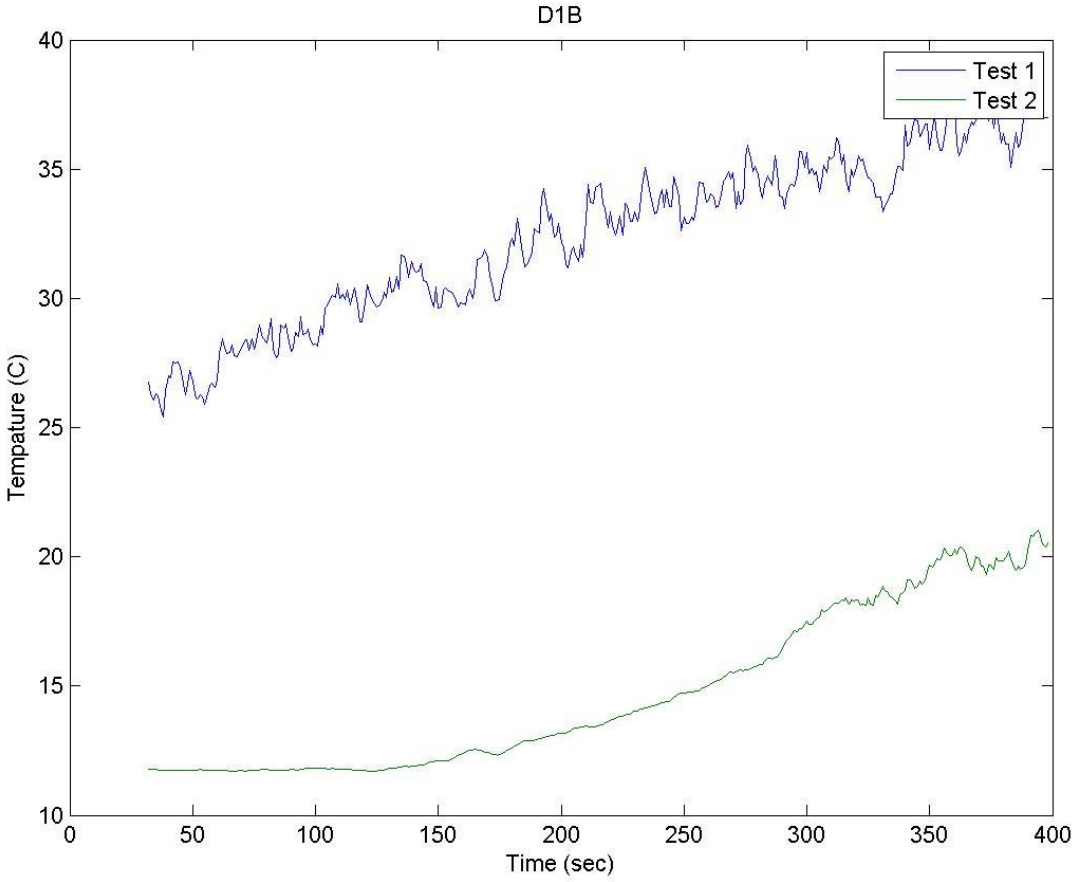
D1B
Test 1
Test 2
Tempature (C)
Time (sec)
40
35
30
25
20
15
10
0
50
100
150
200
250
300
350
400

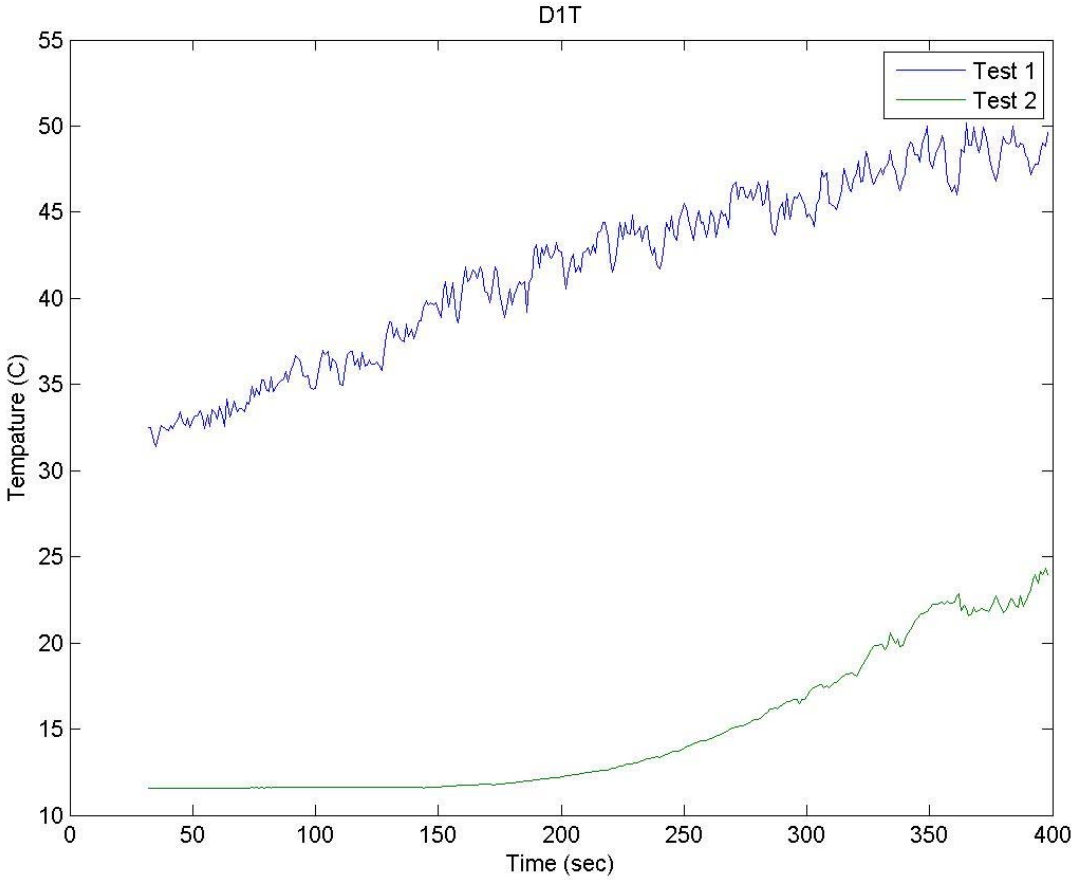
D1T
Test 1
Test 2
Tempature (C)
Time (sec)
55
50
45
40
35
30
25
20
15
10
0
50
100
150
200
250
300
350
400

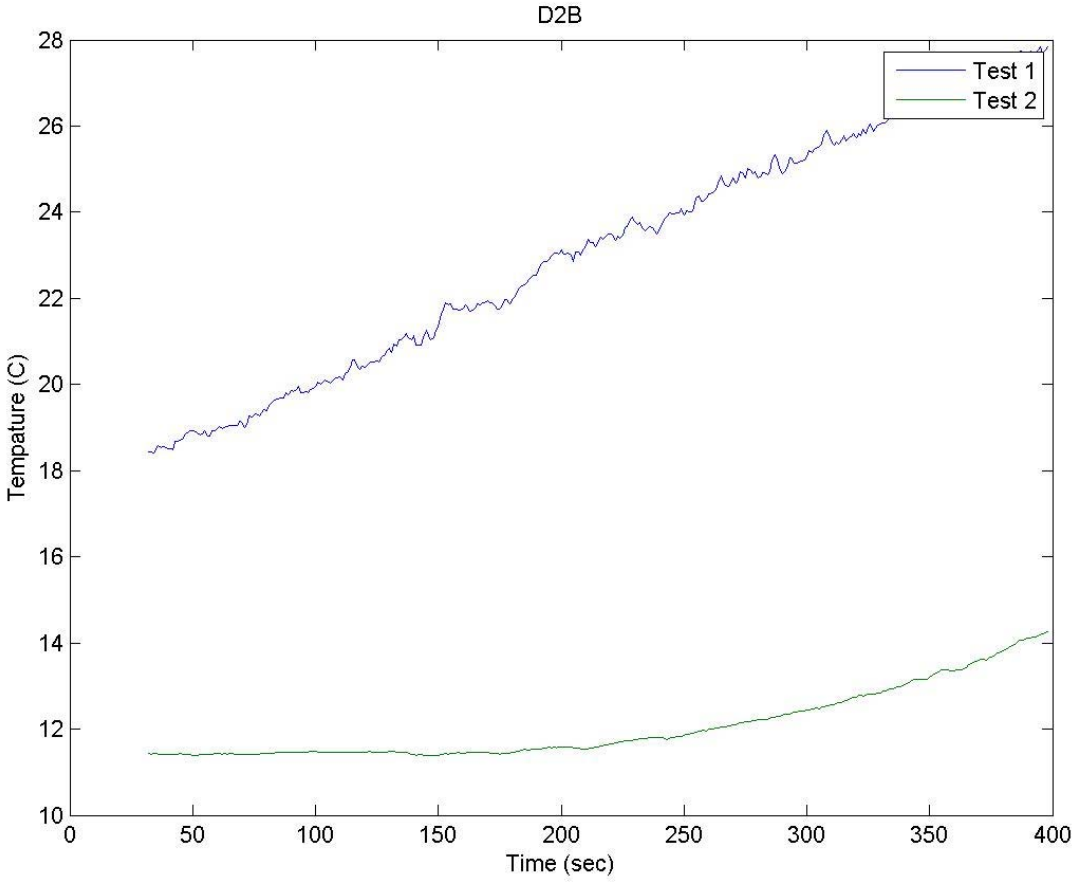
D2B
Test 1
Test 2
Tempature (C)
Time (sec)
28
26
24
22
20
18
16
14
12
10
0
50
100
150
200
250
300
350
400

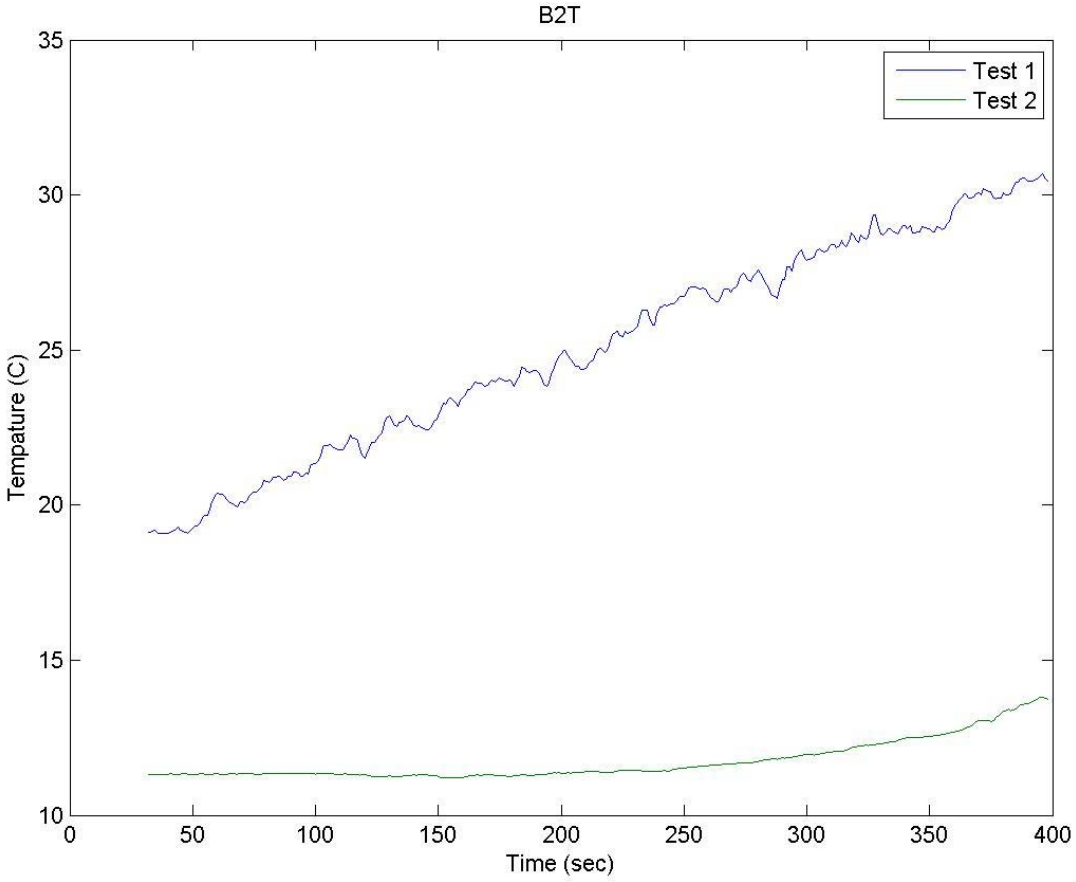
B2T
Test 1
Test 2
Tempature (C)
Time (sec)
35
30
25
20
15
10
0
50
100
150
200
250
300
350
400

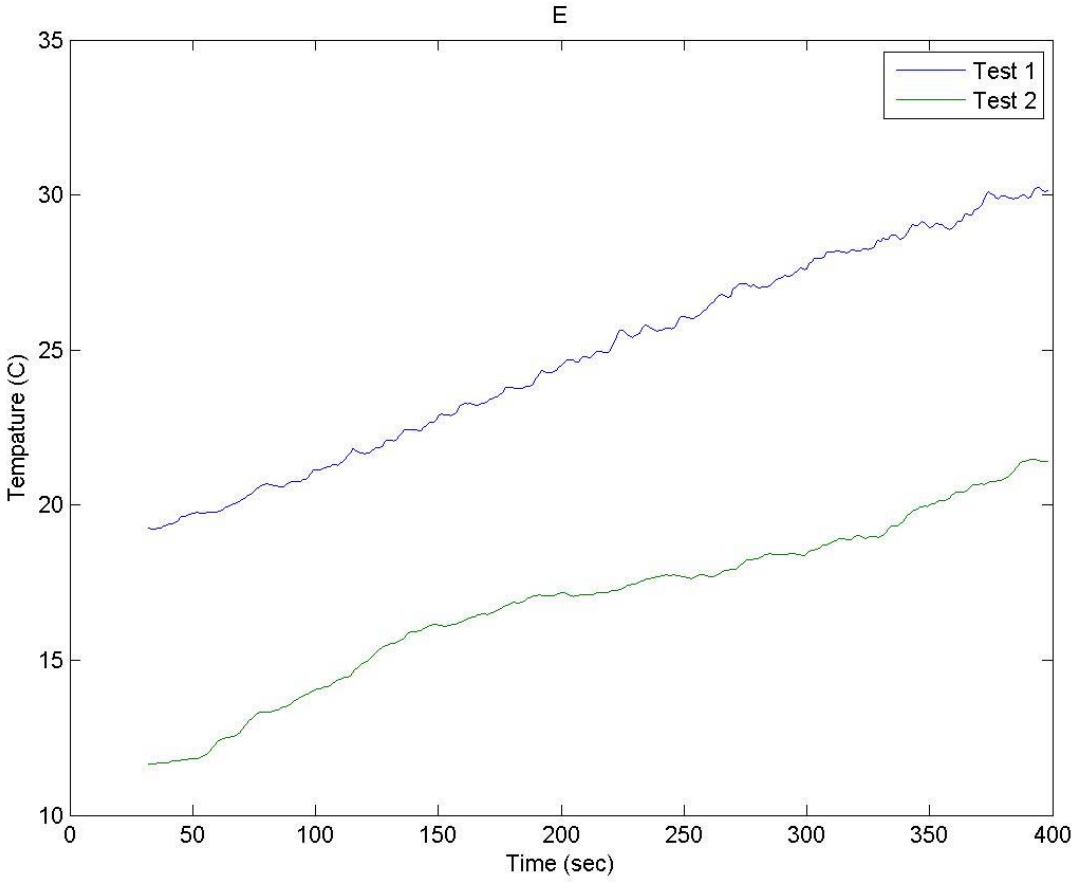
E
Test 1
Test 2
Tempature (C)
Time (sec)
35
30
25
20
15
10
0
50
100
150
200
250
300
350
400

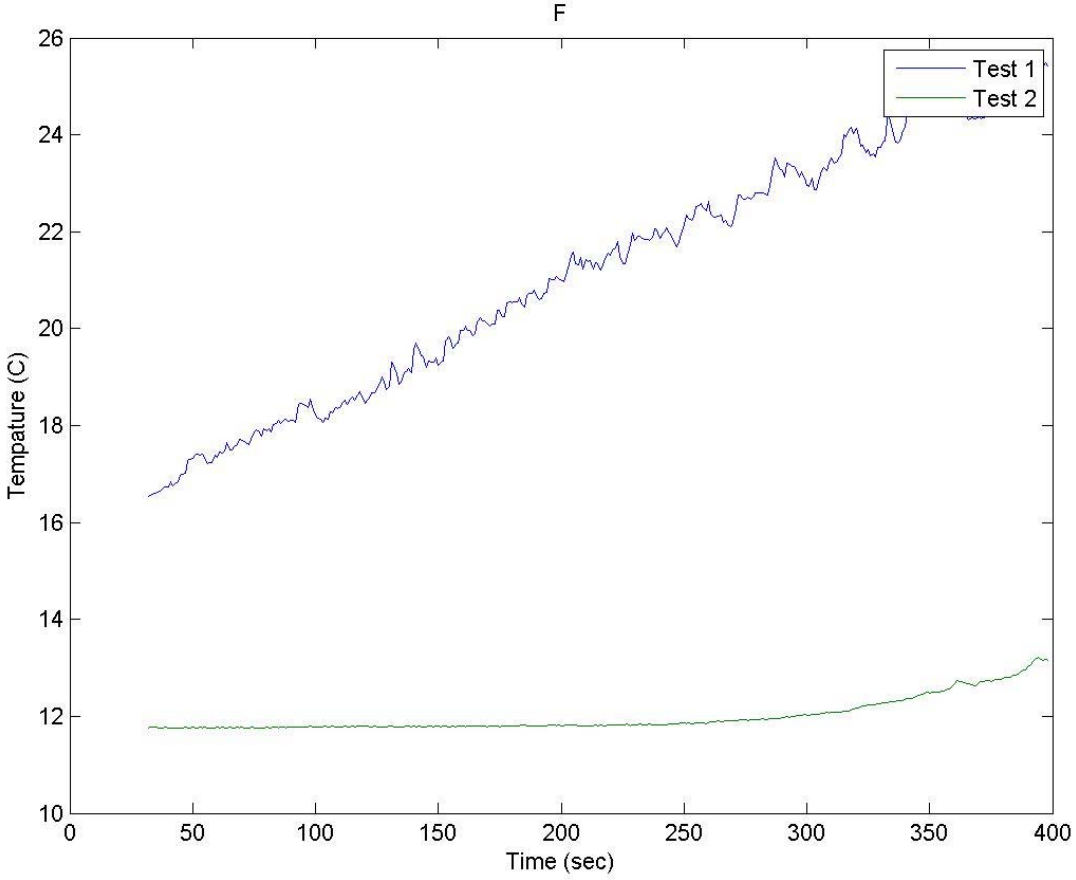
F
Test 1
Test 2
Tempature (C)
Time (sec)
26
24
22
20
18
16
14
12
10
0
50
100
150
200
250
300
350
400

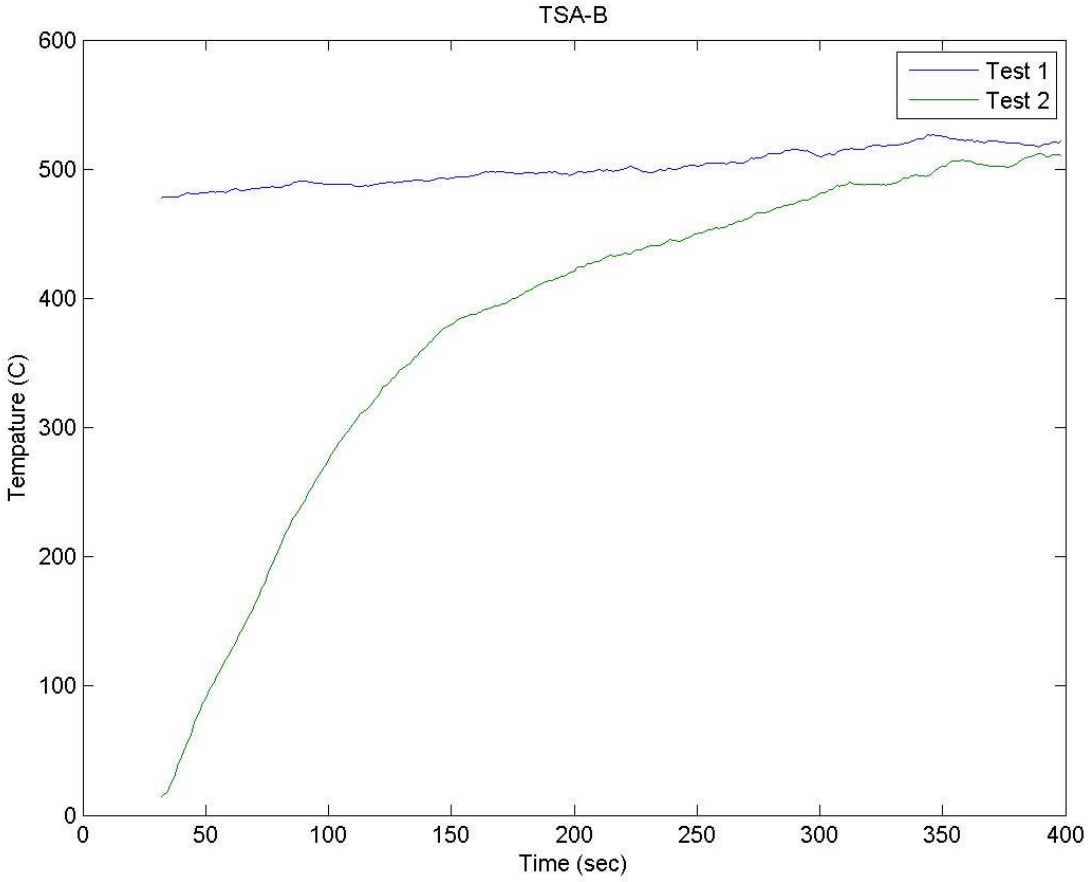
TSA-B
Test 1
Test 2
Tempature (C)
Time (sec)
0
100
200
300
400
500
600
0
50
100
150
200
250
300
350
400

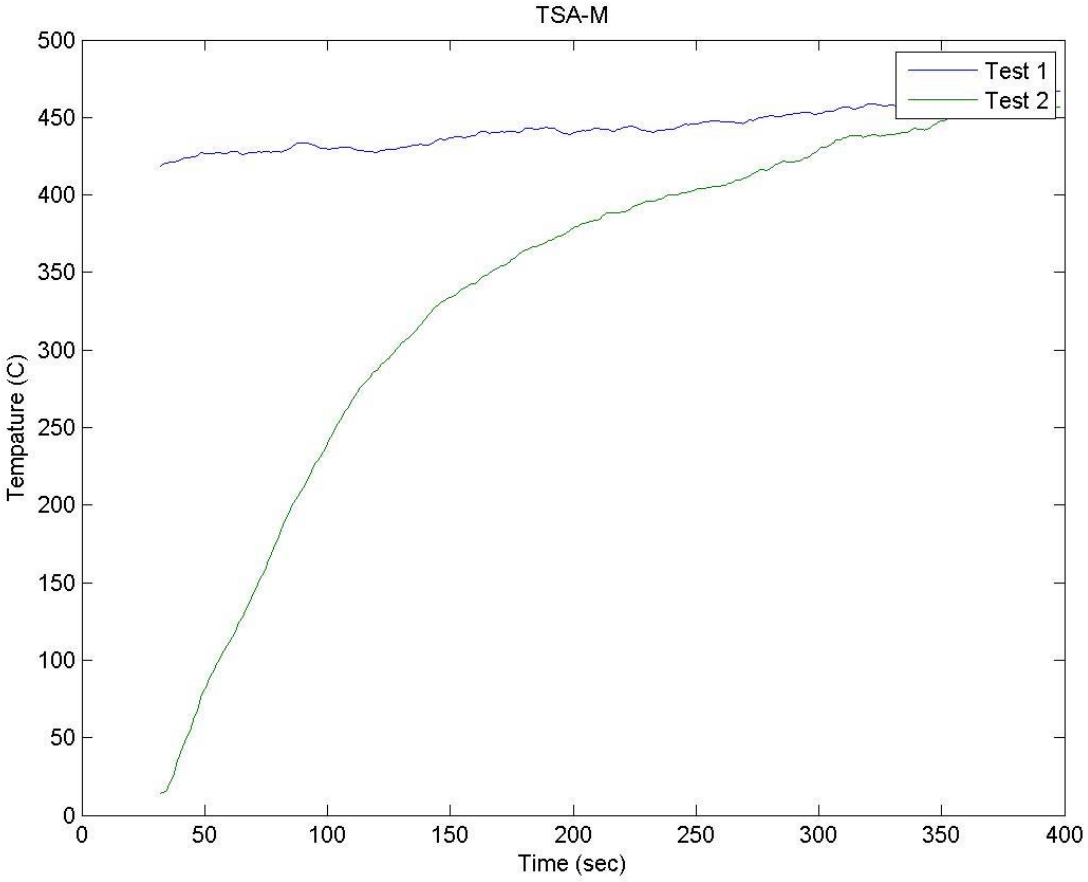
TSA-M
Test 1
Test 2
Tempature (C)
Time (sec)
0
50
100
150
200
250
300
350
400
450
500

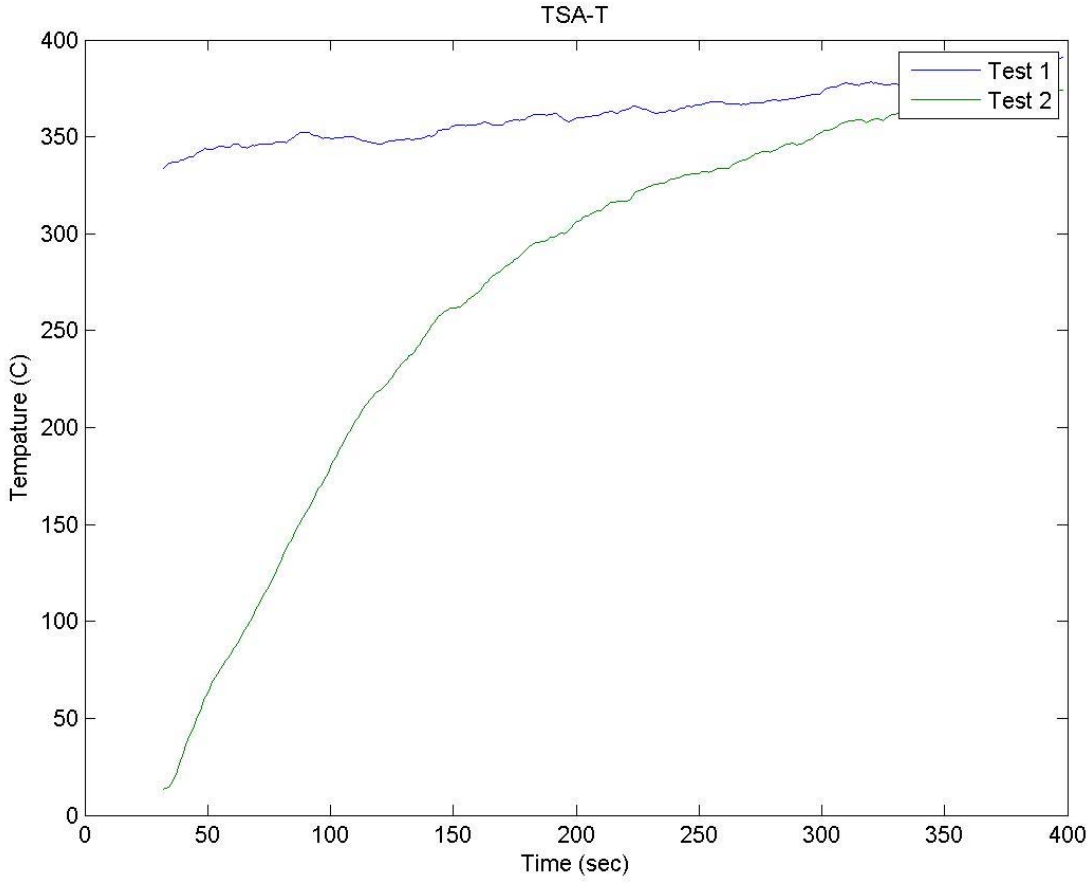
TSA-T
Test 1
Test 2
Tempature (C)
Time (sec)
0
50
100
150
200
250
300
350
400

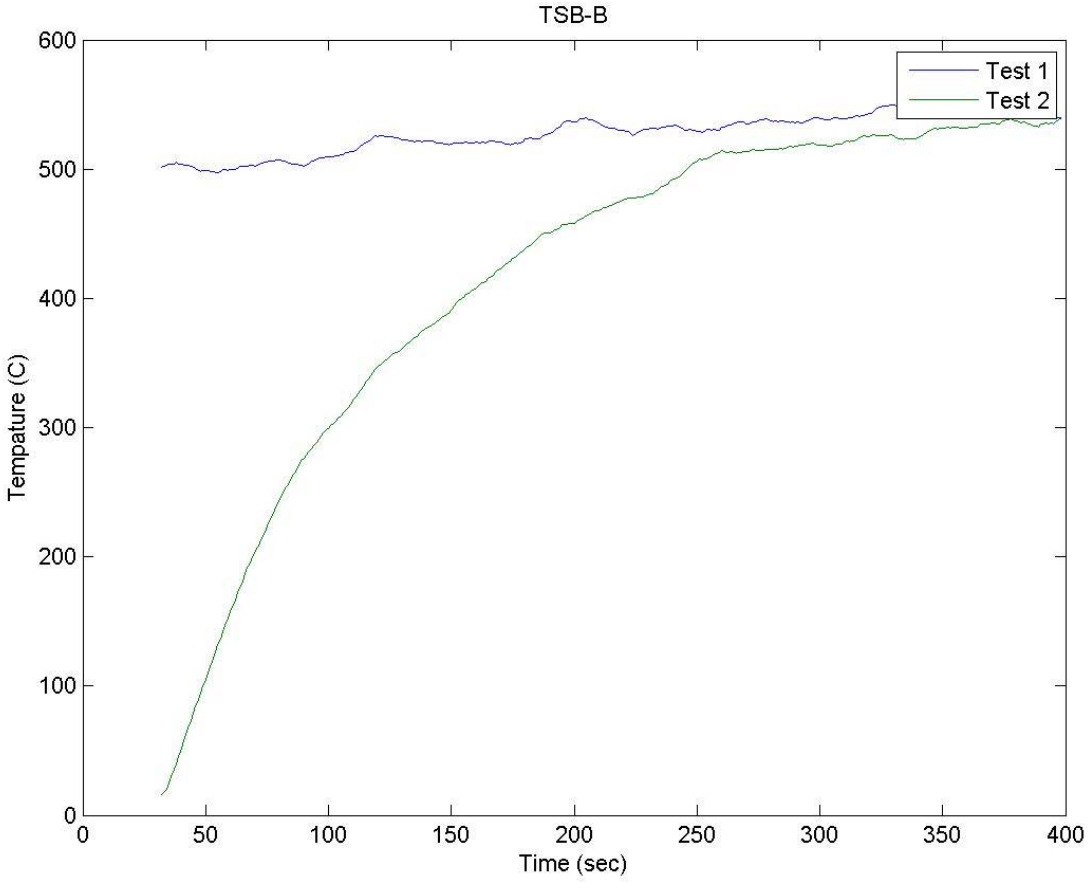
TSB-B
Test 1
Test 2
Tempature (C)
Time (sec)
0
100
200
300
400
500
600
0
50
100
150
200
250
300
350
400

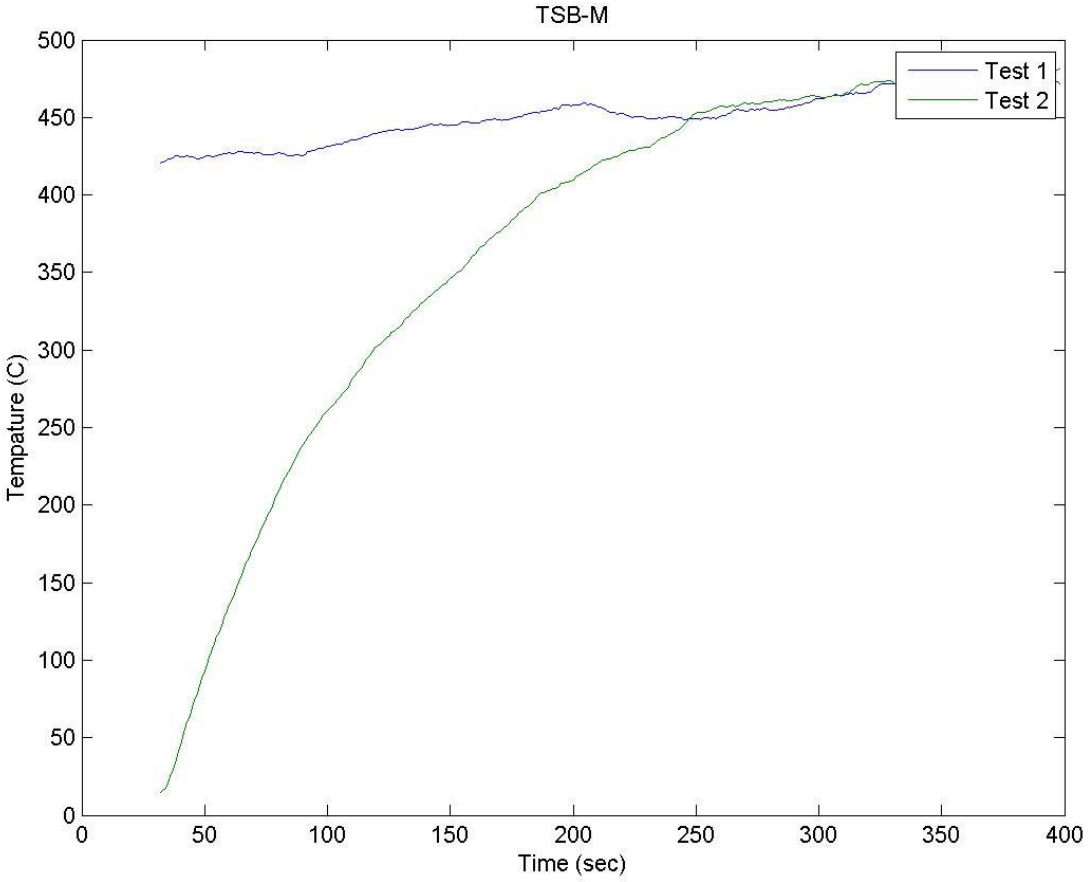
TSB-M
Test 1
Test 2
Tempature (C)
Time (sec)
0
50
100
150
200
250
300
350
400
450
500

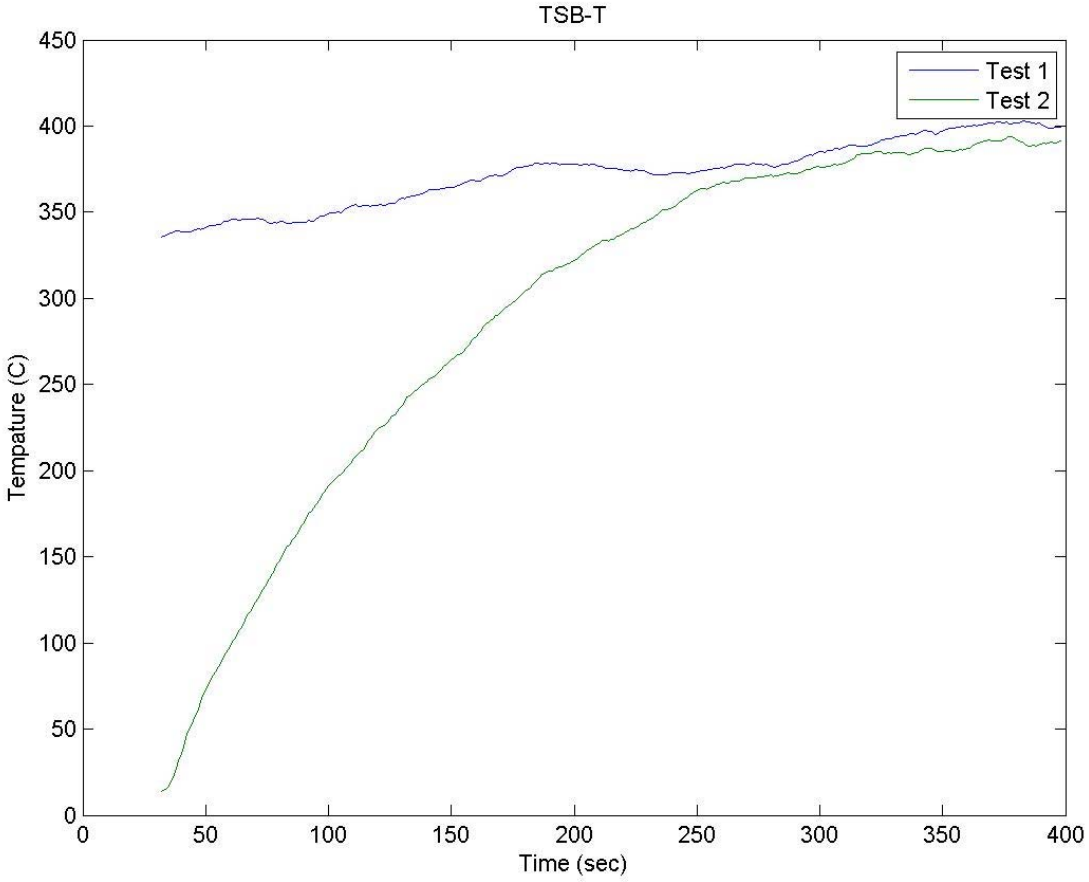
TSB-T
Test 1
Test 2
Tempature (C)
Time (sec)
0
50
100
150
200
250
300
350
400
450

Appendix I: COMSOL Model Compared to Physical Model Data

Spline Joint Data

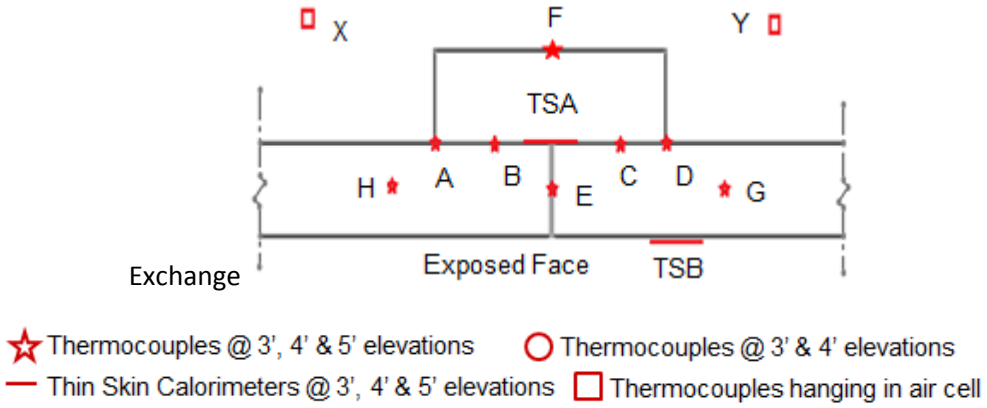

The following graphs show the comparison between the experimental data and the computational data from COMSOL as Time vs. Temp at each instrument at an elevation of 3'. The graph title is the label of each instrument shown in the figure above.

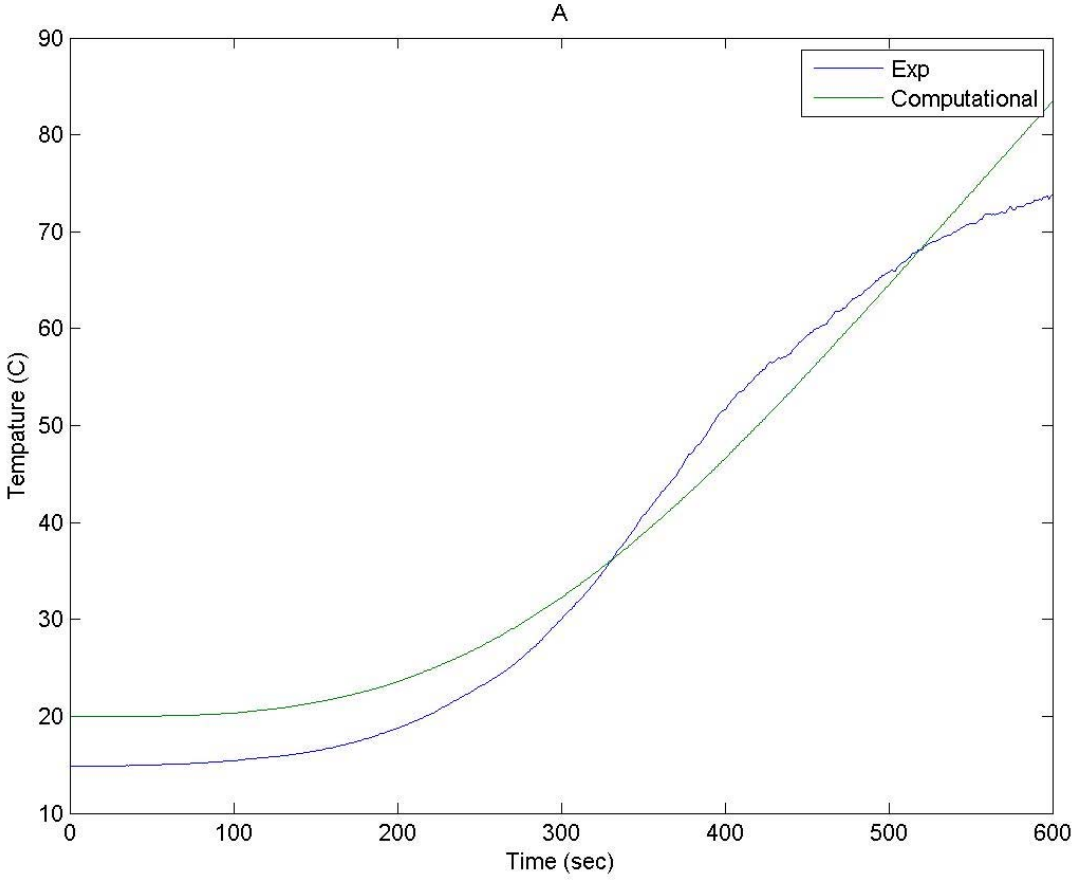
A
Exp
Computational
Tempature (C)
Time (sec)
90
80
70
60
50
40
30
20
10
0
100
200
300
400
500
600

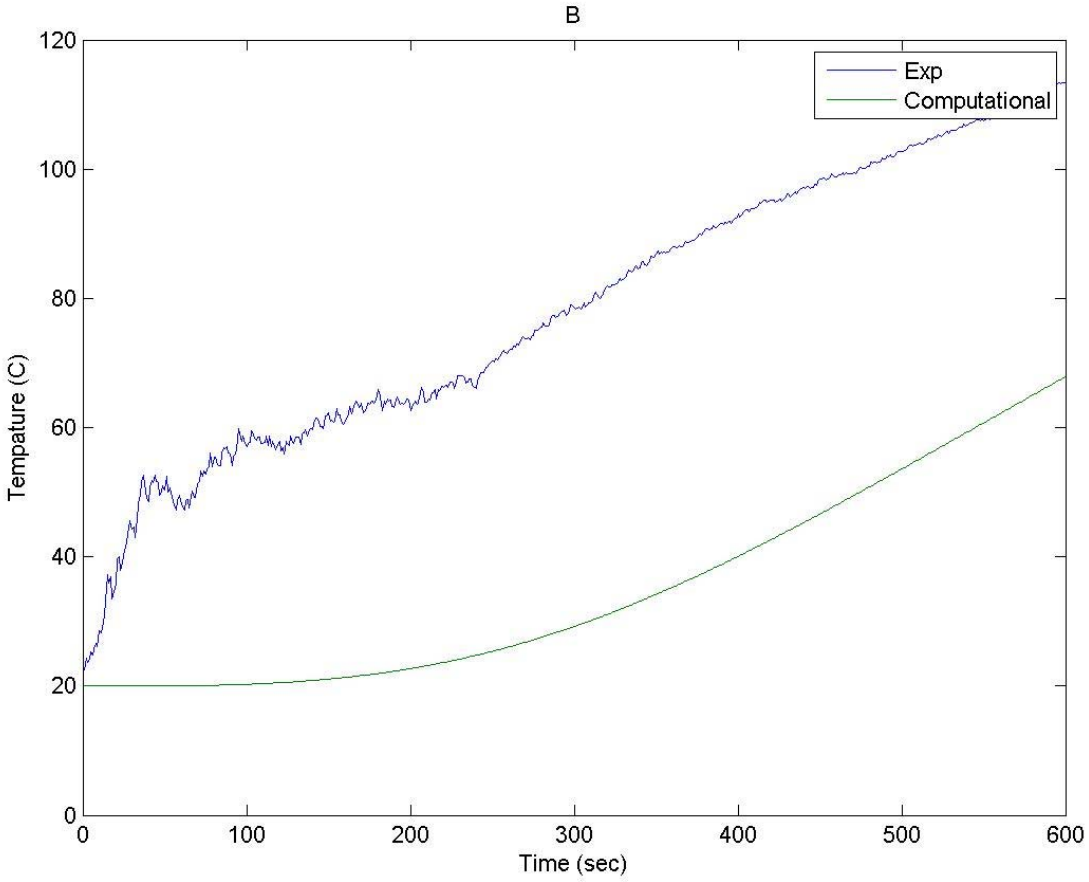
B
Exp
Computational
Tempature (C)
Time (sec)
0
20
40
60
80
100
120
0
100
200
300
400
500
600

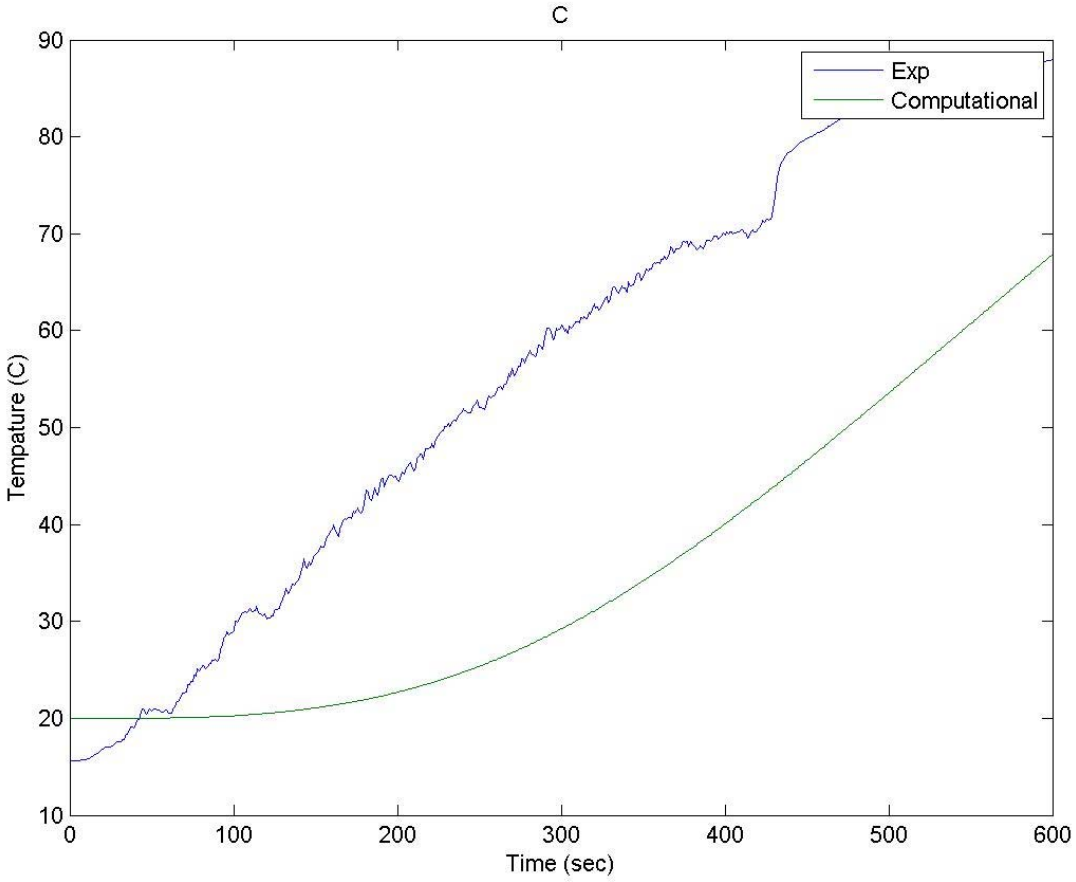
C
Exp
Computational
Tempature (C)
Time (sec)
90
80
70
60
50
40
30
20
10
0
100
200
300
400
500
600

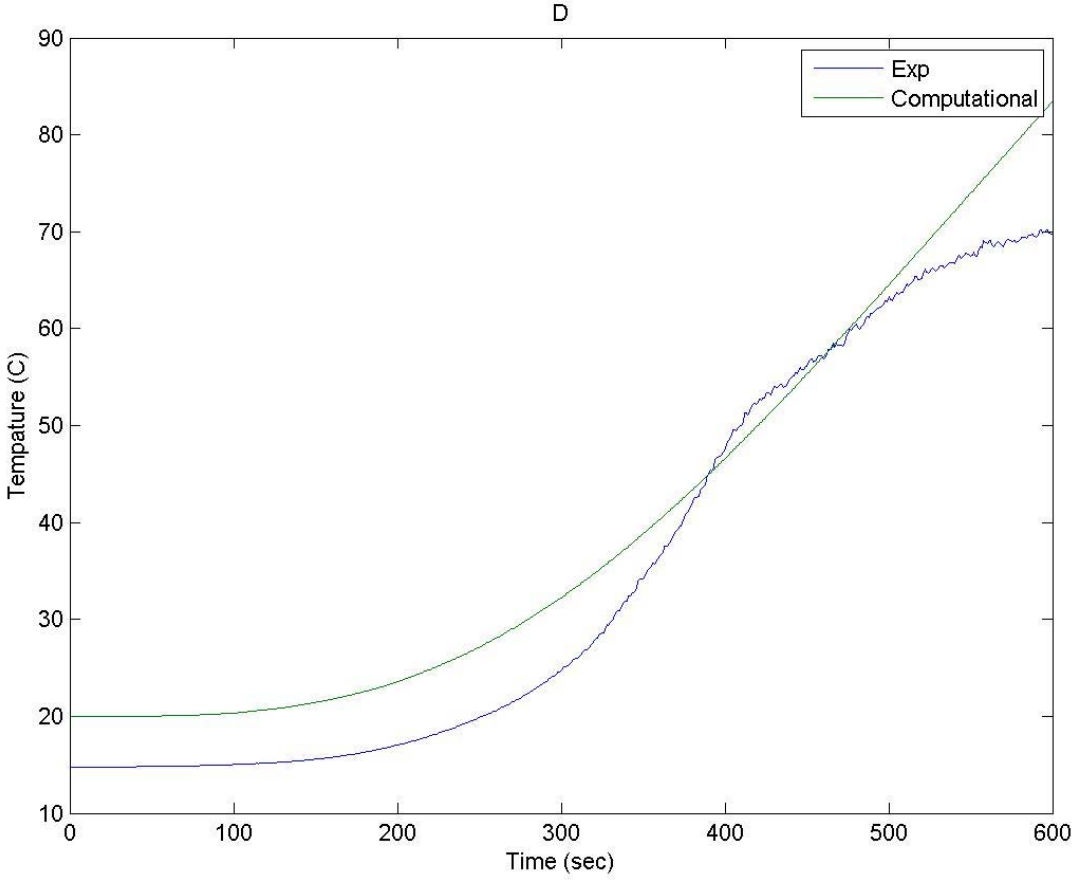
D
Exp
Computational
Tempature (C)
Time (sec)
90
80
70
60
50
40
30
20
10
0
100
200
300
400
500
600

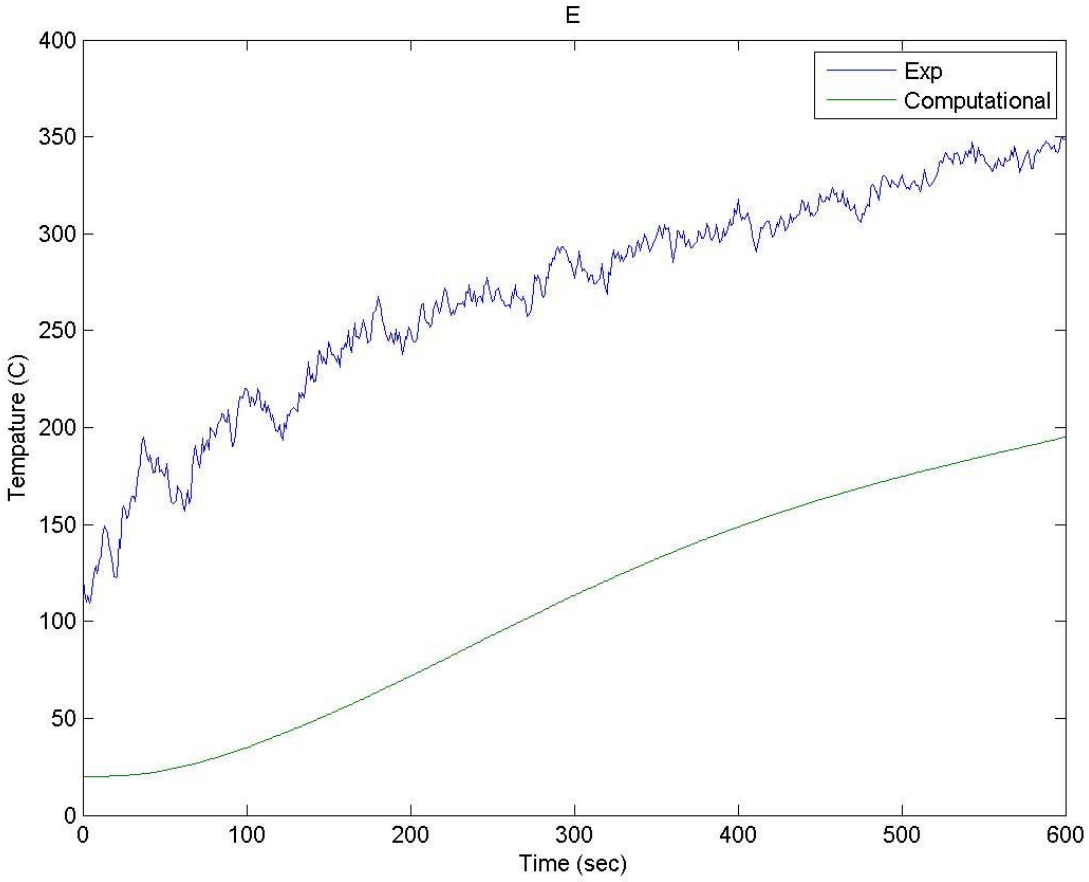
E
Exp
Computational
Tempature (C)
Time (sec)
0
50
100
150
200
250
300
350
400
0
100
200
300
400
500
600

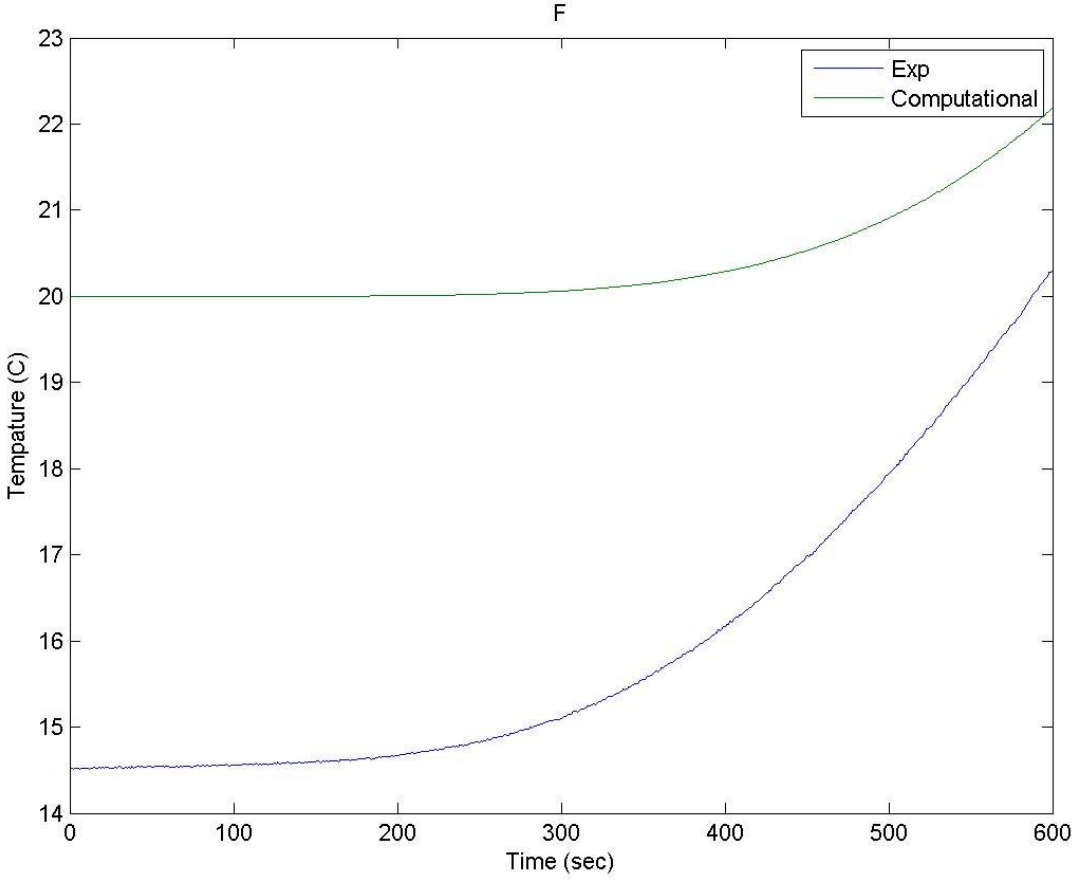
F
Exp
Computational
Tempature (C)
Time (sec)
23
22
21
20
19
18
17
16
15
14
0
100
200
300
400
500
600

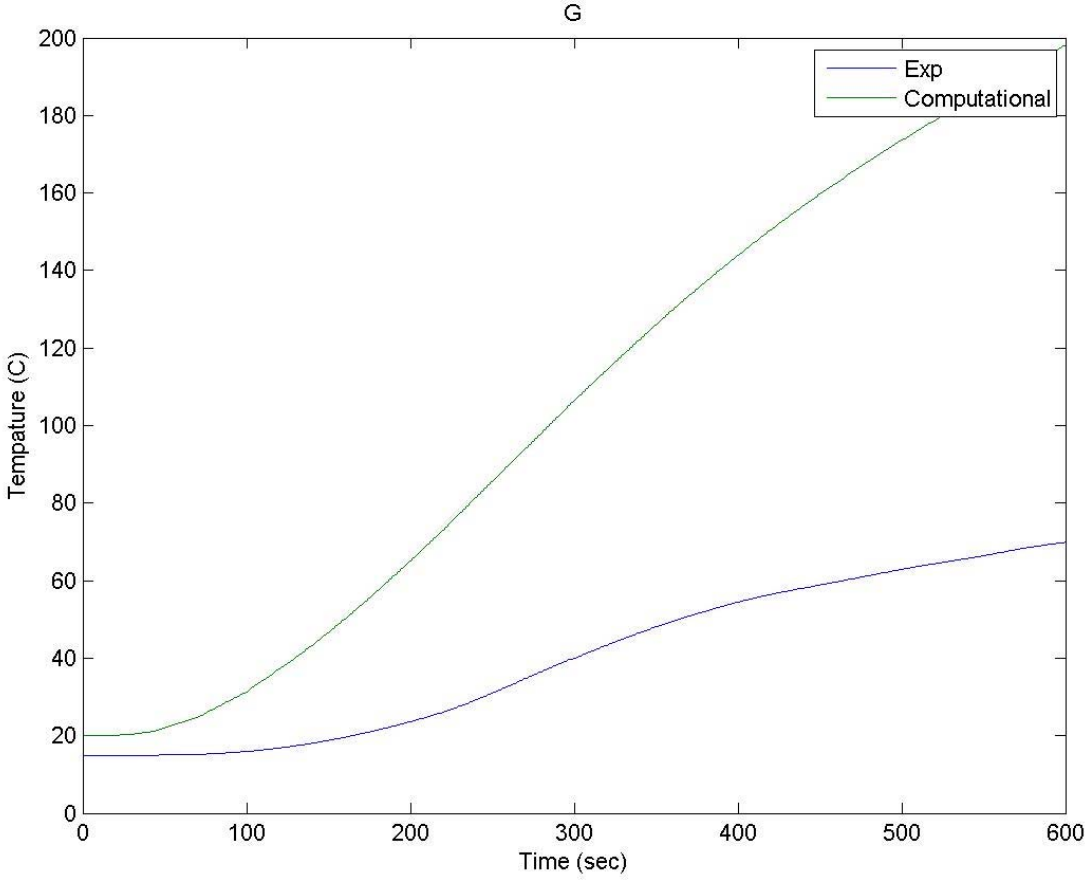
G
Exp
Computational
Tempature (C)
Time (sec)
0
20
40
60
80
100
120
140
160
180
200
0
100
200
300
400
500
600

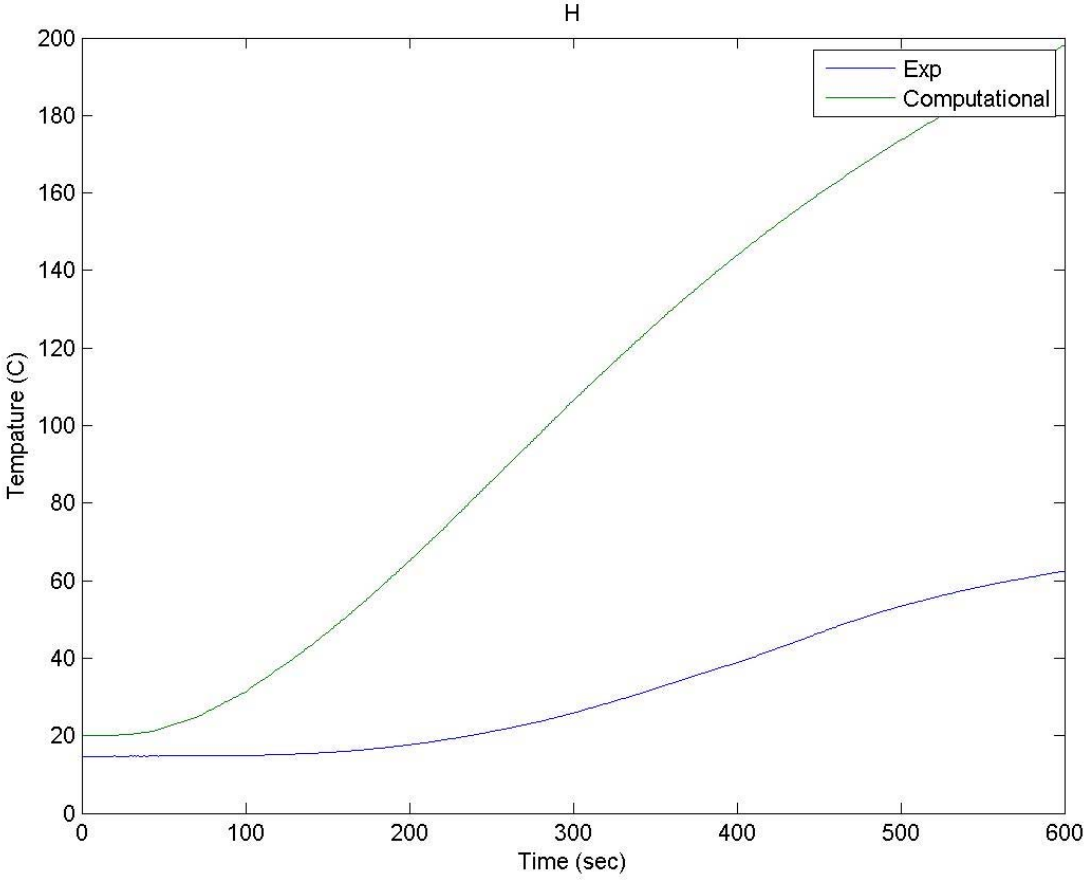
H
Exp
Computational
Tempature (C)
Time (sec)
0
20
40
60
80
100
120
140
160
180
200
0
100
200
300
400
500
600

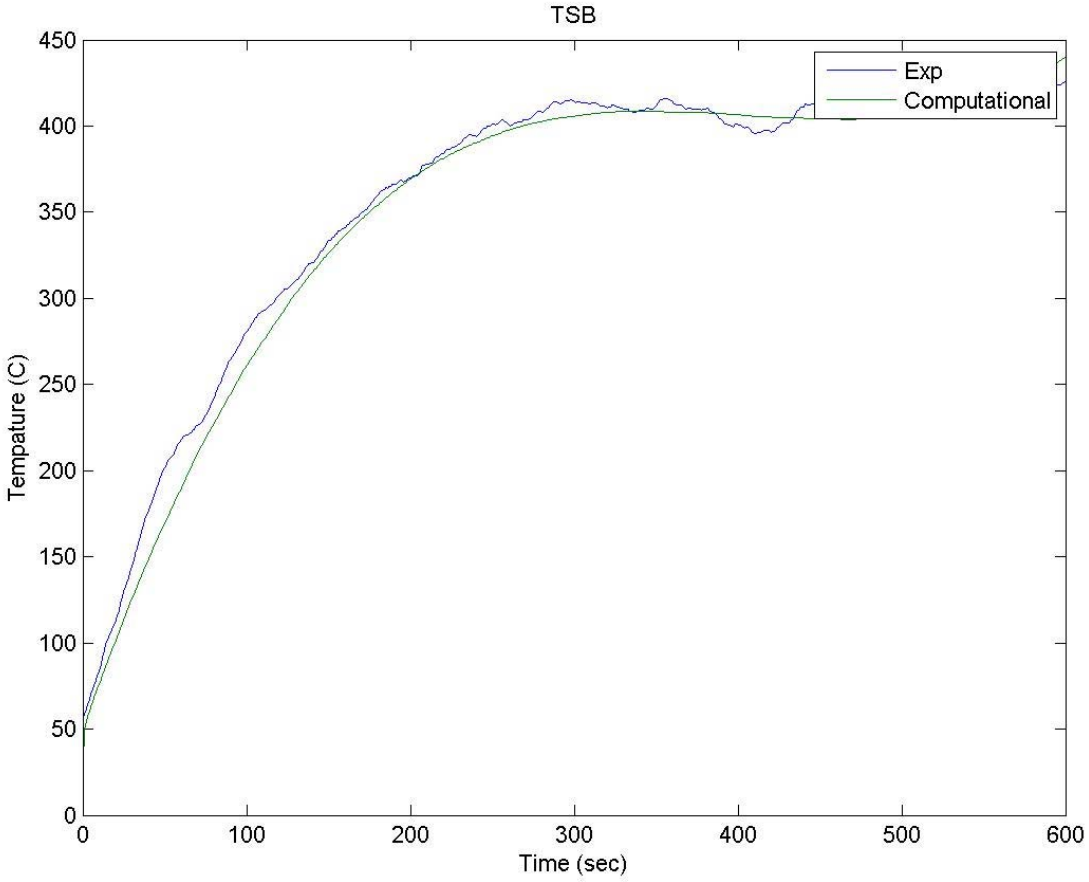
TSB
Exp
Computational
Tempature (C)
Time (sec)
0
50
100
150
200
250
300
350
400
450
0
100
200
300
400
500
600

Overlap Joint Data

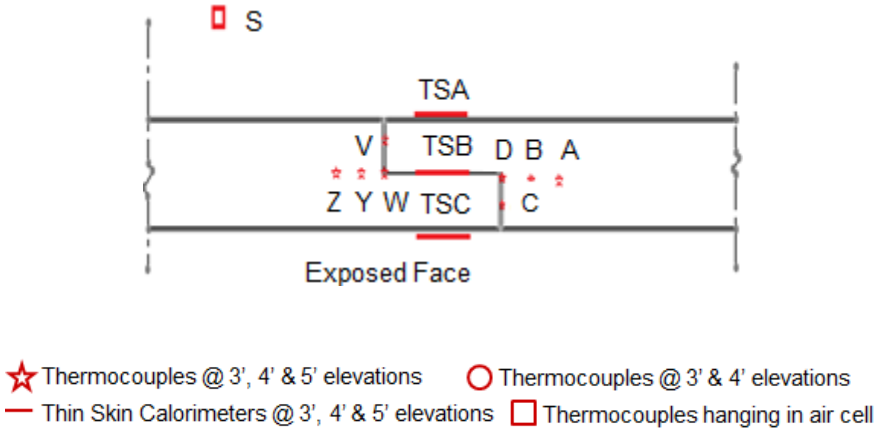

The following graphs show the comparison between the experiment data and the computational data from COMSOL as Time vs. Temp at each instrument at an elevation of 3'. The graph title is the label of each instrument shown in figure above.

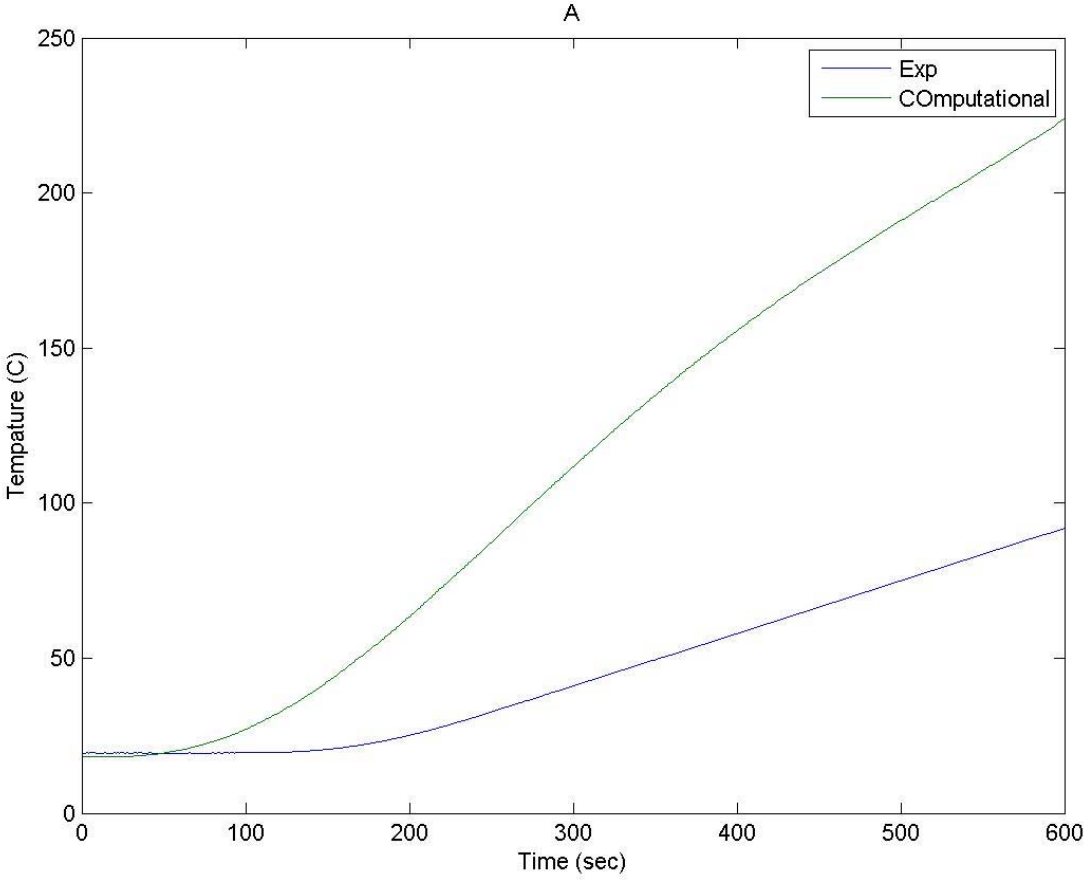
A
Exp
COmputational
Tempature (C)
Time (sec)
0
50
100
150
200
250
0
100
200
300
400
500
600

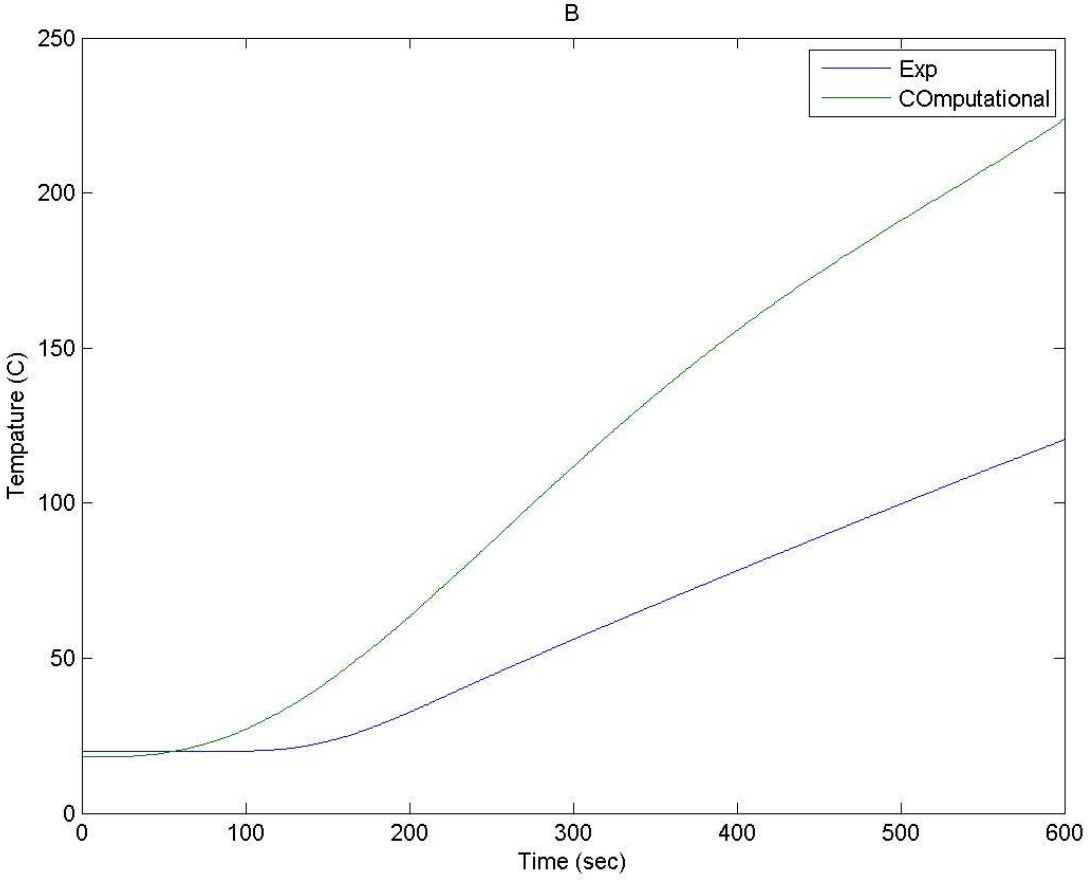
B
Exp
COmputational
Tempature (C)
Time (sec)
0
50
100
150
200
250
0
100
200
300
400
500
600

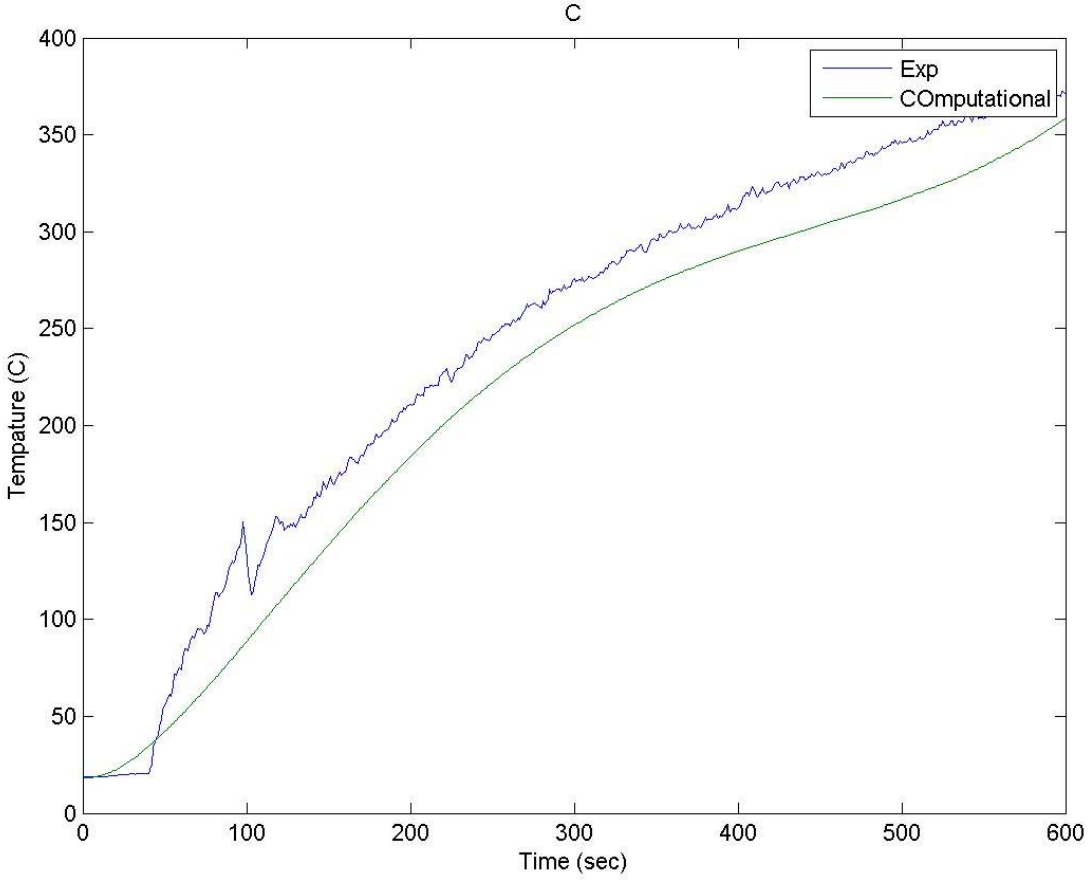
C
Exp
COmputational
Tempature (C)
Time (sec)
0
50
100
150
200
250
300
350
400
0
100
200
300
400
500
600

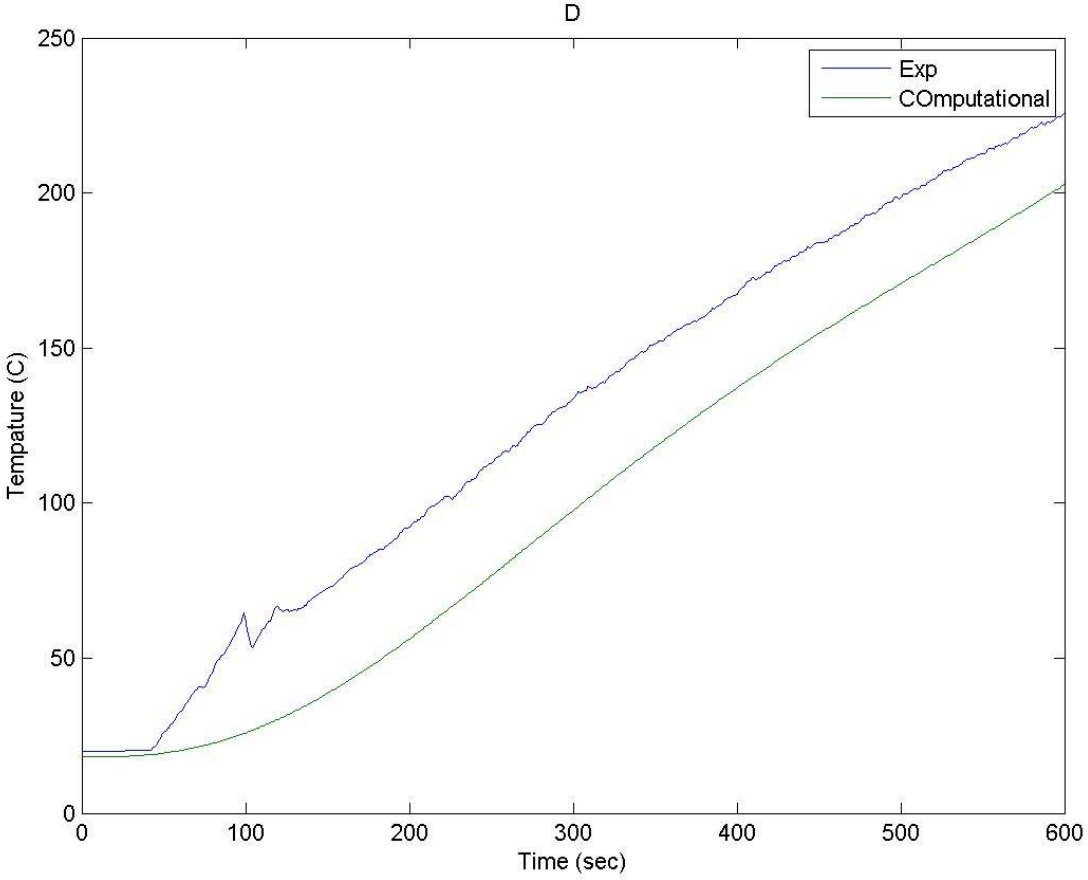
D
Exp
COmputational
Tempature (C)
Time (sec)
0
50
100
150
200
250
0
100
200
300
400
500
600

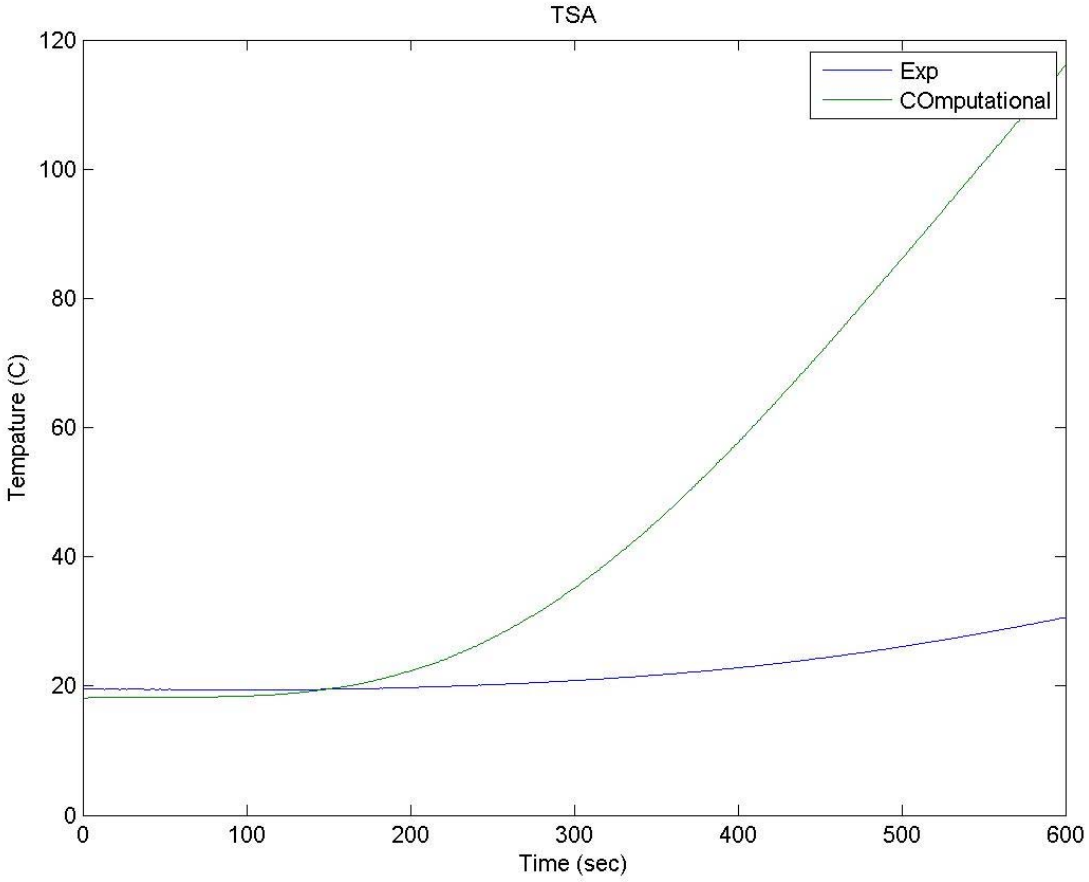
TSA
Exp
COmputational
Tempature (C)
Time (sec)
0
20
40
60
80
100
120
0
100
200
300
400
500
600

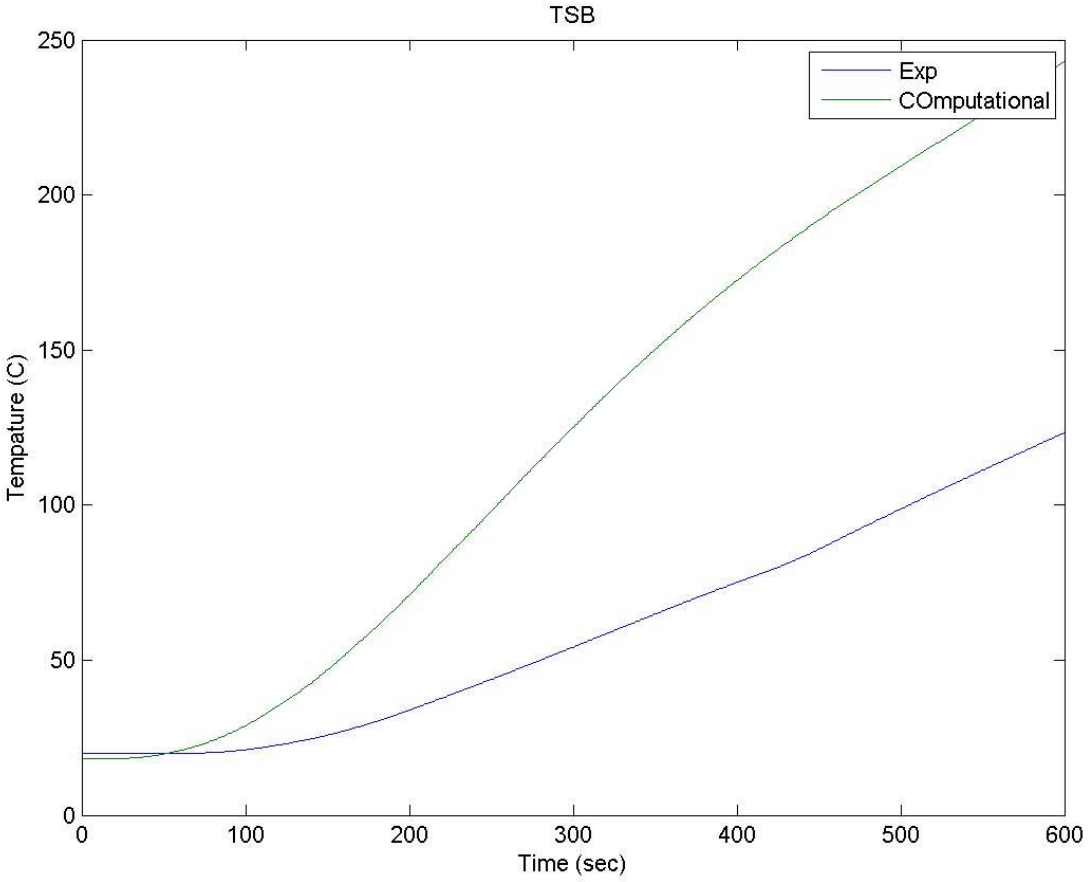
TSB
Exp
COmputational
Tempature (C)
Time (sec)
0
50
100
150
200
250
0
100
200
300
400
500
600

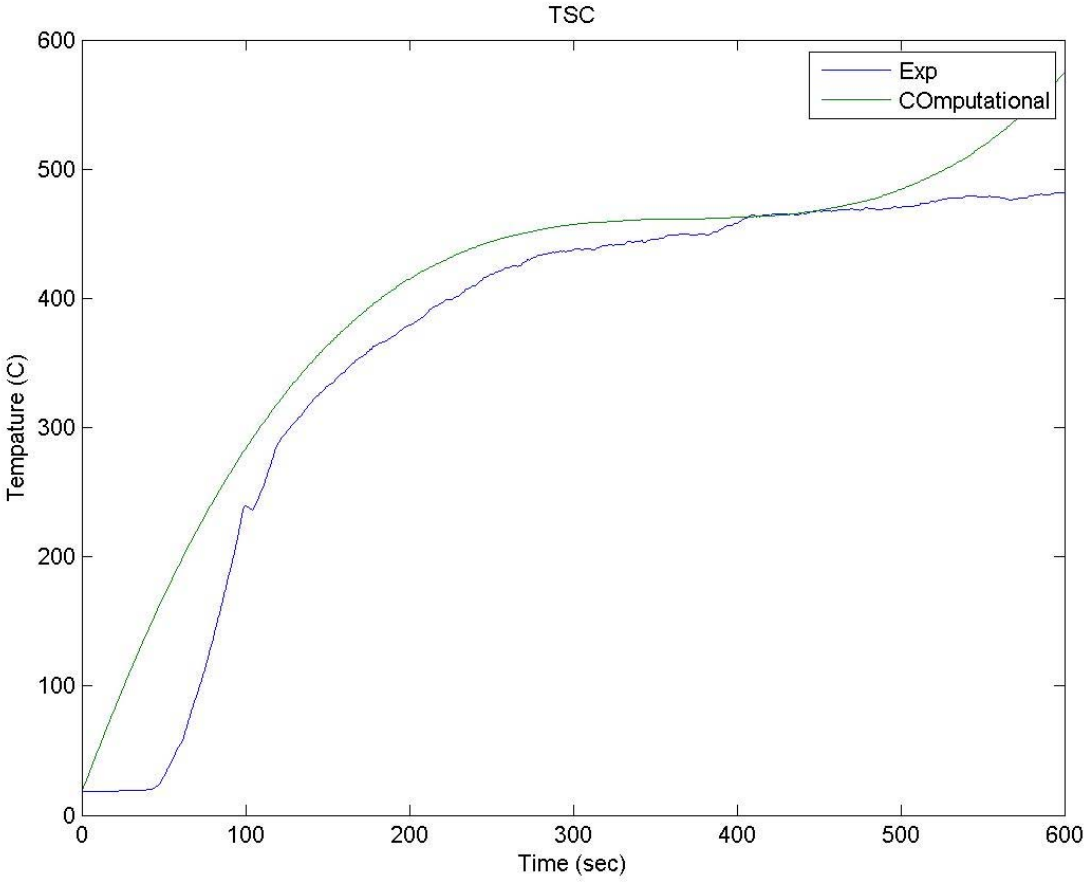
TSC
Exp
COmputational
Tempature (C)
Time (sec)
0
100
200
300
400
500
600

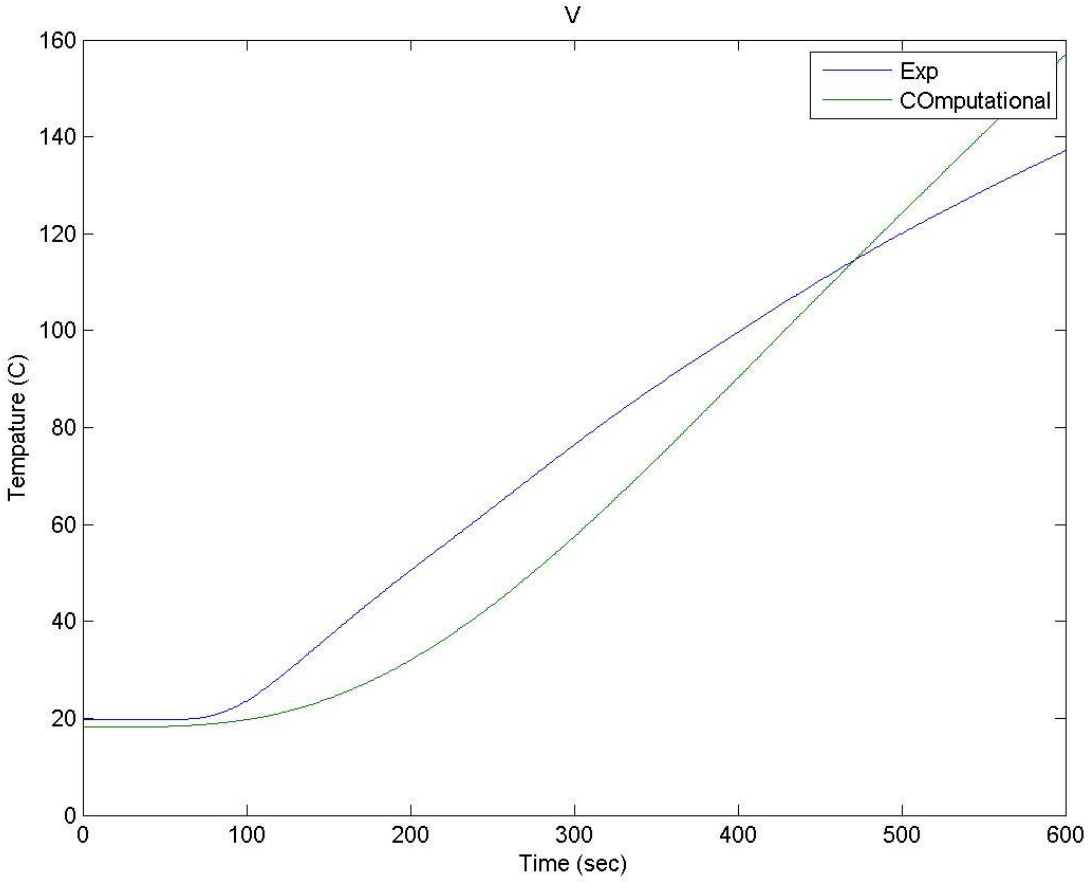
V
Exp
COmputational
Tempature (C)
Time (sec)
0
20
40
60
80
100
120
140
160
0
100
200
300
400
500
600

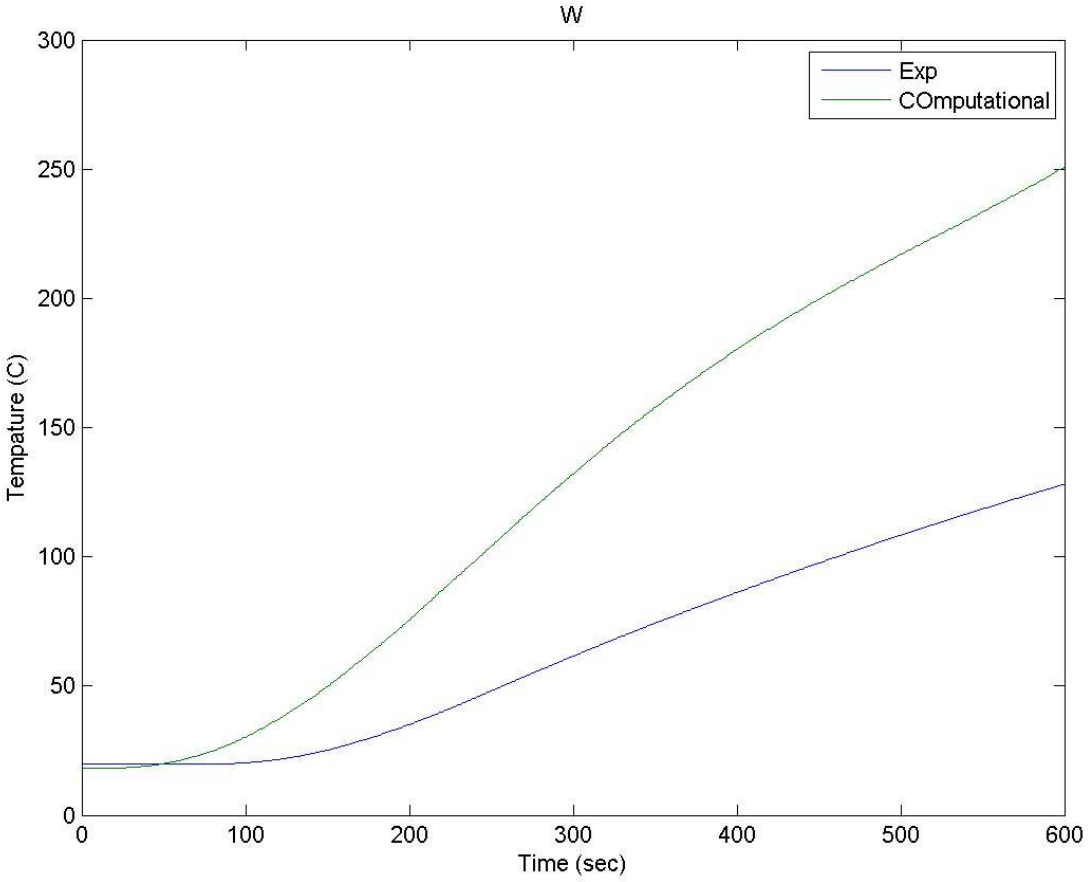
W
Exp
COmputational
Tempature (C)
Time (sec)
0
50
100
150
200
250
300
0
100
200
300
400
500
600

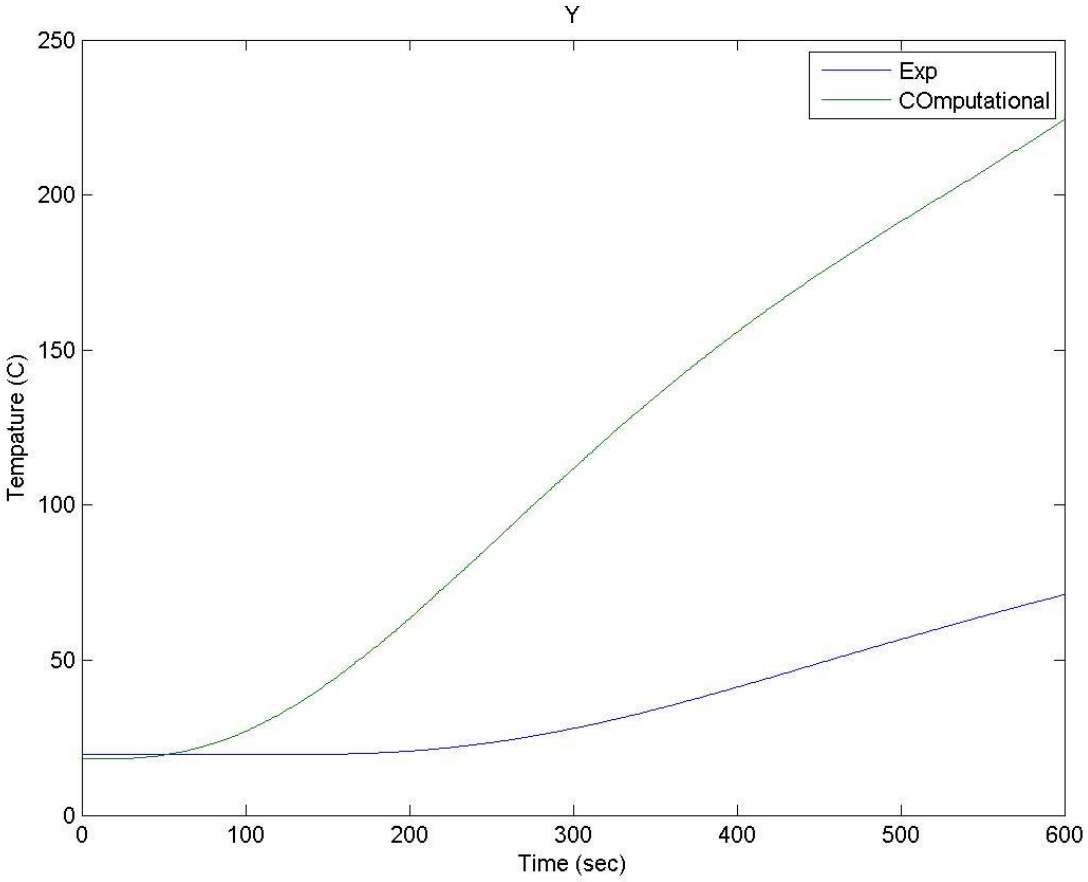
Y
Exp
COmputational
Tempature (C)
Time (sec)
0
50
100
150
200
250
0
100
200
300
400
500
600

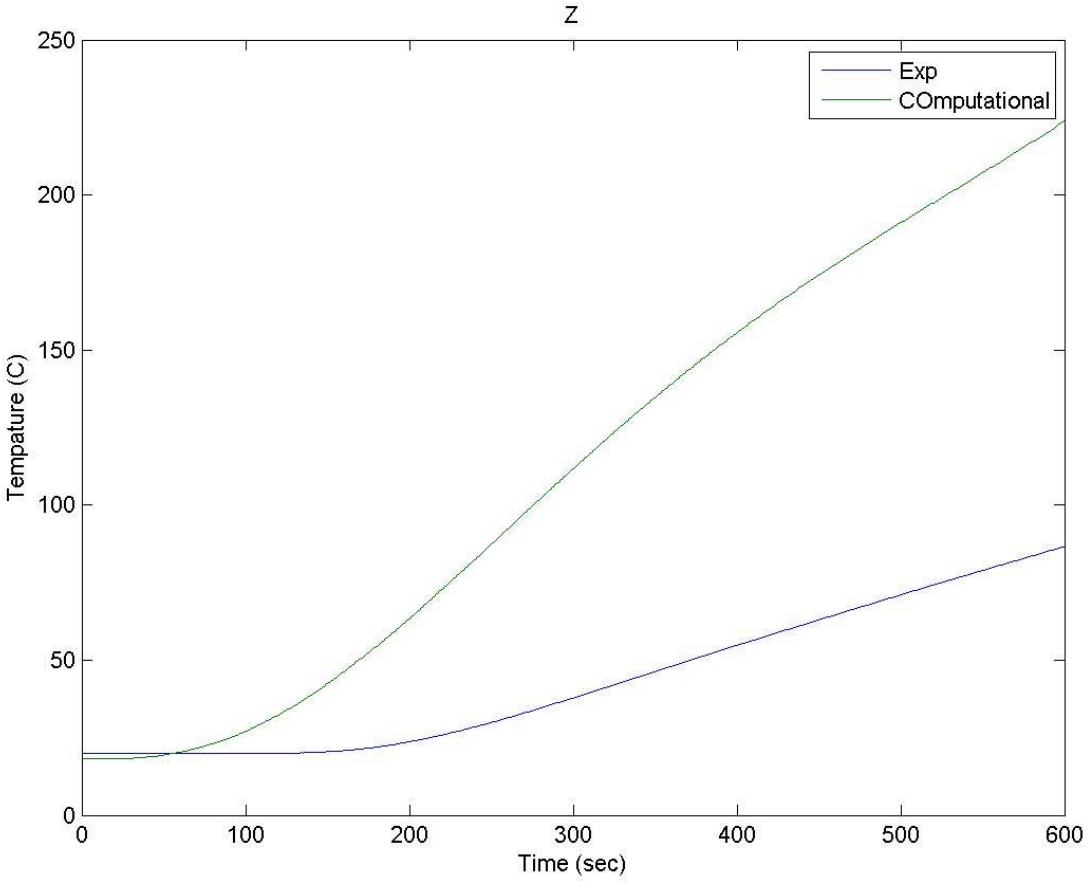
Z
Exp
COmputational
Tempature (C)
Time (sec)
0
50
100
150
200
250
0
100
200
300
400
500
600

Corner Joint Data

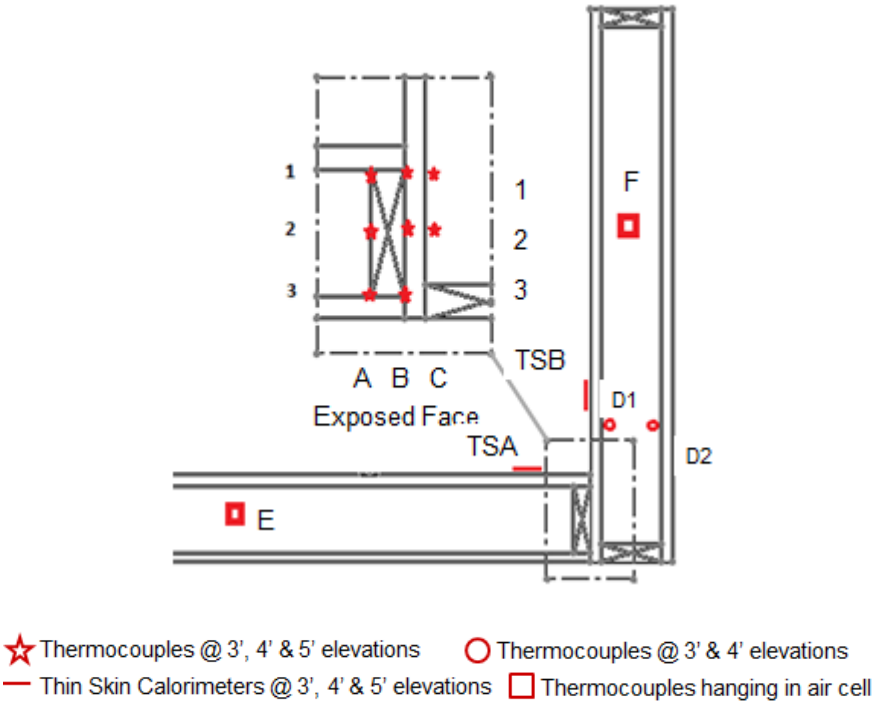

The following graphs show the comparison between the experiment data and the computational data from COMSOL as Time vs. Temp at each instrument at an elevation of 3'. The graph title is the label of each instrument shown in the figure above.

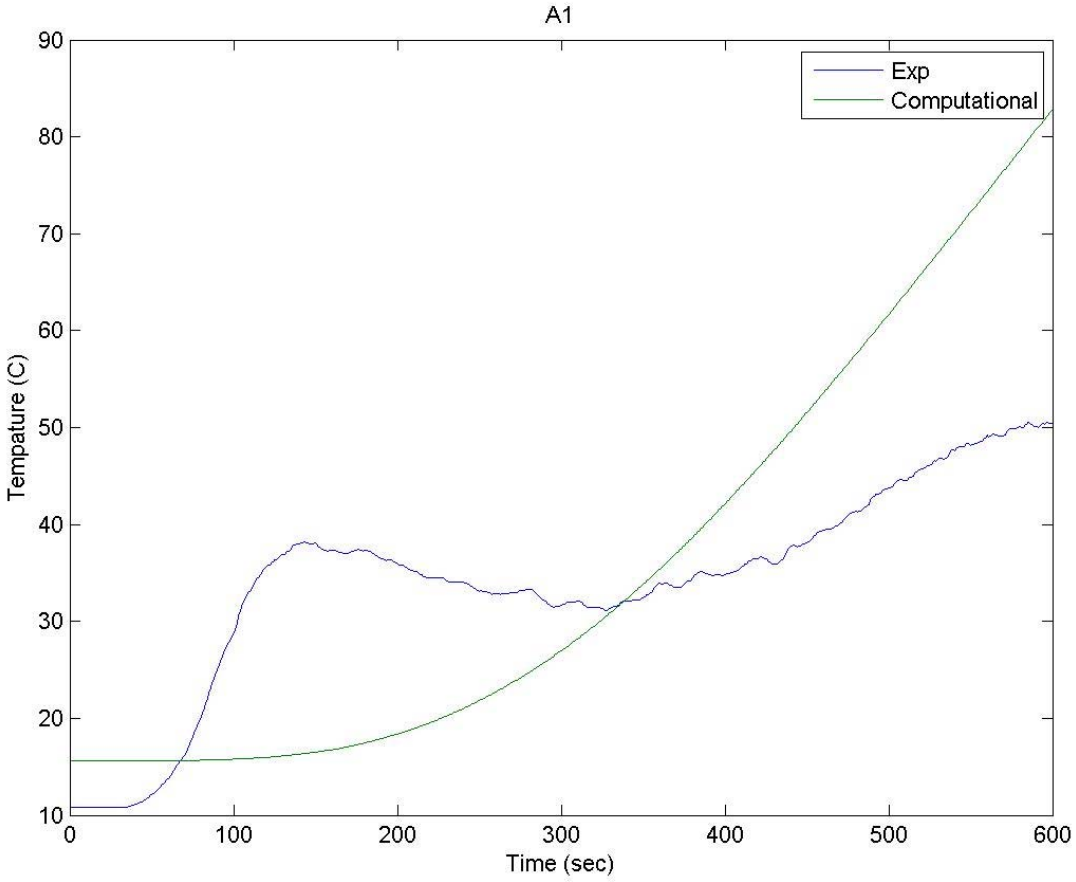
A1
Exp
Computational
Tempature (C)
Time (sec)
90
80
70
60
50
40
30
20
10
0
100
200
300
400
500
600

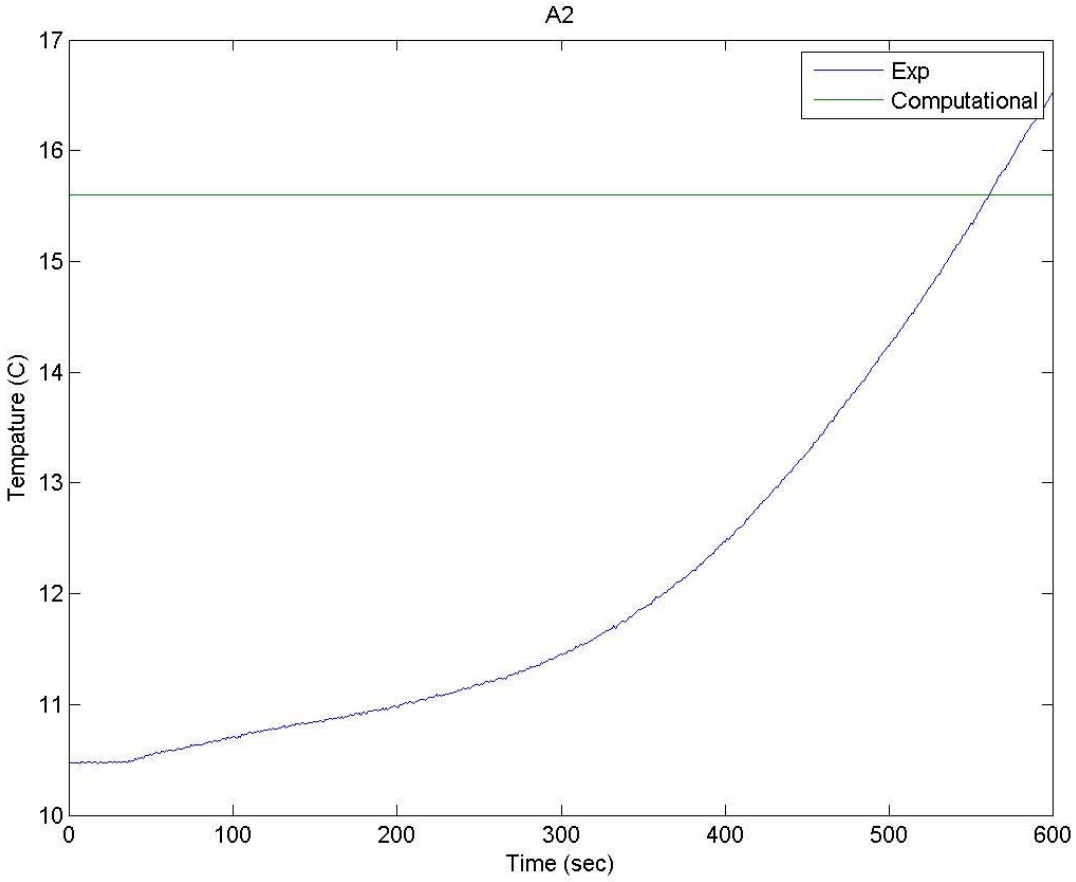
A2
Exp
Computational
Tempature (C)
Time (sec)
17
16
15
14
13
12
11
10
0
100
200
300
400
500
600

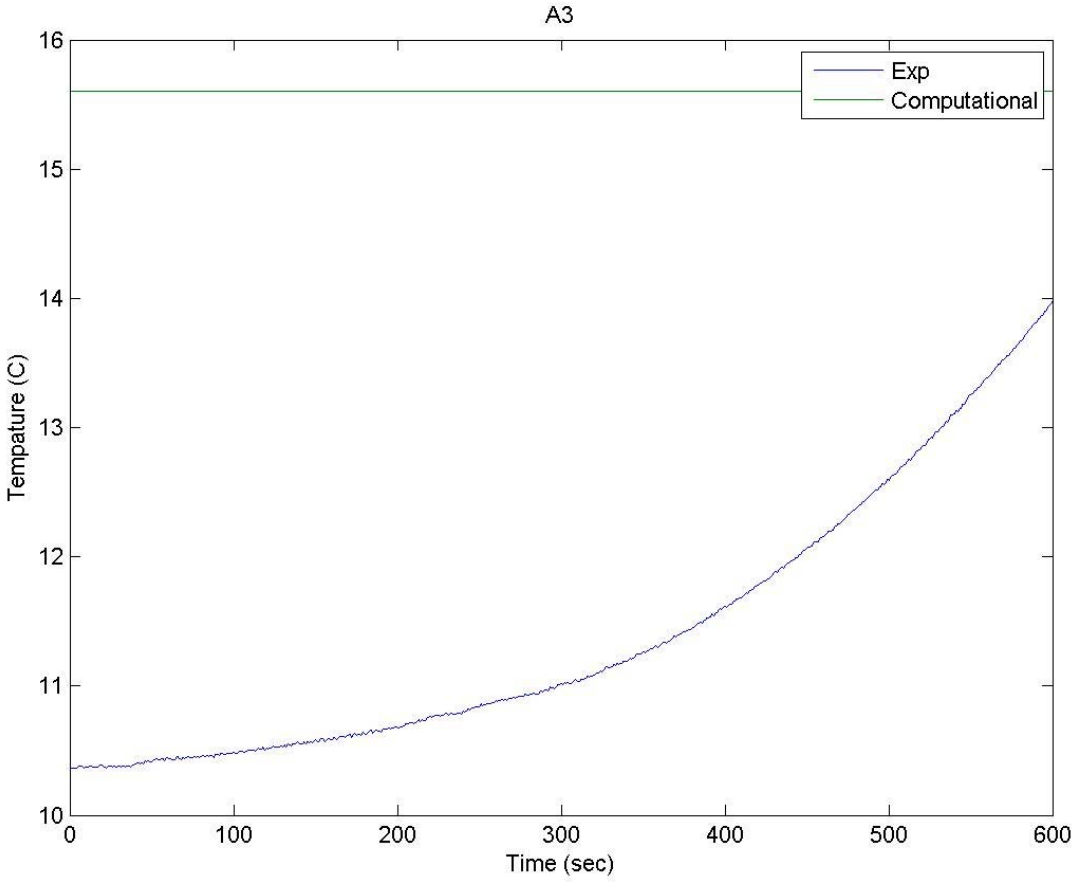
A3
Exp
Computational
Tempature (C)
Time (sec)
16
15
14
13
12
11
10
0
100
200
300
400
500
600

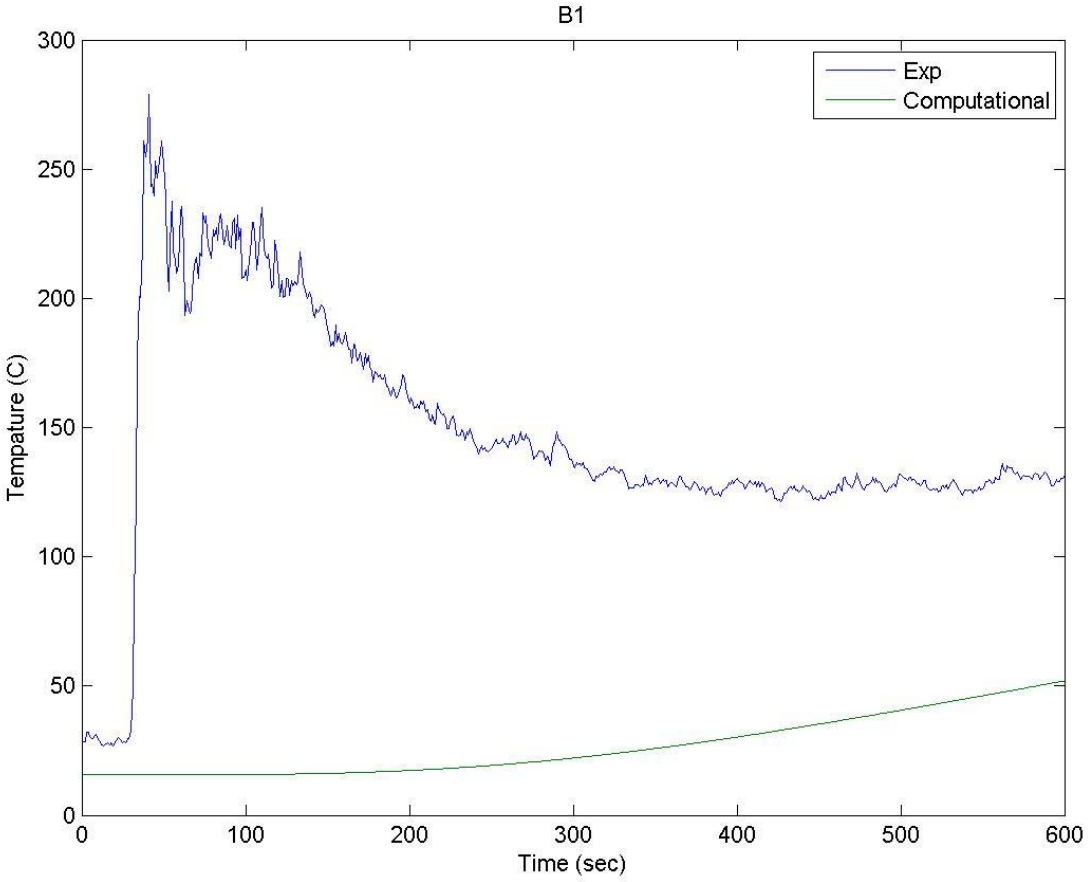
B1
Exp
Computational
Tempature (C)
Time (sec)
0
50
100
150
200
250
300
0
100
200
300
400
500
600

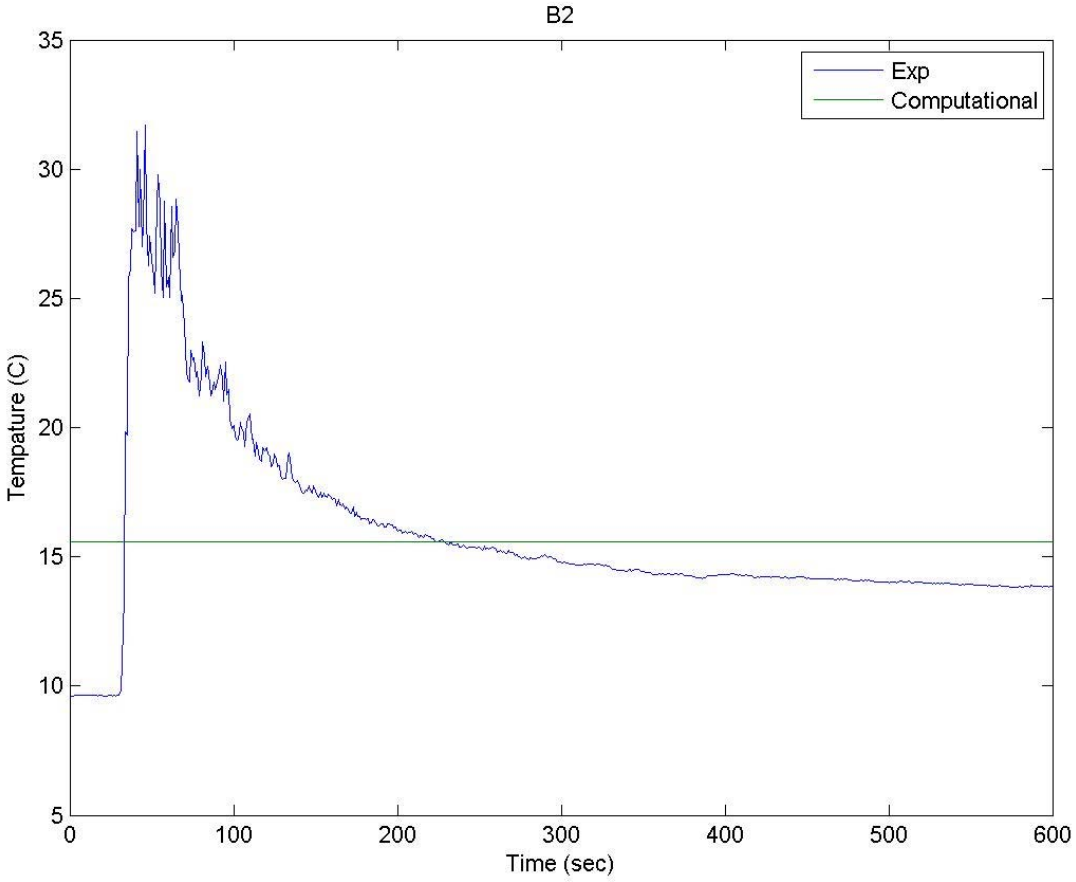
B2
Exp
Computational
Tempature (C)
Time (sec)
35
30
25
20
15
10
5
0
100
200
300
400
500
600

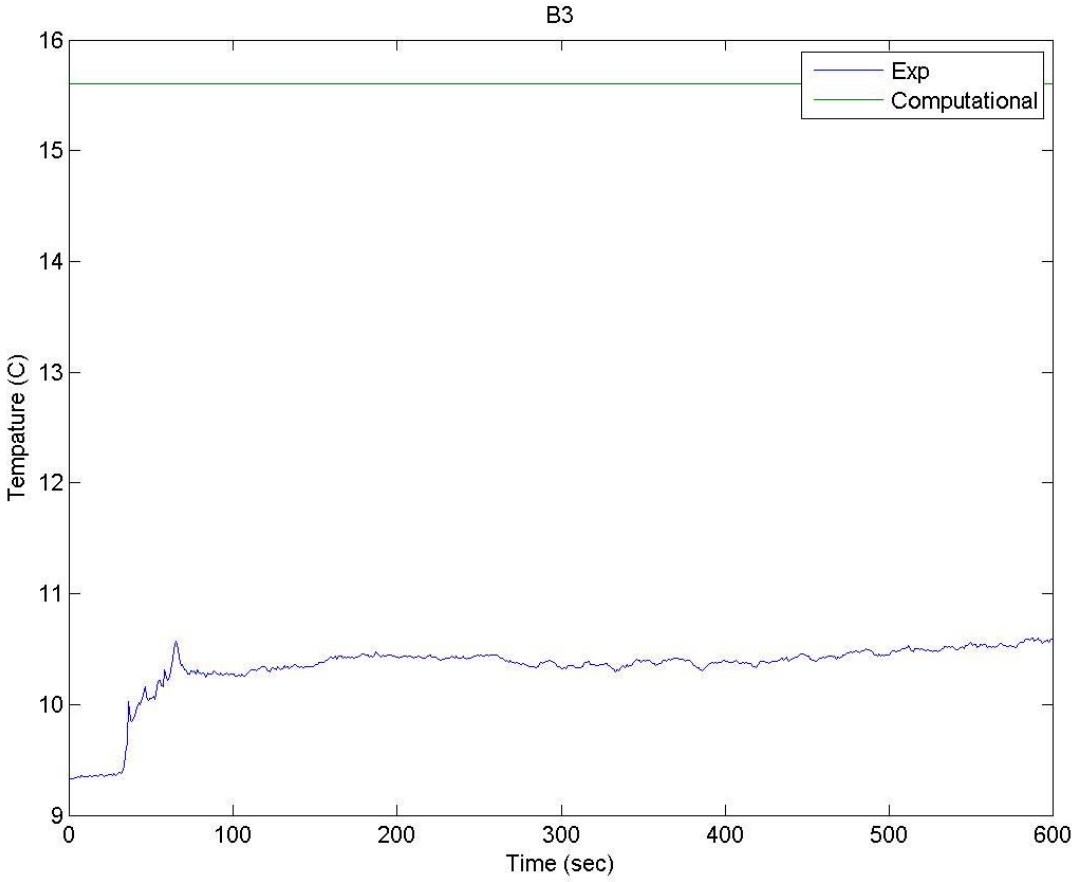
B3
Exp
Computational
Tempature (C)
Time (sec)
16
15
14
13
12
11
10
9
0
100
200
300
400
500
600

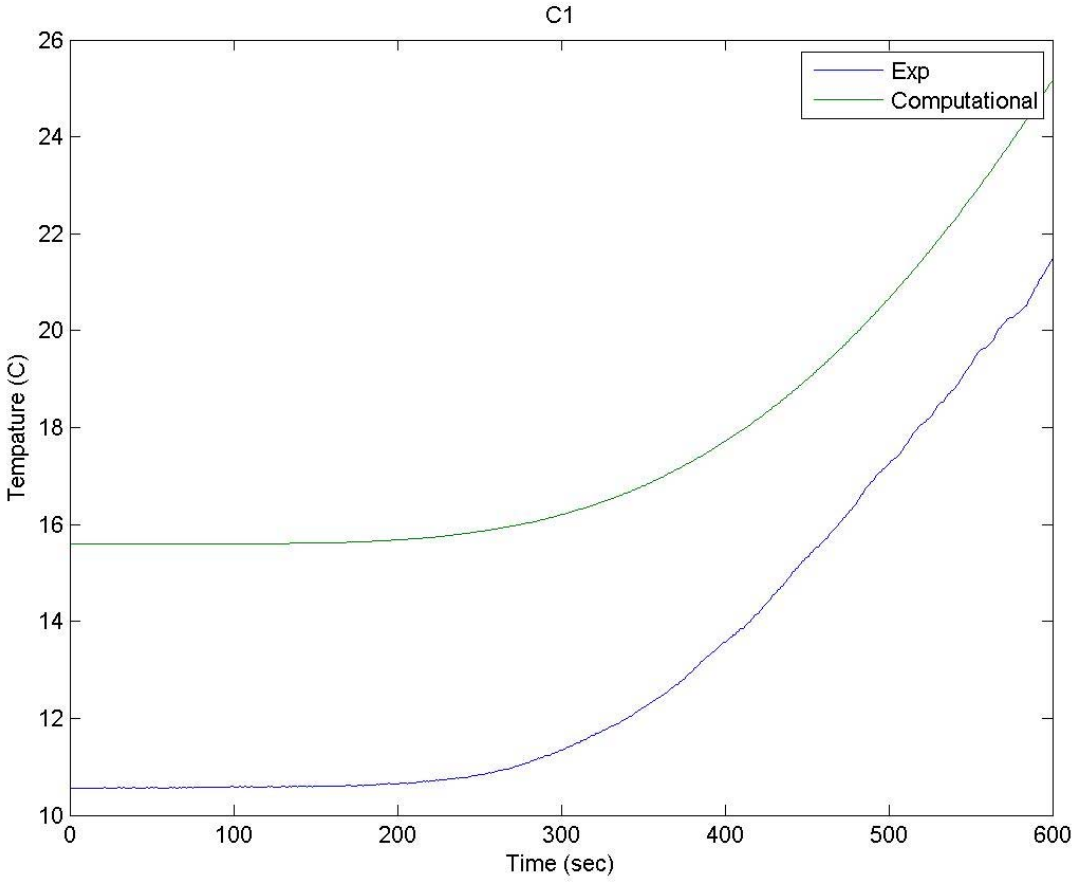
C1
Exp
Computational
Tempature (C)
Time (sec)
26
24
22
20
18
16
14
12
10
0
100
200
300
400
500
600

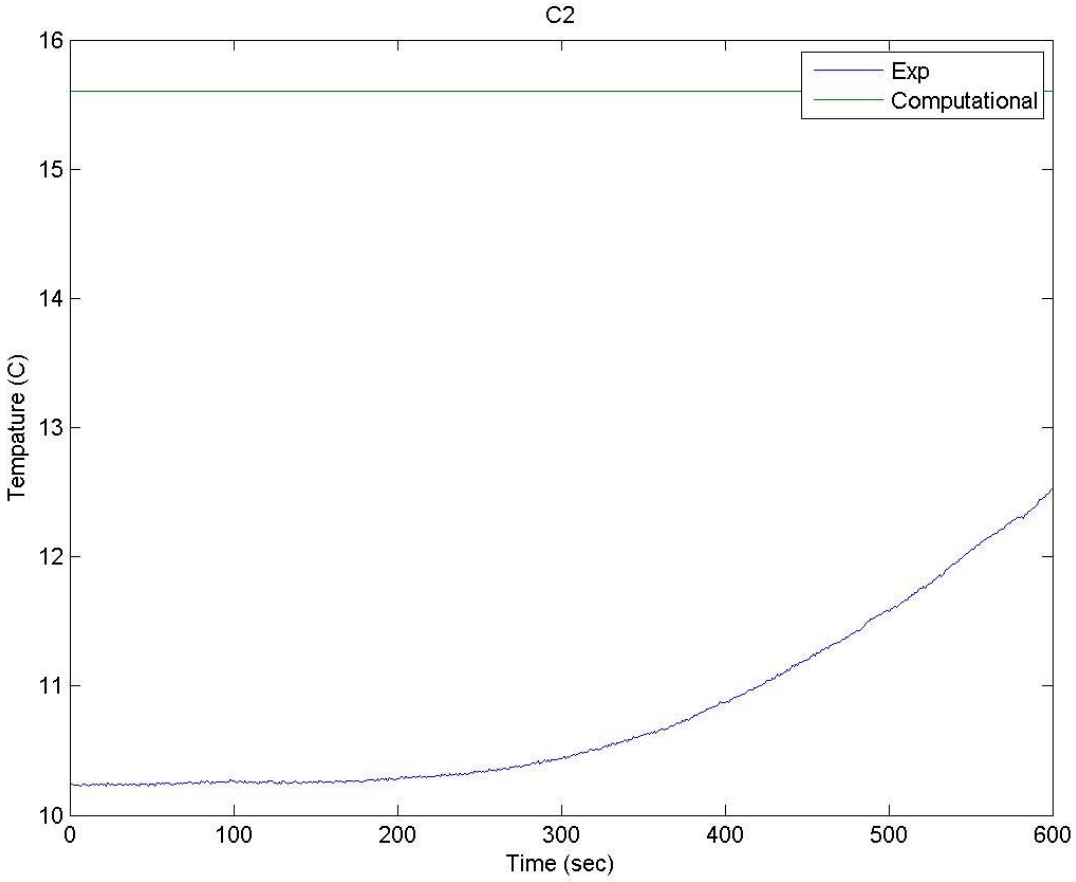
C2
Exp
Computational
Tempature (C)
Time (sec)
16
15
14
13
12
11
10
0
100
200
300
400
500
600

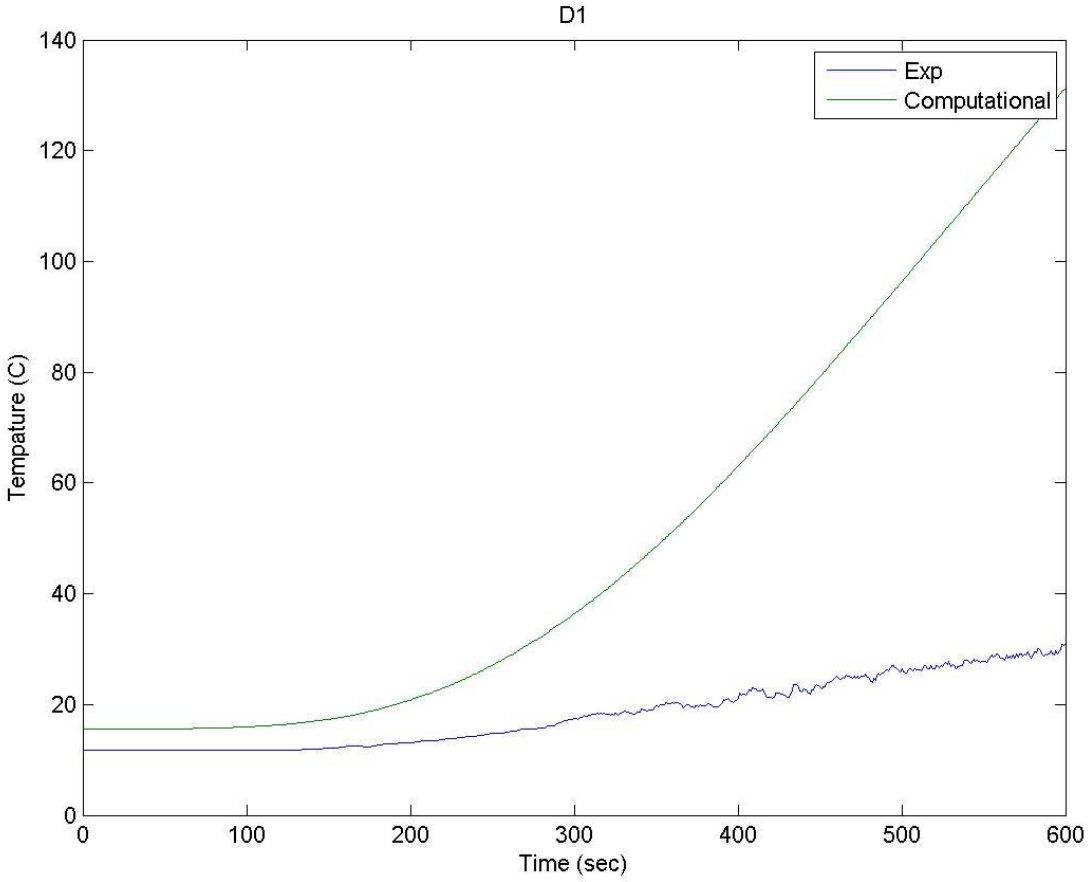
D1
Exp
Computational
Tempature (C)
Time (sec)
0
20
40
60
80
100
120
140
0
100
200
300
400
500
600

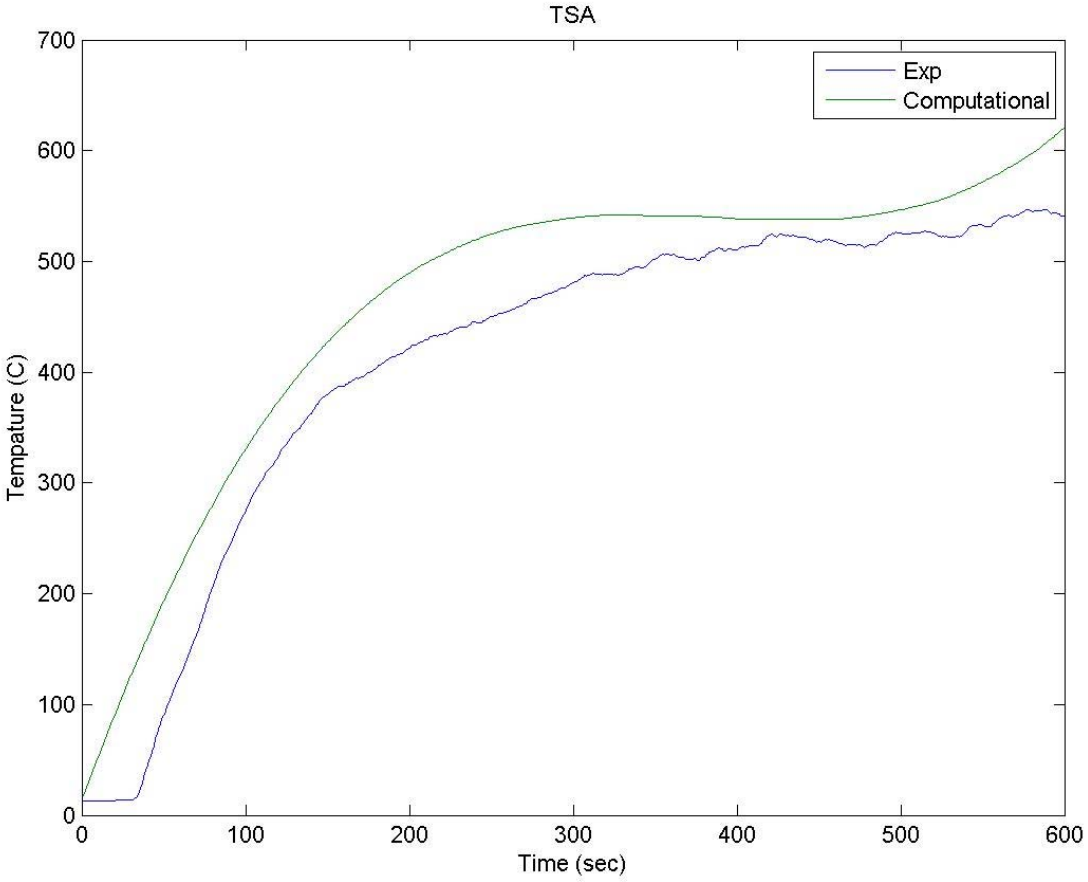
TSA
Exp
Computational
Tempature (C)
Time (sec)
0
100
200
300
400
500
600
700

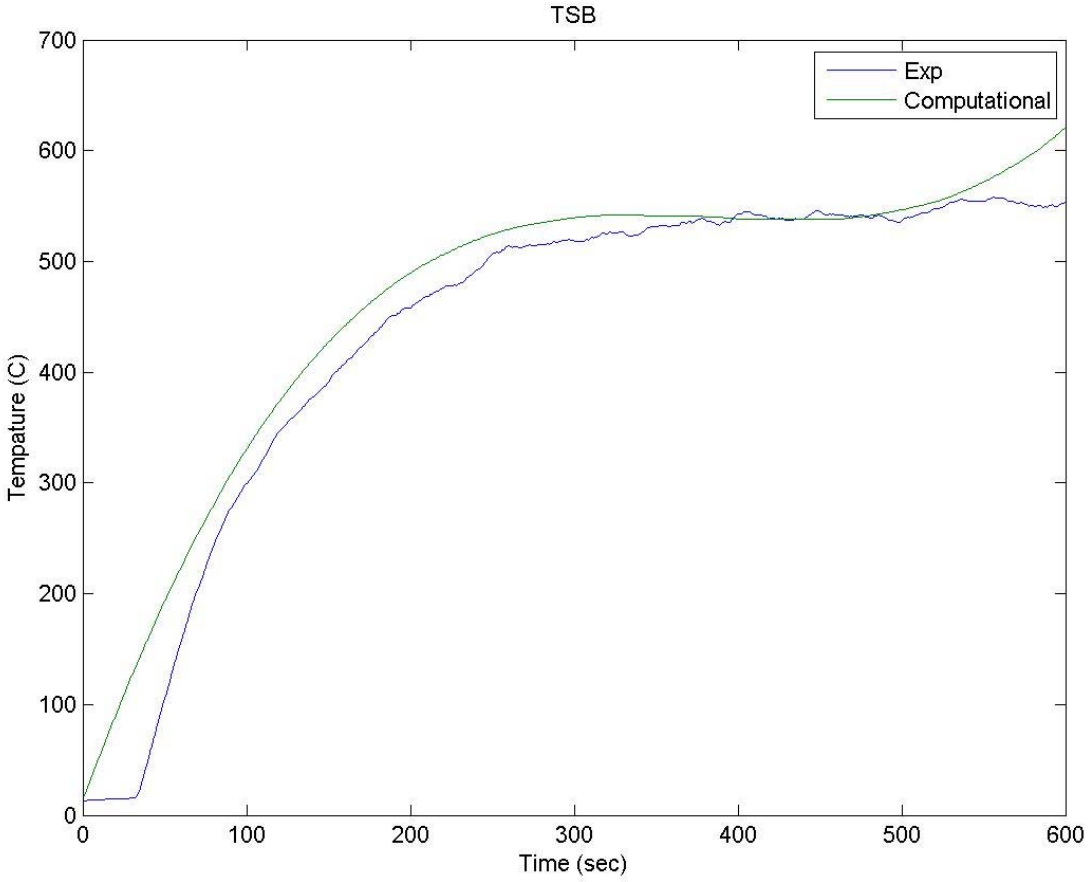
TSB
Exp
Computational
Tempature (C)
Time (sec)
0
100
200
300
400
500
600
700

Bibliography

[12]Alpert, Ronald L., and Richard J. Davis. "Evaluation of Exterior Insulation and Finish System Fire Hazard for Commercial Applications." Journal of Fire Protection Engineering 12 (2002): n. pag. FM Global Research. Web. Oct. 2013.

[13]"Approval Standard for Insulated Wall Constructions." FM Global, Sept. 1974. Web. Sept. 2013. <http://www.fmglobal.com/assets/pdf/fmapprovals/4411.pdf>.

[14]"Architectural Fiberglass, Inc." - 2009/2012 International Building Code. N.p., n.d. Web. 29 Apr. 2014. <http://www.fiberglassafi.com/code_ibc-changes.htm>.

[15]"Building Products." Georgia-Pacific DensGlass Sheathing Fiberglass Mat Gypsum Panels. Georgia Pacific, 31 Dec. 2011. Web. Oct. 2013.

[16]"FM Global Property Loss Prevention Data Sheet: Damage-Limiting Construction." FM Global, April 2012. Web. Sept. 2013. <http://www.fmglobal.com/FMGlobalRegistration/Vshared/FMDS0144.pdf>.

[17]"FM Global Property Loss Prevention Data Sheet: Fire Resistance of Building Assemblies." FM Global, Jan. 2012. Web. Sept. 2013. <http://www.fmglobal.com/FMGlobalRegistration/Vshared/FMDS0121.pdf>.

[18]"FM Global Property Loss Prevention Data Sheet: Fire Tests." FM Global, Jan. 2012. Web. Sept. 2013. <http://www.fmglobal.com/FMGlobalRegistration/Vshared/FMDS0104.pdf>.

[19]"FM Global Property Loss Prevention Data Sheet: Firesafe Building Construction and Materials." FM Global, April 2012. Web. Sept. 2013. <http://www.fmglobal.com/FMGlobalRegistration/Vshared/FMDS0101.pdf>.

[20]"FM Global Property Loss Prevention Data Sheet: Plastics In Construction." FM Global, Feb. 2012. Web. Sept. 2013. <http://www.fmglobal.com/FMGlobalRegistration/Vshared/FMDS0157.pdf>.

[21]Incropera, Frank P. , and David P. DeWitt. Fundamentals of Heat And Mass Transfer. Wiley, print.

[22]RSTSUV, S, and Yaman Yener. *Convective Heat Transfer*. Boca Raton: CRC Press, 1995. Print.

[23]Parker, William J. "An Investigation of the Fire Environment in the ASTM E 84 Tunnel Test." (1977): n. pag. National Bureau of Standards. Web. Oct. 2013.

[24]"Patent US2414060 - Interlocking Wedge Joint for Securing Together Prefabricated Building Panels." Google Books. N.p., n.d. Web. 29 Apr. 2014. <http://www.google.com/patents/US2414060>.

[25]"Pressure-Treated SIP Foundations Are Warm, Dry and Easy to Build -." N.p., n.d. Web. 29 Apr. 2014.<http://stevemaxwell.ca/pressure-treated-sip-foundations-are-warm-dry-and-easy-to- build/>.

[26]Russell, Gordon C. "Patent US3251163 - Clamp Joint Construction for Prefabricated Panels." Google Books. Lockheed Aircraft Group, 5 Apr. 1962. Web. Oct. 2013. <http://www.google.com/patents/US3251163>.

[27]Spencer, Ryan. "Through the Fire: An Overview of the Rigorous Testing Procedures for Fire-Retardant Coatings." Spray Foam Magazine, 1 Mar. 2013. Web. Sept. 2013. <http://sprayfoammagazine.com/through-the-fire-an-overview-of-the-rigorous-testing-procedures-for-fire-retardant-coatings/>.

[28]Stevens, Michael, Elodie Bugnicourt, and Philippe Coutelen. Comparison of Fiber Reinforced Polymers in Global Fire Performance Tests. Tech. London: Interscience Communications, 2009. Print. Ashland Performance Materials, Inc 2009

[29]"Structural Insulated Panels." Green Building Advisor. Gree Building Advisor, May 2012. Web. Sept. 2013. <http%3A%2F%2Fwww.buildingscience.com%2Fdocuments%2Fguides-and-manuals%2Fgm-guide-insulatin%20g-sheathing>.

[30]Vaidya, Amol S. Lightweight Composites for Modular Panelized Construction. Diss. U of Alabama at Brimingham, 2009. N.p.: n.p., n.d. Print.

[31]Williamson, R.B., Revenaugh, A. and Mowrer, F.W. “Ignition Sources in Room Fire Tests and Some Implications for Flame Spread Evaluation.” 1991. Fire Safety Science 3: 657-666. Doi:10.3801/IAFSS.FSS.3-657. Web. Oct. 2013.